



MRC
Mitochondrial
Biology Unit



UNIVERSITY OF
CAMBRIDGE

Investigating the role of mitochondrial
dysfunction in a *Drosophila* model of
C9orf72 ALS/FTD

Wing Hei Au

MRC Mitochondrial Biology Unit

University of Cambridge

Darwin College

This dissertation is submitted for the degree of *Doctor of Philosophy*

September 2022

Thesis Declaration

This thesis is the result of my own work and includes nothing which is the outcome of work done in collaboration except as declared in the Preface and specified in the text. I further state that no substantial part of my thesis has already been submitted, or, is being concurrently submitted for any such degree, diploma or other qualification at the University of Cambridge or any other University or similar institution except as declared in the Preface and specified in the text. It does not exceed the prescribed word limit for the relevant Degree Committee.

Wing Hei Au

September 2022

Abstract

Title: Investigating mitochondrial dysfunction in a *Drosophila* model of *C9orf72* ALS/FTD

Wing Hei Au

Mitochondrial dysfunction is a prevalent feature in many neurodegenerative diseases including Amyotrophic Lateral Sclerosis (ALS) and Frontotemporal Dementia (FTD). ALS is a debilitating and incurable disease characterised by the loss of upper and lower motor neurons leading to symptoms such as muscle weakness and paralysis. Most patients die from respiratory failure after 2–5 years however, only one globally licensed treatment (Riluzole) is available which only prolongs survival by a modest 2–3 months.

A hexanucleotide repeat expansion consisting of GGGGCC (G4C2) in the first intron of *C9orf72* is the most common pathogenic mutation in ALS/FTD. Three disease mechanisms have been proposed including haploinsufficiency and the sequestration of RNA binding proteins at accumulations (foci) of the transcribed RNA. Although intronic, the repeats are translated to produce 5 dipeptide repeat proteins (DPRs) through a mechanism known as repeat associated non-AUG (RAN) translation. Various pathogenic mechanisms have been proposed and it is generally accepted that mitochondrial dysfunction is an early alteration in ALS. Mitochondria are vital organelles important for cellular processes regulating energy metabolism and cell survival. The role of mitochondria specifically in *C9orf72* ALS/FTD has been relatively understudied, especially in an *in vivo* system. Excess production of reactive oxygen species (ROS) and defective mitochondrial dynamics are common features of ALS, but it is not clear whether these phenomena are causative or a consequence of the pathogenic process.

In this thesis, I have utilised 3 different *Drosophila* models of *C9orf72*, including a (i) 36 repeat GGGGCC (G4C2x36), (ii) poly GR36 DPR-only model and (iii) GR1000-eGFP DPR-only model. Firstly, I recapitulated established phenotypic characterisations that have been previously published. Briefly, pan-neuronal expression of the various transgenes exhibit locomotor deficits which I used as a readout for testing different genetic manipulations to modulate and ultimately rescue these behavioural phenotypes. Next, I performed a thorough characterisation of mitochondrial dysfunction in all the models, analysing impacts on ROS, morphology and mitochondrial turnover (mitophagy). I found alterations in mitochondrial morphology, specifically hyperfusion, a reduction in mitophagy, increased ROS production and impaired respiration in these models. Unexpectedly, genetic manipulation to restore

mitochondrial fission/fusion dynamics or boosting mitophagy were unable to rescue the locomotor deficits in larvae. However, genetic upregulation of antioxidants such as mitochondrial superoxide dismutase 2 (SOD2) and catalase were able to rescue impaired larval locomotion. Surprisingly, overexpression of cytosolic superoxide dismutase 1 (SOD1) exacerbated larval crawling phenotypes. Together, these data suggest a causative link between mitochondrial dysfunction, ROS and behavioural phenotypes.

To elaborate on this connection, I investigated whether the nuclear factor erythroid 2-related factor 2 (NRF2)/Keap1 signalling pathway might play a role. I found that NRF2 was translocated to the nucleus suggesting an activation of the pathway. However, there were minimal changes to NRF2 targeting transcript genes although changes were observed using a glutathione S-transferase D1 (*gstD1*-GFP) reporter for NRF2 activity. Despite these variable effects, both genetic reduction in *Keap1* and pharmacological treatment with an NRF2 activator, dimethyl fumarate (DMF), showed a behavioural rescue in climbing activity of G4C2x36 and GR36 flies. While more research is needed, these results provide compelling evidence that mitochondrial oxidative stress is a major upstream pathogenic mechanism leading to downstream mitochondrial dysfunction such as alterations in mitochondrial function and turnover. Consequently, targeting one of the main intracellular defence mechanisms to counteract oxidative stress – the NRF2/Keap1 signalling pathway – could be a viable therapeutic strategy for ALS/FTD.

Acknowledgements

Firstly, of course, I have to thank my supervisor, Dr Alex Whitworth. Thank you Alex for your continued support and guidance throughout the four years of the PhD and also my time as RA in your lab. Thanks for keeping faith in me and I hope we can continue to work together, finish outstanding experiments and publish our work soon!

Next, to all lab members, old and current. Thanks to the ex- lab members, Simo, Tom, Juliette, Joanne and Natalie for their scientific contributions and I'm very happy we are all still in communication, meeting up once in a while to reminisce about the good days and also share how 'successful' (or not sometimes) we all are!

To the current members. Firstly, to Alvaro. You are the one of the main reasons I decided to pursue the PhD in this lab. Thank you for being a great mentor, friend and sometimes adopted father even though the age gap doesn't add up – I know I can count on you for anything and thanks for your scientific input with your big brain. Next to Leonor. Thank you for your continued support, you are always there for me when I needed a pick up and your words of encouragement are always so uplifting. You are one of the cleverest people I've met, and you have such great ideas and scientific curiosity – I'm very lucky to have you on board to discuss results and future experiments together. Also, I can't wait to meet Eddie!! Thanks goes to all the post docs in the lab – Aitor (your passion and positive attitude is inspiring, I wish you luck for everything – 'we are family' sung with your monotonous voice!), Fede (you're destined for great things I know, thank you for being an amazing colleague and friend!) and Ana (I've included you in the post doc category since you are one to me, and thanks for taking care of things when I need and also your scientific input). To all the students in the lab and also my PhD cohort at the MBU, impossible to name all but thanks for making the lab atmosphere great! And to the baby of the lab, but my big sister, Maddy - you are the kindest person and your perseverance and scientific knowledge is great, good luck for your PhD too and thanks for being a great friend! Also, thanks to Hiran from the MBU – thank you for your often sarcastic but mostly useful critical comments and discussions.

Also, thanks to my friends and colleagues from my old lab – Jess, Alan and Dan – without you guys, I would not have been able to learn my basic fly skills and develop my scientific critical mindset and passion for studying C9. Thanks to my best friend Sarah – although we're on opposite sides of the world now, you will always be my bestie and I'm forever

thankful for your support and will always cherish our good times together also with Naune – thanks to you too for checking up on me during the writing stage – loved sharing the writing stress together with you and miss the fun times we've shared together! I'm sorry I haven't named all the friends that have provided me with support and good times!

Lastly, my most heartfelt thanks go to Chris. I'm so lucky to have you in my life – thanks for your continuous love, support and companionship, allowing me to achieve the perfect work/life balance. I am always indebted to my parents, my brother Cheuky and grandparents. Thanks to my dad for his wisdom, my mum for her love, care and food and Cheuky for being the best supportive brother.

Basically, thanks to everyone for making my PhD experience such a good one! The only thing left is to get this work published which will be my thanks to all of you! Much love :D

Table of Contents

Thesis Declaration	iii
Abstract	iv
Acknowledgements	vi
List of Abbreviations	xii
Chapter 1 - Introduction	1
1.1 ALS-FTD Spectrum	2
1.1.1 Amyotrophic Lateral Sclerosis (ALS)	2
1.1.2 Frontotemporal Dementia (FTD)	2
1.1.3 Converging genetic, pathological and clinical features of ALS/FTD	4
1.2 Chromosome 9 Open Reading Frame 72 (C9orf72)	6
1.2.1 C9orf72 Gene and Function	6
1.2.2 Other functions of C9orf72	11
1.2.3 Mechanisms of C9orf72 toxicity	12
1.2.3.1 Loss of function: Haploinsufficiency.....	12
1.2.3.2 Gain of function: RNA toxicity	14
RNA toxicity	14
Evidence for C9orf72 repeat RNA toxicity	15
Evidence against C9orf72 repeat RNA toxicity.....	16
1.2.3.3 Gain of function: Dipeptide repeat proteins (DPRs).....	16
Poly-GA	19
Arginine DPRs – poly-GR and poly-PR	20
1.3 Mitochondria and C9orf72	23
1.3.1 Mitochondrial structure and function	23
1.3.2 Mitochondrial dynamics.....	23
1.3.3 Mitochondrial respiration and ATP production	29
1.3.4 Mitochondrial quality control.....	32
1.4 NRF2/Keap1 system	35
1.4.1 Structure of NRF2 and Keap1	35
1.4.2 NRF2/Keap1 signalling	39
1.4.3 NRF2 and ALS	40
1.5 The use of <i>Drosophila melanogaster</i> as a genetic model system	44
1.6 Thesis Aims	46
Chapter 2 – Materials and Methods	47
2.1 <i>Drosophila</i> husbandry	48
2.1.1 Drug Treatments	49
2.2 Behavioural assays	49
2.2.1 Larval crawling	49
2.2.2 Climbing assay	50
2.3 Immunohistochemistry	50
2.3.1 Mitochondrial morphology, autophagy and mitophagy.....	50
2.3.1.1 Quantification of mitoQC mitolysosomes and mCherry autolysosomes	50
2.3.1.2 Quantification of mitochondrial morphology.....	51
2.3.2 Immunostaining	51
2.3.2.1 Quantification of cncC staining	51
2.3.3 Using mito-roGFP2-Orp1	51
2.3.4 MitoSOX.....	52
2.4 Microscopy	52

2.5 Immunoblotting	52
2.6 Quantitative real-time PCR	53
2.6.1 RNA extraction	53
2.6.2 DNase treatment	53
2.6.3 cDNA synthesis	54
2.6.4 qRT-PCR.....	54
2.7 Mitochondrial respiration	55
2.8 Statistical analysis	56
Chapter 3 – Characterisation of mitochondrial phenotypes in a <i>Drosophila</i> model of <i>C9orf72</i> ALS/FTD	57
3.1 Phenotypic characterisation of <i>C9orf72</i> flies	58
3.1.1 Expression of G4C2x36 repeats and GR36 in the eye harbours a rough eye phenotype .	58
3.1.2 Pan-neuronal expression of GR36 is developmental lethal	60
3.2 Behavioural analysis of <i>C9orf72</i> flies	61
3.2.1 Pan-neuronal expression of G4C2x36 and GR36 causes a larval crawling impairment....	61
3.2.2 Pan-neuronal expression of GR1000 shows a progressive age-related climbing deficit ...	63
3.3 Mitochondrial morphology in <i>C9orf72</i> flies	64
3.3.1 No observable differences in mitochondrial morphology in G4C2x36 and GR36 larval epidermal cells	65
3.3.2 Elongated, hyperfused mitochondria were observed with pan-neuronal expression in the larval ventral ganglion of G4C2x36 and GR36.....	66
3.4 Mitochondrial respiration is compromised in <i>C9orf72</i> flies	67
3.4.1 G4C2x36 flies have a reduction in Complex I and Complex II linked respiration.....	67
3.5 Disrupted mitochondrial quality control in <i>C9orf72</i> flies	70
3.5.1 Reduction in mitophagy is observed in G4C2x36 and GR36 flies using the mito-QC reporter.....	70
3.5.2 Autophagy is perturbed when overexpressing G4C2x36 and poly-GR36.....	72
3.5.3 Increased Ref(2)P and reduced Atg8a-II levels were observed with pan-neuronal expression of G4C2x36.....	74
3.6 Increased oxidative stress in <i>C9orf72</i>	75
3.6.1 Increased mitochondrial ROS was observed in G4C2x36 and GR36.....	75
3.6.2 Increased MitoSOX staining was observed in GR1000 flies.....	77
3.7 Discussion	78
Basic characterisation of <i>C9orf72 Drosophila</i> toolset	78
Mitochondrial morphology	79
Mitochondrial respiration	80
Autophagy and Mitophagy	81
Oxidative stress.....	83
Intracellular superoxide production	83
Intracellular hydrogen peroxide (H ₂ O ₂) production.....	84
3.8 Summary	85
Chapter 4 – Modulating mitochondrial dysfunction to improve <i>C9orf72</i> behavioural fitness	86
4.1 Genetic manipulations of fission and fusion does not rescue <i>C9orf72</i> locomotor phenotypes	87
4.1.1 Promoting fission by overexpressing <i>Tango11</i> or <i>Drp1</i>	87
4.1.2 Decreasing fusion with <i>Opa1</i> and <i>Marf</i> mutants in heterozygosity	90
4.1.3 Manipulating mitochondrial dynamics does not rescue <i>C9orf72</i> motor deficits	92
4.2 Boosting mitophagy does not rescue <i>C9orf72</i> phenotypes	94

4.2.1 Overexpression of <i>Pink1</i> or <i>parkin</i> did not rescue rough eye phenotypes in G4C2x36 and GR36 flies	94
4.2.2 Boosting mitophagy by expressing <i>USP30</i> RNAi had no effect in G4C2x36 and GR36 flies	96
4.2.3 Expression of <i>USP30</i> RNAi had no beneficial effect on larval crawling in G4C2x36 and GR36 flies	98
4.3 Other components – MICOS	99
4.3.1 No rescue was observed in larval crawling when manipulating MICOS components in G4C2x36 and GR36.....	99
4.4 Antioxidants	100
4.4.1 Overexpression of mitochondrial Sod2 and catalase partially rescues larval crawling deficit in G4C2x36 and GR36 models	100
4.4.2 Less elongated mitochondria were found with overexpression of Sod2 and catalase.....	102
4.4.3 No additive effect was observed when overexpressing Sod2 and catalase together	105
4.4.4 Overexpression of mitochondrial Sod2 and catalase also partially rescued adult climbing deficits observed with GR1000 model at day 10.....	106
4.4.5 Partial rescue of mitophagy was observed with overexpression of Sod2	107
4.5 Discussion.....	109
Modulation of mitochondrial dynamics does not rescue <i>C9orf72</i> phenotypes	109
MICOS	110
Modulation of mitophagy does not rescue <i>C9orf72</i> phenotypes	111
Antioxidants.....	112
4.6 Summary.....	114
Chapter 5 – NRF2/cncC and Keap1 signalling.....	115
5.1 Genetic interactions with Keap1	116
5.1.1 Genetic interactions with Keap1 mutants in heterozygosity rescued larval crawling phenotypes in G4C2x36 and GR36 larvae	116
5.1.2 Genetic interactions with Keap1 mutants in heterozygosity rescued adult climbing phenotypes in GR1000 flies	117
5.2 Characterisation of NRF2/cncC in G4C2x36 flies	119
5.2.1 Increased nuclear cncC staining is observed in larval brains of G4C2x36 and GR36.....	119
5.2.2 G4C2x36 flies are able to respond to ROS-inducing paraquat treatment.....	121
5.2.3 Changes in <i>gstD1</i> -GFP levels were observed across time	123
5.2.4 <i>cncC</i> target genes show minimal changes at transcript level	126
5.2.5 Transcript levels of <i>cncC</i> related genes comparing larval and adult G4C2x36 flies	128
5.3 Treatment with NRF2/cncC activator dimethyl fumarate (DMF)	131
5.3.1 DMF treatment rescued climbing phenotypes in G4C2x36 and GR36 flies	131
5.3.2 DMF treatment had little effect on climbing phenotypes in GR1000 flies.....	132
5.4 Discussion.....	134
Localisation of <i>cncC</i> /NRF2.....	134
<i>cncC</i> /NRF2 activity – using the <i>gstD1</i> -GFP reporter	135
<i>cncC</i> /NRF2 activity – transcript levels.....	137
Therapeutic treatments – DMF	138
5.5 Summary.....	139
Chapter 6 – General discussion and future work.....	140
6.1 Summary of Findings	141
6.2 Expanding on our knowledge of compartmentalised ROS damage.....	143
6.3 Alternative oxidative stress responses & contribution from other pathogenic mechanisms	145
6.4 Mitophagy and autophagy	147

6.5 Therapeutic treatments - DMF	148
6.6 Relevance of work	149
6.7 Conclusions	151
References	152

List of Abbreviations

AAV	Adeno-associated virus
ALS	Amyotrophic Lateral Sclerosis
AMBRA1	Autophagy and BECLIN 1 regulator 1
ARE	Antioxidant response element
ARF	ADP-ribosylation factor
ASO	Antisense oligonucleotides
ATG	Autophagy related
ATP	Adenosine triphosphate
BAC	Bacterial artificial chromosome
BBB	Blood brain barrier
BNIP3	Bcl-2 and adenovirus E1B 19 kDa-interacting protein 3
C9orf72	Chromosome 9 Open Reading Frame 72
Cat	Catalase
CCCP	Carbonyl cyanide m-chlorophenyl hydrazone
CHMP2B	Charged Multivesicular body protein
CJ	Cristae Junction
CnC	Cap 'n' collar
CNS	Central nervous system
CUL3	Cullin 3
DCF	Dichlorofluorescein
DENN	Differentially expressed in normal and neoplasia
DHE	Dihydroethidium
DMF	Dimethyl fumarate
DPR	Dipeptide repeat proteins
DRP1	Dynamamin-related protein 1
DUBs	Deubiquitinating enzymes
ETC	Electron transport chain
FIP200	FAK family kinase-interacting protein of 200 kDa
FIS1	Mitochondrial fission 1 protein
FTD	Frontotemporal Dementia
FUNC1	FUN14 domain-containing protein 1
GA	Glycine alanine
GABARAP	GABA Type A Receptor-Associated Protein
GAP	GTPase activating protein
GCL	Glutamate-cysteine ligase
GDP	Guanosine diphosphate
GEF	GDP/GTP exchange factors
GP	Glycine proline
GPX	Glutathione peroxidases
GR	Glycine arginine
GSH	Glutathione
GSSG	Oxidised glutathione
GST	Glutathione S-transferase
GTP	Guanosine triphosphate
H ₂ DCFDA	2',7'-dichlorodihydrofluorescein diacetate

H ₂ O ₂	Hydrogen peroxide
hnRNP	Heterogenous nuclear ribonucleoproteins
HO1	Heme oxygenase 1
HRE	Hexanucleotide repeat expansion
IMM	Inner mitochondrial membrane
IMS	Intermembrane space
iPSC	Induced Pluripotent Stem Cells
Keap1	Kelch-like ECH-associated protein 1
LC-MS	Liquid chromatography–mass spectrometry
LC3	Microtubule-associated protein 1A/1B-light chain 3
LCD	Low-complexity domains
LIR	LC3 interacting region
LLPS	Liquid-liquild phase separation
LMN	Lower motor neurons
MAPT	Microtubule associated protein tau
MFF	Mitochondrial fission factor
MFN	Mitofusins
MICOS	Mitochondrial contact site and cristae organizing system
MitoB/MitoP	MitoBoronic acid/MitoPhenol
MND	Motor Neuron Disease
NCT	Nucleocytoplasmic transport
NDP52	Nuclear dot protein
NF-κB	Nuclear factor kappa-light-chain-enhancer of activated B cells
NRF2	Nuclear factor erythroid 2 p45-related factor 2
OMM	Outer mitochondrial membrane
OPA1	Optic atrophy 1
OPTN	Optineurin
Orp1	Oxidant receptor peroxidase
OXPPOS	Oxidative phosphorylation
PA	Proline alanine
PARL	Presenilin-associated rhomboid-like protease
PGC1α	Peroxisome proliferator-activated receptor gamma coactivator 1-alpha
PINK1	PTEN-induced kinase 1
PPA	Primary progressive aphasia
PQ	Paraquat
PR	Proline arginine
PRX	Peroxiredoxins
RAB	Ras-associated binding
RAN	Repeat associated non-AUG
RBP	RNA binding proteins
RBX1	Ring box protein 1
roGFP	Redox sensitive green fluorescent protein
ROS	Reactive oxygen species
SG	Stress granules
SMCR8	Smith-Magenis chromosome region 8
SOD	Superoxide dismutase
SQSTM1	Sequestosome 1
TBK1	Tank binding protein 1
TCA	Tricarboxylic acid

TDP-43	Transactive DNA response DNA binding protein 43
TEM	Transmission electron microscopy
TIM/TOM	Translocase of the inner/outer membrane
TMD	Transmembrane domain
UAS	Upstream activating sequence
UBQLN2	Ubiquilin 2
ULK1	Unc-51 like kinase 1
UMN	Upper motor neurons
Unc119	Uncoordinated 119
UPS	Ubiquitin proteasome system
USP	Ubiquitin-specific protease
VCP	Valosin-containing protein
VNC	Ventral nerve cord
WDR41	WD repeat-containing protein 41

Chapter 1 - Introduction

1.1 ALS-FTD Spectrum

1.1.1 Amyotrophic Lateral Sclerosis (ALS)

Motor neuron disease (MND) defines a group of neurodegenerative disorders characterised by the degeneration of both upper motor neurons (UMNs) and lower motor neurons (LMNs), leading to motor and extra motor symptoms (Ling *et al*, 2013; Robberecht & Philips, 2013; Hardiman *et al*, 2017; van Es *et al*, 2017; Masrori & Van Damme, 2020). Loss of UMNs may lead to symptoms such as muscle spasticity and hypertonia, whereas degeneration of LMNs can lead to muscle weakness, atrophy and fasciculations (Figure 1.1A) (van Es *et al.*, 2017). Classical amyotrophic lateral sclerosis (ALS) refers to MND in which both UMN and LMN symptoms are present. Approximately 25-30% of patient cases present with bulbar onset which is characterised by symptoms such as dysarthria and dysphagia. Alternatively, patients present with spinal onset ALS which occurs when the disease begins by affecting the motor neurons in a person's limbs. Most patients die 2-3 years after symptom onset from respiratory failure (Masrori & Van Damme, 2020).

1.1.2 Frontotemporal Dementia (FTD)

Frontotemporal dementia (FTD) is characterised by the degeneration of the frontal and temporal lobes leading to clinical symptoms such as cognitive impairment. There are two main subtypes of FTD; primary progressive aphasia (PPA) and the behavioural variant (bvFTD). PPA causes language impairments, including loss of fluency and ability to form speech (non-fluent variant PPA) and patients who lose the understanding of words and the ability to recognise familiar objects and people (semantic variant PPA) (Rohrer *et al*, 2015) (Figure 1.1A). The bvFTD subtype covers two thirds of FTD where symptoms include drastic changes in behaviour, however, it is interesting to note that memory and visuospatial skills are surprisingly preserved in bvFTD (Rademakers *et al*, 2012). Approximately 15% of patients with ALS will develop symptoms which are also present for FTD and 30-50% of patients will exhibit cognitive and behavioural impairment (Masrori & Van Damme, 2020).

ALS-FTD Spectrum

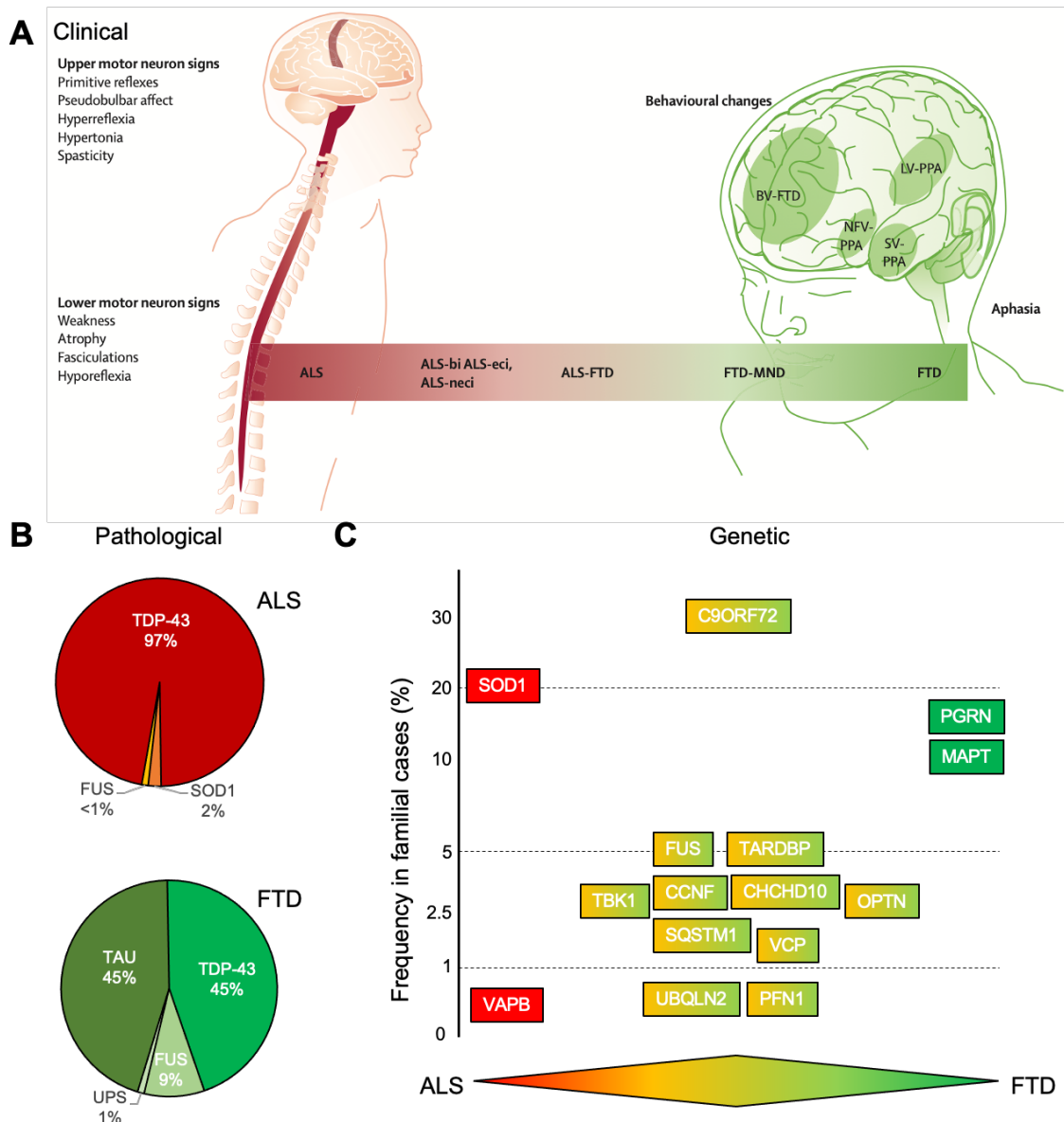


Figure 1.1 - Clinical, pathological and genetic convergence in ALS/FTD

(A) Approximately half of ALS patients develop symptoms relating to motor dysfunction termed classical ALS. However, there are ALS patients who develop degrees of cognitive and behavioural impairment: ALS-bi (ALS with behavioural impairment), ALS-eci (ALS with executive dysfunction symptoms) and ALS-neci (ALS with other cognitive impairments e.g., memory). About 5-10% of patients with ALS also have FTD (ALS-FTD). There are also some FTD patients with motor neuron deficit involvement (FTD-MND). Classical FTD can be further divided into two subtypes: BV-FTD (behavioural variant), and the primary progressive aphasias (PPAs) characterised by language deficits (NFV=non-fluent variant, SV=semantic variant, LV=logopenic variant). (B) Inclusions of TDP-43 and FUS highlight the pathological overlap of ALS and FTD. (C) Schematic reflecting the genetic overlap of ALS and FTD – the genes are distributed according to their mutation frequency in familial cases of ALS and FTD. Figures adapted from (A) van Es *et al.* (2017) (B) Ling *et al.* (2013) and (C) Shahheydari *et al.* (2017).

1.1.3 Converging genetic, pathological and clinical features of ALS/FTD

ALS and FTD are considered to be on two ends of a spectrum due to overlap in clinical, pathological and genetic features underlying both diseases. Clinically, as mentioned above, an FTD diagnosis is present in approximately 15% of ALS patients and up to 50% of ALS patients report cognitive and behavioural changes (Masrori & Van Damme, 2020). Similarly, motor neuron dysfunction is a common feature in approximately 15% of FTD cases (Figure 1.1A) (Lomen-Hoerth *et al*, 2002).

Proteinaceous pathological inclusions are observed in the pure forms of either disease, and some are shared across the spectrum of disorders. Approximately 2% of ALS patients have superoxide dismutase 1 (SOD1) inclusions which are not found in FTD cases (Ling *et al.*, 2013). Conversely, 45% of FTD cases exhibit microtubule-associated protein tau (MAPT) inclusions which are not found in ALS. Fused in Sarcoma (FUS) inclusions are found in both ALS (<1%) and FTD (9%) (Ling *et al.*, 2013). The most common pathological signature observed in both ALS and FTD is the presence of Transactive DNA response (TAR) DNA binding protein with a molecular weight of 43kDa (TDP-43) inclusions where it is observed in around 97% of ALS and 45% of FTD cases (Ling *et al.*, 2013; Masrori & Van Damme, 2020). TDP-43 is an evolutionarily conserved heterogenous nuclear ribonucleoprotein (hnRNP) and its functions include regulation of RNA transcription, splicing and transport as well as microRNA biogenesis (Cohen *et al*, 2011). Under basal conditions, TDP-43 is predominantly in the nucleus and in disease, it becomes mislocalised into the cytoplasm where it becomes abnormally phosphorylated and ubiquitinated (Figure 1.1B) (Arai *et al*, 2006; Neumann *et al*, 2006). Pathological TDP-43 aggregates can consist of full length TDP-43 as well as N terminal and C terminal fragments of the protein (Scotter *et al*, 2015). While cytoplasmic protein inclusions are indicative of gain of toxic properties, cells with TDP-43 aggregates also exhibit loss of nuclear TDP-43 which suggests a loss of TDP-43 function (Ling *et al.*, 2013). A summary of the shared molecular pathology observed across ALS and FTD is shown in Figure 1.1B.

Lastly, overlap and convergence of these two diseases can be seen at the genetic level. Mutations in *SOD1* cause a pure form of ALS, whereas mutations in *MAPT* lies on the opposite end of the spectrum causing a pure form of FTD which is reflected in their formation of distinct toxic aggregates and may suggest different mechanisms underlying pathogenesis (Hardy & Rogavaeva, 2014). Strikingly however, many other genes whose mutations cause FTD are also involved in ALS summarised in a review from Gao *et al* (2017) including valosin-containing protein (VCP) (Watts *et al*, 2004; Johnson *et al*, 2010), charged multivesicular body

ALS-FTD Spectrum

protein 2B (CHMP2B) (Skibinski *et al*, 2005; Parkinson *et al*, 2006), ubiquilin 2 (UBQLN2) (Deng *et al*, 2011) and sequestosome 1 (SQSTM1/P62) (Fecto *et al*, 2011; Rubino *et al*, 2012) (Figure 1.1C). Most of the genes can be categorised into three main categories and suggest a convergence of the cellular and molecular events that lead to degeneration: protein homeostasis, RNA homeostasis and trafficking, and cytoskeletal dynamics; it is important to stress that these mechanisms are not exclusive (Brown & Al-Chalabi, 2017). In 2011, *C9orf72* was found to be the most common genetic cause of both ALS and FTD (DeJesus-Hernandez *et al*, 2011; Renton *et al*, 2011) which will be the focus of this thesis.

1.2 Chromosome 9 Open Reading Frame 72 (*C9orf72*)

1.2.1 *C9orf72* Gene and Function

The hexanucleotide repeat expansion (HRE) in *C9orf72* is the most common genetic mutation in ALS/FTD (DeJesus-Hernandez *et al.*, 2011; Renton *et al.*, 2011). 95% of neurologically healthy individuals will harbour less than 11 hexanucleotide repeats in the *C9orf72* gene, however the pathological threshold has not been established due to somatic instability and somatic mosaicism of the mutation (Balendra & Isaacs, 2018). *C9orf72* ALS/FTD patients can range from having more than 30 to hundreds if not thousands of repeats (Rutherford *et al.*, 2012; Harms *et al.*, 2013). Individuals can have large expansions of repeats within the CNS but a differing intermediate repeat length when analysing blood DNA (Fratta *et al.*, 2015; Gijssels *et al.*, 2016). Similarly, different brain regions exhibit different repeat size lengths too (Beck *et al.*, 2013; van Blitterswijk *et al.*, 2015).

The *C9orf72* gene is located on the short arm of chromosome 9 and is highly conserved, with high degree of homology in mouse (98.13%), rat (97.71%), African clawed frogs (83.96%) and zebrafish (75.97%), however unfortunately, there is no ortholog of *C9orf72* in *Drosophila* (Smeyers *et al.*, 2021). *C9orf72* transcripts are found in most brain regions and spinal cord (DeJesus-Hernandez *et al.*, 2011; Renton *et al.*, 2011) and its expression is highest in myeloid cells involved in innate and adaptive immunity, such as CD14+ monocytes, eosinophils and neutrophils, and lower in lymphoid derived cells such as T and B cells as well as other remaining cell types and tissues throughout the body including the CNS (Rizzu *et al.*, 2016). *C9orf72* mRNA has at least three variants derived from alternative splicing and the use of different transcriptional start sites. Variant 1 (V1) is the shortest transcript which includes non-coding exon 1a and only exons 2-5 as the coding sequence. Variant 3 (V3) also contains non-coding exon 1a as well as exons 2-11 as the coding sequence. Variant 2 (V2) shares exons 2-11 but differs as it contains non-coding exons 1b instead (Smeyers *et al.*, 2021). Alternative splicing of the three RNA variants produces two isoforms– C9-short (24 kDa), 222 aa long encoded by V1 and C9-long (54 kDa), 481aa isoform encoded by V2 and V3 (Figure 1.2) (DeJesus-Hernandez *et al.*, 2011; Renton *et al.*, 2011).

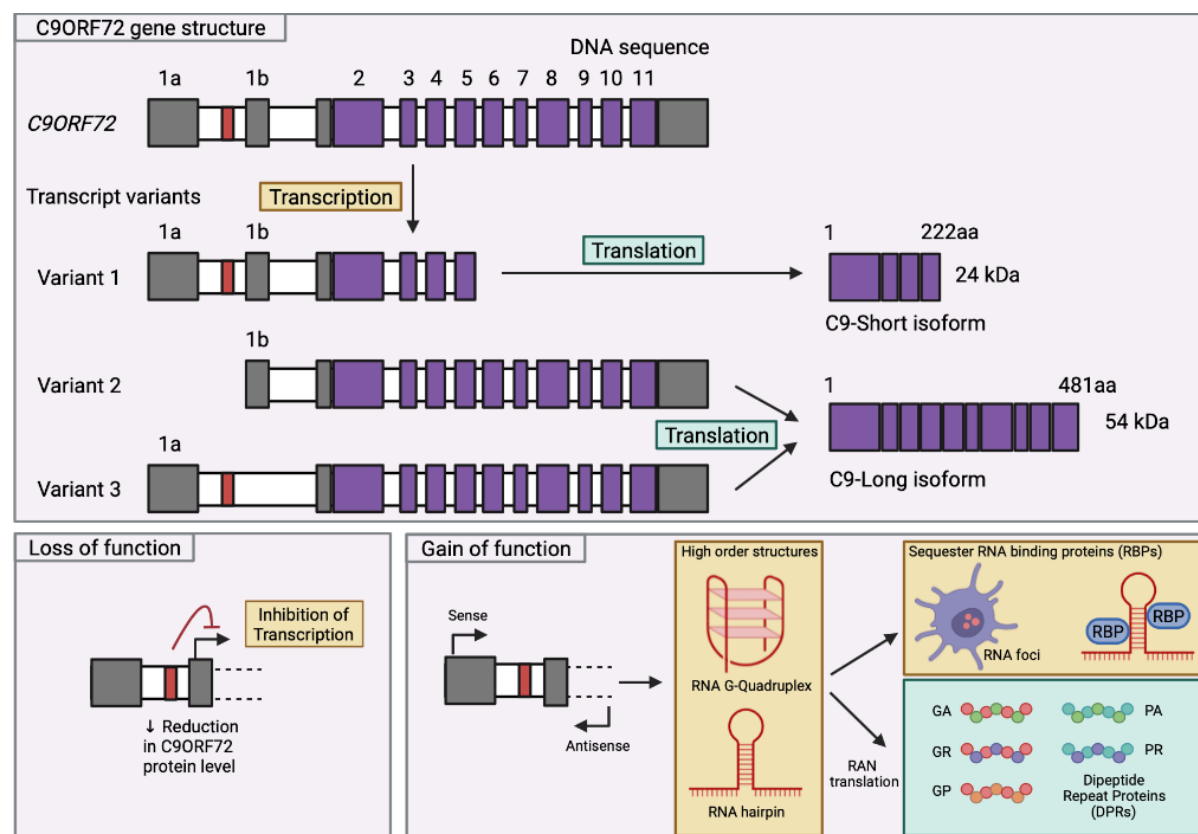


Figure 1.2 – C9orf72 gene structure and function

C9orf72 is made up of two non-coding exons (1a and 1b) and 10 coding exons which give rise to three coding variants: Variant 1 (includes exon 1a and exons 2-5), Variant 2 (includes exon 1b and exons 2-11) and Variant 3 (includes exon 1a and exons 2-11). Alternative splicing of the RNA variants produces two different isoforms: C9-short (encoded by V1) and C9-long (encoded by V2 and V3) which is the predominant isoform. In pathological conditions, the presence of the hexanucleotide repeats can inhibit transcription leading to a reduction of C9orf72 protein levels. Moreover, the hexanucleotide repeat expansion between non-coding exons 1a and 1b are bidirectionally transcribed to produce high order structures, giving rise to RNA G-quadruplex and hairpin that forms RNA foci and can sequester important RNA binding proteins (RBPs). Although intronic, the expanded RNA can also be translated through a mechanism called repeat-associated non-AUG (RAN) translation which produces 5 different dipeptide repeat proteins (DPRs) – poly-GA, poly-GR, poly-GP, poly-PA and poly-PR. Figure adapted from Balendra & Isaacs (2018), Smeyers *et al.* (2021) and Schmitz *et al.* (2021).

C9orf72 can be found mostly in the brain, spinal cord and the immune system, which is in agreement with the expression profile of the transcript. The lack of specific antibodies has been a limiting factor in understanding the role and function of the C9orf72 protein, however recently, the range and specificity of available antibodies has improved (Smeyers *et al.*, 2021). Xiao *et al.* (2015) were amongst the first to generate novel isoform specific antibodies to reveal the distinct subcellular localisation of C9orf72. C9-long was the predominant isoform (Xiao *et*

al., 2015; Frick *et al.*, 2018) and exhibited diffuse cytoplasmic staining in neurons as well as the presence of large speckles in the cytoplasm and dendritic processes of cerebellar Purkinje cells (Xiao *et al.*, 2015). C9-short was localised at the nuclear membrane in control and diseased motor neurons. Moreover, co-immunoprecipitation experiments demonstrated an interaction between the C9orf72 isoforms with importin beta-1 and Ran-GTPase, which are components of the nuclear pore complex. The localisation of C9-long appeared similar when labelling spinal cord tissue, however, changes of relative intensity was observed which may be related to the differences in transcript levels between cases. Most notable was the absence of the large speckles observed in the Purkinje cells. Furthermore, C9-short labelling was diminished or completely absent in motor neurons of C9-ALS and non-C9 ALS cases which correlated with the loss of Importin- β 1 and Ran-GTPase labelling (Xiao *et al.*, 2015). These results show C9orf72 protein may function and affect the nucleocytoplasmic transport pathway which will be discussed later in the thesis. It also highlights the differences between transcript expression as well as antibody and tissue specificity when interpreting results regarding the localisation of a protein. Atkinson *et al.* (2015) also provided evidence to explain differential expression of isoforms present in specific locations. In a mouse model, C9orf72 is detected throughout the mouse brain in a punctate speckled manner, and the localisation of C9orf72 isoforms are dynamic and significantly change during development. Synaptosome preparations also revealed the presence of C9orf72 (mouse isoform 1) in synaptic-rich fractions from mouse adult brain (Atkinson *et al.*, 2015; Frick *et al.*, 2018). Further studies have also revealed interactions of C9orf72 with other organelles, including the Golgi apparatus (Aoki *et al.*, 2017), stress granules (Maharjan *et al.*, 2017), mitochondria (Wang *et al.*, 2021) compartments of the endolysosomal pathway (Sellier *et al.*, 2016; Frick *et al.*, 2018) and lysosomes themselves (Laflamme *et al.*, 2019).

Using bioinformatics analysis, C9orf72 is predicted to show structural homology with the differentially expressed in normal and neoplasia (DENN) family of proteins, which are GDP/GTP exchange factors (GEFs) that activate Rab-GTPases which regulate membrane trafficking (Zhang *et al.*, 2012; Levine *et al.*, 2013). RAB activity is tightly regulated by the constant cycling between two conformational states – an active GTP-bound and an inactive GDP-bound form. This step is mediated by GEFs which exchange GDP for GTP which allows them to be activated and recruited to membranes. Indeed, Farg *et al.* (2014) were amongst the first to demonstrate a role for C9orf72 in endosomal trafficking by showing colocalization and co-immunoprecipitation of C9orf72 with RAB proteins including RAB1, RAB5, RAB7 and RAB11 in neuronal cell lines, primary cortical neurons and human spinal cord motor neurons which implies a role in endocytic transport and later stages of autophagy.

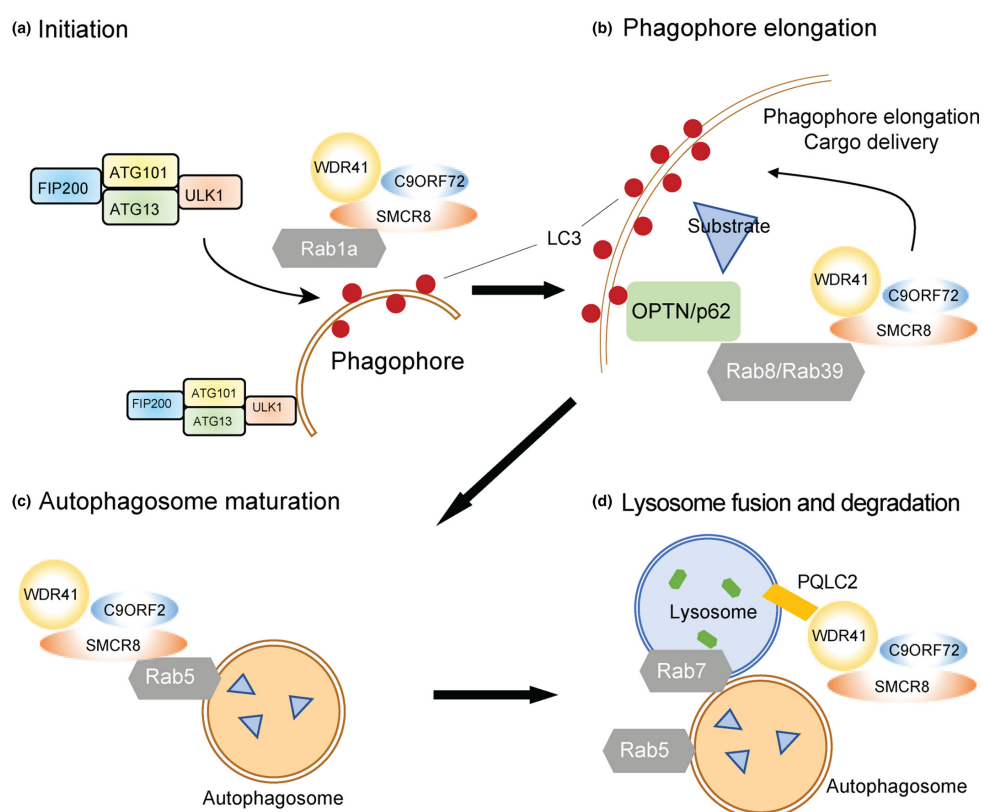


Figure 1.3 The C9orf72 complex and its role in autophagy

(A) C9orf72 forms a complex with SMCR8 and WDR41 which acts downstream of Rab1a GTPase to recruit the ULK1/FIP200/ATG13/ATG101 complex to the phagophore to initiate autophagy. **(B)** The complex also interacts with Rab8a and Rab39b GTPases which bind to Optineurin (OPTN) and p62, proteins essential for substrate delivery to autophagosomes. **(C)** The complex interacts with Rab5 and Rab7, important for autophagosome maturation and finally lysosome fusion and degradation. **(D)** WDR41 targets C9orf72-SMCR8 to the lysosomes via an interaction with the transporter PQ loop repeat containing 2 (PQLC2). Figure from Pang & Hu (2021).

Autophagy is the major intracellular degradation system which delivers cytoplasmic material to the lysosomes (Yim & Mizushima, 2020). Knockout of C9orf72 has been shown to cause defects in starvation-induced autophagy, suggesting that C9orf72 regulates autophagy positively (Sellier *et al.*, 2016; Sullivan *et al.*, 2016; Ugolino *et al.*, 2016). In contrast to Farg *et al.* (2014), Webster *et al.* (2016) weighs more importance for C9orf72 in the initiation step of autophagy where they used two siRNAs that targeted both isoforms of C9orf72 which resulted in a reduction of autophagosome formation. Overexpression of both isoforms induced autophagy which was dependent on the formation of the ULK1 complex composing of Unc-51-like kinase 1 (ULK1), FAK family kinase-interacting protein of 200 kDa (FIP200), autophagy-related 13 (ATG13) and ATG101. They show that C9orf72 mediates interaction of RAB1a with the ULK1 initiation complex to facilitate its trafficking to the phagophore and

therefore initiate autophagosome formation (Figure 1.3A). Sellier *et al.* (2016) demonstrated that C9orf72 is in a complex with Smith-Magenis chromosome region 8 (SMCR8) and WD repeat-containing protein 41 (WDR41) which acts as a GEF for RAB8a and RAB39b (also shown by Yang *et al.* (2016)), which interacts with the p62 autophagy receptor and therefore likely to impact on the formation of autophagosome in autophagy (Figure 1.3B). Phosphorylation of SMCR8 by ULK1 or Tank binding kinase 1 (TBK1) is important to control autophagy in neuronal cells which promotes C9orf72 GEF activity. Sellier *et al.* (2016) also discussed discrepancies between their data with Farg *et al.* (2014) as they observe different RABs being affected, most likely due to differences in methodology as different compositions of Co-IP washing buffers were used. Also, Farg *et al.* (2014) studied C9orf72 in isolation, whereas Sellier *et al.* (2016) studied C9orf72 in a complex. Sullivan *et al.* (2016) further demonstrated that C9orf72/SMCR8/WDR41 forms a ternary complex which interacts with FIP200 identified in Webster *et al.* (2016), therefore consolidating our understanding that formation of the C9orf72 complex promotes interaction of ULK1/FIP200/ATG13/ATG101 complex involved in autophagy initiation.

To summarise, it is clear that C9orf72 interacts with different RABs and has a strong role regulating autophagy at many different levels: firstly during autophagy initiation when C9orf72 forms a protein complex with SMCR8 and WDR41 which acts as a GEF for RAB8a (Sellier *et al.*, 2016) and RAB39b (Sellier *et al.*, 2016; Yang *et al.*, 2016) as well as RAB1a (Webster *et al.*, 2016) and RAB5 (Farg *et al.*, 2014; Shi *et al.*, 2018) to interact with the key autophagy initiation ULK1 complex with FIP200, ATG13 and ATG101 to control autophagic flux (Sellier *et al.*, 2016; Sullivan *et al.*, 2016; Webster *et al.*, 2016; Yang *et al.*, 2016) (Figure 1.3). The interaction of the complex with RAB8a and RAB39b also mediates the recruitment of p62 (Sellier *et al.*, 2016) which targets poly-ubiquitinated proteins for autophagy degradation. Farg *et al.* (2014) also showed that interaction of C9orf72 with RAB7 and RAB11 is important for the final maturation and closure of the autophagosome (Figure 1.3C). Moreover, many C9orf72 knockout models have observable lysosomal defects including defects in lysosomal morphology depicting enlarged lysosomes, increased swollen perinuclear lysosomes, as well as an accumulation of lysosomes and lysosomal enzymes (Amick *et al.*, 2016; O'Rourke *et al.*, 2016; Sellier *et al.*, 2016; Sullivan *et al.*, 2016; Ugolino *et al.*, 2016). Amick *et al.* (2018) went on to show that WDR41 targets C9orf72-SMCR8 to the lysosomes via an interaction with the transporter PQ loop repeat containing 2 (PQLC2) (Amick *et al.*, 2020) (Figure 1.3D).

However, recently two groups have expressed and purified full-length human C9orf72-SMCR8-WDR41 complex, determining the structure at a resolution of 3.2 Å (Tang *et al.*, 2020)

and 3.8 Å by cryo-electron microscopy (Su *et al.*, 2020). Surprisingly, they found that C9orf72 complex acts as a GTPase activating protein (GAP) instead of a GEF for small GTPases such as Rab8a and Rab11a (Tang *et al.*, 2020), where the arginine finger residue R147 of SMCR8 is essential for the GAP activity of the C9orf72 complex (Su *et al.*, 2020; Tang *et al.*, 2020). (Su *et al.*, 2020) also found that the C9orf72 complex acts as a GAP for the ADP-ribosylation factor (ARF) family of GTPases, more specifically ARF1 which promotes mTORC1 activation and ARF6 which regulates actin dynamics – these two interactors have been previously identified in a C9orf72 interactome mass spectrometry-based proteomics screen from Sivadasan *et al.* (2016). In conclusion, there are many candidates for the identification of the Rab GTPase target for the C9orf72 complex, however this still remains elusive. What is certain is that the complex is an important regulator for membrane trafficking and autophagy through its actions on Rab GTPases (Pang & Hu, 2021).

1.2.2 Other functions of C9orf72

C9orf72 has also been shown to play a role in many other processes including inflammation, stress granule dynamics and axonal growth and trafficking.

As described earlier, the expression level of C9orf72 is highest in myeloid cells therefore emphasising its importance in immune regulation (O'Rourke *et al.*, 2016; Rizzu *et al.*, 2016). There have been many C9orf72 knockout mouse models (Koppers *et al.*, 2015; Burberry *et al.*, 2016; Jiang *et al.*, 2016) developed which all produce similar immune abnormalities including age-dependent lymphadenopathy and splenomegaly as well as increased levels of proinflammatory cytokines (Atanasio *et al.*, 2016; O'Rourke *et al.*, 2016; Sullivan *et al.*, 2016). A recent study by Burberry *et al.* (2020) investigated the importance of the microbiome and found that differences in the environment, with regards to variations in the gut microbiota affects C9orf72-deficient mice phenotypes which can be ameliorated with gut microflora transplantations as well as suppression of the gut microflora with antibiotics, even after onset of phenotypes. The variance in the microbiota therefore is extremely important and can explain why certain patients develop ALS/FTD and/or develop different symptoms with/without inflammatory phenotypes.

C9orf72 is also involved in stress granule (SG) formation and degradation (Maharjan *et al.*, 2017; Chitipolu *et al.*, 2018). C9-long was found to be localised to processing bodies (P bodies) and can be recruited to SGs upon stress-related stimuli. CRISPR/Cas9 mediated knockdown of C9orf72 prevented SGs and other SG-associated proteins to form, such as TIA-

1 and HuR. They were found to be downregulated as well as accelerating cell death (Maharjan *et al.*, 2017). C9orf72 also associates with p62 to target SGs for degradation by autophagy (Chitiprolu *et al.*, 2018).

Lastly, C9orf72 can affect axon growth with overexpression leading to increased growth of primary mouse embryonic motor neuron axons with the opposite occurring, exhibiting shortened axons and smaller growth cones, with C9orf72 knockdown (Sivadasan *et al.*, 2016). The authors proposed that C9orf72 interacts with cofilin, which is a protein important for regulating actin dynamics affecting axon growth (Sivadasan *et al.*, 2016). To summarise, there has been a substantial growth in our understanding of what C9orf72 does in relation to regulating autophagy and inflammation as well as other roles including stress granule formation and axonal growth. With new studies showing the cryo-EM structure of C9orf72, we are only starting to understand how C9orf72 in a complex with SCRM8 and WDR41 functions as a GAP, therefore more research is needed to complete our understanding of C9orf72 cellular functions.

1.2.3 Mechanisms of *C9orf72* toxicity

There are three main proposed mechanisms of toxicity underlying *C9orf72* ALS/FTD. Firstly, the repeat expansion could disrupt transcription leading to a reduction of the C9orf72 protein and therefore cause a loss of function of the gene. Second, the HRE can be bidirectionally transcribed and form secondary sense and antisense RNA structures to sequester important RNA binding proteins. Thirdly, although intronic, the HRE can be translated via repeat associated non-AUG (RAN) translation to form potentially toxic dipeptide repeat proteins (DPRs) from the sense strand (poly-GA, poly-GR and poly-GP) and the antisense strand (poly-PA and poly-PR). In the following section, the disease mechanisms will be discussed in further detail (Figure 1.2).

1.2.3.1 Loss of function: Haploinsufficiency

In a large scale *C9orf72* expansion carrier study, van Blitterswijk *et al.* (2015) use quantitative real time PCR and digital molecular barcoding techniques to assess transcript levels in the cerebellum and frontal cortex in human post-mortem tissue. They found decreased expression of V1 and V2 (strongest association was observed for V2) but no reduction was observed in V3. Moreover, they showed the presence of truncated transcripts and pre-mRNAs that could be used as templates for RAN translation. Many other research

groups have also found a similar trend where V2 seems to be the most prominent change in patient material (DeJesus-Hernandez *et al.*, 2011; Mori *et al.*, 2013; Waite *et al.*, 2014). Similar reductions in V1 and V2 levels were also found in blood samples (Jackson *et al.*, 2020) and they also detected hypermethylation of the *C9orf72* promoter. This suggests that epigenetic modifications may also contribute to the reduction of *C9orf72* including hypermethylation in the promoter region, methylation of the HRE or histone trimethylation (Belzil *et al.*, 2013). Since V2 is located in the promoter region, the repeat expansion may be more susceptible to the binding and/or function of polymerases and transcription factors compared to V1 and V3, which are located on the first intron hence they are less susceptible to transcriptional modifications (Braems *et al.*, 2020).

The overall consensus in the literature is that there is a reduction in protein levels too, however, these observations are heavily influenced based on where the measurements are taken. For example, cerebellar proteins are inconsistent (Braems *et al.*, 2020) ranging from 80% reduction (Sivadasan *et al.*, 2016; Frick *et al.*, 2018) to no change (Waite *et al.*, 2014; Xiao *et al.*, 2015). To complicate matters, patients with large repeat expansions have increased expression of C9-short whereas intermediate repeat carriers have a higher expression of C9-long (Xiao *et al.*, 2015; Cali *et al.*, 2019) which suggests a repeat length dependent effect on expression level and isoform distribution (Braems *et al.*, 2020).

As previously discussed, *C9orf72* plays a role in endolysosomal trafficking and autophagy, therefore impairments in these cellular functions would be predicted to result from *C9orf72* loss of function. Knockdown of *C9orf72* inhibits autophagy induction (Webster *et al.*, 2016; Frick *et al.*, 2018) and overexpression of *C9orf72* can activate autophagy leading to an increase in autophagosomes. However, the relevance of *C9orf72* in autophagy for disease pathogenesis is still unclear (Balendra & Isaacs, 2018).

When investigating *in vivo* LOF models, a loss of *C9orf72* in zebrafish (Ciura *et al.*, 2013) and *C. elegans* by using a null mutation of the *C9orf72* worm orthologue, *F18A1.6*, also called *alfa-1* (Therrien *et al.*, 2013) was found to produce motor deficits however, it has to be noted that the homology of the human *C9orf72* orthologues differ a lot (21% in *C. elegans*, 75% in zebrafish compared to 98% in mice) and could explain the phenotypic differences observed since most *C9orf72* knockout mice models failed to recapitulate ALS or FTD phenotypes, suggesting that *C9orf72* loss of function is insufficient to precipitate disease (Balendra & Isaacs, 2018). Depleting levels of *C9orf72* expression by administration of antisense oligonucleotides (ASOs) throughout the CNS of adult mice achieved a reduction of 30% and 40% of control levels in the spinal cord and brain respectively. However, it is well

tolerated and does not result in any neuropathology or behavioural phenotypes in the mice (Lagier-Tourenne *et al.*, 2013). Selective depletion of *C9orf72* from neurons and glial cells also did not induce motor neuron degeneration or exhibit defective motor function or decreased survival (Koppers *et al.*, 2015). Consistent with these findings in mouse models, no loss of function *C9orf72* mutations in human have been identified to cause ALS/FTD (Harms *et al.*, 2013). The lack of motor neuron degeneration is striking; however, these models do present with many immune phenotypes including changes to myeloid and lymphoid cell populations, enlarged lymph nodes, increased levels of inflammatory cytokines and splenomegaly (Atanasio *et al.*, 2016; O'Rourke *et al.*, 2016; Sullivan *et al.*, 2016). This is in line with cellular studies showing *C9orf72* transcripts are most prevalent in myeloid cells (Rizzu *et al.*, 2016) and therefore further supports *C9orf72* involvement in regulating the immune response. Taken together, the murine models have shown that loss of *C9orf72* alone is unlikely to be the main pathogenic cause. However, a recent paper from Zhu *et al.* (2020) suggested a direct form of cooperative pathogenesis between the loss and gain of function mechanisms whereby *C9orf72* haploinsufficiency impairs clearance of DPRs, hypersensitising motor neurons to the toxic effects of DPRs. This supports the hypothesis that loss of *C9orf72* function synergises with repeat dependent gain of toxicity mechanisms.

1.2.3.2 Gain of function: RNA toxicity

C9orf72 repeat expansion can be transcribed into RNA foci and also translated to form dipeptide repeat proteins (DPRs) but which is the main contributor to gain of toxic function in the disease is debatable. Here we discuss the arguments for these gain of function mechanisms (Figure 1.2).

RNA toxicity

RNA foci are formed by transcription of the HRE in both the sense and antisense direction and have been observed in most brain regions in *C9orf72* ALS/FTD patients and often coincide in the areas affected by ALS/FTD (Cooper-Knock *et al.*, 2015; DeJesus-Hernandez *et al.*, 2017). Interestingly, TDP-43 has not been found to directly interact with RNA foci (Lagier-Tourenne *et al.*, 2013; Chew *et al.*, 2015). The repeat RNA forms secondary structures, including stable G-quadruplexes and hairpins, which mediate the sequestration of important RNA binding proteins (RBPs) (Haeusler *et al.*, 2014) and therefore lead to RNA toxicity by disruption of gene regulation, translation and splicing (Sareen *et al.*, 2013; Xu *et al.*, 2013). There have been numerous studies depicting interactions of repeat RNA with RBPs in

human tissue, *in vivo* and *in vitro* assays. These include various heterogeneous nuclear ribonucleoproteins (hnRNPs) (Mori *et al.*, 2013; Conlon *et al.*, 2016), THO complex subunit 4 (ALYREF) (Cooper-Knock *et al.*, 2014), serine/arginine-rich splicing factor 1 (SRSF1), SRSF2, (Cooper-Knock *et al.*, 2014; Hautbergue *et al.*, 2017), double stranded RNA specific editase B2 (ADARB2), (Donnelly *et al.*, 2013), nucleolin (Haeusler *et al.*, 2014), Pur-alpha (Xu *et al.*, 2013), and Zfp106 (Celona *et al.*, 2017). Haeusler *et al.* (2014) showed that nucleolin, an essential nucleolar protein binds specifically to G-quadruplexes, which is also mislocalised in patient cells and induce nucleolar stress. Moreover, repeat RNA was shown to interact with RanGAP, a key regulator of nucleocytoplasmic transport (Zhang *et al.*, 2015). The authors did not detect DPRs using dot blotting in their G4C2x30 repeat *Drosophila* model but could not rule out undetectable levels of DPRs having an effect. Others have gone on to show that DPRs cause nucleocytoplasmic transport deficits (Freibaum *et al.*, 2015; Jovicic *et al.*, 2015). Lastly, all these RBPs listed have not been consistently found in all studies which may be explained by the use of different methodologies and models therefore it is important to establish how RBPs are mechanistically linked to pathogenesis (Balendra & Isaacs, 2018).

Evidence for C9orf72 repeat RNA toxicity

There are a few *in vivo* models supporting repeat RNA-mediated toxicity. Firstly, Wen *et al.* (2014) used primary and cortical neurons transfected with constructs encoding intronic expanded repeats that do not initiate RAN translation. They found expression of G4C2 transcripts by fluorescence *in situ* hybridisation analysis and using longitudinal live cell imaging showed that the transfected cortical neurons survived significantly less than control. The G4C2x30 *Drosophila* model described previously exhibited eye and motor neuron damage too (Xu *et al.*, 2013; Zhang *et al.*, 2015). Both studies did not detect any DPRs and therefore attributed toxicity to repeat RNA however, DPRs can be hard to detect, especially the toxic poly-GR therefore it is hard to make such concrete conclusions (Balendra & Isaacs, 2018). Moreover, a zebrafish model with sense repeat length of 10 – 35 repeats and antisense length of 35 – 70 repeats was able to induce toxicity in motor axons however, no DPRs could be detected in these models suggesting that the RNA toxicity is the sole culprit. They also used RNA only constructs with 70 and 108 repeats and observed toxicity in this model too, further supporting repeat RNA mediated toxicity (Swinnen *et al.*, 2018). However, there are other studies which argue against RNA toxicity.

Evidence against *C9orf72* repeat RNA toxicity

Mizielinska *et al* (2014) generated 'RNA-only' transgenic flies whereby stop codons were used in all reading frames of both sense and antisense directions in the repeat constructs allowing expression of RNA but not translation of the repeats into DPRs. These RNA-only flies expressed up to 288 repeats, were able to form RNA foci and sequester endogenous RBPs, however, no detectable toxicity was seen. Tran *et al* (2015) also generated a transgenic *Drosophila* model expressing 160 repeats flanked by human intronic and exonic sequences of *C9orf72*. Although abundant nuclear sense RNA foci were seen in neurons and glial cells, no evidence of neurodegeneration was observed. Their explanation for the lack of toxicity is due to the inefficient export of the repeat RNA to the cytoplasm where translation of DPRs occurs. In summary, there is evidence from numerous studies depicting interactions of repeat RNA with RBPs in human tissue, *in vivo* and *in vitro* assays which affect various cellular processes including splicing, translation and nucleocytoplasmic transport. However, Burguete *et al* (2015) showed that RNA foci altered trafficking in neurites and perturbed RNA granule function, ultimately leading to neuritic defects. Moreover, a recent study from Coyne *et al* (2020) showed that repeat RNA can initiate pathogenic cascades, leading to decreased nuclear POM121, thereby affecting nuclear pore composition and altering the localisation of nucleocytoplasmic transport proteins, ultimately increasing the flies' sensitivity to stressor induced neuronal death. *Drosophila* lack POM121, which may explain the lack of toxicity shown in previous models, as POM121 is an important initiator of RNA toxicity (Coyne *et al.*, 2020; Dubey *et al*, 2022). To summarise, the balance of evidence has shown that repeat RNA may not be the dominant contributor to the gain of toxic function in the disease.

1.2.3.3 Gain of function: Dipeptide repeat proteins (DPRs)

Repeat associated non-AUG (RAN) translation occurs in *C9orf72* ALS/FTD where, although intronic, the expanded repeats are still translated lacking a traditional ATG start codon (Green *et al*, 2017) to form dipeptide repeat proteins (DPRs): glycine-alanine (GA), glycine-proline (GP) and glycine-arginine (GR) from the sense strand and proline-alanine (PA), glycine-proline (GP) and proline-arginine (PR) from the antisense strand (Mori *et al.*, 2013). DPRs are present in all areas of the brain including the cerebellum, hippocampus, basal ganglia, frontal and motor cortices as well as skeletal muscle (Al-Sarraj *et al*, 2011; Ash *et al*, 2013; Sharpe *et al*, 2021). These DPR inclusions are often cytosolic and stellate-shaped, p62 positive, ubiquitin-positive but TDP-43 negative within neurons and glia (Schludi *et al*, 2015). Intranuclear and para-nucleolar DPR aggregates have also been observed but appear

less frequently (Wen *et al.*, 2014; Schludi *et al.*, 2015). The most abundant DPR is poly-GA in post-mortem tissue (May *et al.*, 2014; Zhang *et al.*, 2014), however, the most toxic DPR has been shown to be the arginine DPRs – poly-GR and poly-PR (Mizielinska *et al.*, 2014; Mackenzie *et al.*, 2015).

In vivo mouse models that recapitulate behavioural phenotypes, as well as clinical and pathologic features of the disease are extremely pivotal for investigating disease mechanisms. There are numerous transgenic approaches to introduce the *C9orf72* hexanucleotide repeat mutation including adeno-associated virus (AAV)-mediated expression and generation of bacterial artificial chromosome (BAC) transgenic mouse models (Batra & Lee, 2017). Chew *et al.* (2015) produced the first *C9orf72* mouse model using AAV-mediated CNS overexpression of G4C2x66 repeats. It recapitulated the disease well as motor and behavioural phenotypes were present by 6 months, with RNA foci (only sense foci were analysed), high to moderate levels of GA and GP aggregates, but low levels of GR in the cortex shown. Phospho-TDP-43 inclusions were also found in the cortex and neuronal loss was observed at 6 months.

There have been a few BAC transgenic *C9orf72* mouse models produced which all use slightly different methodologies and mouse strains which resulted in having different behavioural and pathological phenotypes. BAC models are arguably better to use as they include the presence of endogenous transcription and translation regulatory sequences which are important for spatiotemporal control of expression (Batra & Lee, 2017). Peters *et al.* (2015) used a BAC construct containing exons 1-5 and 300 or 500 repeats. Jiang *et al.* (2016) also adopted a similar approach but instead used 110 or 450 repeats and showed no motor deficits but mild neurodegenerative behavioural phenotypes as spatial and working memory deficits and anxiety were observed at 12 months. The third BAC model expressed the full gene and protein with 100–1000 repeats (O'Rourke *et al.*, 2016). All three models were produced on C57BL/6J genetic backgrounds and developed RNA foci and DPRs in the CNS but surprisingly failed to recapitulate TDP-43 pathology, neuronal loss or develop any strong motor or cognitive phenotypes. Liu *et al.* (2016) generated a BAC transgenic containing the full gene with different lines containing repeat lengths up to 500 repeats (C9-500) on a FVB/NJ genetic background. Significantly, these models developed RNA foci (both sense and antisense), DPR aggregates, TDP-43 pathology and neurodegeneration. Interestingly, a subset of female mice developed an early onset form of the disease exhibiting inactivity, sudden weight loss, hind limb paralysis and ultimately death at 3-6 months which the authors termed 'acute-onset rapidly progressive'. The other subset developed a slower progressive phenotype (12-17 months). Differences shown between the mouse models can potentially be explained by different genetic backgrounds of the mice, as well as expression levels of the G4C2 repeat RNA expression

and repeat lengths used. Furthermore, C57BL/6J mice express a mutant nicotinamide nucleotide transhydrogenase (Nnt) gene, a mitochondrial protein located at the IMM, which is involved in glucose-mediated insulin secretion and regulates mitochondrial NADPH levels and mitochondrial redox balance (Freeman *et al*, 2006). Due to a mutation of the Nnt gene, the inbred mouse strain C57BL/6J is protected from oxidative stress (Nickel *et al*, 2015) and therefore the substrain chosen may contribute to reasons explaining a lack of phenotype from Peters *et al*. (2015), Jiang *et al*. (2016) and O'Rourke *et al*. (2016).

Since the C9-500 mouse from Liu *et al*. (2016) is a promising model for research as it recapitulates disease phenotypes well, it has been used in the wider community however, discrepancies between behavioural and pathological phenotypes have been reported in multiple lab. Mordes *et al* (2020) did not detect any survival or motor phenotypes previously described by Liu *et al*. (2016). In contrast, Nguyen *et al* (2020b) used the same mice and showed decreased survival, motor neuron loss and behavioural abnormalities, despite not observing changes in weight loss, grip strength or open field abnormalities as described by Liu *et al*. (2016). This study elegantly used a human-derived recombinant antibody against poly-GA and showed phenotypic improvements. Nguyen *et al* (2020a) published a response paper highlighting the differences between all the studies and included new data from two other groups which also used the C9-500 mice which also observed decreased survival and behavioural phenotypes. To summarise their findings, background strain problems (FVB-NJ mice have reported increased seizures which may mask disease phenotypes), methodological differences and environmental conditions are key elements to consider when raising these mice and may explain the differences in phenotypes observed. Taken together, these mouse models albeit showing variable extents of neurodegeneration and clinical phenotypes, all represent valuable tools to dissect the molecular mechanisms underlying the pathogenesis of the disease.

However, to determine which of the gain of function hypotheses is more likely to contribute to pathogenesis, many groups have succeeded in studying potential cytotoxicity of DPRs independently of RNA toxicity using alternative codon construct models. In these constructs, DPRs are generated from a non-G4C2 sequence downstream of a conventional ATG start codon. This allows the generation of DPRs without RNA aggregation since G4C2 repeats are absent.

Poly-GA

Using a synthetic GA with 15 repeats model system, poly-GA has been shown to aggregate into flat, amyloid-like, ribbon-type fibrils, forming a parallel beta sheet structure which are neurotoxic and have the potential to transmit between cells in neuroblastoma cells (Chang *et al*, 2016; Edbauer & Haass, 2016). Due to similarities analogous to the formation of amyloid beta fibrils in Alzheimer's disease, Edbauer & Haass (2016) hypothesise that *C9orf72* pathogenesis also follows a similar cascade of events where there is an increased production, aggregation and failure to clear poly-GA and, therefore, trigger downstream events such as TDP-43 pathology ultimately leading to neurodegeneration. Aggregation-prone *C9orf72* ALS/FTD poly-GA form filamentous structures that were shown to cause neurotoxicity by inducing ER stress in cultured cells and primary neurons (Zhang *et al.*, 2014). These aggregates colocalised with both p62 and ubiquitin and contributed to neurodegeneration by activating caspase 3, impairing neurite outgrowth and inhibiting the ubiquitin–proteasome system (UPS) to induce endoplasmic reticulum (ER) stress, hence, causing neurotoxicity in the absence of RNA foci. Specifically, May *et al.* (2014) showed that poly-GA sequestered Unc119, a transport factor for myristoylated proteins, which inhibited its function regulating axonal protein trafficking. Moreover, quantitative mass spectrometry revealed that many interactors of poly-GA showed enrichment of UPS proteins suggesting recruitment and inhibition of the proteasome. Guo *et al* (2018) dissected the molecular architecture of the protein aggregates using cryo-electron tomography and found that poly-GA exists as densely packed twisted ribbons that recruit the 26S proteasome complexes, suggesting stalled degradation and, hence, impaired proteasome function. In addition, Unc119 overexpression partially rescues poly-GA toxicity (May *et al.*, 2014). Both rolipram treatment used to boost proteasome activity and overexpression of the proteasome protein PSMD11 rescued poly-GA aggregation and TDP-43 pathology in primary neurons (Khosravi *et al*, 2020).

Mouse models of poly-GA have exhibited behavioural deficits and neuronal loss at 6 months as well as exhibit rare phosphorylated TDP-43 inclusions thereby the toxicity was attributed to aggregated GA. Zhang *et al* (2016) also showed in their mouse model using AAV-mediated CNS overexpression of GFP-GA50 that poly-GA sequestered and impaired HR23, proteins involved in proteasomal degradation as well as proteins associated with nucleocytoplasmic transport such as RanGAP1 and Pom121. Although poly-GA has been associated with toxicity via impairment of the UPS, poly-GA is expressed at high levels in most models and when compared with arginine-containing DPRs models, it appears less toxic (Mizielinska *et al.*, 2014; Wen *et al.*, 2014; Freibaum *et al.*, 2015). Therefore, despite being the most abundant DPR, it is unclear whether poly-GA is toxic at physiologically relevant levels

(Freibaum & Taylor, 2017). For example, in *Drosophila* models, Mizielinska *et al.* (2014) generated protein-only constructs which used alternative codons found in the repeats; the arginine-rich DPRs – GR36 and PR36 developed a degenerative eye phenotype however, GA36 and PA36 had no effect. These data suggest that alanine-containing DPRs are relatively benign and the arginine-containing DPRs are the more toxic species which will be discussed in the following section.

Arginine DPRs – poly-GR and poly-PR

There have been a lot of studies focussing on overexpression of the arginine-rich DPRs and have found them to be toxic in many model systems – in cells, primary neuron cultures and iPSCs. Many *in vivo* models such as zebrafish (Swaminathan *et al.*, 2018) and *Drosophila* models (Mizielinska *et al.*, 2014; Wen *et al.*, 2014; Freibaum *et al.*, 2015; Yang *et al.*, 2015; Solomon *et al.*, 2018) have shown that overexpression of poly-GR and poly-PR result in developmental issues, reduced survival and have locomotor phenotypes. Researchers have postulated that this is due to their positive charge and high polarity. Kwon *et al.* (2014) showed that synthetic GR20 and PR20 peptides were able to enter cells and migrate to the nucleus due to the nature of the positive charge from the arginine residues mimicking nuclear localisation signals. The peptides associate with the periphery of the nucleoli which perturb ribosomal RNA production and therefore cause cell death.

There have been many different downstream mechanisms implicated in *C9orf72* ALS/FTD described in the literature comprising of RNA metabolism, proteostasis, nervous system-specific processes such as axonal transport, other cellular processes including DNA damage, mitochondrial function and nucleocytoplasmic transport and systemic functions involving the immune system (Balendra & Isaacs, 2018).

In 2015, three elegant studies published back-to-back and found nucleocytoplasmic transport (NCT) is perturbed in *C9orf72* ALS/FTD. Freibaum *et al.* (2015) conducted a genetic screen using G4C2x58 *Drosophila* lines and the fly eye as a readout for modifiers which included components of the nuclear pore complex and components related to export of nuclear RNA and import proteins. Moreover, immunostaining of endogenous Lamin C demonstrated the nuclear envelope was abnormal and had a ‘frayed’ phenotype. Similarly, Zhang *et al.* (2015) performed a candidate-based genetic screen with G4C2x30 *Drosophila* lines using protein interactors identified from their previous study Donnelly *et al.* (2013). They found that RanGAP, a key regulator of NCT, suppressed neurodegeneration. Enhancing nuclear import

or suppressing nuclear export was also able to suppress neurodegeneration. Lastly, Jovicic *et al.* (2015) performed a yeast screen and identified including karyopherins and effectors of Ran-mediated NCT.

However, not all studies have observed the same disruption of NCT. I was involved in investigating the link between *C9orf72*, possible NCT effects and TDP-43 pathology in *C9orf72 Drosophila* models (Solomon, Stepto and Au *et al.*, 2018). We found that expression of G4C2x38 and GR64 cause TDP-43 to mislocalise and accumulate in the cytoplasm of neurons. In turn, excess cytosolic TDP-43 enhanced DPR levels leading to mislocalisation of nuclear import protein karyopherin- α and a vicious feedback loop of TDP-43 and KPNA dysfunction, ultimately resulting in neurodegeneration. Interestingly, other components of NCT such as RanGAP and Nup50 were not altered, similar to findings from Saberi *et al.* (2018) where they also did not find evidence for nuclear membrane proteins, RanGAP and lamin B1 and Nup205 in spinal motor neurons and motor neurons of the motor cortex containing poly-GR aggregates of *C9orf72* ALS cases.

Moreover, in 2016, a flurry of studies were published regarding *C9orf72* and phase separation. Lee *et al.* (2016) analysed poly-GR and poly-PR interactomes in human cells by affinity purification followed by liquid chromatography with tandem mass spectrometry (LC-MS/MS). Both Lee *et al.* (2016) and Lin *et al.* (2016) used similar approaches and demonstrated how poly-GR and poly-PR interact with proteins containing low-complexity domains (LCDs) in many RNA binding proteins (RBPs) such as TDP-43, hnRNPA1 and Ataxin-2. Other protein interactors include components of membrane-less organelles such as G3BP, Caprin and USP10 (Lee *et al.*, 2016) which have been shown to form a complex mediating stress granule condensation (Kedersha *et al.*, 2016). Arginine is a highly polar, positively charged amino acid and these properties allow arginine-rich DPRs to interact with LCDs of RBPs, resulting in liquid-liquid phase separation (LLPS) and LLPS ultimately contribute to the formation of membrane-less organelles. Lee *et al.* (2016) and Boeynaems *et al.* (2017) showed that GR and PR altered phase separation of LCD-containing proteins and poly-GR and poly-PR themselves are able to phase separate with proteins or nucleic acids forming liquid droplets *in vitro* and accumulate in membrane-less organelles such as stress granules and the nucleolus therefore disrupting their normal function such as their assembly and dynamics. Lee *et al.* (2016) also performed an *in vivo* RNAi screen to assess the functional significance of the hits from the DPR interactomes using GFP-GR30 *Drosophila* lines and found that most genetic modifiers encode components of membrane-less organelles such as the nuclear pore complex, nucleolus, nuclear speckles, Cajal bodies and stress granules. Furthermore, Zhang *et al.* (2018) showed that cellular stress disrupts NCT by localising NCT

transport factors into stress granules. Moreover, inhibiting stress granule assembly by Ataxin-2 knockdown alleviated NCT defects and neurodegeneration in cells and a G4C2x30 *C9orf72* *Drosophila* model. Taken together, these data identify abnormal phase separation to be an important pathological cellular phenomenon and NCT defects as a key pathogenic event. Since LLPS is essential for the formation of membrane-less organelles such as stress granules, Zhang *et al.* (2018) provide evidence to link stress granule assembly and NCT deficits in the pathogenesis of *C9orf72* ALS/FTD.

To summarise, many studies have focussed on arginine-DPR mediated gain of function toxicity. More research is needed to determine which downstream mechanisms are most important and address whether different DPRs or repeat RNAs can act synergistically to elicit downstream effects. In the next section, the focus of attention is concentrated on the relevance of another potentially important downstream mechanism/consequence: mitochondrial dysfunction.

1.3 Mitochondria and *C9orf72*

1.3.1 Mitochondrial structure and function

Mitochondria are double membrane bound organelles found in most eukaryotic cells and are essential for life with vital roles in aerobic oxidative phosphorylation generating more than 90% of the cell's adenosine triphosphate (ATP) (Harris & Das, 1991). Beyond their functions with energy production, they are also important for processes involving lipid and amino acid synthesis/metabolism, calcium regulation as well as repurposing waste generated from other cellular processes (Rossmann *et al*, 2021). Neurons are long lived and have high metabolic requirements (Nicholls & Budd, 2000), therefore, they may be more susceptible to damage from mitochondrial dysfunction. This is predominantly why many neurodegenerative diseases, including ALS have been linked to mitochondrial dysfunction which include changes to mitochondrial dynamics and morphology, defective oxidative phosphorylation and impaired quality control (Smith *et al*, 2019). In the following section, a comprehensive overview of mitochondrial dysfunction specifically in *C9orf72* ALS/FTD will be discussed (Table 1.1).

1.3.2 Mitochondrial dynamics

Mitochondria are highly dynamic organelles which undergo cycles of fission and fusion important for many cellular processes which regulate mitochondrial number, size and localisation in the cytosol (Liesa *et al*, 2009; Westrate *et al*, 2014; Tilokani *et al*, 2018). Mitochondria fission occurs when a single mitochondrion divides into two daughter mitochondria and is often upregulated when stress levels are elevated (Zemirli *et al*, 2018). Fission also facilitates the removal of damaged mitochondria by a specialised form of autophagy, termed mitophagy (Kim *et al*, 2007). Moreover, during the G2/M phase of the cell cycle, fragmentation of the mitochondria is also observed (Otera *et al*, 2013). On the other hand, fusion of mitochondria is when two mitochondria come together and form one mitochondrion which allows distribution of mitochondrial metabolites and proteins as well as stimulation of OXPHOS activity (Mishra & Chan, 2016). Mitochondria have two membranes with the outer mitochondrial membrane (OMM) facing the cytosol, and the inner mitochondrial membrane (IMM) protruding into the mitochondrial matrix (Figure 1.4A). Fission is mediated by dynamin related protein 1 (DRP1) and fusion is regulated by two steps, where mitofusin 1 and 2 (MFN1, MFN2) are involved at the OMM and Optic atrophy 1 (OPA1) at the IMM (Chan, 2012; Tilokani *et al.*, 2018).

Table 1.1 Summary of the involvement of mitochondria in C9orf72 ALS/FTD studies
 PubMed search for keywords - mitochondria- and - C9orf72-. A summary of studies investigating mitochondrial phenotypes in various *in vivo* and *in vitro* systems exploring mitochondrial morphology, regulation of calcium, respiration, mitochondrial DNA biogenesis, ATP production, oxidative stress and axonal transport of mitochondria. Additional information section outlines key findings from the studies that are important.

Study	System	Mitochondrial phenotypes						Additional information	
		Morphology/dynamics	Calcium mishandling/ Membrane potential	Respiration	Mitochondrial DNA	ATP	Oxidative stress		Axonal homeostasis
Baldwin et al., (2016)	<i>Drosophila</i> : G4C2x36, PR36, RO36 (neuropeptidergic CCAP-GAL4)							Disruption of mitochondrial transport in G4C2x36 and PR36, but not RO36	
Dafinca et al., (2016)	C9ORF72 iPSC-derived motor neurons • C9ORF72 patient fibroblasts • C9ORF72 fibroblasts grown in galactose medium	Swollen mitochondria, abnormal cristae structures	<ul style="list-style-type: none"> Loss of calcium homeostasis Decrease in membrane potential Increase in ER stress 						
Onesto et al., (2016)		Mixed populations of elongated, short and round-shaped mitochondria	Increase in mitochondrial membrane potential	Increased in oxygen consumption	Increased mitochondrial DNA content and mass	Increase in ATP production	Increased ROS		
Lopez Gonzalez et al., (2016)	• C9ORF72 iPSC-derived motor neurons • <i>Drosophila</i> : GR80 (wing specific driver VG-GAL4)		Increase in mitochondrial membrane potential				<ul style="list-style-type: none"> Increase in DNA damage Increase in ROS 	Interactome analysis with HEK293 cells with GR80-GFP vs control - two-thirds of the hit ribosomal proteins are mitochondrial ribosomal proteins	
Konrad et al., (2016)	Fibroblasts from patients with sporadic ALS, primary lateral sclerosis (PLS), ALS/PLS with C9ORF72 mutations		Increase in mitochondrial membrane potential	No changes in OCR		No changes in ATP content			
Choi et al., (2019)	GR80 inducible mouse model	<ul style="list-style-type: none"> EM: Disruption of IMM and loss of cristae Shorter mitos in primary cortical neurons isolated from GR80 mice Increased levels of DRP1 and decreased levels of OPA1 		Decreased activities of mitochondrial complexes I and V			<ul style="list-style-type: none"> Increase in DNA damage GR binds to ATP5A1 and decreases ATP5A1 expression level in the cortex of GR80 mice 	GR is localised in the mitochondria	
Lynch et al., (2019)	C9ORF72 iPSC-derived skeletal myocytes	Decrease in <i>TMM9</i> from RNA seq and RTqPCR		Decrease in <i>NDUFB11</i> and <i>ATP5A1</i> from RNA seq and RTqPCR			Increased susceptibility to oxidative stress		Increase in <i>RHOJ</i> from RNA seq and RTqPCR

Mitochondria and *C9orf72*

Study	Mitochondrial phenotypes					Additional information			
	System	Morphology/dynamics	Calcium mishandling/ Membrane potential	Respiration	Mitochondrial DNA		ATP	Oxidative stress	Axonal homeostasis
Li et al., (2020) a	<ul style="list-style-type: none"> <i>Drosophila</i>: Flag-GR80 (muscle-specific driver MHC-GAL4) FLAG-GR80-transfected HEK293T C9ORF72-ALS Patient Fibroblasts 	<ul style="list-style-type: none"> Alteration of Mitochondrial Contact Site and Cristae Organizing System (MICOS) Structure Small, swollen and round mitochondria devoid of electron-dense matrix material Altering fission-fusion balance by the loss- or gain-of-function of Dp1, Fis1, or Marf had no obvious effect on GR80 toxicity 	<ul style="list-style-type: none"> Increase in mitochondrial membrane potential High Ca²⁺ levels 	Complex I activity was elevated, whereas Complex II-V were unaltered		Increased ATP production	Increased ROS		<p>Rescue of Mitochondrial Defects in C9ORF72 - ALS/FTD Patient Fibroblasts by Genetic Manipulation of MICOS Components</p> <ul style="list-style-type: none"> GR can act as an MTS and therefore is cotranslationally imported into the mitochondria Stalled translation of GR on mitochondrial surface triggers ROC and CTE, promoting GR aggregation and toxicity
Li et al., (2020) b	<ul style="list-style-type: none"> <i>Drosophila</i>: Flag-GR80 (muscle-specific driver MHC-GAL4) FLAG-GR80-transfected HEK293T 								<ul style="list-style-type: none"> Mitochondrially encoded transcripts downregulated in C9 MNS (CI, CV, mitochondrial small and large ribosomal subunits) but not nuclear subunits Overexpression of PGC1α rescues axonal phenotypes
Mehhta et al., (2021)	<ul style="list-style-type: none"> C9ORF72 iPSC-derived motor neurons C9ORF72 PM spinal cord tissue 			<ul style="list-style-type: none"> Impaired basal and maximal respiration T. transcriptomic analysis - reduced expression of ETC genes 	<ul style="list-style-type: none"> No changes in mitochondrial copy number 	<ul style="list-style-type: none"> Shorter axons Fewer motile in proximal and distal axons 			<ul style="list-style-type: none"> Mitochondrially encoded transcripts downregulated in C9 MNS (CI, CV, mitochondrial small and large ribosomal subunits) but not nuclear subunits Overexpression of PGC1α rescues axonal phenotypes
Debska-Vielhaber et al., (2021)	C9ORF72 skin fibroblasts			Enzymatic activity nor respiration affected		Decreased ATP levels			No antioxidant effect was observed as there was no initial observation of mitochondrial impairment compared to data from other sALS and FALS groups
Wang et al., (2021)	<ul style="list-style-type: none"> C9ORF72 KO MEFs derived motor neurons C9ORF72 iPSC-derived motor neurons 	General morphology-mitochondrial area and branch length unaltered in C9ORF72 KO MEFs	C9ORF72 KO MEFs are more depolarised	<ul style="list-style-type: none"> Multiple proteins of OXPHOS including CI were downregulated, CI-mediated OXPHOS specifically is most important involving TIMMDC1 NADH levels increased Glycolysis pathway enhanced 		ATP production rate decreased			Endogenous C9ORF72 resides to the IMM and mitochondrial import is dependent on the AIFM1/CHCHD4 complex

Study	System	Mitochondrial phenotypes							Additional information
		Morphology/dynamics	Calcium mishandling/ Membrane potential	Respiration	Mitochondrial DNA	ATP	Oxidative stress	Axonal homeostasis	
Fumagalli et al., (2021)	<ul style="list-style-type: none"> • C9ORF72 iPSC-derived spinal motor neurons • Drosophila: GR36, PR36, GR100, PR100 (Chemosensory neurons dpr-GAL4) 								Physical interaction studies demonstrate that arginine-rich DPRs associate with motor complexes and the unstructured tubulin tails of microtubules.
Gomez-Suaga et al., (2022)	DPR-transfected SH-SY5Y neuronal cells (EGFP-tagged 125 poly-GA, poly-GR and poly-PR DPRs)		Disruption of ER-mitochondria Ca ²⁺ exchange						
Sung and Lloyd (2022)	Drosophila: G4C2x30, G4C2x36, RO36 (motor neuron vGlut-GAL4)								Increased static lysosomes, impaired trafficking of late endosomes and dense core vesicles but unaffected axonal transport of mitochondria

Fission starts in the matrix where the replication of mtDNA marks the site for endoplasmic reticulum recruitment (Friedman *et al*, 2011; Lewis *et al*, 2016). Pre-constriction at the mito-ER contact site occurs before the oligomerisation of DRP1. Many mitochondrial bound proteins, including mitochondrial fission 1 (FIS1), mitochondrial fission factor (MFF) and mitochondrial dynamic proteins of 49 and 51kDa (MiDs – MiD49 and MiD51) recruit DRP1 to the mitochondria (Loson *et al*, 2013). It is important to note that whilst these proteins have been identified to play a role in fission, the exact mechanisms are still controversial and unclear (Liu *et al*, 2020). For example, FIS1 is not required for DRP1 recruitment to the OMM in basal conditions (Otera *et al*, 2016) yet overexpression of FIS1 can still cause mitochondrial fragmentation in the absence of DRP1 (Liesa *et al*, 2019). It has been suggested that FIS1 can induce fragmentation by increasing fission and decreasing fusion where fusion is blocked by inhibiting the function of MFN1, MFN2 and OPA1 (Yu *et al*, 2019). DRP1 oligomerises into a ring like structure and GTP hydrolysis causes a conformational change which enhances pre-existing mitochondrial constriction (Mears *et al*, 2011) (Figure 1.4).

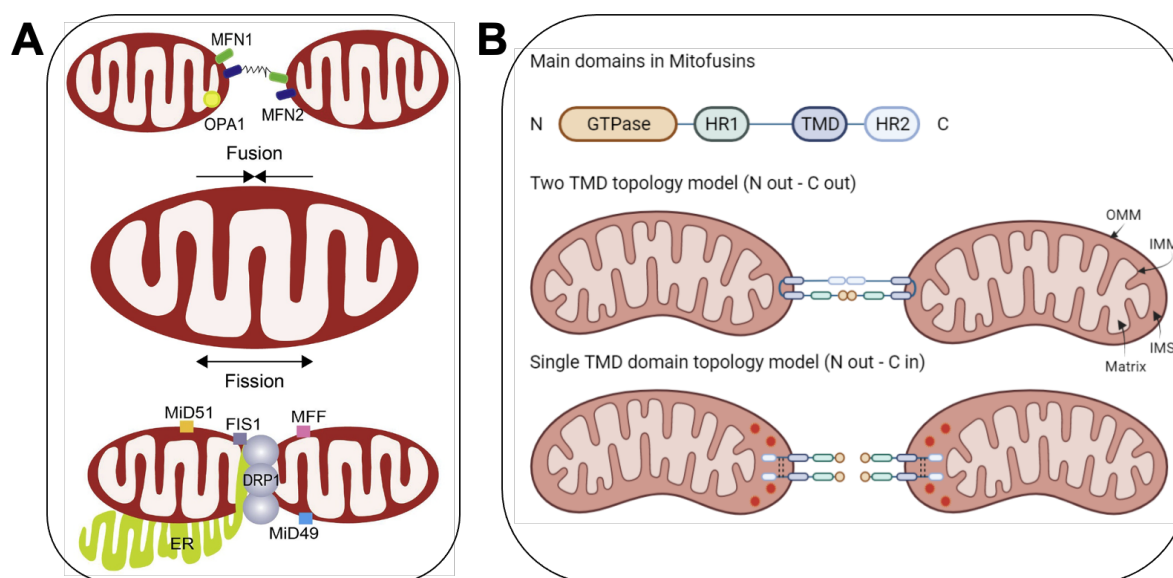


Figure 1.4 – Mitochondrial fission and fusion

(A) Mitochondria fission begins when the ER is recruited to the constriction site, marked by mtDNA replication. OMM proteins including FIS1, MFF, MiD49 and MiD51 are responsible for recruiting DRP1 to mitochondria. DRP1 oligomerises in a ring like structure as depicted and GTP hydrolysis causes a conformational change to enhance constriction. OMM fusion involves Mitofusins (MFN1 and MFN2) whereas IMM fusion is coordinated by OPA1. **(B)** Two main models of mitochondrial fusion depicting possible topologies of MFNs. With two transmembrane domains (TMD), both the N- and C- terminal harbouring the GTPase and the coil-coil heptad repeat 1 and 2 (HR1, HR2) of MFN is exposed to the cytoplasm, tethering two adjacent mitochondria together. Mattie *et al* (2018) suggested a new model based on new metazoan MFN topology highlighting a single TMD hence the C- terminus is in the IMS

and exposed to potential oxidised environments from ROS production (red stars) to enhance fusion by forming redox mediate disulphide bonds (dotted lines) promoting tethering or GTPase activity. **(A)** From Liu *et al.* (2020) **(B)** Adapted from Cohen & Tareste (2018) and Tilokani *et al.* (2018).

In mammals, fusion is characterised by three main steps. First, tethering of two opposing mitochondria occurs by interactions with the HR2 and/or GTPase domains of mitofusins 1 and 2 (MFN1, MFN2) (Tilokani *et al.*, 2018), GTP binding (Qi *et al.*, 2016) and/or hydrolysis (Cao *et al.*, 2017) results in conformational changes of the MFNs leading to mitochondrial docking. GTPase-dependent power stroke or GTP-dependent oligomerisation leads to the completion of OMM fusion (Qi *et al.*, 2016; Cao *et al.*, 2017). IMM fusion is regulated by OPA1 which can be alternatively spliced to long forms (L-OPA1) and proteolytically cleaved to short forms (S-OPA1). L-OPA1 and cardiolipins interact which drives the tethering of the two IMM and fusion occurs via OPA1-dependent GTP hydrolysis (Tilokani *et al.*, 2018; Liesa *et al.*, 2019). Recently, a different model of OMM fusion has been proposed based on new metazoan topology of MFNs which is mediated by redox signalling (Tilokani *et al.*, 2018). Mattie *et al.* (2018) suggests that the MFN C-terminus resides in the IMS instead and an oxidised environment due to reactive oxygen species (ROS) production as well as an increased concentration of oxidised glutathione (GSSG) can lead to the formation of two disulphide bonds within the IMS domains. These bonds induce the dimerisation and oligomerisation of MFNs which in turn induces tethering and/or GTPase activity required for OMM fusion (Figure 1.4B). This model therefore suggests a link between oxidative stress and the promotion of mitochondria fusion.

In the literature, many neurodegenerative diseases, including ALS, have shown an imbalance of the interplay between fission and fusion (Smith *et al.* (2019), Table 1.1). Onesto *et al.* (2016) used *C9orf72* human fibroblasts grown in galactose media in their study and found a mixed population of elongated, short and round shaped mitochondria, whereas mutant *TARDBP* fibroblasts showed a much stronger phenotype with a fragmented mitochondria network. Mitochondrial dynamics were also assessed by western blot analysis for FIS1 and MFN1. MFN1 levels were significantly increased compared to control in mutant *C9orf72* fibroblasts suggesting an imbalance between fission and fusion levels. Moreover, transmission electron microscopy (TEM) revealed swollen mitochondria as well as abnormalities in cristae structure in an iPSC model of *C9orf72* (Dafinca *et al.*, 2016). Gao's group has also reported abnormal mitochondrial morphology *in vivo* utilising their GR80 inducible mouse model and Flag-GR80 *Drosophila* model. TEM from the prefrontal cortex of young 3- and 6-month-old GR80 mice revealed disruption of the IMM and loss of cristae with a more pronounced effect at 6 months, suggesting an age-related accumulation of toxicity

(Choi *et al.*, 2019). In line with their observations on mitochondrial fragmentation, Choi *et al.* (2019) detected an increase in DRP1 and decrease in OPA1 levels in 9-month-old mice. Furthermore, muscle mitochondrial defects were evident in Flag-GR80 transgenic flies (Li *et al.*, 2020). Swollen mitochondria were observed in the indirect flight muscles, and TEM pictures showed round mitochondria devoid of electron-dense matrix material and aberrant cristae structure, which is similar to what was seen in Dafinca *et al.* (2016). Interestingly, altering mitochondrial dynamics by genetic manipulation using loss or gain of function of DRP1, FIS1 or Marf (*Drosophila* homolog of Mitofusin) had no obvious effect on GR80 toxicity (Li *et al.*, 2020). This raises the question of the importance of mitochondrial morphology and dynamics in relation to disease pathogenesis.

1.3.3 Mitochondrial respiration and ATP production

Mitochondria are known for being the 'powerhouse of the cell' as they are required to generate energy in the form of ATP mainly by oxidative phosphorylation (OXPHOS) at the electron transport chain (ETC) which spans across the IMM except for Complex II (Zhao *et al.*, 2019). The ETC is composed of transmembrane complexes I to IV and ATP synthase (CV) and two electron carriers – ubiquinone (CoQ) and cytochrome C (Cyt c) (Figure 1.5). Electrons from NADH and FADH₂, produced in the tricarboxylic acid (TCA) cycle, are transferred via a series of redox reactions down the ETC. Firstly, electrons are donated to CI which causes a reduction of CoQ into CoQH₂. The CoQH₂ is then oxidised by CIII where the electrons are passed to Cyt c. The reduced Cyt C is then oxidised by CIV where molecular oxygen is reduced as the final electron acceptor to produce water (Sazanov, 2015). Through this series of redox reactions, protons are pumped from the matrix across the IMM to the IMS. The accumulated protons and reduction of protons from the IMM create a gradient i.e. mitochondrial membrane potential, favouring the protons to traverse through CV/ATP synthase and drive ATP synthesis. Ultimately, this proton motive force drives the conversion of ADP to ATP (Mazat *et al.*, 2013; Area-Gomez *et al.*, 2019).

Under physiological conditions, 0.2-2% of electrons leak out of the ETC which reacts with oxygen to produce superoxide. Superoxide dismutase (SOD) enzymes catalyse the dismutation of superoxide generating hydrogen peroxide, which itself plays a role in many signalling pathways including cell proliferation, differentiation and migration (Holmstrom & Finkel, 2014), or react with redox active metals such as iron to generate the hydroxy radical through the Fenton/Haber-Weiss reaction (Wang *et al.*, 2018; Zhao *et al.*, 2019). 11 sites have been identified in mammalian mitochondria to produce both superoxide and hydrogen

peroxide, the main ones from the ETC are highlighted in Figure 1.5 (Brand, 2010; Zhao *et al.*, 2019). Excess ROS production from the mitochondria is widely known to be detrimental and closely linked to many neurodegenerative diseases including ALS (Smith *et al.*, 2019).

Since mitochondria are the main site of ROS generation, they have multiple anti-oxidant defence mechanisms in place to counteract excessive production of ROS. SODs are the first line of defence against oxygen free radicals. SOD1 is mainly cytosolic and can be found in the IMS, where it removes superoxide generated from the IMM (Han *et al.*, 2001). However, SOD2 is the major mitochondrial enzyme. Chemically, superoxide is a negatively charged free radical anion, which reacts with itself, catalysed by SOD dismutation reaction to form hydrogen peroxide and oxygen. Superoxide is relatively short lived and due to its charge does not readily pass through cell membranes, whereas hydrogen peroxide can freely traverse membranes. Despite being an important signalling molecule, excessive hydrogen peroxide is also detrimental to the cell, therefore, tight regulation of ROS homeostasis is needed. Hydrogen peroxide can be degraded to water and molecular oxygen by catalase, mainly present in peroxisomes. However, catalase is not present in the mitochondria and therefore the glutathione peroxidases (GPxs), peroxiredoxins (Prx) and thioredoxin (Trx) system are required instead to reduce hydrogen peroxide (Lubos *et al.*, 2011). GPx-1 is the most abundant member of the GPx family which is localised in the cytosol, mitochondria and peroxisomes. It uses reduced glutathione (GSH) as a cofactor to reduce hydrogen peroxide, forming oxidised glutathione (GSSG).

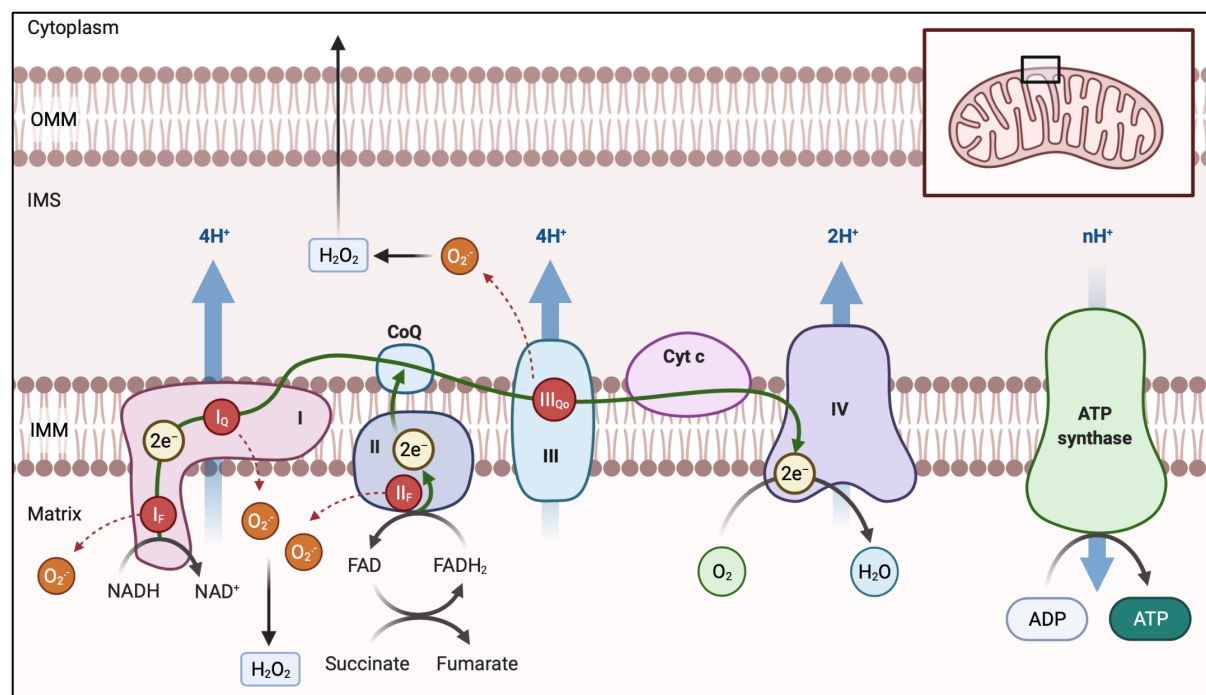


Figure 1.5 – Electron transport chain and sites of superoxide production

The electron transport chain (ETC) is composed of enzymatic complexes (I-V) and two free electron carriers – CoQ and Cyt C. Electrons transferred from NADH and FADH₂ are passed down the ETC to molecular oxygen, coupled with the generation of a proton gradient across IMM which drives ATP synthesis at ATP synthase. Sites of superoxide production in the complexes are also indicated. Modified using BioRender 'Electron transport chain' template, content adapted from Zhao *et al.* (2019) and Li *et al.* (2021).

In *C9orf72* iPSC-derived motor neurons, Dafinca *et al.* (2016) showed up to 30% reduction in mitochondrial membrane potential compared to controls. However, Onesto *et al.* (2016) found membrane hyperpolarisation and increased ATP production as well as respiration in *C9orf72* patient fibroblasts. Furthermore, Mehta *et al.* (2021) investigated cellular energetics in *C9orf72* iPSC-derived motor neurons and found impaired basal and maximal mitochondrial respiration which implicates abnormalities in the ETC. To further explore this, Mehta *et al.* (2021) performed RNA-seq using human iPSC-derived *C9orf72* motor neurons. Transcriptomic analysis identified dysregulation in pathways implicated in OXPHOS, as well as changes with mitochondrial small and large ribosomal subunits. Validation of hits using qRT-PCR and western blot confirmed dysregulation of mostly complex I and IV and importantly, examination of human *C9orf72* post-mortem spinal cord tissue using RNA *in situ* hybridisation corroborated their result by showing reduced expression of complexes I and IV in ventral horn spinal motor neurons. Interestingly, genetic manipulation of mitochondrial biogenesis by overexpressing PGC1 α in *C9orf72* motor neurons corrected the bioenergetic deficit and rescued other dysregulated mitochondrial phenotypes. Consistently, Wang *et al.*

(2021) used mouse embryonic fibroblasts isolated from *C9orf72* knockout and wild-type mice to show that *C9orf72* is imported into the IMS and stabilises translocase of inner mitochondrial membrane domain containing 1 (TIMMDC1) which is necessary for the assembly of complex I.

Specifically, it has been shown that poly-GR itself may be important in linking mitochondrial dysfunction and oxidative stress. Lopez-Gonzalez *et al* (2016) showed an increase in DNA damage, oxidative stress and mitochondrial membrane potential in iPSC-derived *C9orf72* motor neurons. They also performed an interactome analysis with GR80 expressed in HEK293 cells compared to control where they identified many mitochondrial ribosomal proteins which are required for the translation of the mitochondrial complexes. In a mouse model expressing GR80, Choi *et al.* (2019) found increased DNA damage, oxidative stress and decreased activities of mitochondrial complexes I and V. Poly-GR was also shown to bind to the mitochondrial complex V component ATP5A1, which enhanced its ubiquitination and degradation which is consistent with findings showing reduced ATP5A1 protein levels in both the mouse model and patient brains. Moreover, Li *et al.* (2020) observed an increase in oxidative stress, mitochondrial membrane potential and ATP production in their Flag-GR80 *Drosophila* model when expressed in the muscle. Interestingly, they saw that complex I activity was elevated however Complex II-V were unaffected.

Taken together, all the results highlight the involvement of oxidative stress and the connection between *C9orf72* itself, or poly-GR in the mitochondria and its influence on mitochondrial metabolism and respiration is extremely important.

1.3.4 Mitochondrial quality control

Extensively damaged or stressed mitochondria can be targeted for degradation by a selective form of autophagy termed mitophagy. It is required to maintain steady mitochondrial turnover and metabolic homeostasis (Youle & Narendra, 2011). PINK1/parkin-mediated mitophagy is one of the more studied mechanisms. PINK1 is a mitochondria-targeted serine/threonine kinase and in healthy mitochondria, PINK1 is imported into the mitochondria through TIM/TOM complexes, translocases of the inner and outer membrane where it is processed by mitochondrial proteases such as mitochondrial processing peptidase (MPP) and presenilin-associated rhomboid-like protease (PARL) resulting in proteasomal degradation of PINK1 (Greene *et al*, 2012). Parkin is a cytosolic E3 ubiquitin ligase and is responsible for the formation of mono- and poly-ubiquitin chains on various substrates.

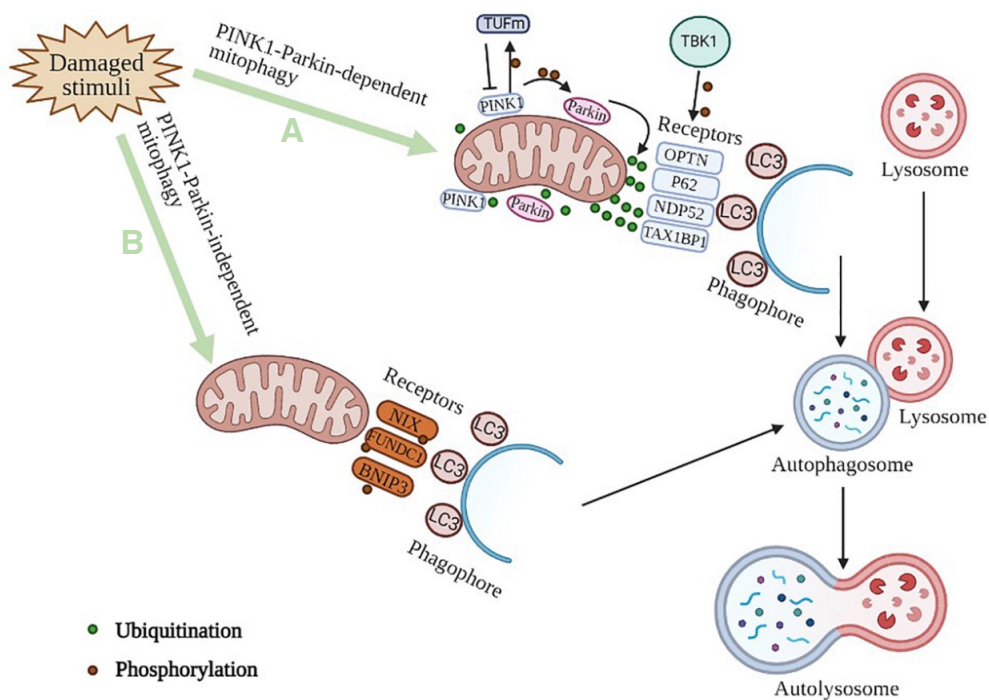


Figure 1.6 PINK1-Parkin-mediated mitophagy

(A) PINK1-Parkin dependent mitophagy: upon mitochondrial depolarisation, PINK1 stabilises on the OMM and phosphorylates ubiquitin and recruits and activate Parkin, which can be amplified by ubiquitinating mitochondrial surface proteins, creating a feed-forward amplification loop. PINK1 can also limit the level of mitophagy by activating a non-canonical function of the mitochondrial Tu translocation elongation factor (TUFm) by phosphorylating TUFm at serine 222. Recruitment of ubiquitin-binding autophagy receptors such as OPTN, p62, NDP52 and TAX1BP1 leads to local phagophore formation at damaged mitochondria. TBK1 phosphorylation of these receptors enhances interactions between LC3 and ubiquitin therefore enhancing mitophagy. The polyubiquitinated mitochondria are engulfed by autophagosomes subsequently fusing with lysosomes to form autolysosomes where contents are degraded. **(B)** PINK1-Parkin-independent mitophagy: alternative pathways triggering mitophagy are mediated by mitophagy receptors such as NIX, FUNDC1 and BNIP3. Figure adapted from (Zhu *et al*, 2021).

When the mitochondria are damaged, the loss of mitochondrial membrane potential leads to blockade of PINK1 import and thereby it stabilises on the OMM where it phosphorylates ubiquitin at serine 65 and recruits Parkin to further ubiquitinate OMM proteins. Phospho-ubiquitination of OMM proteins such as MFN1 and MFN2 creates a feed-forward amplification cascade, providing further substrates for PINK1 phosphorylation and recruitment of more Parkin molecules marking mitochondrion for degradation. PINK1 can also limit the level of mitophagy by activating a non-canonical function of the mitochondrial Tu translocation elongation factor (TUFm) by phosphorylating TUFm at serine 222 (Lin *et al*, 2020). The

polyubiquitinated mitochondria are subsequently engulfed by autophagosomes which fuses with lysosomes, thereby resulting in the formation of autolysosomes for degradation (Lazarou *et al*, 2015; Nguyen *et al*, 2016) (Figure 1.6). Deubiquitinating enzymes (DUBs) regulate ubiquitin signals and therefore play an important role in modulating mitophagy. For example, Ubiquitin-specific processing protease 30 (USP30) is localised at the OMM and negatively regulates mitophagy by hydrolysis of K6 and K11 linked chains of parkin substrates (Bingol *et al*, 2014; Cunningham *et al*, 2015).

Optineurin (OPTN), nuclear dot protein (NDP52) and p62 are autophagy receptors that have been shown to translocate to damaged mitochondria leading to the recruitment of microtubule-associated protein 1A/1B light chain 3A (LC3) (Figure 1.3). The autophagy receptors comprise of a LC3 interacting region (LIR) domain which enables interaction with LC3 proteins on the autophagosome membrane. It has also been shown that OPTN and NDP52 are required for the recruitment of ULK1 to initiate phagophore and autophagosome formation (Lazarou *et al.*, 2015; Nguyen *et al.*, 2016). Moreover, there are alternative pathways that have been reported to trigger mitophagy that are PINK1/Parkin independent. Other mitophagy receptors that are located on the OMM containing LC3 interacting region (LIR) motifs which also interact with LC3 (Khalil & Lievens, 2017) include Bcl-2 and adenovirus E1B 19 kDa-interacting protein 3 (BNIP3) and Nix/BNIP3L (BNIP3-Like) (Novak *et al*, 2010; Rikka *et al*, 2011), Autophagy and BECLIN 1 regulator 1 (AMBRA1) (Strappazzon *et al*, 2015) and FUN14 domain-containing protein 1 (FUNDC1) (Liu *et al*, 2012) (Figure 1.6).

Interestingly, OPTN, and its kinase TBK1 and SQSTM1/p62 are all ALS-linked genes. OPTN translocation is dependent on parkin recruitment and disruption of this process with ALS-associated E478G ubiquitin binding-deficient mutation led to defective mitophagy and accumulation of damaged mitochondria in CCCP-treated HeLa cells highlighting a role for mitophagy in ALS pathogenesis (Wong & Holzbaur, 2014). Moreover, TBK1 was found to be co-recruited with OPTN to depolarised mitochondria where OPTN is phosphorylated by TBK1 at serine 177. Inhibition using siRNA or depletion of TBK1 using TBK1-E696K mutants blocks efficient autophagosome formation in CCCP-treated HeLa cells (Moore & Holzbaur, 2016). Moreover, TBK1 has been found to phosphorylate p62 and NDP52 as well as OPTN, enhancing its ability to link ubiquitin and LC3 (Oakes *et al*, 2017).

As discussed before, *C9orf72* is involved in the initiation of autophagy and has also been implicated in regulating lysosomal function (Amick *et al.*, 2016; Yang *et al.*, 2016) however its role in mitophagy is relatively understudied and therefore more research is needed to elucidate whether mitophagy is important in *C9orf72* ALS/FTD.

1.4 NRF2/Keap1 system

The nuclear factor erythroid 2 p45-related factor 2 (NRF2)/ Kelch-like ECH-associated protein 1 (Keap1) pathway is an important stress response to protect against oxidative and electrophilic stresses. NRF2 is negatively suppressed by its interaction with Keap1 under homeostatic conditions and is responsible for regulating the expression of more than 250 genes involved in cellular protection against oxidative and electrophilic stresses and inflammatory agents as well as the maintenance of mitochondrial function and cellular redox state (Hayes & Dinkova-Kostova, 2014; Jimenez-Villegas *et al*, 2021).

1.4.1 Structure of NRF2 and Keap1

NRF2 is a basic region leucine zipper transcription factor belonging to the Cap 'n' Collar (CnC) family and comprises of seven domains with different functions to control NRF2 activity – Nrf2-ECH homology 1-7 (Neh) domains (Figure 1.7A). Neh2 domain contains the DLG and ETGE motifs, which interact with Keap1 and are important for the subsequent Keap1-mediated proteasomal degradation of NRF2 (Figure 1.7B). Neh1 contains a CNC domain and basic region essential for DNA binding as well as a leucine zipper region important for dimerization with sMAF (Figure 1.7C). Neh3-5 regions are transcriptional activation domains which binds to various components of the transcriptional regulatory machinery (He *et al*, 2020). Neh6 domain is needed for the phosphorylation-based regulation of NRF2 activity (Chowdhry *et al*, 2013) and Neh7 interacts with retinoic X receptor alpha (RXR α), which represses NRF2 activity (Wang *et al*, 2013).

NRF2 and Keap1 are well conserved in *Drosophila* (Pitoniak & Bohmann, 2015). Cap 'n' Collar (CnC) proteins were first identified in *Drosophila melanogaster* (Mohler *et al*, 1991) and the CnC locus is transcribed in three transcript isoforms, CncA, CncB and CncC. CncC is the longest isoform which contains an additional N terminal domain homologous to NRF2 (Kobayashi *et al*, 2002) and was demonstrated to have a similar antioxidant stress response in adult flies (Sykiotis & Bohmann, 2008). Of interest, the DLG and ETGE motifs are conserved from the Neh2 domain (Figure 1.7A,B). The amino acid sequence of Neh1 domain, especially the basic region in the middle of this domain is highly conserved (Figure 1.7A,C).

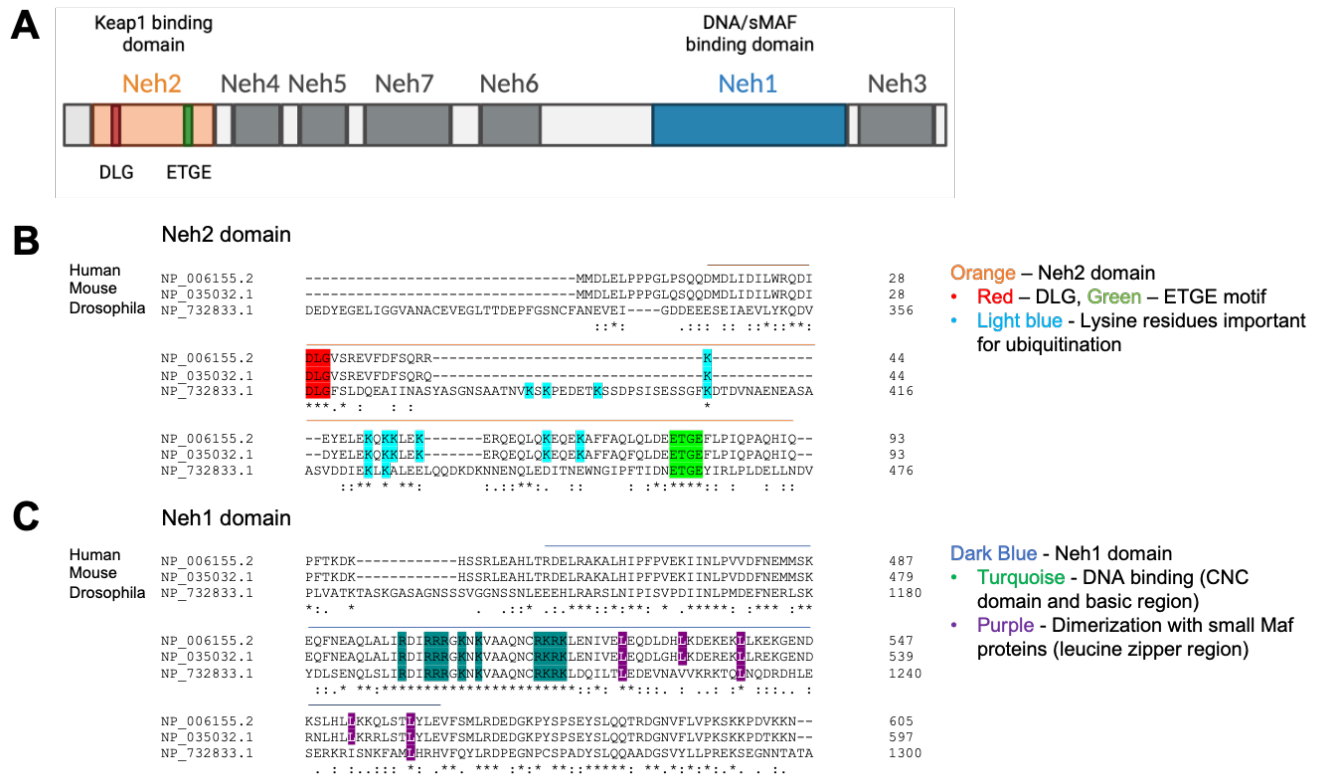


Figure 1.7 NRF2 structure and homology comparison

(A) Schematic of NRF2 protein in humans including the Neh domains. The Neh2 domain is important for binding with Keap1, and Neh1 domain is important for DNA binding and dimerization with small Maf proteins (sMAF). Adapted from Fuse & Kobayashi (2017) **(B)** Alignment of key functional elements in the Neh2 domain from human, mouse and *Drosophila*. The DLG and ETGE motifs are conserved in the fly, lysine residues important for ubiquitination are somewhat conserved. **(C)** Comparison of the Neh1 domain from human, mouse and *Drosophila*. The CNC domain and basic region essential for DNA binding is well conserved. The leucine zipper region important for dimerization with sMAF is also somewhat conserved. Mostly importantly, Sykiotis & Bohmann (2008) have shown that there is an analogous NRF2-Keap1 system in *Drosophila*.

NRF2/Keap1 signalling

Kelch-like ECH-associated protein 1 (Keap1) is a cysteine-rich protein, serving as an adaptor protein for the Cullin 3 (CUL3)-dependent E3 ubiquitin ligase complex with Ring box protein 1 (RBX1). NRF2 is basally lowly expressed in all cell types due to the Keap1-mediated constitutive proteasomal degradation. Keap1 comprises of 3 main domains (Figure 1.8A) including the broad complex-tramtrack-bric a brac (BTB) domain, the intervening region (IVR) (Figure 1.8B) and double glycine repeat (DGR)/Kelch repeat domains (Figure 1.8C). The N terminal BTB domain is essential for the formation of the homodimer of Keap1 (Figure 1.8B). Keap1 binds NRF2 via its C terminal Kelch domain by interacting with the DLG and ETGE motifs in the Neh2 domain of NRF2 (Figure 1.8B). The cysteine residues in Keap1 are highly reactive and can function as sensor amino acids to detect stress, the important residues are summarized in Figure 1.8A (Dinkova-Kostova & Abramov, 2015; Holmstrom *et al*, 2016; Fuse & Kobayashi, 2017).

NRF2/Keap1 signalling

The IVR domain consists of the nuclear export sequence (NES) and also contains stress sensing cysteine residues. Cysteine 151 is most prominently studied and is known determined to be an important cysteine for the detection of electrophiles, such as dimethyl fumarate (DMF). This particular cysteine is not conserved in the same amino acid however, there is a cysteine adjacent to this position and the ARE reporter gene was shown to be activated by diethyl-maleate (DEM) treatment (Chatterjee & Bohmann, 2012). **(C)** Keap1 binds NRF2 via its C terminal Kelch domain by interacting with the DLG and ETGE motifs in the Neh2 domain of NRF2. The six double glycine repeats are also a key structure feature of the Kelch domain.

1.4.2 NRF2/Keap1 signalling

Under basal homeostatic conditions, Keap1 binds to CUL3 via its BTB domain, which leads to Keap1 homodimerisation. The CUL3-RBX1-Keap1 ubiquitin ligase complex interacts with the DLG and ETGE motifs in the Neh2 domain of NRF2 via its C terminal Kelch domain of Keap1. The high-affinity ETGE motif binds to the Kelch domain of Keap1 and the lower affinity DLG motif binds to the second Keap1 dimer. This leads to polyubiquitination of NRF2 at the lysine-rich region (KKKKKKK) in the cytoplasm and is targeted to the proteasome for degradation (Figure 1.9). Under oxidative stress, electrophiles and ROS react with the several cysteine sensors of Keap1, including cysteine 151 (C151), C273 and C288 (Figure 1.9B). The modification of the cysteine residues causes a conformational change which disrupts the weak, low-affinity binding between the DLG motif and Kelch domain of Keap1, leading to its dissociation with NRF2. NRF2 translocates to the nucleus where it binds with small Maf proteins (sMAFs), forming a heterodimer which then binds to the ARE (antioxidant responsive element) sequences on target cytoprotective genes, thus activating their transcription (Figure 1.9) (Dinkova-Kostova & Abramov, 2015; Holmstrom *et al.*, 2016; Fuse & Kobayashi, 2017).

Moreover, there are Keap1-dependent but cysteine-independent mechanisms whereby proteins such as p62/sequestosome1 (SQSTM1) also contains ETGE motifs which compete with NRF2 for Keap1 binding, leading to Keap1 sequestration and NRF2 stabilisation (Komatsu *et al.*, 2010). There are also other means of NRF2 degradation which are Keap1 independent including β TrCP-SKP1-CUL1-RBX1 and WDR3-CUL4-DDB1 mediated degradation which also results in NRF2 ubiquitination and degradation by interacting with different NRF2 domains (Rada *et al.*, 2011; Chowdhry *et al.*, 2013; Lo *et al.*, 2017).

NRF2 downstream target genes include a range of proteins with detoxification, antioxidant and anti-inflammatory properties, with the purpose to maintain redox balance (Hirotsu *et al.*, 2012). Some examples of redox genes include heme oxygenase 1 (HO1),

NADPH quinone dehydrogenase (NQO1), glutathione S-transferase (GST), two subunits of glutamate-cysteine ligase (GCL) and glutamate-cysteine ligase modifier (GCLM, the rate-limiting enzyme for GSH synthesis). Antioxidant genes include SOD1, catalase, sulfiredoxin, thioredoxin, and peroxiredoxin (Bono *et al.*, 2021). NRF2 also regulates other cellular pathways including several autophagy-related genes that have common ARE sequences in their promoters including NDP52, SQSTM1, ULK1 and ATG7 as well as blocking pro-inflammatory cytokine transcription including IL-6 and IL-1 β (Bono *et al.*, 2021).

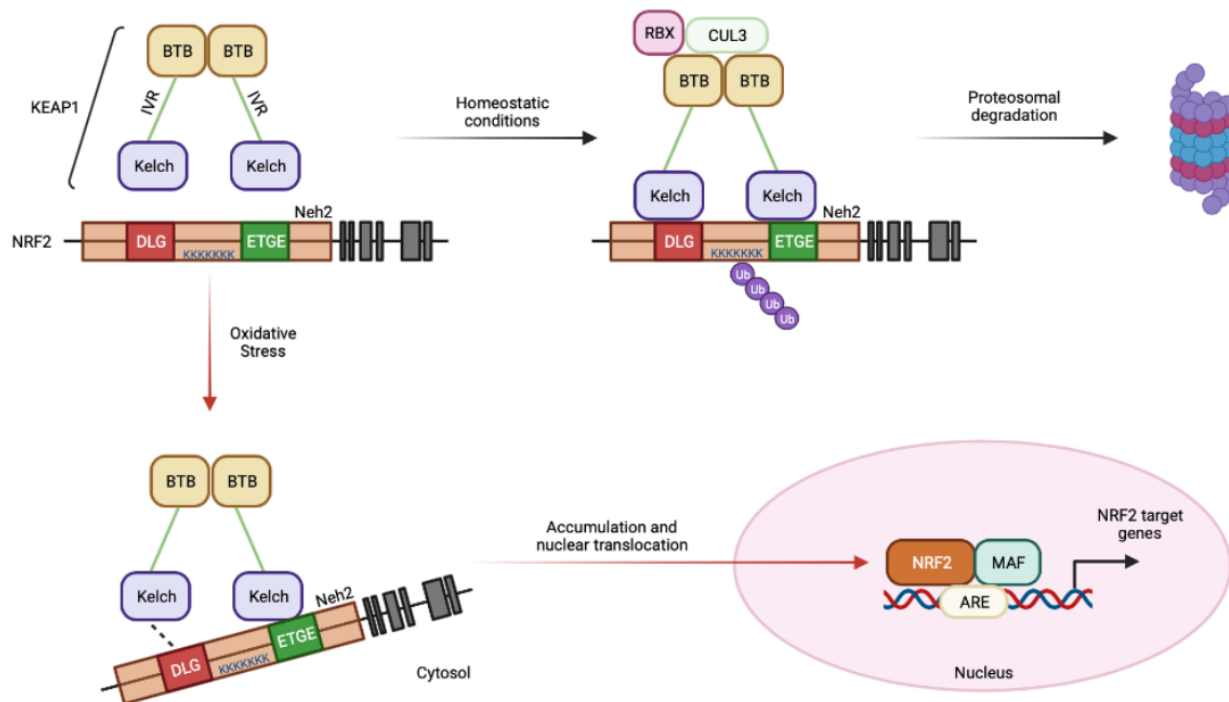


Figure 1.9 NRF2/Keap1 signalling

Under basal conditions, Keap1 forms a ubiquitin E3 ligase complex with CULLIN 3 (CUL3) and Ring box protein 1 (RBX1) by binding to the DLG and ETGE motifs from NRF2. This leads to the polyubiquitination of NRF2 resulting in proteasomal degradation in the cytoplasm. During oxidative stress, exposure to electrophiles or ROS is detected by the reactive cysteine residues in Keap1, causing a conformational change whereby NRF2 dissociates from Keap1 and in turn accumulates and translocate to the nucleus, heterodimerizes with small Maf (sMAF) proteins, bind to ARE of cytoprotective genes, thereby acting as a master regulatory transcription factor.

1.4.3 NRF2 and ALS

The NRF2 pathway has been shown to be affected in ALS patients as well as in *in vitro* and animal models of the disease however, there are contrasting views on how the pathway is dysregulated (Table 1.2). Post mortem tissue from ALS patients revealed a reduction of

NRF2/Keap1 signalling

NRF2 mRNA and protein expression in neurons in the motor cortex and spinal cord, whereas Keap1 mRNA expression was increased in the motor cortex only, however similar protein expression levels were observed (Sarlette *et al*, 2008). The authors did emphasise that since the ALS samples are from end-stage disease, it is not possible to rule out a role for Keap1 in motor neuron death as expression levels may have been altered in earlier stages of the disease (Sarlette *et al.*, 2008). Moreover, one cannot exclude the possibility that the NRF2 axis could be activated at the early stages of the disease since a reduction of NRF2 was observed (Jimenez-Villegas *et al.*, 2021).

Most studies investigating the NRF2/Keap1 pathway have focussed on the SOD1-linked ALS. Deletion of NRF2 in different SOD1 mouse models (G93A model (Guo *et al*, 2013; Vargas *et al*, 2013); G85R model (Vargas *et al.*, 2013); H46R model (Hadano *et al*, 2016) did not change the progression of the disease, suggesting NRF2 may not be the sole mediator for the induction of cytoprotective antioxidant genes and therefore may not be the key protective mechanism against neurodegeneration (Guo *et al.*, 2013). However, despite not observing any detrimental effect associated with the lack of NRF2, specific overexpression in neurons or type II skeletal muscle fibres delayed disease onset, but did not extend survival in SOD1^{G93A} mice highlighting the tissue and cell type specificity involved in the regulation of the NRF2 pathway (Vargas *et al.*, 2013). Kraft *et al* (2007) had similar findings by crossing ALS mouse models with an antioxidant response element (ARE) reporter mouse to understand the spatio-temporal activation. They showed an early and intense NRF2 activation in distal skeletal muscles and progress in a retrograde fashion since lower levels of activation at symptom onset in spinal cord MNs and astrocytes were observed (Kraft *et al.*, 2007). Moreover, it is important to recognise that using global, non-inducible knockouts of NRF2 may cause many compensatory pathways to occur and therefore not portray the complete picture.

Other studies have observed evidence indicating that the NRF2 pathway is perturbed. Nardo *et al* (2013) performed a motor neuron transcriptome analysis with laser captured motor neurons isolated from the lumbar ventral spinal cords of two strains of SOD1 transgenic mice – the rapid progressive strain (129Sv) compared to the slowly progressive strain (C57). The expression of NRF2 mRNA was increased in the motor neurons of the slowly progressive C57 strain from disease onset whereas an increase in NRF2 levels was only observed at the end stage of the disease for the fast progressive 129Sv strain. Immunohistochemical analysis performed on the lumbar spinal cord at the onset of the disease identified no upregulation of NRF2 protein in the slow progressive C57 strain, whereas a reduction was observed in the fast progressive 129Sv strain. Moreover, downregulation of pathways involving mitochondrial function was only observed in the fast progressive 129Sv strain. This suggests that the rapidly

progressive strain may have mitochondrial phenotypes in early pathogenesis accompanied by a weak NRF2 response which also may explain the fast progressive nature of this strain. NRF2 protein levels were also reduced in primary motor neuron cultures from SOD1^{G93A} transgenic mice (Pehar *et al*, 2007) and overexpression of NRF2 in NSC-34 SOD1^{G93A} cells was able to significantly decrease oxidative stress and increase cell survival (Nanou *et al*, 2013).

Mimoto *et al* (2012) evaluated the temporal and spatial changes of NRF2, Keap1 and its downstream stress response proteins HO-1, TRX and heat shock protein 70 (HSP70) throughout the MN degeneration in the spinal cord of SOD1^{G93A} mice. Keap1 protein levels were progressively decreased from early (63%) to late symptomatic stages (58%), whereas NRF2 dramatically increased in the anterior lumbar cord with accumulation in the MN nucleus (to 229%) and 471% at 18 weeks when glial like cells also became positive. In contrast, downstream stress response proteins showed only a small significant increase in MNs that correlated with an increased number of glial cells after the symptomatic stage (149% to 280%) (Mimoto *et al.*, 2012).

Finally, in a different ALS model, Moujalled *et al* (2017) used ALS patient fibroblasts harbouring a TDP-43^{M337V} mutation and NSC-34 motor neuronal cell lines carrying the TDP-43^{Q331K} mutation and performed RNA binding immunoprecipitation studies. This revealed an enrichment of NRF2 and GPX1 transcripts bound to heterogeneous nuclear ribonucleoprotein K (hnRNP K) protein, which is an RNA-binding protein. hnRNP K was found to be mislocalised and its altered metabolism subsequently impairs the oxidative stress response in cells due to aberrant translation of key antioxidant proteins (Moujalled *et al.*, 2017). Of note, Braems *et al* (2022) found that hnRNP K was found to be mislocalised in *C9orf72* ALS/FTD patient tissue and overexpression of hnRNP K was sufficient to suppress DNA damage in a *C9orf72* zebrafish model.

Altogether, these studies support the hypothesis that reinforcement of the NRF2/Keap1 pathway could represent a promising therapeutic strategy for neuroprotection in ALS (Jimenez-Villegas *et al.*, 2021).

Table 1.2 Summary of NRF2 findings in the literature

A summary of NRF2 observations in the literature for ALS from human post mortem tissue as well as *in vivo* and *in vitro* systems; emphasis on NRF2 mRNA transcript and protein levels as well as mRNA transcripts and protein levels of NRF2 downstream target genes. Other significant genes of interest and additional information of interest is also documented.

Model system	Study	NRF2		NRF2 downstream genes		Other significant genes of interest/notes
		mRNA	protein	mRNA	protein	
Human post mortem						
Post mortem tissue	Sarlette et al., (2008)	↓	↓			↑ Keap1 mRNA
Cultured cells and animal models						
SOD1 ^{G93A} NSC34 cells	Kirby et al., (2005)	↓	↓	Gsta3, G6pdx, Ak1c13 ↓	PRDX3, G6PD ↓	
SOD1 ^{G93A} MNs	Peher et al., (2007)	↓		GclC, GclM ↓		
SOD1 ^{G93A} NSC34 cells	Wang et al., (2014)	↓	↓	HO-1, NQO1 ↓	HO-1, NQO1 ↓	
SOD1 ^{G93A} rats	Vargas et al., (2005)	↑	↑	HO-1 ↑		
SOD1 ^{G93A} x ARE reporter	Kraft et al., (2007)					↑ NRF2 activity based on reporter, initiating from distal muscles
SOD1 ^{G93A} mice	Mimoto et al., (2012)		↑		HO-1, TRX ↑	↓ Keap1 protein, region specific changes observed anterior vs dorsal lumbar spinal cord
SOD1 ^{G93A} mice	Guo et al., (2013)				HO-1, NQO1, GclC, GclM ↑	↑ Keap1 protein
TDP-43 ^{M337V} patient fibroblasts	Moujalled et al., (2017)	↑	↑	HMOX1, GPX1 ↑	GPX1, NQO1 ↑	↑ Keap1 protein, no changes in response to sodium arsenite
TDP-43 ^{G331K} mice		↑		HMOX1, NQO1 ↑	GclM, GPX1, NQO1 no change	
TDP-43 ^{M337V} NSC34 cells	Tian et al., (2017)		↑ nuclear NRF2 ↓ total and cyto NRF2	NQO1 ↓		

1.5 The use of *Drosophila melanogaster* as a genetic model system

Drosophila melanogaster are an excellent model organism and have been extensively used to study neurodegenerative diseases. Flies have a range of complex behaviours including sleep, learning and memory, and navigation which can be monitored as these behaviours decline with age and in the presence of disease genes (Anoar *et al.*, 2021). The *Drosophila* genome is fully sequenced, has only 4 chromosomes and currently estimates 13,821 genes; 65% of human genes are homologous to *Drosophila* genes and there is homology in the structure and function of proteins found to be involved in neurodegeneration (Hirth, 2010). Moreover, *Drosophila* can be used to recapitulate phenotypic features of disease well and expression of specific genes can be manipulated in a time and tissue-specific manner, facilitating the study of disease progression. This is easily achieved using the GAL4/UAS bipartite system whereby selective expression and knockdown of target genes can be achieved in a cell and tissue specific manner (Brand & Perrimon, 1993). The system consists of two parts: the yeast transcription factor GAL4 and the upstream activating sequence (UAS). GAL4 is typically expressed under the control of a tissue specific enhancer and binds to the UAS which initiate transcription of the gene of interest downstream of the UAS in a tissue specific manner. This system is activated when two transgenic lines, the GAL4 driver line and the UAS responder line are combined, usually by defined crossing schemes (Figure 1.10).

Drosophila also have a relatively short lifespan, rapid generation times and low maintenance costs, therefore are ideal for conducting genetic screens as well as studying neurodegenerative diseases including *C9orf72* ALS/FTD. Firstly, *Drosophila* do not have a *C9orf72* orthologue therefore loss of function experiments are not possible. However, gain of function toxicity can be investigated. Pure repeat models have been produced which contain the G4C2 sequence thereby producing repetitive RNA and theoretically all five of the DPRs and have shown to cause toxicity (Xu *et al.*, 2013; Mizielinska *et al.*, 2014; Freibaum *et al.*, 2015; Solomon *et al.*, 2018). In order to elucidate the contribution of repeat RNA, fly models expressing repeat RNA only (RO) have been developed by inserting stop codons every 12 GGGGCC repeats to prevent translation. Antisense RNA models as well as pathologically relevant repeat length RNA (up to 1000 repeats) were generated by (Moens *et al.*, 2018). All of the RNA only models were shown to form RNA foci and sequester RNA binding proteins however, do not cause overt toxicity suggesting that repeat RNA alone is insufficient to cause neurodegeneration (Sharpe *et al.*, 2021). To dissect DPR protein only toxicity, a variety of DPR only constructs have been developed by the expression of transgenes generated using

alternative codon sequences for each different DPR (Mizielinska *et al.*, 2014; Wen *et al.*, 2014; Freibaum *et al.*, 2015; Yang *et al.*, 2015; Boeynaems *et al.*, 2016; Solomon *et al.*, 2018; West *et al.*, 2020) whereby arginine-rich DPR only flies have been found to be the most toxic. In conclusion, a combination of flies can be used to determine the molecular mechanisms underpinning disease.

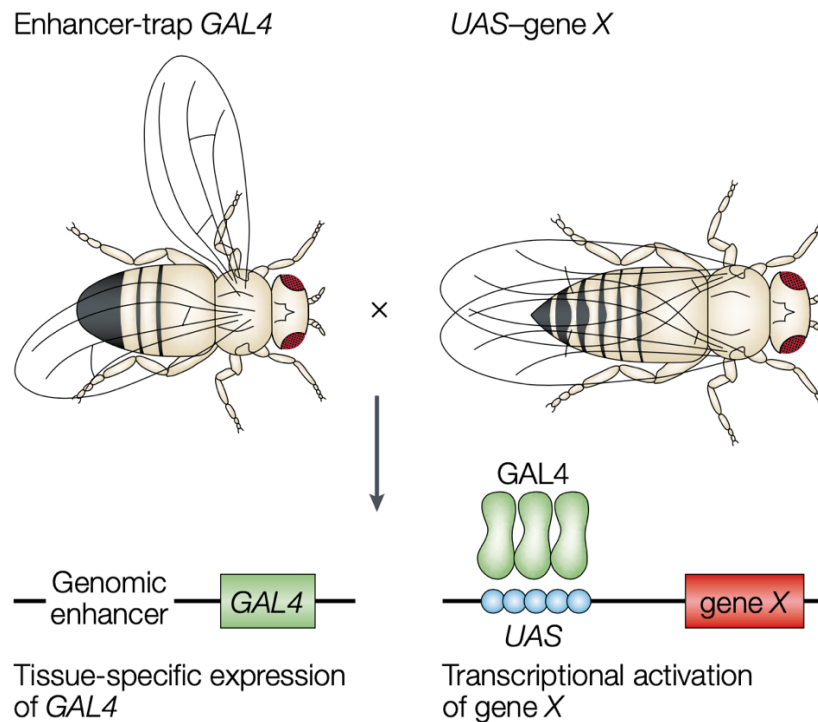


Figure 1.10 GAL4/UAS System

Two transgenic lines are crossed together, the enhancer-trap GAL4 x UAS gene X. The yeast transcriptional activator GAL4 can be used to regulate tissue-specific gene expression by binding to the upstream activating sequence (UAS), which initiates transcription of the gene X of interest downstream of the UAS. Figure from St Johnston (2002).

1.6 Thesis Aims

Mitochondria are vital organelles important for cellular processes regulating energy metabolism and cell survival. The role of mitochondria specifically in *C9orf72* ALS/FTD has been relatively understudied, especially in an *in vivo* system. Excess production of reactive oxygen species (ROS) and defective mitochondrial dynamics are common features of ALS, but it is not clear whether these phenomena are causative or a consequence of the pathogenic process. Therefore, this project aimed to provide a comprehensive *in vivo* characterisation of mitochondrial dysfunction in a *Drosophila* model of *C9orf72* ALS/FTD and aim to elucidate the underlying mechanisms behind the disease progression and pathogenesis.

Chapter 3 provides a thorough analysis of different aspects of mitochondrial dysfunction in *C9orf72* ALS/FTD using various models including a G4C2x36 repeat model, and alternative codon constructs, GR36 and GR1000. Mitochondrial morphology, autophagy and mitophagy, mitochondrial respiration and oxidative stress were investigated. These results provided fundamental groundwork to characterise mitochondrial phenotypes present.

Chapter 4 aimed to build on results found in Chapter 3 and rescue mitochondrial phenotypes and behavioural motor impairments observed in the *C9orf72* flies. Genetic interactions were tested including mitochondrial dynamics genes, mitophagy-related genes and antioxidant genes.

In Chapter 5, since only overexpression of antioxidant genes, mitochondrial Sod2 and catalase were beneficial, the causative link between mitochondrial dysfunction, ROS and behavioural phenotypes were explored by investigating the main intracellular defence mechanisms to counteract oxidative stress i.e. the NRF2/Keap1 signalling pathway.

Chapter 2 – Materials and Methods

2.1 *Drosophila* husbandry

Flies were maintained at 25 °C in Sanyo incubators (MIR-254) with a 12:12 hour light/dark cycle on food containing cornmeal, agar, molasses, yeast and propionic acid. Fly stocks were kept at 18°C and experimental crosses at 25 °C. Flies used in this study is listed in Table 2.1.

Table 2.1. *Drosophila* lines used in this study, with source and ID

Genotype	Source	ID
GAL4 drivers		
nSyb-GAL4	BDSC	BDSC_51635
D42-GAL4	BDSC	BDSC_8816
GMR-GAL4	BDSC	BDSC_1104
arm-GAL4	BDSC	BDSC_1560
Dip-γ-GAL4 (MI03222)		Carillo et al., (2015)
C9orf72 lines		
UAS-G4C2x3		Mizielinska et al., (2014)
UAS-G4C2x36		Mizielinska et al., (2014)
UAS-GR36		Mizielinska et al., (2014)
UAS-GR1000-eGFP		West et al., (2020)
Controls		
w[1118]	BDSC	BDSC_6326
UAS-lacZ	FlyORF	F005035
UAS-luciferase RNAi	BDSC	BDSC_31603
UAS-mito.HA.GFP	BDSC	BDSC_8443
Antioxidant lines		
UAS-Sod1	BDSC	BDSC_33605
UAS-Sod2	BDSC	BDSC_24492
UAS-catalase	BDSC	BDSC_24621
UAS-mito.Catalase		Radyuk et al., (2010)
Mitochondrial dynamics lines		
UAS-Tango11.HA	FlyORF	F002828
UAS-Drp1.WT	JK Chung	
Opa1[s3475]	BDSC	BDSC_12188
Marf[B]	Hector Sandoval, Hugo Bellen	
Mitophagy/autophagy lines		
UAS-mitoQC (attP16)	Our lab	Lee et al., (2018)
UAS-USP30 RNAi	NIG	3016R-2
UAS-GFP.mCherry.Atg8a	BDSC	BDSC_37749

UAS-Atg5 RNAi	BDSC	BDSC_34899
UAS-HA-Pink1.WT	JK Chung	
UAS-Tc-Pink1	Our lab	Woodroof et al., (2011)
UAS-park.C2	Leo Pallanck	Greene et al., (2003)
MICOS lines		
UAS-Opa1-RNAi	VDRC	KK106290
UAS-dMitofilin-myc	Xinnan Wang	
UAS-Letm1-HA	FlyORF	F001238
Oxidative stress lines		
UAS-mito-roGFP2-Orp1	BDSC	BDSC_67667
cncC/Keap1 lines		
UAS-cncC	Linda Partridge	Sykiotis and Bohmann (2008)
Keap1[del]	Linda Partridge	Castillo et al., (2016)
gstD1-GFP (II)	Linda Partridge	Sykiotis and Bohmann (2008)

BDSC = Bloomington Drosophila Stock Center (RRID:SCR_006457), FlyORF = Zurich ORFeome Project (Bischof et al., 2013), NIG = National Institute of Genetics, VDRC = Vienna Drosophila Reference Center (RRID:SCR_013805).

2.1.1 Drug Treatments

For food supplemented with 10 mM paraquat (Sigma) or 7 μ M dimethyl fumarate (DMF, Sigma), standard *Drosophila* food was used but prepared with $\frac{3}{4}$ parts of water. After cooling to 50 °C, the remaining part of water is added with the compounds dissolved in a concentration of 4X for the desired concentration. All flies were flipped into freshly prepared supplemented food every 2-3 days.

2.2 Behavioural assays

2.2.1 Larval crawling

Wandering third instar larvae (only larvae from the tube wall) were used (n = 8-15). Each larva was placed in the middle of a 1 % agar plate, where they were left to acclimatise for 30 seconds. After, the number of forward and backward peristaltic waves were counted for 60 seconds.

2.2.2 Climbing assay

Unless specified, adult males were collected the day before the experiment in groups of 15-22. On the day of the experiment, flies were placed in the climbing room for 30 minutes to acclimatise to the temperature (around 22-23 °C), then transferred into test tubes for another 30 minutes. Flies were then placed in a counter-current apparatus as previously described (Greene et al., 2003). After tapping the flies to the bottom of the tube, ten seconds were given for the flies to climb to the upper portion of the apparatus (10 cm). Flies that reached the upper portion i.e. climbed 10 cm or more, were shifted into the adjacent chamber. After five successive trials, the number of flies in each chamber was counted and the average score was calculated and expressed as a climbing index.

2.3 Immunohistochemistry

2.3.1 Mitochondrial morphology, autophagy and mitophagy

Third instar larval brains were dissected in phosphate buffered saline (PBS) and fixed with 4 % formaldehyde (FA) (Thermo Scientific)/PBS for 20 minutes at room temperature. For the mitophagy mito-QC reporter, the 4 % FA/PBS was adjusted to pH 7. Samples were then washed in PBS followed water to remove salts. Prolong antifade mounting media (Thermo Scientific) was used to mount the samples and imaged the day after.

2.3.1.1 Quantification of mitoQC mitolysosomes and mCherry autolysosomes

Confocal images were processed using FIJI (Image J). The quantification of mitolysosomes was performed as described in Lee et al., (2018) using Imaris (version 9.0.2) analysis software. Briefly, a rendered 3D surface was generated corresponding to the mitochondrial network (GFP only). This surface was subtracted from the mCherry signal which overlapped with the GFP-labelled mitochondrial network, defining the red only mitolysosomes puncta with an estimated size of 0.5 μm and a minimum size cut-off of 0.2 μm diameter determined by Imaris (n = 6-8 animals, at least 10 cells were analysed per animal).

The quantification of autolysosomes was performed using FIJI (Image J) with the 3D Objects Counter Plugin. An area of interest was selected by choosing 6-10 cells per image. The threshold was based on matching the mask with the fluorescence. All puncta larger than 0.049 μm^3 was considered an autolysosome.

2.3.1.2 Quantification of mitochondrial morphology

After acquisition of images, each cell was classified using a scoring system where morphology was scored as fragmented, WT/tubular or fused/hyperfused. All images were blinded and quantified by three independent investigators.

2.3.2 Immunostaining

After fixing as described in 2.3.1, tissues were permeabilised in PBS with 0.3 % TritonX-100 (PBS-T) and blocked using 1 % bovine serum albumin (BSA) in PBS-T for 1 hour at room temperature. Tissues were then incubated with primary antibody, diluted in 1 % BSA in PBS-T overnight at 4 °C. Three 5-minute washes were performed using PBS-T, and then incubated with the appropriate secondary antibody diluted in 1 % BSA in PBS-T for 1 hour. After, two 5-minute washes in PBS-T were performed followed by a final 10-minute wash in PBS. If Hoechst was used to stain the cell nuclei, this was added at 1:10,000 in the first wash after secondary antibody incubation. Tissues were mounted on slides using Prolong antifade mounting media. A list of primary and secondary antibodies used in this study is given in Table 2.2.

2.3.2.1 Quantification of cncC staining

All acquired images were taken with the same laser and gain during acquisition, which allowed a threshold to be set in FIJI that was consistent for all images. For each brain, using the Hoechst signal, 10 nuclei from the central part of the larval CNS and 10 from the periphery were quantified to minimise bias. This was overlaid onto the cncC channel and the mean intensity within the nuclei was measured using the ROI manager.

2.3.3 Using mito-roGFP2-Orp1

Mitochondrial ROS imaging was performed using the mito-roGFP2-Orp1 reporter lines (BDSC_67667). Third larval instar brains were dissected in PBS in a Poly-D-Lysine coated 35 mm dish (MatTek) and imaged by excitation at 488 nm (reduced) or 405 nm (oxidized), with emission detected at 500-530 nm. Images were acquired using an LSM880 confocal microscope (Zeiss) equipped with a Nikon Plan-Apochromat 20X/0.8 NA objective. The maximum intensity of projected z stacks from imaged brains was quantified using ImageJ and the ratio of 405/488 nm was calculated.

2.3.4 MitoSOX

2-3 adult brains at a time at day 15 were dissected in phosphate buffered saline (PBS), incubated in 20 μM of MitoSOX (ThermoFisher) for 30 minutes in the dark, washed with PBS for three times, mounted on MatTek dishes and imaged immediately. Images were acquired using an LSM880 confocal microscope (Zeiss) equipped with a Nikon Plan-Apochromat 20X/0.8 NA objective. The maximum intensity of projected z stacks from imaged brains was quantified using ImageJ.

2.4 Microscopy

Fluorescence imaging was conducted with a Zeiss LSM 880 (Carl Zeiss MicroImaging) equipped with Nikon Plan-Apochromat 40X/1.3 NA oil immersion objective. For mito-QC imaging, the Andor Dragonfly spinning disk microscope was used, equipped with a Nikon Plan-Apochromat 100x/1.45 NA oil immersion objective and iXon camera. Z stacks were acquired with 0.2 μm steps.

2.5 Immunoblotting

Proteins were isolated from either larval brains or adult heads using RIPA lysis buffer (50 mM pH 7.4 Tris, 1 M NaCl, 0.1 % SDS, 0.5 % sodium deoxycholate and 1 % NP-40) supplemented with cOmplete mini EDTA-free protease inhibitors (Roche). After protein quantification using bicinchoninic acid assay (BCA) (Thermo Fisher), 4X Laemmli buffer (BioRad) containing 1:10 β -mercaptoethanol (Sigma) was added. Samples were boiled at 95 $^{\circ}\text{C}$ for 10 minutes and resolved by SDS-PAGE using 4-20 % or 10 % precast gels (BioRad), depending on the molecular weight of the desired protein, and transferred onto nitrocellulose membrane (BioRad) using a semi-dry BioRad TransBlot system. Membranes were blocked with 5 % (w/v) dried skimmed milk powder (Instant Milk Marvel) in Tris-buffered saline (TBS) with 0.1 % Tween-20 (TBS-T) for 1 hour at room temperature and probed with the appropriate primary antibodies diluted in TBS-T overnight at 4 $^{\circ}\text{C}$. After three 10-minute washes in TBS-T, the membranes were incubated with the appropriate horse radish peroxidase (HRP-conjugated) secondary antibodies (Dako) diluted in 5 % milk in TBS-T for 1 hour at room temperature. Membranes were washed finally three times for 10 minutes in TBS-T and detection was achieved with ECL-Prime detection kit (Amersham). All primary and secondary antibodies used are listed in Table 2.2.

Table 2.2. Primary and secondary antibodies used for immunofluorescence and western blot

Purpose	Primary antibodies	Dilution	Source/ID
IF	rabbit anti-cncC	1:500	Yu Fengwei's lab
WB	rabbit anti-GFP	1:1000	Abcam, ab294
	mouse anti-tubulin	1:5000	Sigma, T9026
	rabbit anti-Ref2(P)	1:1000	Abcam, ab178440
	rabbit anti-SOD1	1:1000	Sigma, HPA001401
	rabbit anti-GABARAP	1:1000	Abcam, ab109364
Purpose	Secondary antibodies	Dilution	Source/ID
WB	goat anti-mouse HRP	1:10000	Abcam, ab6789-1
	goat anti-rabbit HRP	1:10000	Invitrogen, G21234
IF	goat anti-rabbit AF488	1:500	Invitrogen, A11008
Purpose	Others	Dilution	Source/ID
WB	Hoechst	1:10000	Invitrogen, H3570

IF = immunofluorescence, WB = western blot

2.6 Quantitative real-time PCR

2.6.1 RNA extraction

Whole flies were snap frozen and vortexed in a 15 ml falcon before being emptied out onto a dish sitting on top of dry ice. Approximately 30 heads were collected using a paint brush and placed into a 2 ml tube containing 1.4 mm ceramic beads (Fisherbrand), also on dry ice to minimise any RNA degradation. 400 µl of TRI Reagent (Sigma) was added and placed into Minilysis machine where the programme was set to maximum speed for 10 seconds. The samples were placed back on ice for 5 minutes before two further rounds of lysing. Direct-zol RNA miniprep (Zymo) RNA extraction kit was used following manufacturer's instructions. Briefly, RNA purification was achieved by adding equal amounts of 100 % ethanol to the lysed sample in Tri Reagent, mixed and centrifuged. Rounds of Direct-zol RNA Prewash and RNA wash buffer followed by centrifugation proceeded. RNA was eluted with nuclease free water (ThermoFisher) with the final volume of 15 µl.

2.6.2 DNase treatment

TURBO DNA-free Kit (Invitrogen) was used to remove contaminating DNA by following manufacturer's instructions. Briefly, 0.1 volume of 10X TURBO Dnase Buffer and 0.1 µl of

TURBO Dnase enzyme was added to the RNA and incubated at 37 °C for 30 minutes. A further 0.1 µl of TURBO Dnase enzyme was added and incubated at 37 °C for another 30 minutes. 0.1 volume/2 µl (whichever volume is greater) of Dnase Inactivation Reagent was added, mixed well and incubated for 5 minutes at room temperature. Samples were centrifuged and the supernatant containing the RNA was transferred to a fresh tube carefully without disturbing the pellet to avoid contamination. RNA concentration was measured using a Nanophotometer (Implen).

2.6.3 cDNA synthesis

cDNA was synthesised using Thermo Scientific Maxima H Minus cDNA synthesis kit following manufacturer's instructions. Equivalent (500 µg) total RNA underwent reverse transcription for each sample. Briefly, a mixture of RNA, 10X dsDNase buffer, dsDNase and nuclease free water was mixed together and incubated at 37 °C for 2 minutes and placed back on ice to chill. Next, a mixture of Maxima cDNA H Minus Synthesis Master Mix (5X, containing reverse transcriptase, Rnase inhibitor, dNTPs, oligo (dT)₁₈ and random hexamer primers in reaction buffer) and nuclease free water was added, mixed and incubated in a preheated PCR machine with the programme consisting of 25 °C for 10 minutes, 50 °C for 15 minutes and 85 °C for 5 minutes. cDNA was stored in -20 °C if used directly or -70 °C for long term storage.

2.6.4 qRT-PCR

Gene-specific primers were designed such that oligos spanned an intron whenever possible while some were taken from the literature. A list of all the primers used are in Table 2.3. Thermo Scientific Maxima SYBR Green/ROX was used following manufacturer's instructions. Briefly a master mix containing Maxima SYBR Green/ROX qPCR Master Mix, 0.6 µM of forward and reverse primers and nuclease free water was made up and added into a 96-Well Reaction Plate MicroAmp Optical (VWR International). Template DNA was added to the wells, centrifuged briefly and placed into the Quant Studio 3 RT-PCR machine. The two-step cycling protocol was used consisting of an initial denaturation at 95 °C for 10 minutes followed by 40 cycles of denaturation at 95 °C for 15 seconds and annealing/extension at 60 °C for 1 minute. The specificity of primers was assessed by melting curve profile and their efficiency ranged from 0.95 to 1.03. The relative transcript levels of each target gene were normalised to a geometric mean of *RpL32* and *Tub84b* reference genes, using the comparative Ct method (Schmittgen and Livak, 2008).

Table 2.3. Primers used for qRT-PCR in this study

Primer	Sequence 5'-3'
cncC	GAGGTGGAAATCGGAGATGA
	CTGCTTGTAGAGCACCTCAGC
Keap1	TGGCCAGCGTGGAGTGCTAC
	TTGCAGCAACACCCGCTCCA
gstD1	CCGTGGGCGTTCGAGCTGAACA
	GCGCGAATCCGTTGTCCACCA
gclC	ATACCGACCATAACGAAGAAGTACCAGA
	ATACTTATCTCATTCCGTCCATTCTCCGT
Sod1	CCAAGGGCACGGTTTTCTTC
	CCTCACCGGAGACCTTCAC
Sod2	GTGGCCCGTAAAATTCGCAA
	GCTTCGGTAGGGTGTGCTT
Catalase	CCAAGGGAGCTGGTGCTT
	ACGCCATCCTCAGTGTAGAA
RpL32	AAACGCGGTTCTGCATGAG
	GCCGCTTCAAGGGACAGTATCTG
Tubulin (Tub84b)	TGGGCCCGTCTGGACCACAA
	TCGCCGTCACCGGAGTCCAT

2.7 Mitochondrial respiration

Mitochondrial respiration was monitored at 25 °C using an Oxygraph-2k high resolution respirometer (OROBOROS Instruments). Standard oxygen calibration was performed before the start of every experiment. 15-20 day 5 old adult heads per replicate for each genotype was extracted using forceps and placed in 100 µl of Respiration buffer (RB) (120 mM sucrose, 50 mM KCl, 20 mM Tris-HCl, 4 mM KH₂PO₄, 2 mM MgCl₂, 1 mM EGTA and 1 g/l fatty acid-free BSA, pH 7.2). This was homogenised on ice using a pestle with 20 strokes. 1 ml of RB was added to the homogenate and passed through a 1 ml syringe with a piece of cotton wool inside to remove the debris. This was repeated with another 1 ml of RB. In total, 2.1 ml of homogenate was added into the respiratory chambers. For coupled 'state 3' assays, saturating concentrations of substrates including 10 mM glutamate, 2 mM malate, 10 mM proline and 2.5 mM ADP was added to measure Complex I linked respiration. 0.15 µM rotenone was added to inhibit Complex I and a further 10 mM succinate was added to measure Complex II linked respiration. Data acquisition and analysis were carried out using Datlab software (OROBOROS Instruments).

2.8 Statistical analysis

GraphPad Prism 9 was used to perform all statistical analyses. Climbing data was analysed using Kruskal-Wallis non-parametric test with Dunn's correction for multiple comparisons. Data are presented as mean \pm 95% confidence interval. Larval crawling, number of mitolysosomes and autolysosomes count, WB and qPCR quantification was analysed using one-way ANOVA test with Bonferroni post hoc for multiple comparisons. Data are presented as mean \pm SD. Mitochondria morphology was quantified using Chi squared test. Unpaired t-tests with Welch's correction for unequal standard deviation was used for respiratory Oroboros analysis. All statistical tests and n numbers are stated in the figure legends.

Chapter 3 – Characterisation of
mitochondrial phenotypes in a *Drosophila*
model of *C9orf72* ALS/FTD

Chapter 3. Characterisation of mitochondrial phenotypes in a *Drosophila* model of *C9orf72* ALS/FTD

Background and Aims

Drosophila melanogaster is an excellent animal model which recapitulates phenotypic features of disease well, for which expression of specific genes can be manipulated in a time and tissue specific manner using the GAL4/UAS system, facilitating the study of disease progression.

Mitochondrial dysfunction is a prevalent feature in many neurodegenerative diseases including Amyotrophic Lateral Sclerosis (ALS) and Frontotemporal Dementia (FTD). The role of mitochondria specifically in *C9orf72* ALS/FTD has been relatively understudied, especially in an *in vivo* system. Excess production of reactive oxygen species (ROS) and defective mitochondrial dynamics are common features of ALS, but it is not clear whether these phenomena are causative or a consequence of the pathogenic process. Therefore, in this chapter, using three different *Drosophila* models of *C9orf72* developed in Adrian Isaacs' lab (Mizielinska *et al.*, 2014) and Ryan West's lab (West *et al.*, 2020), I aimed to investigate and characterise mitochondrial phenotypes in the pathogenic processes of these models.

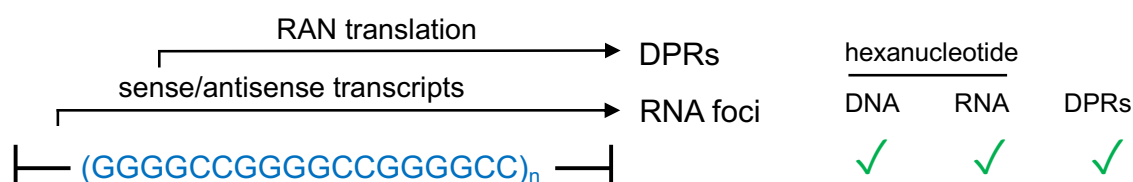
3.1 Phenotypic characterisation of *C9orf72* flies

3.1.1 Expression of G4C2x36 repeats and GR36 in the eye harbours a rough eye phenotype

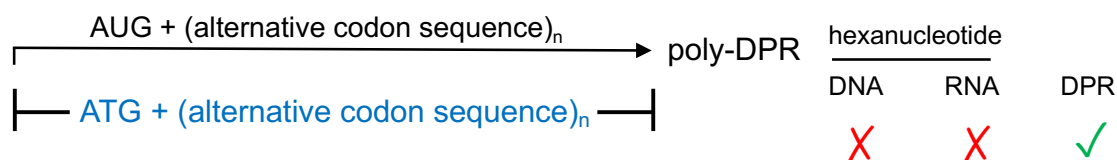
At the start of the project, I used four *Drosophila* transgenic lines from Mizielinska *et al* (2014) which carry a range of 'pure repeats' under the UAS promoter (Figure 3.1A). These included a 'pure repeats' model containing a short non-pathological GGGGCC-repeat length of 3 and a longer pathogenic 36 repeats, which will now be referred to as G4C2x3 and G4C2x36. Mizielinska *et al.* (2014) showed that only sense transcripts were detected in their models, but not antisense transcripts. RNA fluorescent *in situ* hybridisation (FISH) showed that their 103 pure repeat model was able to generate RNA foci (Mizielinska *et al.*, 2014). Of note, the study did not show any FISH performed in the G4C2x36 model used in our current study, however, since the longer repeat model was able to generate RNA foci, it is assumed that the shorter G4C2x36 model would too, but this remains to be confirmed. Moreover, poly-

GR and poly-GP is also present in the G4C2x36 model shown by immunoblot. The G4C2x3 acts as an excellent control as it has been shown that the shorter length constructs show no phenotype (no foci or DPRs) and are benign (Mizielinska *et al.*, 2014). I also made use of three ‘protein-only’ alternative codon constructs, only producing the DPRs i.e., GR36, PR36 and GA36 (Mizielinska *et al.*, 2014) (Figure 3.1A). The constructs were generated by using alternative codons to those found within the G4C2 repeat. My aim was to use these models together with the pure repeats model to disentangle the differences between repeat RNA and DPR protein toxicity, as well investigate the differences in toxicity between the individual DPRs.

A Pure repeat transgene:



Transgenes encoding DPRs without hexanucleotide DNA:



B

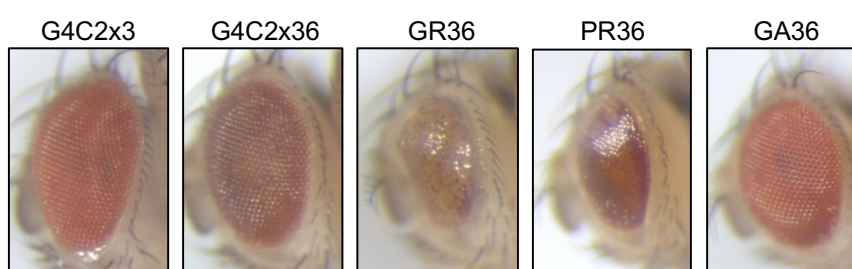


Figure 3.1 Expression of G4C2x36 and arginine-rich DPRs, poly-GR and poly-PR are toxic

(A) Schematic depicting *C9orf72* models used in this study. The pure repeats model contains the hexanucleotide repeat sequence, and produces both RNA foci and DPRs. The DPR only models use alternative codon sequences to produce only one DPR protein and lack the repeat sequence. Figure adapted from (Sharpe *et al.*, 2021). **(B)** *GMR-GAL4* was used to express G4C2x36, GR36, PR36 and GA36 in the compound eye which were compared to the G4C2x3 control (n=6 images taken, but more than 30 flies were assessed visually to confirm the phenotypes observed).

Firstly, it was important to recapitulate the phenotypes observed in (Mizielinska *et al.*, 2014) to validate the models before investigating mitochondrial function. Indeed, when I used *GMR-GAL4* to express the five transgenes in the eye, a mild rough-eye phenotype was seen in G4C2x36 compared to the G4C2x3 control (Figure 3.1B) The arginine-rich DPR constructs GR36 and PR36 developed degenerative, strong rough-eye phenotypes compared to the normal G4C2x3 control compound eye highlighting how toxic these DPRs are. In addition, the GA36 showed no overt phenotype which demonstrated that poly-GA is not toxic, at least in *Drosophila* (Figure 3.1B).

3.1.2 Pan-neuronal expression of GR36 is developmental lethal

Next, I wanted to investigate the expression of the repeats and DPRs in a neuronal context and therefore used a pan-neuronal driver, *nSyb-GAL4*. Development of larvae for the G4C2x3, G4C2x36 and GA36 was normal and no developmental delay was observed. For the arginine-containing DPRs, GR36 and PR36 were L3 developmental lethal and the GR36 larvae were also substantially thinner. For the G4C2x36 and PR36, their appearance was moderately thinner compared to the G4C2x3 control (Figure 3.2). Finally, when the G4C2x36 flies eclosed, some of the flies had a wing phenotype where the wings do not fully open. This suggests that there was some toxicity in the flies in the developmental stage that was not reflected in the appearance of the larvae. GA36 showed no overt phenotype after eclosion and appeared the same as the control, G4C2x3 (Figure 3.2).

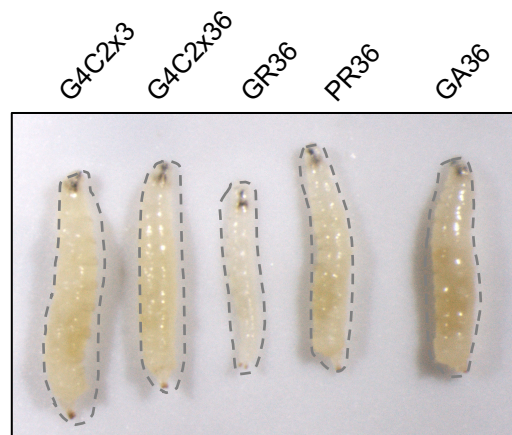


Figure 3.2 Pan-neuronal expression of arginine DPRs are developmental lethal

nSyb-GAL4 was used to express the repeats and DPRs. GR36 larvae were substantially thinner compared to the control, G4C2x3. G4C3x36 and PR36 were also moderately thinner compared to GA36 and the control, G4C2x3 (n=6 images taken, but more than 30 larvae were assessed visually to confirm the phenotypes observed).

3.2 Behavioural analysis of *C9orf72* flies

3.2.1 Pan-neuronal expression of G4C2x36 and GR36 causes a larval crawling impairment

To establish a paradigm for analysing motor function, the key clinical feature of ALS, larval crawling and adult climbing behavioural assays were carried out. Transgenes were expressed via the pan-neuronal driver *nSyb-GAL4*. For larval crawling, I counted the number of forward and backward peristalsis wave movements for a minute after 30 seconds habituation on an agar plate. There was a significant reduction in larval crawling (number of peristaltic waves) when expressing G4C2x36 compared to the control of G4C2x3. The same is observed when expressing PR36, and GR36 larvae showed an even stronger larval motor deficit. GA36 however had no larval crawling impairment (Figure 3.3A)

Adult climbing behaviour was analysed by expression of the repeats and DPRs selectively in motor neurons using *D42-GAL4*. A similar behavioural trend was observed compared to the larval crawling where a mild climbing impairment was seen with G4C2x36 and PR36, whereas GR36 exhibited an even lower climbing performance compared to the control G4C2x3. GA36 also had no climbing deficit (Figure 3.3B). These data fit with the observations published by Mizielinska *et al.* (2014) where they have observed that the arginine-rich DPRs are the most toxic species in flies.

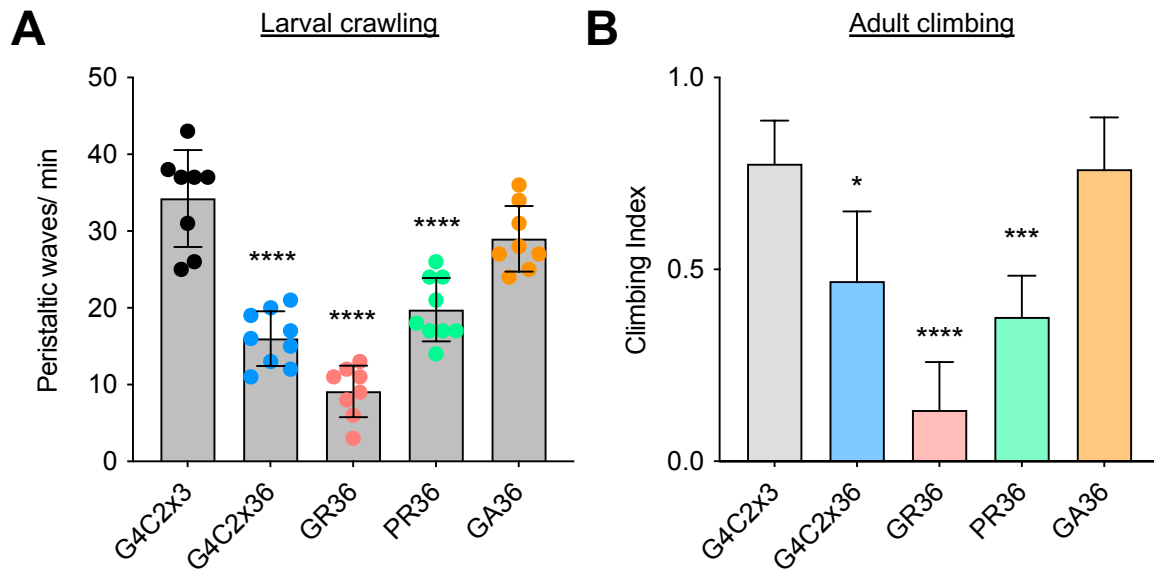


Figure 3.3 Strong motor impairment was observed for arginine-rich *C9orf72* *Drosophila* models

(A) Expression of the repeats and DPRs was achieved using a pan-neuronal driver, *nSyb-GAL4* and the number of peristalsis waves were recorded. Statistical analysis was performed using one-way ANOVA with Bonferroni multiple comparison test: **** $p < 0.0001$ compared to control G4C2x3, chart shows mean \pm SD, $n = 8-10$. **(B)** Adult climbing ability was assessed by expression in motor neurons using *D42-GAL4*. Statistical analysis was performed using Kruskal-Wallis non parametric test with Dunn's correction: * $p < 0.05$, *** $p < 0.001$, **** $p < 0.0001$, compared to control G4C2x3. Chart shows mean \pm 95% CI, $n = 60-100$ flies.

3.2.2 Pan-neuronal expression of GR1000 shows a progressive age-related climbing deficit

During my investigation, more *Drosophila* transgenic models have been generated to dissect the molecular mechanisms contributing to neurodegeneration in ALS/FTD. West *et al.* (2020) generated novel models using physiologically relevant repeat length DPRs to represent the known pathological lengths in humans. They generated transgenic flies expressing DPRs with more than 1000 repeats in length and showed that these animals exhibit age related motor decline as well as neurodegeneration. DPR constructs were generated using semi-randomised alternative codons with an EGFP tag. Moreover, West *et al.* (2020) demonstrated that the EGFP tag does not show any effect on DPR localisation or pathology. I utilised their UAS-GR1000-EGFP fly line to complement my studies with my GR36 data. For simplicity, this line will be referred to simply as GR1000.

Using the same approach, I used *nSyb-GAL4* to express GR1000 pan-neuronally and observed no developmental phenotypes. Early in life, up to 2 days post eclosion, GR1000 showed no climbing impairment compared to aged-matched GFP controls (Figure 3.4). However, a significant decline in motor function from 10 to 20 days post eclosion was observed. At day 20, the flies could not climb at all (Figure 3.4). This is in line with West *et al.* (2020). Although they used a different assay to monitor motor function by tracking climbing speed instead, they observed no variance to wild type at 7 days, after which a significant decline in motor function was seen from 7 to 28 days post eclosion.

In summary, the strong phenotypes observed and its reproducibility in the *C9orf72* flies from Mizielska *et al.* (2014) and West *et al.* (2020) provide good models to investigate the role of mitochondria in ALS/FTD pathogenesis.

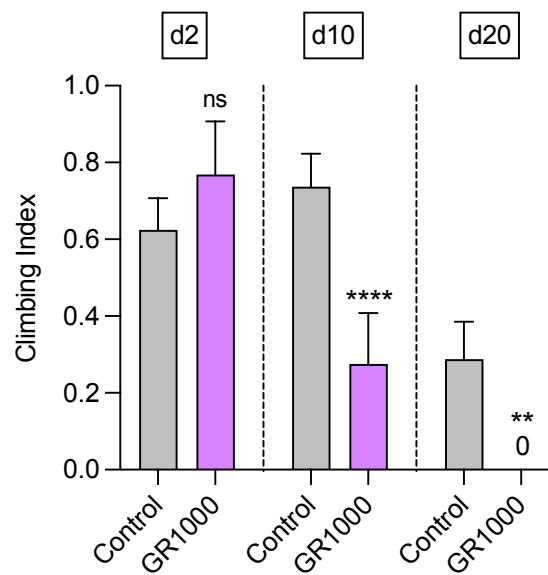


Figure 3.4 GR1000 flies exhibit an age-related motor impairment

Adult climbing ability was assessed by expression in neurons using *nSyb-GAL4* at day 2, day 10 and day 20. Statistical analysis was performed using Kruskal-Wallis non parametric test with Dunn's correction: ns = non significant, ** $p < 0.01$, **** $p < 0.0001$, compared to control (*nSyb>mito.GFP*). Chart shows mean \pm 95% CI, $n = 60-100$ flies.

3.3 Mitochondrial morphology in *C9orf72* flies

As I established the utility of the various fly lines in recapitulating aspects of the pathophysiology of *C9orf72* ALS/FTD, I next aimed to explore the mechanisms of mitochondrial involvement in the disease. Mitochondria are dynamic and undergo fission and fusion events and this is known to occur in response to changes in ROS levels and oxidative stress as well as other physiological stimuli. There have been many reports that implicate impaired mitochondrial dynamics in the aetiology of ALS (Smith *et al.*, 2019). Onesto *et al.* (2016) observed mitochondrial fragmentation even though there appeared to be an increase in Mfn1 levels in *C9orf72* ALS/FTD patient fibroblasts. Moreover, transmission electron microscopy (TEM) revealed swollen mitochondria as well as abnormalities in cristae structure in an iPSC model of *C9orf72* (Dafinca *et al.*, 2016).

To investigate mitochondrial morphology *in vivo*, the repeats and DPR-only transgenes were expressed and mito.GFP was used to label the mitochondria. I analysed two different tissues, the larval epidermal cells and larval CNS, and used two different drivers (*armadillo-GAL4* and *nSyb-GAL4*) to overexpress mito.GFP and the transgenes to monitor morphology changes.

3.3.1 No observable differences in mitochondrial morphology in G4C2x36 and GR36 larval epidermal cells

Firstly, I used a ubiquitous driver, *armadillo-GAL4* to overexpress mito.GFP and the transgenes in the larval epidermal cells. This was analysed first as it is a good tissue to observe an extensive mitochondrial network. In G4C2x3 control samples, mitochondria are typically a mixture of short round and long tubular morphologies (Figure 3.5), which was also seen for all the other genotypes; therefore no observable phenotype could be detected. A limitation that needs to be considered is that *armadillo-GAL4* is a mild, ubiquitous driver and no larval crawling phenotypes were observed (data not shown); contrary to that seen when expressing using the pan-neuronal driver; hence, the driver may not be strong enough to show any mitochondrial phenotypes in this particular tissue.

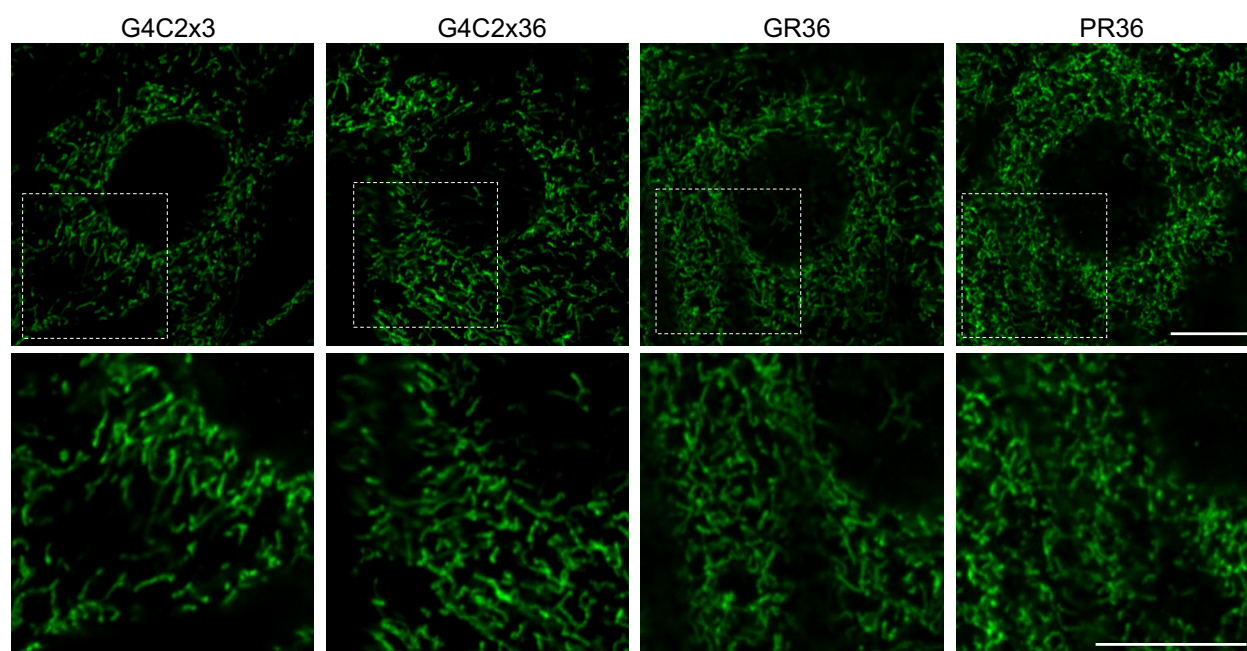


Figure 3.5 Mitochondrial morphology differences were not observed in G4C2x36, GR36 and PR36 larval epidermal cells

Confocal images of larval epidermal cells labelling mitochondria using overexpression of mito.GFP with G4C2x36, GR36 and PR36 compared to control, G4C2x3. Dotted box shows region zoomed in on the bottom panel. Both low and high magnification scale bar = 10 μ m, n=8.

3.3.2 Elongated, hyperfused mitochondria were observed with pan-neuronal expression in the larval ventral ganglion of G4C2x36 and GR36

Next, I used a pan-neuronal driver, *nSyb-GAL4* to overexpress the transgenes in the larval brain. To be consistent, an equivalent group of cells in the middle of the ventral ganglion were analysed (Figure 3.6A). In G4C2x3 control samples, mitochondria are typically a mixture of short, round and long tubular morphologies. GA36 showed no observable changes in mitochondrial morphology and resembled the control (Figure 3.6B). However, for G4C2x36, GR36 and PR36, mitochondria were more elongated, hyperfused and therefore often seemed clumped (Figure 3.6B). I quantified these observations using a scoring system to characterise the overall mitochondrial morphology for each cell – fragmented, tubular for WT appearance, fused and hyperfused. The quantification supported my qualitative observations where G4C2x36 as well as the arginine-rich DPRs have more elongated and hyperfused mitochondria (Figure 3.6C). These observations suggest that there is an alteration in mitochondrial dynamics in neuronal cells.

(Disclaimer note: All of the mitochondrial morphology experiments in Chapters 3 and 4 were performed in one big experiment, therefore the quantification for the controls is the same, however, different representative images are chosen for different figures. The graphs are separated for ease of reading and flow of the thesis.)

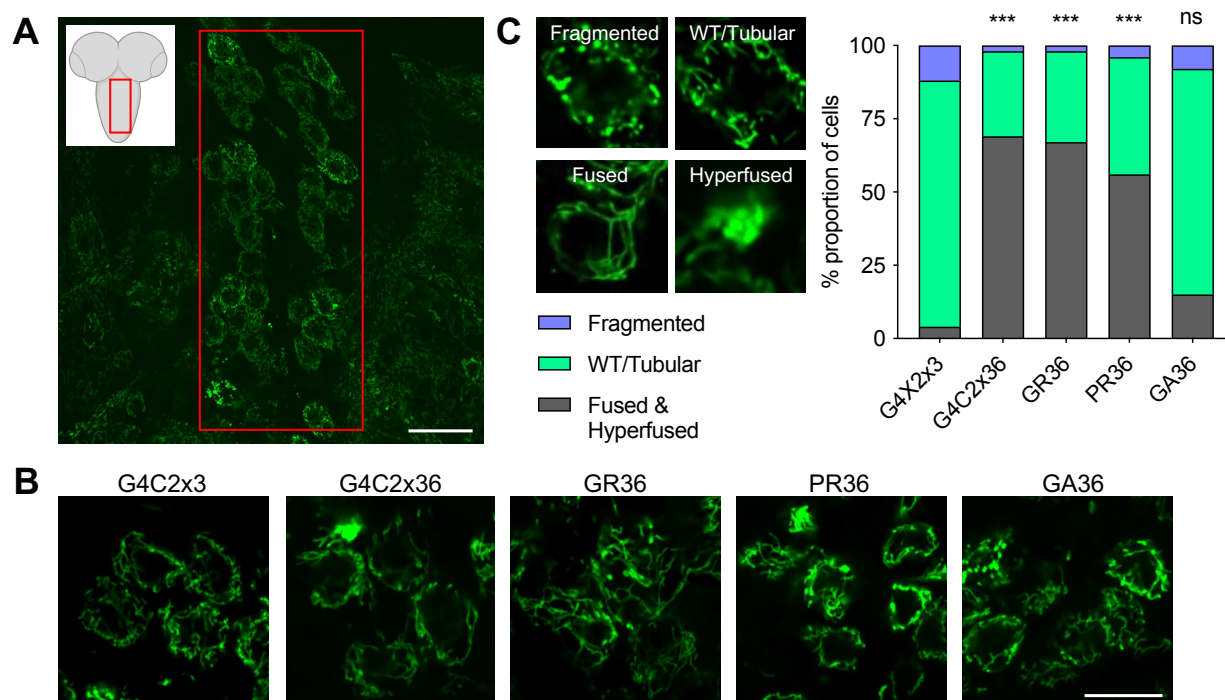


Figure 3.6 Mitochondria are hyperfused when overexpressing 36 repeats and arginine DPRs in larval ventral ganglion

(A) Representative confocal images of the ventral ganglion of larval brains and red box shows region of interest chosen for each brain, scale bar = 50 μ m. (B) Mitochondria are labelled with mito.GFP, using pan-neuronal driver *nSyb-GAL4*, co-expressing G4C2x36, GR36, PR36 and GA36, comparing the morphology with G4C2x3, scale bar = 10 μ m. (C) A scoring system was used to characterise the mitochondrial morphology for each cell – fragmented, tubular for WT appearance, fused and hyperfused. Statistical analysis was performed using Chi squared test: *** $p < 0.001$, ns = not significant, n=8-10.

3.4 Mitochondrial respiration is compromised in *C9orf72* flies

3.4.1 G4C2x36 flies have a reduction in Complex I and Complex II linked respiration

Defective mitochondrial respiration, ATP production and oxidative stress are prevalent features of many neurodegenerative diseases including *C9orf72* ALS/FTD. Mehta *et al.* (2021) investigated cellular energetics in *C9orf72* iPSC-derived motor neurons and found impaired basal and maximal mitochondrial respiration which implicates abnormalities in the ETC. Validation of their RNA-seq hits using qRT-PCR and immunoblot confirmed dysregulation of mostly complex I and IV. Importantly, examination of human *C9orf72* post-mortem spinal cord

tissue using RNA *in situ* hybridisation corroborated their result by showing reduced expression of complexes I and IV in ventral horn spinal motor neurons. Poly-GR itself may be important linking in mitochondrial dysfunction and oxidative stress. Lopez-Gonzalez *et al.* (2016) performed an interactome analysis with GR80 expressed in HEK293 cells compared to control where they identified many mitochondrial ribosomal proteins which are required for the translation of the mitochondrial transcripts. In a mouse model expressing GR80, Choi *et al.* (2019) found increased DNA damage, oxidative stress and decreased activities of mitochondrial complexes I and V. Poly-GR was also shown to bind to the mitochondrial complex V component ATP5A1 (Choi *et al.*, 2019).

To investigate the metabolic consequences of expression of G4C2x36, high-resolution respiratory was performed on day 5 fly heads by Oroboros. Specifically, we measured complex I- and complex II-linked oxygen consumption. For complex I-linked respiration, glycine, proline and malate were used as substrates. For complex II-linked respiration, succinate was used as the substrate, and rotenone was used as a complex I inhibitor. Compared to other standard Oroboros protocols, proline was used as it has been shown to enhance respiration in insects Teulier *et al* (2016). Interestingly, both complex I and complex II-linked respiration was reduced in G4C2x36 compared to G4C2x3 control flies (Figure 3.7). Since I have only optimised this assay with adult flies, I was unable to perform this with the GR36 flies as they are developmental lethal.

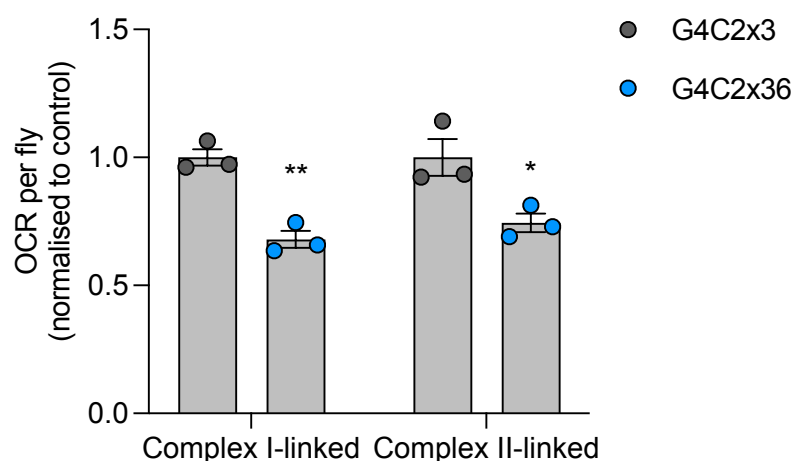


Figure 3.7 Pan-neuronal expression of G4C2x36 leads to an impaired respiration

Oxygen consumption rate (OCR) of complex I and complex II in day 5 fly heads with pan-neuronal expression of G4C2x3 and G4C2x36 using *nSyb-GAL4*. Results are presented as mean \pm SEM and statistical tests were performed using unpaired t-tests with Welch's correction for unequal standard deviation where * $p < 0.05$, ** $p < 0.01$. Data points indicate individual runs each containing 20 fly heads ($n=3$ runs).

3.5 Disrupted mitochondrial quality control in *C9orf72* flies

3.5.1 Reduction in mitophagy is observed in G4C2x36 and GR36 flies using the mito-QC reporter

Impaired mitophagy has also been implicated in many neurodegenerative diseases including ALS. I wanted to use our *Drosophila* mitophagy reporter, mito-QC (Lee *et al.*, 2018), to observe mitophagy *in vivo* in the *C9orf72* models (Figure 3.8B). Briefly, the mito-QC mitophagy reporter uses a tandem GFP-mCherry fusion protein targeted to the outer mitochondrial membrane (OMM). Mitolysosomes are marked when GFP is quenched by the acidic environment but mCherry is still able to fluoresce, resulting in 'red-only' puncta (Lee *et al.*, 2018). I analysed mitophagy in the larval brain by overexpressing mito-QC under *C9orf72* conditions with the pan-neuronal driver *nSyb-GAL4*.

An equivalent group of motor neurons in the middle of the ventral ganglion was analysed and quantified across the *C9orf72* models (Figure 3.6A). For G4C2x36, GR36 and PR36, the mitochondria appear to be more hyperfused, with a clumped appearance, as observed previously (Figure 3.6). Of note, the GR36 has smaller cells as well which is also reflected in the thin nature of the larvae (Figure 3.2). In conjunction, there are significantly fewer 'red-only' mitolysosomes under these conditions compared to the controls G4C2x3 (Figure 3.8A) quantified using IMARIS (Figure 3.8C). Again, the mitochondrial network in the GA36 was similar to control, G4C2x3, and there were similar numbers of mitolysosomes present as well (Figure 3.8A,C). In summary, there is less mitophagy when expressing the repeats and arginine-rich DPRs compared to controls. This is an interesting novel result as mitophagy *in vivo* using *C9orf72* *Drosophila* models have yet to be explored.

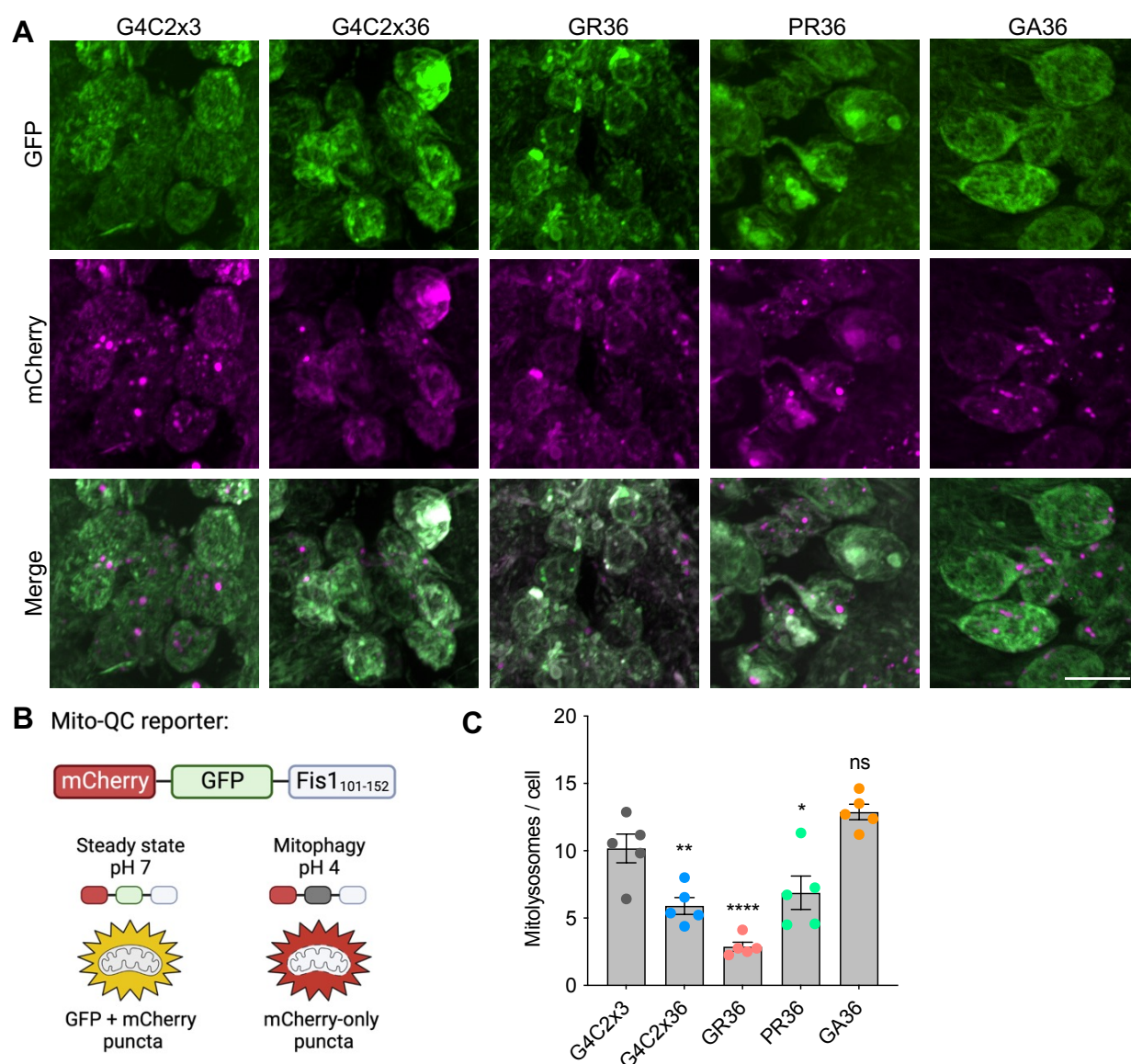


Figure 3.8 G4C2x36 and GR36 have reduced levels of mitophagy

(A) Confocal microscopy images of the mito-QC reporter in *C9orf72* conditions using pan-neuronal driver *nSyb-GAL4* expressed in larval ventral ganglion. Mitolysosomes are evident as GFP-negative, mCherry-positive red only puncta. Scale bar = 10 μ m. **(B)** Schematic of mito-QC reporter from Lee *et al.* (2018) which consists of a tandem-tagged mCherry-GFP fusion protein which is targeted to the OMM by the C-terminus of Fis1. Briefly, at normal steady states, cytosolic mitochondria, both mCherry and GFP fluoresce. However, under mitophagy when damaged mitochondria are engulfed in lysosomes, the acidic environment quenches the GFP, resulting in 'mCherry-only' puncta called mitolysosomes. **(C)** Quantification of number of mitolysosomes per cell using IMARIS. Statistical analysis was performed using one-way ANOVA with Bonferroni multiple comparison test: * $p < 0.05$, ** $p < 0.01$, **** $p < 0.0001$, ns = not significant, mean \pm SD, $n = 5$.

3.5.2 Autophagy is perturbed when overexpressing G4C2x36 and poly-GR36

After investigating mitophagy, I wanted to explore whether general autophagy was also perturbed. However, during my investigation, Cunningham *et al* (2020) had similar questions and showed that expression of expanded G4C2 repeats is sufficient to disrupt autophagy in many *Drosophila* models of *C9orf72*, leading to an accumulation of p62 and ubiquitinated protein aggregates. Nevertheless, it was important to assess whether the results were recapitulated in our model system. Using a tandem tagged GFP-mCherry-Atg8a reporter (Figure 3.9B), I aimed to monitor autophagic flux. The Atg8 family is represented by two members in *Drosophila* where Atg8a has been shown to be required for the formation of autophagosomes and Atg8b is largely restricted to the male germline (Scott *et al*, 2007). The reporter labels non-acidified autophagic compartments (phagophore and autophagosomes) with both GFP and mCherry signals (green and red). Fusion with acidic late endosomes or lysosomes will cause the GFP signal to quench, hence, mCherry signal remains and is detectable as red only puncta. Most cells undergoing autophagy will display a combination of both green and red autophagosomes and red only autolysosomes which has been characterised by Juhasz and colleagues (Mauvezin *et al*, 2014; Nagy *et al*, 2015).

Firstly, I overexpressed the GFP-mCherry-Atg8a reporter with the *C9orf72* conditions, as well as adding an additional *Atg5* RNAi condition to verify that the assay was performing appropriately. Using *Atg5* RNAi, I would expect to see an impairment in autophagy and therefore a reduction in the number of autolysosomes, which is indeed shown in Figure 3.9A,C, validating the assay conditions. However, surprisingly, there was a lack of GFP puncta in the larval brain. There were very few studies in the literature which use this reporter in *Drosophila* larval brains, therefore it was hard to understand why this is the case. Despite this limitation of not being able to quantify autophagosomes (GFP and mCherry colocalization), I was still able to quantify mCherry-positive puncta which should equate to the number of autolysosomes. There was a significant reduction in the number of autolysosomes per cell in G4C2x36 and GR36 conditions compared to the G4C2x3 control (Figure 3.9A, C). Thus, these results corroborate findings from Cunningham *et al.* (2020) to suggest that autophagy is perturbed, and further support my previous findings on mitophagy.

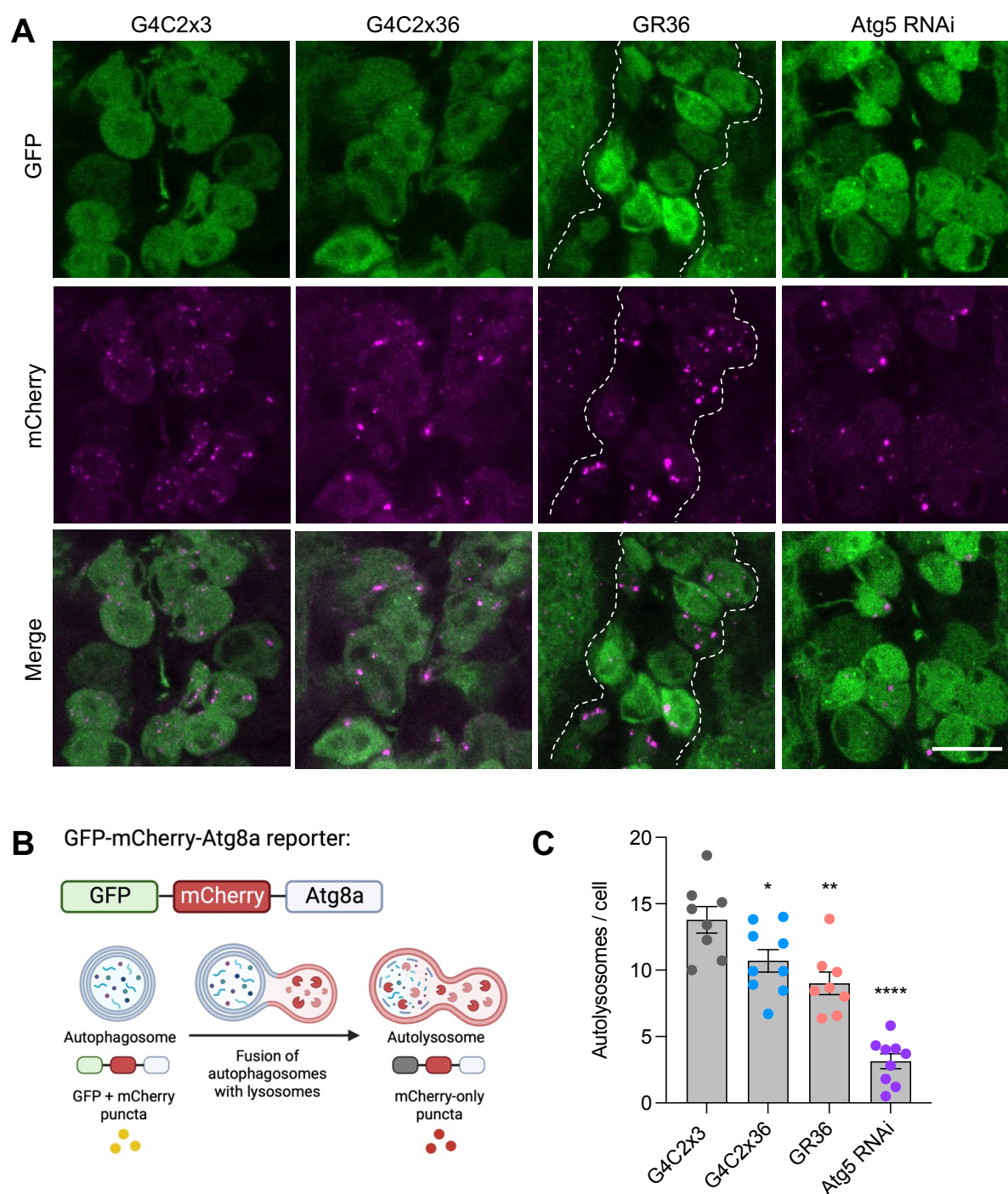


Figure 3.9 G4C2x36 and GR36 exhibit perturbed autophagy

(A) The GFP-mCherry-Atg8a reporter with *C9orf72* transgenes was co-expressed in the larval brain with a pan-neuronal *nSyb-GAL4* driver. Only the motor neurons were used to monitor autophagy marked by the boundaries indicated with the dotted white line, scale bar = 10 μ m. (B) A schematic depicting the GFP-Cherry-Atg8a reporter from Nezis *et al* (2010). Briefly, tandem-tagged Atg8a protein emits GFP and mCherry fluorescence in nonacidic structures such as autophagosomes. Under acidic conditions, the GFP is quenched and mCherry-only puncta labelling the autolysosomes are observed. (C) Only mCherry positive puncta was quantified using a FIJI Image Objects Counter plugin. Data is represented mean \pm SD, statistical analysis was performed using one-way ANOVA with Bonferroni

multiple comparison test vs G4C2x3 control with significance indicated as * $p < 0.05$, ** $p < 0.01$ and **** $p < 0.0001$, $n = 8-10$.

3.5.3 Increased Ref(2)P and reduced Atg8a-II levels were observed with pan-neuronal expression of G4C2x36

To corroborate/substantiate the reporter assay results, I used other autophagy assays to develop a more complete picture regarding autophagic flux. Firstly, I measured the levels of the p62 homologue, Ref(2)P, in G4C2x36 flies. Ref(2)P is an autophagy adaptor that can interact with ubiquitin conjugated to a target protein as well as LC3/GABARAP on autophagosomes. With pan-neuronal expression of the G4C3x36 repeats using *nSyb-GAL4* at day 5, I extracted the heads and performed a western blot to measure Ref(2)P/p62 levels (Figure 3.10A). Although there was a trend towards an increase, this did not reach statistical significance (Figure 3.10B).

Moreover, I used an anti-GABARAP (subfamily of Atg8) antibody where the processed protein (lipid conjugated) Atg8-II migrates at a faster rate than the unprocessed (non-lipidated form) and can accumulate to high levels in cells with high rates of autophagy. However, in my results, there appears to be a reduction in the lipidated Atg8a-II form in G4C2x36 compared to the control, G4C2x3 (Figure 3.10A). In brain tissues, the non-lipidated form is highly expressed (Klionsky *et al.*, 2021) and therefore it was not possible to quantify the lipidated form. A decrease in Atg8a-II levels relative to the tubulin loading control may indicate a defect in autophagosome induction and/or in Atg8a lipidation (Nagy *et al.*, 2015). These findings need to be interpreted with caution as the current experiment was conducted without including lysosomal inhibitors in the analysis and therefore can lead to an incorrect interpretation of the result. Nevertheless, my results suggest that under *C9orf72* conditions, autophagic flux is perturbed.

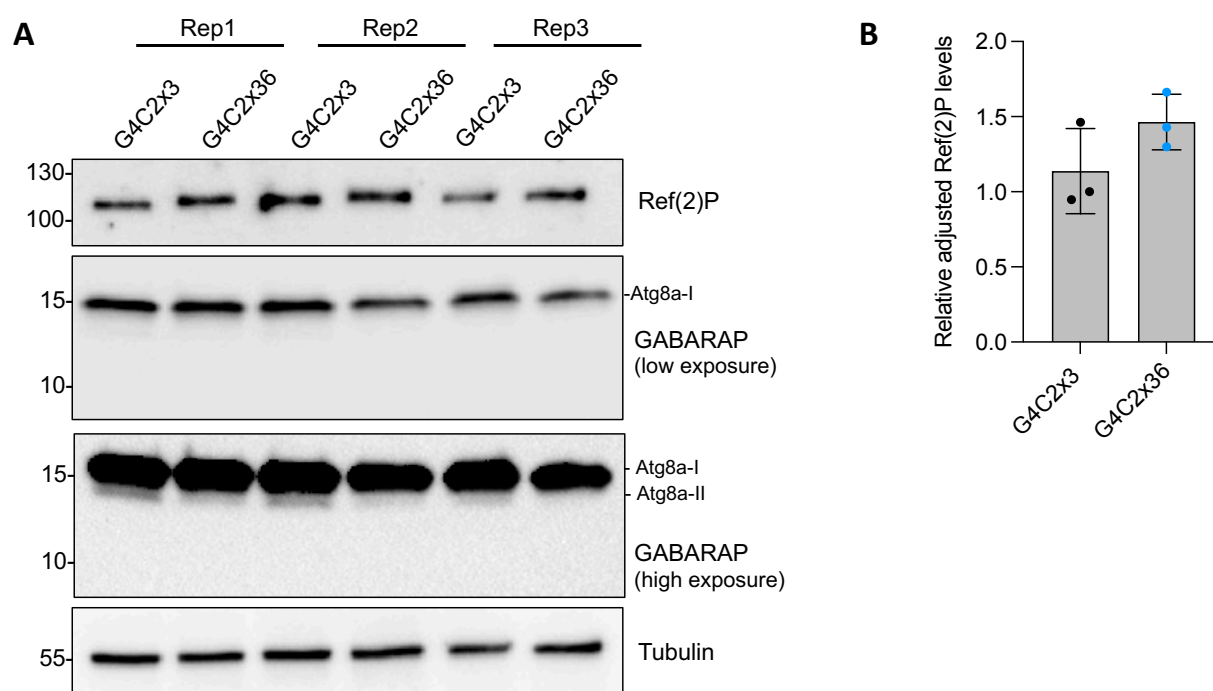


Figure 3.10 Immunoblotting levels of Ref(2)P/p62 and GABARAP in G4C2x36 flies

(A) Immunoblotting of Ref(2)P/p62 and GABARAP in G4C2x3 and G4C2x36 day 5 fly brains (pan-neuronal expression *with nSyb-GAL4*). Tubulin was used as a loading control. A low and high exposure for GABARAP is depicted, where high exposure shows the lipidated Atg8a-II clearer. **(B)** Quantification of Ref(2)P levels (n=3 reps (replicates)), statistical analysis was performed using unpaired t-test with Welch's corrections p=0.181.

3.6 Increased oxidative stress in *C9orf72*

3.6.1 Increased mitochondrial ROS was observed in G4C2x36 and GR36

Increased levels of ROS and ROS-associated damage have been widely reported in ALS (Smith *et al.*, 2019). Lopez-Gonzalez *et al.* (2016) has previously reported an increase in DNA damage, oxidative stress and mitochondrial membrane potential in iPSC-derived *C9orf72* motor neurons. In a mouse model expressing GR80, Choi *et al.* (2019) found increased DNA damage, oxidative stress and decreased activities of mitochondrial complexes I and V.

To investigate specifically the relation between mitochondria and oxidative stress in *C9orf72*, I used a mito-roGFP2-Orp1 reporter fly line to assess the production of mitochondrial ROS by hydrogen peroxide (Figure 3.11A). Hydrogen peroxide causes conformational changes to the oxidant receptor peroxidase (Orp1) which is fused to a redox-sensitive green

fluorescent protein (roGFP2) (Gutscher *et al*, 2009; Albrecht *et al*, 2011). Firstly, I confirmed the reporter responded as expected, by exogenously applying a reductant (DTT) and, separately, an oxidant (DA). After calibration of the biosensor response, I overexpressed the *C9orf72* transgenes along with the reporter pan-neuronally in the larval CNS. An increase in mitochondrial H_2O_2 was observed in both G4C2x36 and GR36 compared to G4C2x3 control (Figure 3.11B,C).

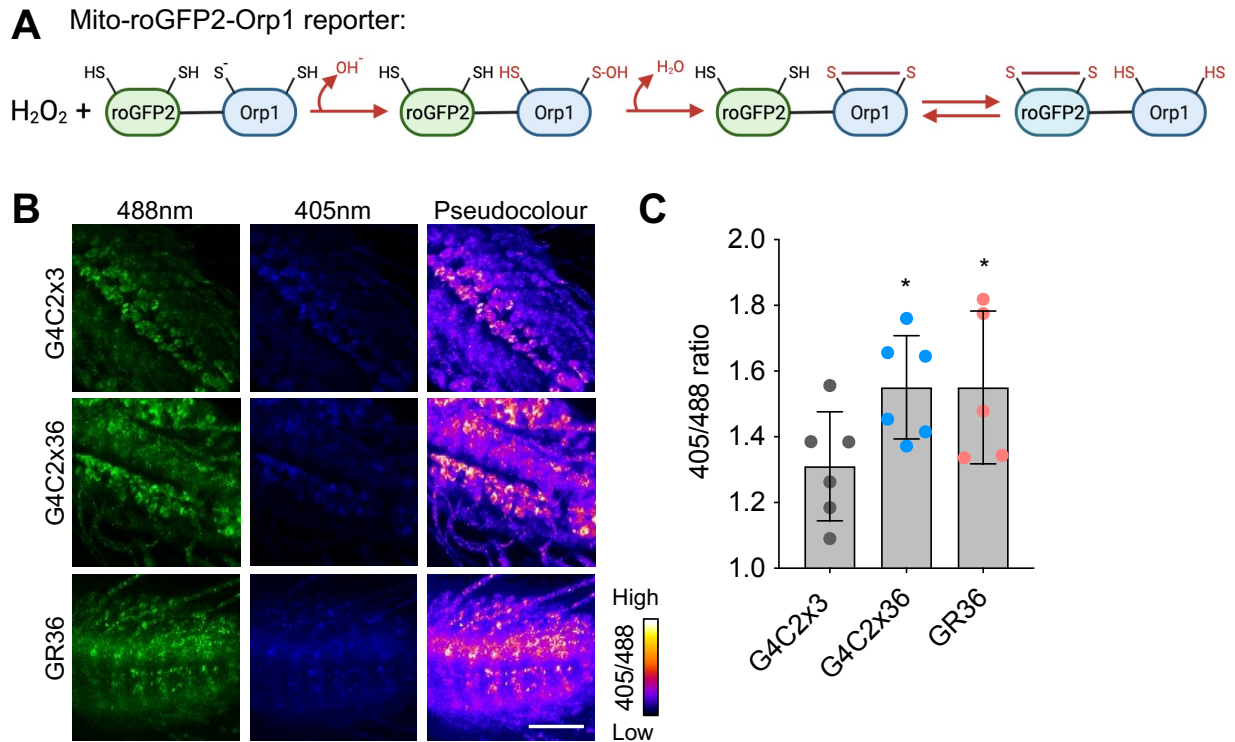


Figure 3.11 G4C2x36 and GR36 show increased mitochondrial ROS

(A) Schematic depicting the H_2O_2 biosensing flies - mito-roGFP2-Orp1 reporter from Albrecht *et al.* (2011). Briefly Orp1, a thiol peroxidase, mediates roGFP2 oxidation by H_2O_2 which leads to a shift in its excitation maxima of roGFP2 from 488 to 405. **(B)** The mito-roGFP2-Orp1 reporter was co-expressed with *C9orf72* transgenes using *nSyb-GAL4*, a pan-neuronal driver to assess mitochondrial ROS in the larval brain. Pseudocolour representative images of the larval brain is shown where an increase in mitoROS is evident in G4C2x36 and GR36 compared to G4C2x3 control, scale bar = 50 μm . **(C)** Quantification of 405/488 ratio, statistical analysis was performed using one-way ANOVA with Bonferroni multiple comparison test with significance indicated as * $p < 0.05$, $n = 6$.

3.6.2 Increased MitoSOX staining was observed in GR1000 flies

Mitochondrial (and cytosolic) superoxide indicators are hard to use for larval brains as the tissue is too thick for the dyes to penetrate well. However, for the GR1000 flies, we were able to use MitoSOX instead to measure mitochondrial superoxide. In collaboration with Maddy Twyning in the lab, we dissected out the adult brains at day 15 and observed an increase in MitoSOX intensity in GR1000 flies compared to control (Figure 3.12). It will be interesting to investigate the cross talk between oxidative stress and other pathogenic mechanism as well as attempt to rescue the phenotypes with genetic manipulations with various antioxidants to determine the specific pathways and compartments involved with all our *C9orf72* models.

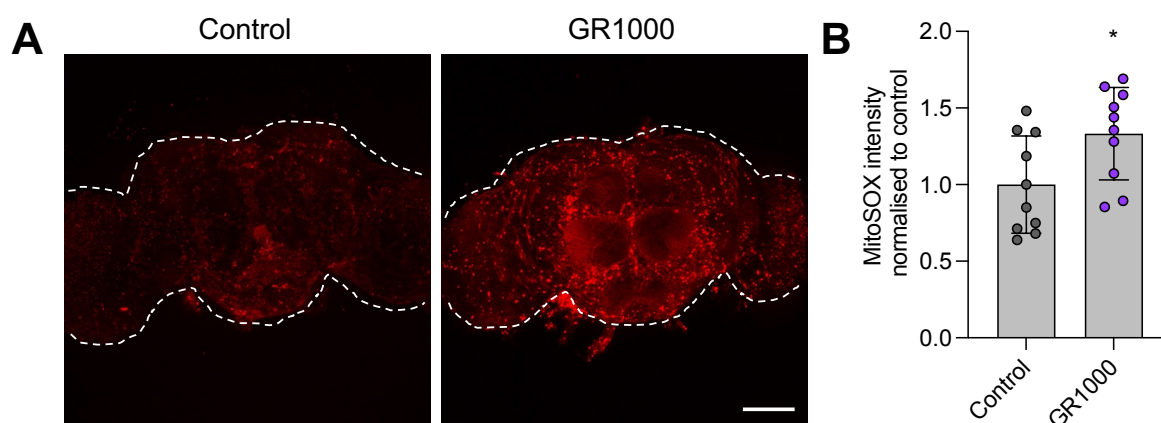


Figure 3.12 MitoSOX staining in GR1000 is increased

(A) Pan-neuronal expression of GR1000 and control, mito.GFP with *nSyb-GAL4*. MitoSOX intensity was measured at day 15. White dotted line indicates adult brain boundaries, scale bar = 100 μ m. **(B)** Statistical analysis was performed using two-tailed t-test with Welch's corrections where * $p < 0.05$, $n = 10$.

3.7 Discussion

Mitochondrial dysfunction has been linked to many neurodegenerative diseases including *C9orf72* ALS/FTD. In this chapter, I aimed to analyse different aspects of mitochondrial function to investigate its potential role in initiating disease pathogenesis by utilising different *Drosophila* models of *C9orf72* developed in Adrian Isaac's lab (Mizielinska *et al.*, 2014) and Ryan West's lab (West *et al.*, 2020).

Basic characterisation of *C9orf72* *Drosophila* toolset

It is important to remember that *Drosophila melanogaster* does not have a *C9orf72* ortholog and therefore we are not able to investigate any loss of function mechanisms. We can however explore the toxicity associated with the gain of function with either the RNA and/or the DPRs. The pure repeats model contains the G4C2 sequence and produces both repetitive RNA and the five DPRs. Before using the G4C2x3 and G4C2x36 flies to investigate mitochondrial dysfunction, it was essential to recapitulate findings from the original publication as the basis for follow-on work. Transgene expression within the *Drosophila* compound eye has been used frequently to assess genetic interactions and perform genome-wide modifier screens. Expressing transgenes in the eye also allows the investigation of toxicity that would be lethal if expressed elsewhere, such as pan-neuronally or ubiquitously. Indeed, when *GMR-GAL4* was used to express G4C2x36, there was a rough eye phenotype compared to the G4C2x3 control which was also observed in Mizielinska *et al.* (2014). Moreover, increasing the length to 103 repeats produced a more severe phenotype (Mizielinska *et al.*, 2014) which suggests that there is a length-dependent toxicity. I also observed a larval locomotor deficit as well as adult climbing impairment when expressing G4C2x36 pan-neuronally compared to G4C2x3 control. Mizielinska *et al.* (2014) used adult-only pan-neuronal expression of the repeats to show a reduced lifespan as well as an impairment in climbing. I chose not to use the gene-switch GAL4 system as I wanted to recapitulate the presumed life-long expression of the G4C2 repeats therefore expression of the repeats/DPRs from development was important for my aim.

Similar observations were made in other studies which also did not use the gene-switch GAL4 system. Freibaum *et al.* (2015) generated pure repeat models with lengths of 8, 28 and 58 copies. They found a length and dose dependent rough eye phenotype when expressing these constructs in the *Drosophila* eye using *GMR-GAL4*. Moreover, toxicity was also observed when these repeats were expressed in other tissues. Expression of two copies

of G4C2x58 in motor neurons led to small larvae with an impaired locomotor activity using a motor neuron driver *OK371-GAL4*. This result is similar to the observations I have made with the G4C2x36 model. Xu *et al.* (2013) also generated a pure repeats model with 30 repeats with an EGFP tag. They observed progressive neurodegeneration in the eye (using *GMR-GAL4*) and motor neurons (using *OK371-GAL4*) with age. At day 28, the eye phenotype progressively worsened (using *GMR-GAL4*) and a reduction in locomotor activity was observed (using *OK371-GAL4*). Freibaum *et al.* (2015) went on to perform a genetic modifier screen in the *Drosophila* eye and found that the expansion compromises nucleocytoplasmic transport and Xu *et al.* (2013) found an interaction with RNA binding protein, Pur-alpha.

Although the repeats present a good model to study *C9orf72* gain of toxicity mechanisms, it is not possible to distinguish between the relative contribution of either RNA or DPR toxicity. To overcome the limitations of pure repeat models, DPR-only fly models have been developed to isolate DPR toxicity. Arginine-rich dipeptide repeat proteins have been shown to be the most toxic species in multiple model systems (Kwon *et al.*, 2014; Wen *et al.*, 2014; Jovicic *et al.*, 2015) and cause toxicity via a range of mechanisms as reviewed by Sharpe *et al.* (2021) including nucleocytoplasmic transport (Freibaum *et al.*, 2015; Jovicic *et al.*, 2015; Zhang *et al.*, 2015), DNA damage (Lopez-Gonzalez *et al.*, 2016) and stress granule dysfunction (Lee *et al.*, 2016; Boeynaems *et al.*, 2017). As reported by Mizielinska *et al.* (2014), I was able to recapitulate their basic characterisation results and also observed a rough eye phenotype using *GMR-GAL4* and a larval crawling locomotor deficit when expressed pan-neuronally with *nSyb-GAL4*. West *et al.* (2020) developed a novel fly model expressing GR at a length of 1000 repeats which represents a more physiologically relevant model to use as the repeat length in patients ranges from more than 20 to thousands of repeats. These flies present less acute toxicity and displays a more progressive age-related neurodegeneration. When expressed pan-neuronally, I was able to see a climbing deficit at day 10. To summarise, I have chosen a variety of suitable tools to use and managed to recapitulate previous findings which I will use to study mitochondrial dysfunction in *C9orf72* ALS/FTD.

Mitochondrial morphology

There are a large variety of assays to study mitochondrial form and function in detail in live and fixed *Drosophila* tissue (Wang *et al.*, 2016b; Sen & Cox, 2017; Anoar *et al.*, 2021). Some examples of them are general-purpose dyes such as the cell-permeant mitochondrion-selective MitoTracker Green to visualise mitochondria and observe mitochondrial mass (Rana

et al, 2017). A limitation that I have encountered throughout my investigation is that since my predominant tissue of interest is the larval VNC, it is very hard to optimise and use dyes as the tissue is extremely thick and hard for the dyes to penetrate through. However, I was able to use fluorescent genetically encoded probes such as UAS-mito.GFP to express in specific tissues using cell-type specific GAL4 drivers to monitor mitochondrial morphology. There is some evidence in the literature that suggests differences in mitochondrial morphology however, the results are not consistent. For example, Onesto *et al.* (2016) used *C9orf72* human fibroblasts grown in galactose media and found a mix population of elongated, short and round shaped mitochondria whereas mutant TDP-43 fibroblasts showed a much stronger phenotype with a fragmented mitochondria network. However, Dafinca *et al.* (2016) used transmission electron microscopy (TEM) and observed swollen mitochondria as well as abnormalities in cristae structure in a *C9orf72* iPSC model. Moreover, mitochondria in primary cortical neurons isolated from mice expressing 80 GR repeats, are also shorter in length and less motile compared to mitochondria in wild-type neurons. Differences in morphology between the studies are likely due to the different systems used as well as cell types. For example, neurons are more susceptible to mitochondrial dysfunction due to their high energetic demands. Also, they have long axonal processes and are long-lived post-mitotic cells therefore any defective organelles by cell division cannot be diluted out (Itoh *et al*, 2013; Anoar *et al.*, 2021).

In my study, at first, I did not observe any differences in mitochondrial morphology in the larval epidermal cells between all the *C9orf72* genotypes. However, in larval brains with pan-neuronal expression of the repeats and DPRs, I observed hyperfused, elongated mitochondria in G4C2x36, GR36 and PR36. There are two main differences between these two assays. Firstly, I used *armadillo-GAL4* to drive expression in the epidermal cells, but this is a weak ubiquitous driver and therefore it may not be strong enough to cause a phenotype. Secondly, as previously discussed, differences in morphology could be due to the different cell types (epidermal cells vs brain) used as well. Excess fusion between mitochondria may serve as a stress response to mitigate the effects of the damage through exchange of proteins and lipids with other healthy mitochondria and therefore maximise oxidative capacity in response to toxic stress (Youle & van der Bliek, 2012).

Mitochondrial respiration

Other assays that can be used to study mitochondrial biology and physiology include measuring oxygen consumption using a high-resolution Oxygraph-2k, Oroboros. It is a very

powerful technique which can also be used to measure mitochondrial membrane potential, ATP production as well as ROS production. In a mouse model expressing GR80, Choi *et al.* (2019) found increased DNA damage, oxidative stress and decreased activities of mitochondrial complexes I and V. Poly-GR was also shown to bind to the mitochondrial complex V component ATP5A1, which enhanced its ubiquitination and degradation which is consistent with findings showing reduced ATP5A1 protein levels in both the mouse model and patient brains. Moreover, Li *et al.* (2020) observed an increase in oxidative stress, mitochondrial membrane potential and ATP production in their Flag-GR80 *Drosophila* model when expressed in the muscle. Interestingly, they saw that complex I activity was elevated, however Complex II-V were unaffected. In contrast, I found a reduction in Complex I in addition to Complex II linked respiration. It will be interesting to use other techniques such as blue native-PAGE gel analysis to see if other complexes are structurally affected, as well as their enzymatic activity using in-gel activity assays. An initial line of my investigation involved studying the relationship between mitochondria, poly-GR and TDP-43. TDP-43 has been shown to colocalise and accumulate in the mitochondria in individuals with ALS and FTD (Wang *et al.*, 2016a; Wang *et al.*, 2019). The hypothetical model of mitochondrial TDP-43 mediating TDP-43-induced mitochondrial dysfunction is as follows: TDP-43 colocalises and accumulates in the mitochondria, and preferentially binds to ND3 and ND6 mRNAs which inhibits their translation, therefore TDP-43 would reduce CI assembly and impair mitochondria function and morphology. Consequently, it would be interesting to investigate the relationship between *C9orf72*, TDP-43 and mitochondrial dysfunction.

Autophagy and Mitophagy

Many techniques can also be used to explore autophagy and mitophagy in *Drosophila*. Initially in my study, autophagy was a main topic of investigation, however Cunningham *et al.* (2020) identified Ref(2)P, a key regulator of autophagy, as a potent suppressor of neurodegeneration and provided evidence for disruption of autophagy in *C9orf72* ALS/FTD *Drosophila* models. Autophagolysosomal defects were attributed to the loss of nuclear localisation of transcription factor Mitf (*Drosophila* homolog of TFEB) and suppressing nucleocytoplasmic transport defects was sufficient to rescue Mitf nuclear localisation, thereby restoring autophagy and lysosome function, ultimately rescuing neurodegeneration (Cunningham *et al.*, 2020). Mitophagy, on the other hand, has not been very well studied in *C9orf72* ALS/FTD and therefore I set out to recapitulate some autophagy findings and explore what happens with mitophagy.

Firstly, I used the GFP-mCherry-Atg8a reporter to follow autophagic flux. The low lysosomal pH quenches the GFP signal after autophagosome-lysosome fusion. This means that autophagosomes will appear as GFP-positive and mCherry-positive puncta whereas autolysosomes will only be positive for mCherry. However, when I used this reporter in the larval brain, I was not able to visualise GFP puncta. This was not a problem with the reporter itself since I tested the reporter in other tissues, such as the fat body (data not shown). After further literature searches, Bedont *et al* (2021) used this reporter in the adult brain but instead of fixation, they used live imaging in haemolymph, an incubation medium, and successfully observed GFP and mCherry puncta. I would like to optimise this tool by using live imaging in media too. In the meantime, I used my initial preliminary data to quantify mCherry-positive puncta as a proxy for the number of autolysosomes in the brain. I found that there is a reduction in the number of autolysosomes which suggests that there is reduced induction of autophagy but conversely could also suggest an increase in degradation and turnover.

To complement the reporter results, immunoblot was used to detect the levels of Ref(2)P and Atg8a/GABARAP, to investigate autophagic flux. A reduction of the lipidated Atg8a-II was observed which could indicate a reduction in flux, i.e., in the number of autophagosomes and autophagy-related structures. Ref(2)P, *Drosophila* homologue of p62, is also often used to complement this assay as it directly binds to Atg8a and is selectively degraded by autophagy. There was a trend for an increase in Ref(2)P levels which corroborates the findings from Cunningham *et al.* (2020) and suggests that there may be a disruption of autophagy. These findings need to be made with caution as the current experiments were carried out without including inhibitors in the analysis, which can result in incorrect interpretation of the result. It is important to measure the amount of Atg8a-II delivered to the lysosomes by comparing in the presence and absence of bafilomycin A1 (a vacuolar H⁺-ATPase inhibitor) or lysosomotropic agents (e.g., chloroquine) to inhibit lysosomal degradation of Atg8a-II to determine the basal autophagic activity (Jiang & Mizushima, 2015). In the lab, we have currently optimised the use of chloroquine in flies (bafilomycin A1 cannot be used as it is toxic for flies as it disrupts the mTOR pathway) and therefore this experiment can be improved to provide a more definitive interpretation of whether autophagy is not induced or there is an increase in autophagic degradation i.e. flux. In summary, whilst the conclusion is not concrete, my findings suggest that there may be less fusion events between the autophagosome and lysosome suggesting a defect in flux due to problems in the initiation stage of autophagy.

Since there is a perturbation of autophagy in the *C9orf72* flies, I hypothesised that mitophagy will also be disrupted. Indeed, using the mito-QC reporter developed in the lab,

there was a reduction in the number of mitolysosomes in G4C2x36 and GR36. The next step will be to determine whether boosting mitophagy can alleviate *C9orf72* phenotypes which will be addressed and discussed in detail in the next chapter.

Oxidative stress

Excess ROS production from the mitochondria is widely known to be detrimental and closely related to many neurodegenerative diseases including ALS (Smith *et al.*, 2019). Specifically, it has been shown that poly-GR itself may be important in linking mitochondrial dysfunction and oxidative stress. Lopez-Gonzalez *et al.* (2016) showed an increase in DNA damage and oxidative stress in iPSC-derived *C9orf72* motor neurons. Choi *et al.* (2019) also found increased DNA damage, oxidative stress and decreased activities of mitochondrial complexes I and V. Moreover, Li *et al.* (2020) observed an increase in oxidative stress, mitochondrial membrane potential and ATP production in their Flag-GR80 *Drosophila* model when expressed in the muscle. To determine whether ROS is a main player in the pathogenesis, I also measured the amount of ROS in the G4C2x36, GR36 and GR1000 fly models. By using a mito-roGFP2-Orp1 reporter, I was able to observe an increase in mitochondrial ROS in the G4C2x36 and GR36 larval brains. Moreover, an increase in mitochondrial ROS was also observed in the GR1000 model using MitoSOX.

Intracellular superoxide production

There are many limitations to consider when measuring ROS and oxidative damage in cells and *in vivo*. Murphy *et al* (2022) published guidelines for recommendations for using and interpreting such data. To understand oxidative stress, one needs to understand their tools and which ROS species are measured.

Throughout my studies, there have been various problems with penetration of dyes. Firstly, I attempted to use dihydroethidium (DHE) to measure intracellular superoxide production. MitoSOX is a mitochondrially-targeted hydroethidine to detect mitochondrial superoxide production by quantifying fluorescence yet the use of both probes can be misleading as the probes produces both ethidium, a non-specific oxidation product and the superoxide-specific product 2-hydroxyethidium. As these two products overlap in their fluorescence spectra, it is not possible to differentiate between the two. During my studies, I was not able to use DHE with larval brains as there were problems with the optimisation step. When oxidised, the ethidium intercalates into nucleic acids and emits fluorescence, however,

when I investigated the signal in larval brains, the localisation pattern as well as fluorescence emitted was extremely variable and unreliable even after trying different mounting techniques as well as adjusting concentration of DHE used.

MitoSOX had similar problems and due to the thickness of the larval brain, the dye did not penetrate well and only labelled the outline of the brain. Penetration of the dye was not a problem with the adult brain however, and therefore MitoSOX was used to measure mitochondrial superoxide production in GR1000 adult brains. In the future, I would like to revisit some larval brain experiments. ROS investigation was performed in the early days of my studies and I have acquired more knowledge and skill since then, therefore I may be able to improve the investigational set up. Furthermore, I have already used flow cytometry to quantify mitochondrial ROS using MitoSOX in *C9orf72* Neuro2a cells (kind gift from Dr. Guillaume Hautbergue) where increased ROS was observed (data not shown). I have since developed plans to further use this *in vitro* system to complement my *in vivo* fly work. Finally, accurate quantification of 2-hydroxyethidium products can be achieved using liquid chromatography-mass spectrometry (LC-MS) in cellular systems (Zielonka *et al*, 2008; Murphy *et al.*, 2022) therefore this approach can potentially be used instead of looking at the larval system. MitoNeoD can also be used, which is a modified version of MitoSOX as it contains neopentyl groups which prevents intercalation into DNA as well as a carbon-deuterium bond to enhance its selectivity for O₂⁻ over non-specific oxidation and therefore reduce the limitations described (Shchepinova *et al*, 2017).

Intracellular hydrogen peroxide (H₂O₂) production

Since I am interested in looking at the different ROS species as well as their compartment-wise response, I tried various tools to measure intracellular hydrogen peroxide (H₂O₂) production. My first attempt was to use 2',7'-dichlorodihydrofluorescein diacetate (H₂DCFDA) to measure H₂O₂. Upon oxidation, the non-fluorescent H₂DCFDA is converted to the highly fluorescent 2',7''-dichlorofluorescein (DCF), yet the fluorescence of DCF is sensitive to local oxygen levels as well as pH and therefore interpretation of results must be made with caution. Moreover, it has been proven that it is not specific for any particular ROS (Zielonka *et al*, 2012). Furthermore, H₂DCFDA is only oxidised by H₂O₂ when it is converted to a more reactive species by redox-active metals or haem proteins (Murphy *et al.*, 2022). Strict controls such as adding a positive control, e.g. D-amino acid oxidase to induce a H₂O₂ response as well as negative controls, such as gene knockouts or inhibitors to abolish the ROS-generating process must be considered in the experimental set-up. However, even with all these controls

in mind, I could not optimise H₂DCFDA to use in the larval brain as I came across a similar issue as the DHE used previously. The larval brain is too thick for complete penetration of the dye therefore I used genetically encoded fluorescent protein sensors instead.

The mito-roGFP2-Orp1 reporter is sensitive to H₂O₂ changes, as a redox-sensitive green fluorescent protein (roGFP) is coupled to a hydrogen peroxide sensor protein peroxidase, Orp1 which mediates roGFP2 oxidation by H₂O₂ and leads to a shift in its excitation maxima of roGFP2 from 488 to 405. It is a good *in vivo* tool to measure production of hydrogen peroxide since the redox-dependent fluorescence ratio displayed by roGFP2 is insensitive to pH changes in the physiological range (Schwarzlander *et al.*, 2008; Albrecht *et al.*, 2011). Moreover, expression of cytosolic or mitochondrial roGFP2-Orp1 in *Drosophila* allows the measurement of physiologically relevant changes in H₂O₂ levels with compartment-specific resolution. Unfortunately, the cyto-roGFP2-Orp1 was extremely weak and I was not able to optimise this tool in this study.

Lastly, a ratiometric mass spectrometry probe, MitoBoronic acid (MitoB), can be used to measure H₂O₂ within the mitochondrial matrix (Cocheme *et al.*, 2011). MitoB is converted into its phenol product, MitoPhenol (MitoP) in response to H₂O₂ and therefore the rate of MitoP to MitoB conversion reflects the mitochondrial matrix H₂O₂ concentration. The technique is an extremely valuable *in vivo* tool developed to measure H₂O₂. However, it can be technically challenging as the probe needs to be injected into the fly which then requires quantification by LC-MS which may be laborious if a simple fluorescent probe with the right controls used can provide the same answer.

3.8 Summary

In summary, I have presented some interesting insights into various parameters of mitochondrial dysfunction in different *C9orf72* *Drosophila* models of ALS/FTD and discussed the merits as well as the limitations present when interpreting the results. The next step is to investigate the underlying pathogenic mechanisms associated with changes in mitochondrial morphology, defective mitophagy and oxidative stress-associated neurodegeneration

Chapter 4 – Modulating mitochondrial
dysfunction to improve *C9orf72*
behavioural fitness

4. Modulating mitochondrial dysfunction to improve *C9orf72* behavioural fitness

Background and Aims

In Chapter 3, I observed that expression of G4C2x36 or GR36 repeats in the larval brains caused hyperfused mitochondria. Moreover, a reduction of mitophagy was observed. To determine whether excess fusion or mitophagy are primary causes for pathogenesis, I aimed to modulate mitochondrial dynamics by manipulating key mitochondrial fission and fusion factors as well as boost mitophagy to assess whether these manipulations can suppress *C9orf72* behavioural motor impairments.

At this stage of the project, I wanted to concentrate my focus on the G4C2x36 repeats model and poly-GR toxicity using the GR36 and GR1000 models. GA36 was benign and did not have any mitochondrial phenotypes therefore it was dropped. PR36 was also dropped as it had similar phenotypes to GR36. In the future, it may be worthwhile to revisit these genotypes to further investigate the differences between the different DPRs and their relevant toxicity.

4.1 Genetic manipulations of fission and fusion does not rescue *C9orf72* locomotor phenotypes

4.1.1 Promoting fission by overexpressing *Tango11* or *Drp1*

Drp1 is recruited to the OMM by mitochondrial fission factors, forming a ring-like structure. This is followed by GTP hydrolysis of Drp1 leading to mitochondrial fission. To determine whether excess fusion is a primary cause of pathogenesis, I first increased fission by overexpression of the key mitochondrial fission factors, *Mff* (*Tango11* in *Drosophila*) and *Drp1*. Using pan-neuronal overexpression of *Tango11* in the larval brain with *nSyb-GAL4*, I did not observe any differences in the proportion of cells containing hyperfused mitochondria comparing G4C2x36, LacZ with G4C2x36, *Tango11* (69% vs 57%) and GR36, LacZ with GR36, *Tango11* (67% vs 63%) therefore the majority of mitochondria were still hyperfused (Figure 4.1). However, both expression of G4C2x3, *Tango11* compared to G4C2x3, LacZ control exhibited an unusual phenotype. As shown in Figure 4.1, there were often 'accumulations' of mitochondria which had a long 'tail'. These accumulations occur in all the

genotypes, even in the control. This often skewed the quantification as there appeared to be more elongated mitochondria in the control as well.

Overexpression of *Drp1* has been well established in the literature to fragment the mitochondria. There were some differences, in particular comparing G4C2x36, LacZ with G4C2x36, *Drp1* where there seems to be fewer cells with hyperfused mitochondria (69% vs 45%). However, no differences were observed comparing GR36, LacZ with GR36, *Drp1* (67% vs 60%). Although, it must be noted that there does not seem to be more fragmented mitochondria in the control comparing G4C2x3, LacZ with G4C2x3, *Drp1* (Figure 4.1) which raises the question of whether small differences in morphology can easily be detected in the larval brain with this set-up.

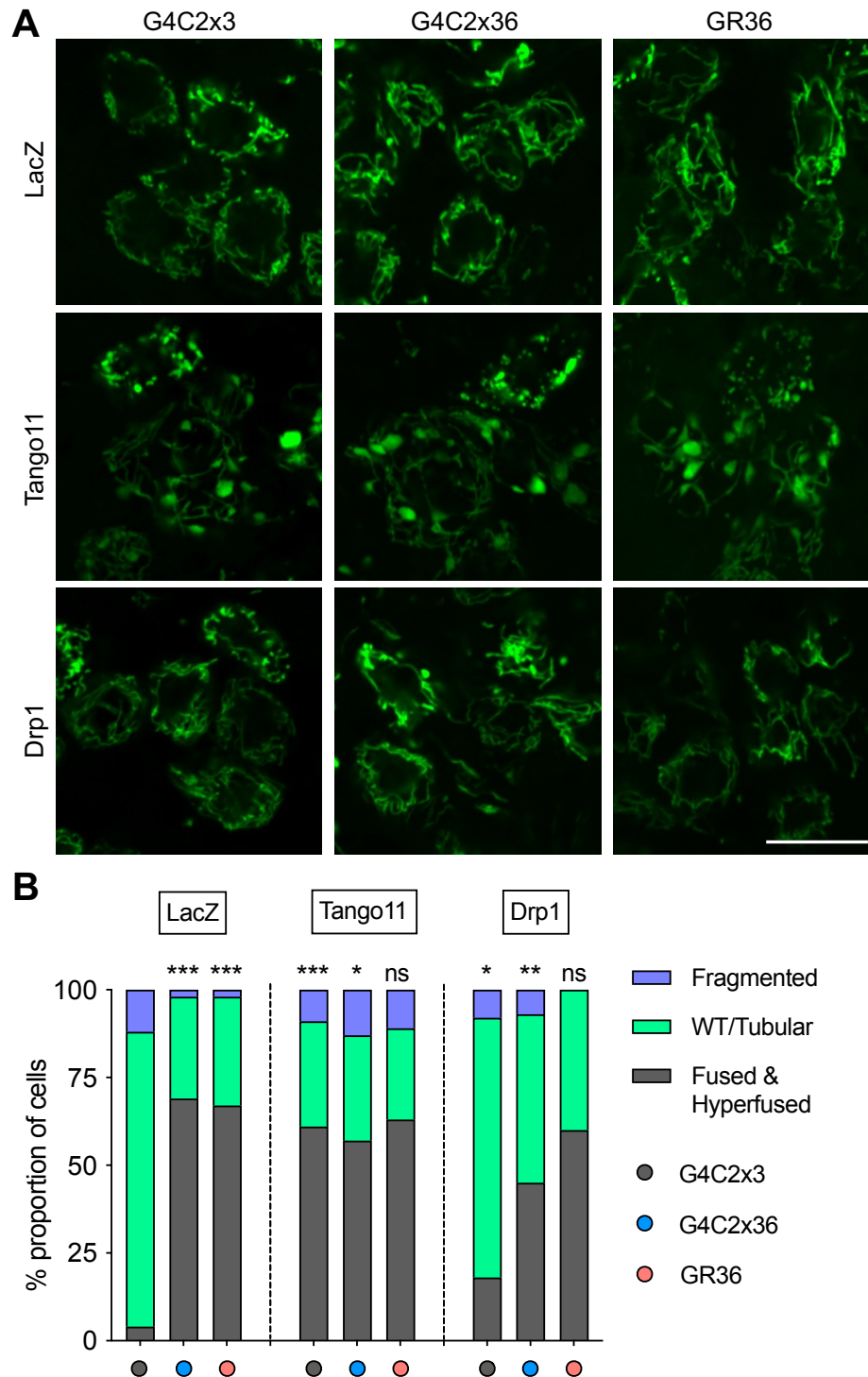


Figure 4.1 Genetic manipulation with fission factors – *Tango11* and *Drp1*

(A) Confocal microscopy of the ventral ganglion of larval brains. Mitochondria are labelled with mito.GFP when overexpressed with pan-neuronal driver *nSyb-GAL4*, scale bar = 10 μ m. Genetic manipulations focussing on promoting fission was used by overexpressing *Tango11* and *Drp1* in *C9orf72* conditions. **(B)** Quantification of mitochondrial morphology using a scoring system established in Figure 3.6. Statistical analysis was performed using Chi squared test. Comparisons for the first LacZ

group are against G4C2x3, LacZ. Otherwise, all the comparisons are against their respective control (LacZ) condition. * $p < 0.05$, ** $p < 0.01$, *** $p < 0.001$, ns = not significant, $n = 8-10$.

4.1.2 Decreasing fusion with *Opa1* and *Marf* mutants in heterozygosity

Next, I tried to reduce fusion by decreasing levels of the pro-fusion factors *Opa1* and *Marf* by using these mutants in heterozygosity. I found that heterozygous loss-of-function mutations of *Opa1* did not alter mitochondrial morphology in the control (G4C2x3, LacZ vs G4C2x3 *Opa1*^{-/+}) nor in the G4C2x36, LacZ vs G4C2x36, *Opa1*^{-/+} comparison (69% vs 62% hyperfused mitochondria). However, there were some differences when comparing GR36, LacZ vs GR36, *Opa1*^{-/+} (67% vs 46% hyperfused mitochondria).

Similar results were observed using heterozygous loss-of-function mutations of *Marf*. I found that mitochondrial morphology was not affected in the control (G4C2x3, LacZ vs G4C2x3 *Marf*^{-/+}). There were some differences observed in the G4C2x36, LacZ vs G4C2x36, *Marf*^{-/+} comparison (69% vs 50% hyperfused mitochondria). Moreover, stronger differences were shown when comparing GR36, LacZ vs GR36, *Marf*^{-/+} (67% vs 40% hyperfused mitochondria).

In summary, there are apparent differences observed in mitochondrial morphologies when co-expressing mitochondrial dynamics genes under *C9orf72* conditions. All these transgenic lines modulating mitochondrial fission or fusion have been tested and used in many studies before, albeit in different tissues and conditions. Further experiments may be needed to investigate in more detail the effects of these genes in a neuronal environment. Another factor that needs to be considered is the UAS/GAL4 ratio. In the co-overexpression experiments, I used one copy of *nSyb-GAL4* driver to express three copies of UAS transgenes including UAS-mito.GFP, UAS-C9 and UAS-dynamics. This may mask any effects observed and account for the lack of phenotype observed in the G4C2x3 controls.

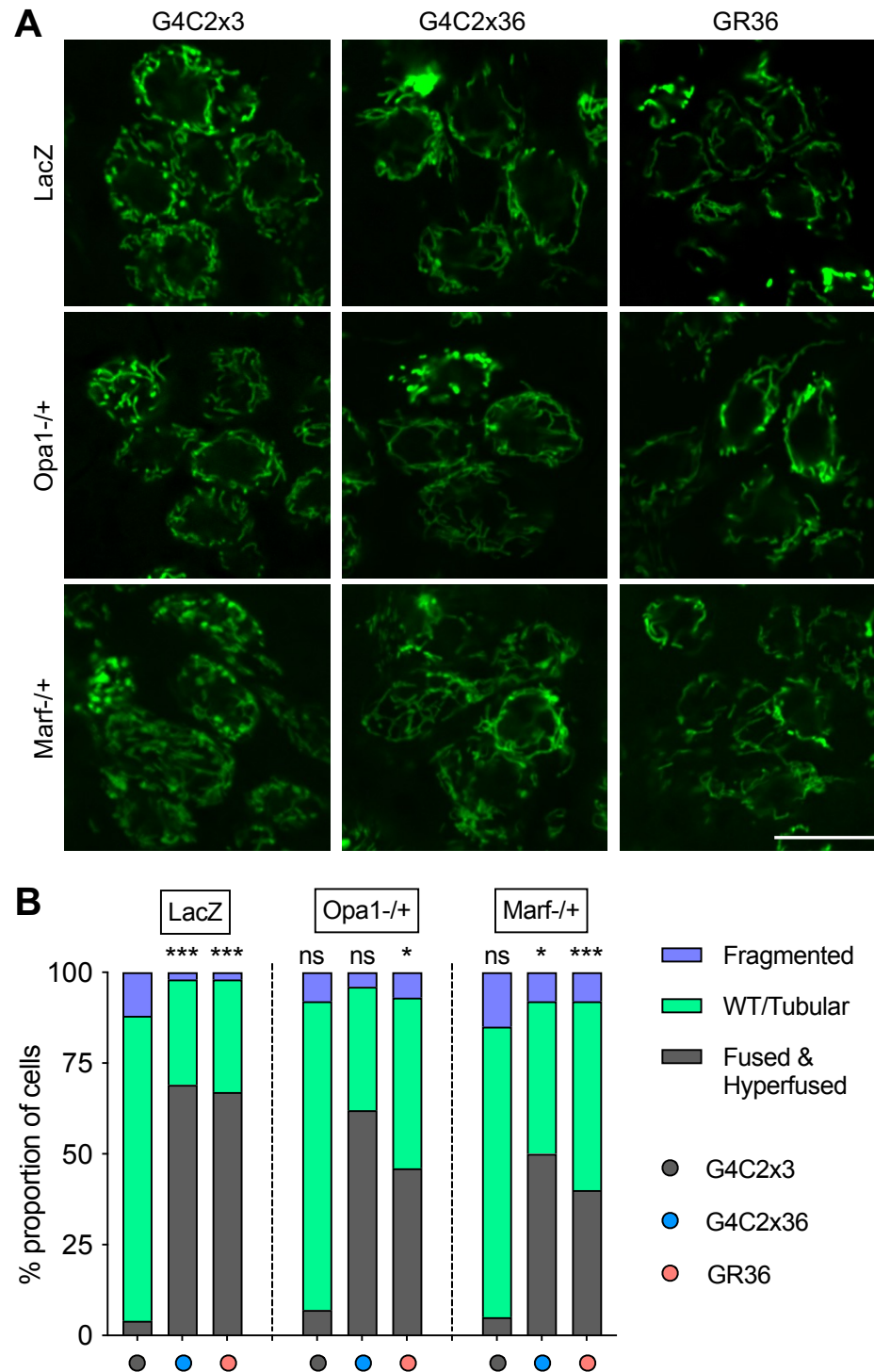


Figure 4.2 Genetic manipulation with fusion factors – *Opa1* and *Marf*

(A) Confocal microscopy of the ventral ganglion of larval brains. Mitochondria are labelled with mito.GFP when overexpressed with pan-neuronal driver *nSyb-GAL4*, scale bar = 10 μ m. Genetic manipulations focussing on promoting fusion using heterozygous loss-of-function mutations of *Opa1* and *Marf* in *C9orf72* conditions. (B) Quantification of mitochondrial morphology using a scoring system established in Figure 3.6. Statistical analysis was performed using Chi squared test. Comparisons for

the first LacZ group are against G4C2x3, LacZ. Otherwise, all the comparisons are against their respective control (LacZ) condition. * $p < 0.05$, *** $p < 0.001$, ns = not significant, $n = 8-10$.

4.1.3 Manipulating mitochondrial dynamics does not rescue *C9orf72* motor deficits

After examining mitochondrial morphology under *C9orf72* conditions, I wanted to test whether genetic manipulations of mitochondrial dynamics genes had an impact on behavioural outputs. Since some manipulations elicited changes in mitochondrial morphology, I hypothesised that increasing fission or decreasing fusion could affect *C9orf72* motor behaviour and help determine whether dynamics play a role in the pathogenesis.

I repeated the same genetic manipulations used in the microscopy analysis, but instead performed larval crawling. Firstly, the combinations of the different mitochondrial dynamic genes with G4C2x3 did not harbour any larval crawling phenotype. This shows that overexpression of *Tango11* and *Drp1* or heterozygous loss of *Opa1* and *Marf* are well tolerated in the larval stage (Figure 4.3).

Next, while expression of G4C2x36 recapitulated the previously observed larval crawling deficit (Figure 3.3), manipulation of the various mitochondrial fission/fusion genes was not sufficient to rescue this behavioural phenotype. In fact, expression of G4C2x36 with heterozygous *Marf* mutants significantly worsened the phenotype, with some larvae barely able to crawl (Figure 4.3). A similar pattern was observed with GR36. Overexpression of *Tango11* or *Drp1*, or heterozygous *Opa1* did not affect motor behaviour (Figure 4.3). However, expression of GR36 in heterozygous *Marf* mutants significantly worsened larval crawling, though no changes in *Marf* levels were measurable by western blot analysis (data not shown) – most of these larvae stayed in the same spot on the agar plate with few peristaltic waves and ‘wriggling’ in the same spot

Taken together, these data suggest that fission and fusion do not play an important role in *C9orf72* pathogenesis and the mitochondrial morphology phenotypes observed are likely a downstream consequence.

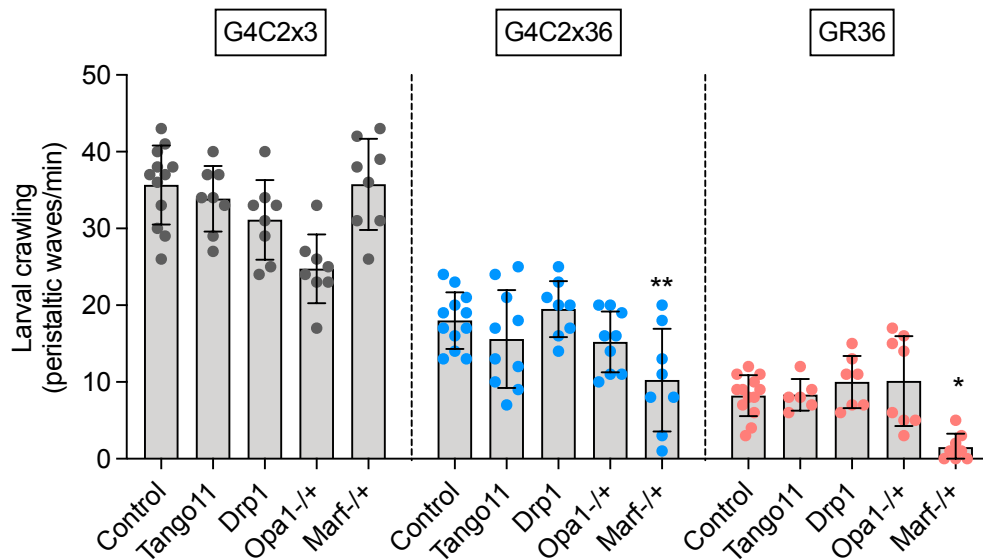


Figure 4.3 Genetic manipulation of fission and fusion does not rescue *C9orf72* larval crawling deficits

Genetic manipulations with overexpression of pro fission factors, *Tango11* and *Drp1* as well as heterozygous reduction of pro fusion factors *Opa1* and *Marf*. Expression of the repeats and DPRs was achieved using a pan-neuronal driver, *nSyb-GAL4* and the number of peristalsis waves was recorded. Statistical analysis was performed using one-way ANOVA with Bonferroni multiple comparison test. Comparisons for the first LacZ group are against G4C2x3, LacZ. Otherwise, all the comparisons are against their respective control (LacZ) condition. * $p < 0.05$, ** $p < 0.01$, chart shows mean \pm SD, $n = 6-12$.

4.2 Boosting mitophagy does not rescue *C9orf72* phenotypes

4.2.1 Overexpression of *Pink1* or *parkin* did not rescue rough eye phenotypes in G4C2x36 and GR36 flies

In Chapter 3, I observed reduced mitophagy in *C9orf72* flies (Figure 3.8). Upon loss of inner mitochondrial membrane potential, PINK1 stabilises and accumulates on the outer mitochondrial membrane to phosphorylate resident ubiquitin which recruits the E3 ubiquitin ligase Parkin to execute the mitophagic process. Khalil *et al* (2015) found mitochondrial spheroids in non-apoptotic photoreceptor neurons in a *Drosophila* model of Huntington's Disease. These spheroids are characteristic of cells where mitophagy is blocked. They found that *PINK1* overexpression alleviated mitochondrial spheroid formation and counteracted neurotoxicity by restoring ATP levels, neuronal integrity and improving survival. Hence, I wanted to test whether boosting mitophagy could rescue the *C9orf72* phenotypes.

I expressed the G4C2x36 and GR36 in the *Drosophila* eye using *GMR-GAL4* and used two *PINK1* overexpression lines as well as a *parkin* overexpression line to investigate whether these genes could modulate the toxicity present in the eye. Surprisingly, neither *PINK1* nor *parkin* overexpression rescued the *Drosophila* rough eye phenotype present with G4C2x36 and GR36 (Figure 4.4). Moreover, in the crosses that were set up, upon eclosion, some males also presented with a folded wings phenotype in *GMR>G4C2x36, Tc-Pink1* and *GMR>G4C2x36, park[C2]*. Furthermore, only males eclosed for *GMR>GR36, park[C2]*. These results suggest that not only do they not rescue the eye phenotypes, overexpression of *PINK1* and *parkin* may even worsen the phenotypes present (Figure 4.4). It is to be noted that overexpression of PINK1 and parkin has not been shown to activate mitophagy therefore more exploratory work is needed.

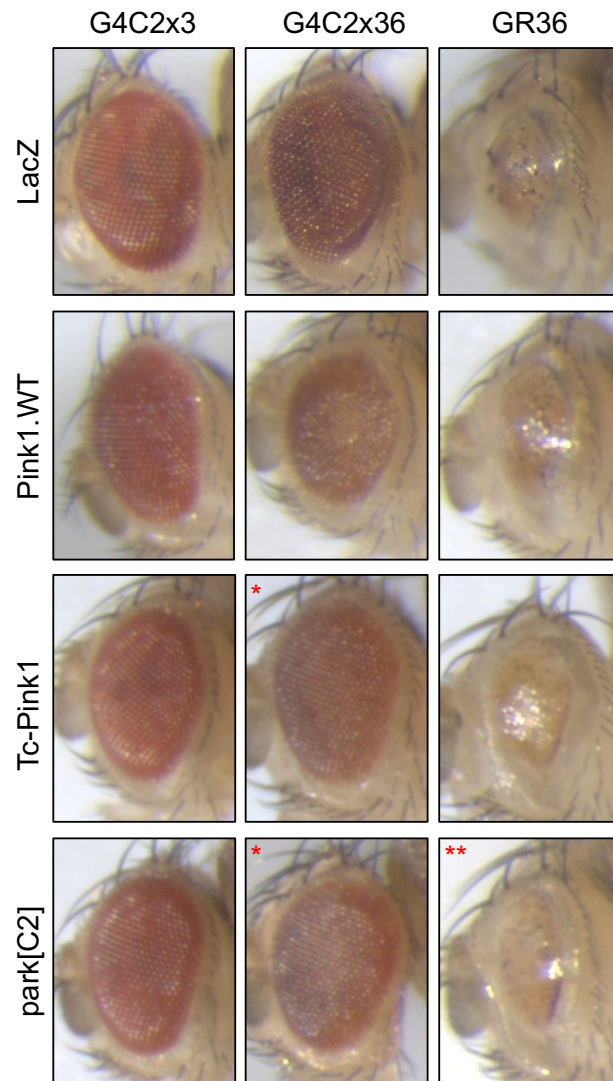


Figure 4.4 Overexpression of *PINK1* and *parkin* do not rescue *C9orf72* rough eye phenotypes
GMR-GAL4 was used to overexpress G4C2x36 and GR36 in the compound eye together with overexpression of *Pink1* and *parkin* (n=6 images taken; more than 30 flies were assessed visually to confirm the phenotypes observed). Single red asterisk depicts some males were observed with folded wings. Double red asterisks indicates that only males eclosed from the cross.

4.2.2 Boosting mitophagy by expressing *USP30* RNAi had no effect in G4C2x36 and GR36 flies

As an alternative approach to boost mitophagy I next targeted the mitochondrial deubiquitylase *USP30*. Knockdown of *USP30* has been shown to rescue defective mitophagy caused by pathogenic mutations in parkin and improves mitochondrial integrity in *parkin*- or *PINK1*-deficient flies (Bingol *et al.*, 2014).

To visualise mitophagy *in vivo*, I employed the mito-QC reporter again to investigate whether *USP30* RNAi could boost mitophagy in the larval brains. Using *nSyb-GAL4*, I overexpressed the G4C2x3 with luciferase RNAi (as a control RNAi) and compared this to G4C2x3, *USP30* RNAi. Using IMARIS to quantify the number of mitolysosomes, I observed that *USP30* RNAi significantly increased the number of mitolysosomes per cell indicating that mitophagy was boosted (Figure 4.5). However, when I looked at the other *C9orf72* conditions, *USP30* RNAi was not sufficient to rescue the reduced mitophagy phenotype observed with G4C2x36 and GR36 (Figure 4.5).

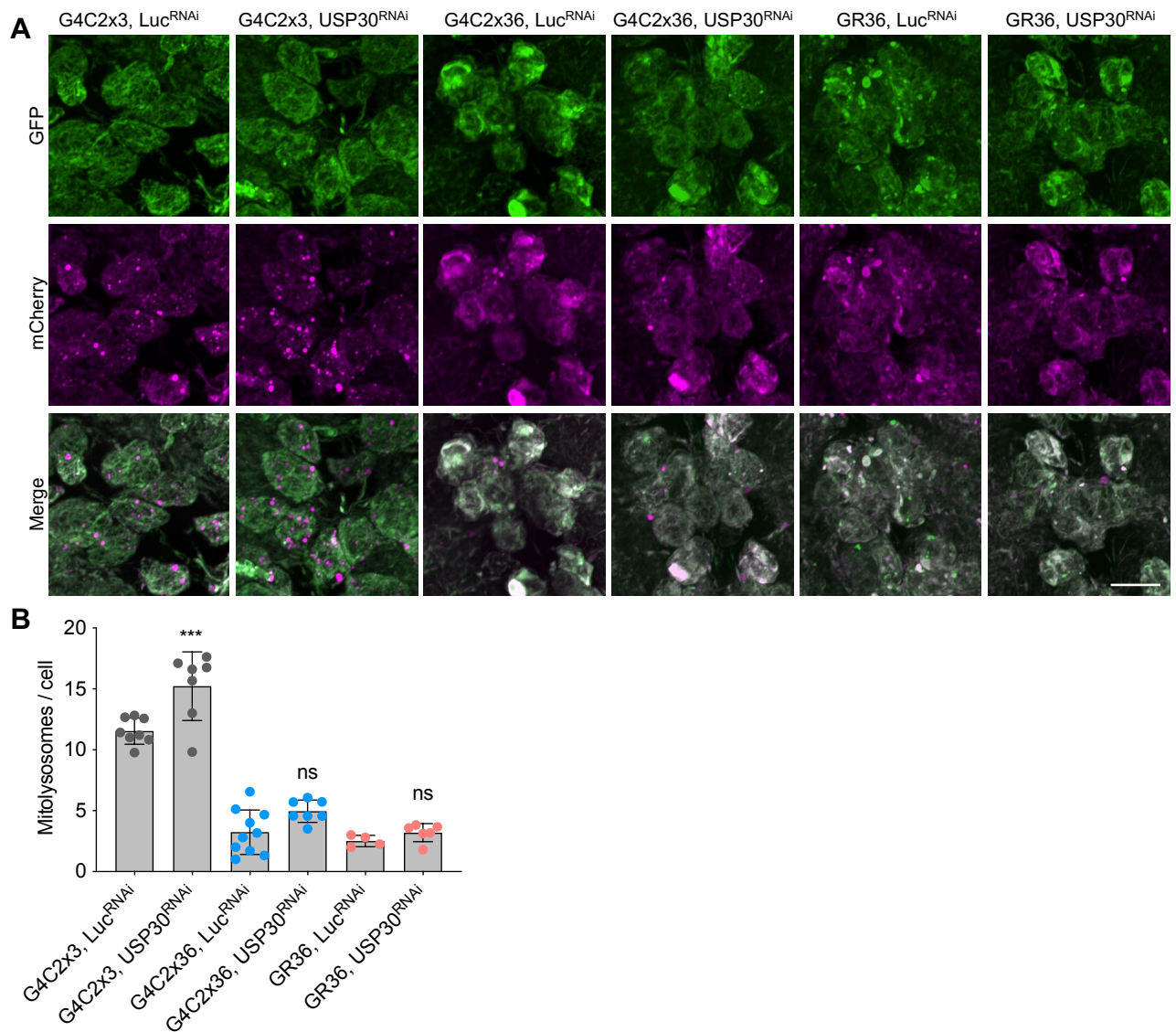


Figure 4.5 Boosting mitophagy with *USP30* RNAi does not rescue *C9orf72* phenotypes

(A) Confocal microscopy images of the mito-QC reporter in *C9orf72* conditions and *USP30* RNAi (*USP30^{RNAi}*) using pan-neuronal driver *nSyb-GAL4* expressed in larval ventral ganglion. Control luciferase RNAi (*Luc^{RNAi}*) was used to balance the UAS/*GAL4* ratio. Mitolysosomes are evident as GFP-negative, mCherry-positive red only puncta. Scale bar = 10 μ m. **(B)** Quantification of number of mitolysosomes per cell using IMARIS. Statistical analysis was performed using one-way ANOVA with Bonferroni multiple comparison test: *** $p < 0.001$, ns = not significant, chart shows mean \pm SD, $n = 4-8$.

4.2.3 Expression of *USP30* RNAi had no beneficial effect on larval crawling in G4C2x36 and GR36 flies

Moreover, pan-neuronal expression of G4C2x36 and GR36 with *USP30* RNAi did not improve the larval crawling deficit (Figure 4.6). Taken together, these data corroborate the lack of behavioural rescue and suggests that mitophagy is not a primary cause but a downstream consequence in *C9orf72* pathogenesis.

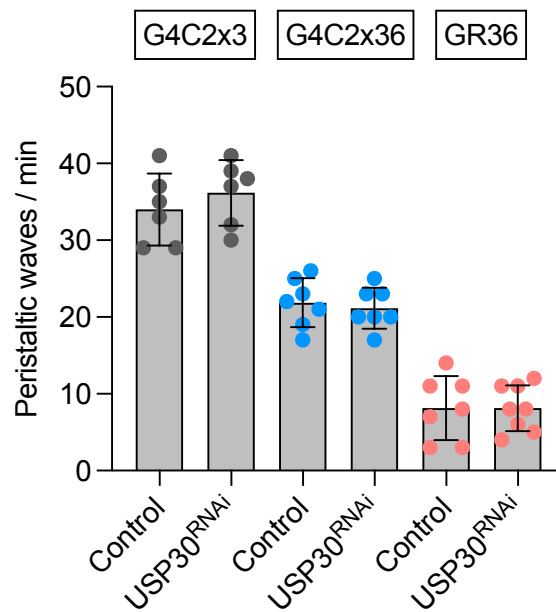


Figure 4.6 Reduction of *USP30* to boost mitophagy does not improve *C9orf72* larval crawling phenotypes

Pan-neuronal expression of G4C2x36 and GR36 with *USP30*^{RNAi} and the number of peristalsis waves was recorded. Statistical analysis was performed using one-way ANOVA with Bonferroni multiple comparison test. All the comparisons are against their respective control (*Luc*^{RNAi}) condition – data not significant, chart shows mean \pm SD, n=6-8.

4.3 Other components – MICOS

4.3.1 No rescue was observed in larval crawling when manipulating MICOS components in G4C2x36 and GR36

During my investigation, Li *et al.* (2020) explored the contribution of muscle in the manifestation of ALS phenotypes as opposed to other studies focussing on motor neurons. They showed that in *Drosophila* muscle, poly-GR entered the mitochondria and interacted with components of the Mitochondrial Contact Site and Cristae Organisation System (MICOS) localised at cristae junctions, which is responsible for proper architecture of the mitochondrial inner membrane.

Consequently, I wanted to recapitulate these results but in my neuronal settings instead to investigate whether this interaction is also observed in this tissue. I targeted various MICOS components by using an *Opa1*-RNAi line, which also has a role in cristae junction (CJ) remodelling (Frezza *et al.*, 2006). I also used *Drosophila* *MIC60/Mitofilin* overexpression and Leucine-zipper and EF-hand-containing Transmembrane protein 1 (*Letm1*) overexpression to attempt to rescue the *C9orf72* larval crawling deficit. However, co-expression with any of the MICOS components did not rescue the larval crawling phenotype (Figure 4.7). This suggests that this interaction may be less relevant in neuronal tissues.

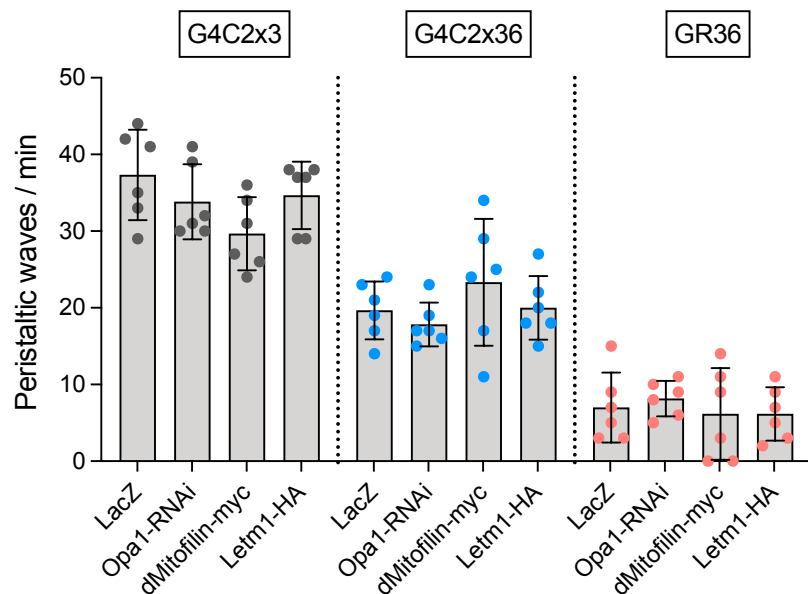


Figure 4.7 Genetic manipulation with MICOS components did not rescue *C9orf72* larval crawling phenotype

Genetic manipulations with overexpression of MICOS components, *Opa1 RNAi*, *dMitofillin* as well as *Letm1*. Overexpression of the repeats and DPRs was achieved using a pan-neuronal driver, *nSyb-GAL4* and the number of peristalsis waves was recorded. Statistical analysis was performed using one-way ANOVA with Bonferroni multiple comparison test, no significance was found when compared to the respective LacZ control, chart shows mean \pm SD, n=6.

4.4 Antioxidants

4.4.1 Overexpression of mitochondrial Sod2 and catalase partially rescues larval crawling deficit in G4C2x36 and GR36 models

Increased ROS has been implicated in many models of neurodegenerative diseases including ALS (Smith *et al.*, 2019) and I observed an increase in mitochondrial ROS using a mito-roGFP2-Orp1 reporter (Figure 3.11). There are several enzymes that function to suppress oxidative stress. Dismutation of the superoxide anion is catalysed by superoxide dismutase enzymes, Sod1 and Sod2, to molecular oxygen and hydrogen peroxide, which can be converted to water by catalase. I hypothesised that an excess of ROS production in the *C9orf72* fly models might contribute to the larval crawling and adult climbing deficits observed. Therefore, I obtained *Drosophila* lines to overexpress cytosolic Sod1, mitochondrial Sod2, catalase and a mitochondrially tagged catalase (mito.Cat). The different natural or induced

subcellular localisations would allow me to assess any differences between different compartments of the cell.

Firstly, I co-expressed the G4C2 repeat and protein-only DPR transgenes with either Sod1 or Sod2 and assessed larval crawling. Surprisingly, overexpression of the cytosolic Sod1 significantly worsened the larval crawling deficit observed for G4C2x36 and GR36 compared to the G4C2x3 control. For GR36, Sod1, the larvae did not crawl at all during the assay conditions. In contrast, overexpression of mitochondrial Sod2 significantly rescued the larval crawling for G4C2x36 and GR36 (Figure 4.8). Overexpression of either catalase or mitochondrial catalase (mito.Cat) also partially rescues the larval crawling impairment observed for both G4C2x36 and GR36 as well (Figure 4.8).

Thus, cytosolic Sod1 exacerbates the larval crawling phenotype whereas mitochondrial Sod2 and catalase are beneficial, suggesting that there is an excess of ROS production in the *C9orf72* models, although the detrimental effects of Sod1 remains to be elucidated.

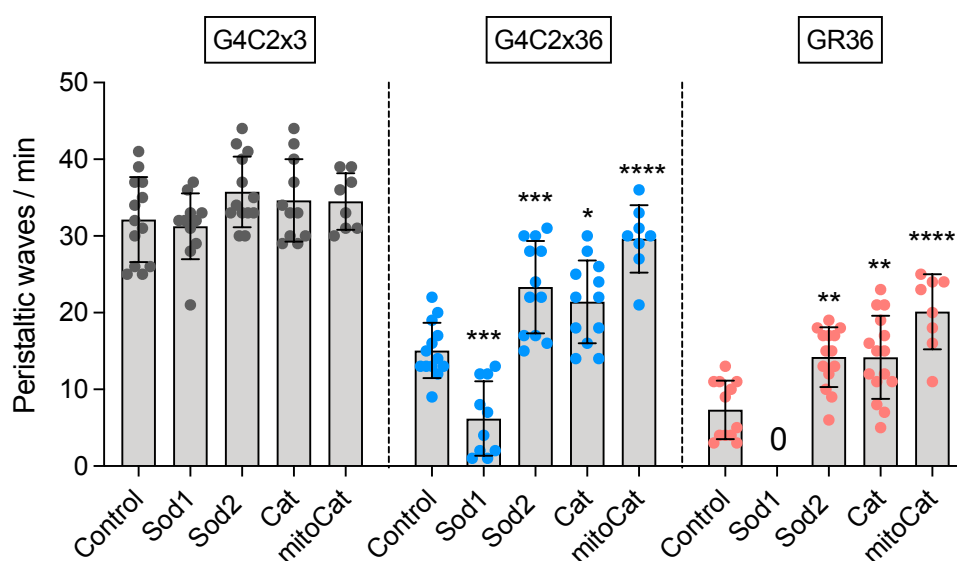


Figure 4.8 Overexpression of Sod2 and catalase partially rescued *C9orf72* larval crawling

Larval crawling was assessed by co-expressing the repeats and DPRs with antioxidant enzymes Sod1, Sod2, catalase and mitochondrially tagged catalase (mito.Cat) using the pan-neuronal driver – *nSyb-GAL4*. Control is overexpressing an inert UAS-lacZ. Statistical analysis was performed using one-way ANOVA with Bonferroni multiple comparison test: * $p < 0.05$, ** $p < 0.01$, *** $p < 0.001$ and **** $p < 0.0001$. 0 indicates no moving larvae could be selected for experimenting. Chart shows mean \pm SD, $n = 10-15$.

4.4.2 Less elongated mitochondria were found with overexpression of Sod2 and catalase

Next, I examined whether co-expressing the *C9orf72* transgenes with antioxidant lines altered the mitochondrial morphology. Less elongated mitochondria were observed when comparing G4C2x36, *LacZ* with G4C2x36, *Sod2* (69% vs 53% hyperfused mitochondria) as well as GR36, *LacZ* with GR36, *Sod2* (67% vs 47%) (Figure 4.9).

Similar results were observed when co-expressing the *C9orf72* transgenes with catalase and mito.Cat, less elongated mitochondria were observed when comparing G4C2x36, *LacZ* with G4C2x36, *Cat* (69% vs 47% hyperfused mitochondria), GR36, *LacZ* with GR36, *Cat* (67% vs 48% hyperfused mitochondria) as well as G4C2x36, *LacZ* with G4C2x36, mito.Cat (69% vs 36% hyperfused mitochondria) (Figure 4.10). However, there was not a significant difference observed when comparing the different scoring categories in GR36, *LacZ* vs GR36, mito.Cat (67% vs 56% hyperfused mitochondria) (Figure 4.10). Taken together, the change in the number of fused mitochondria correlates well with the improvement observed in larval crawling.

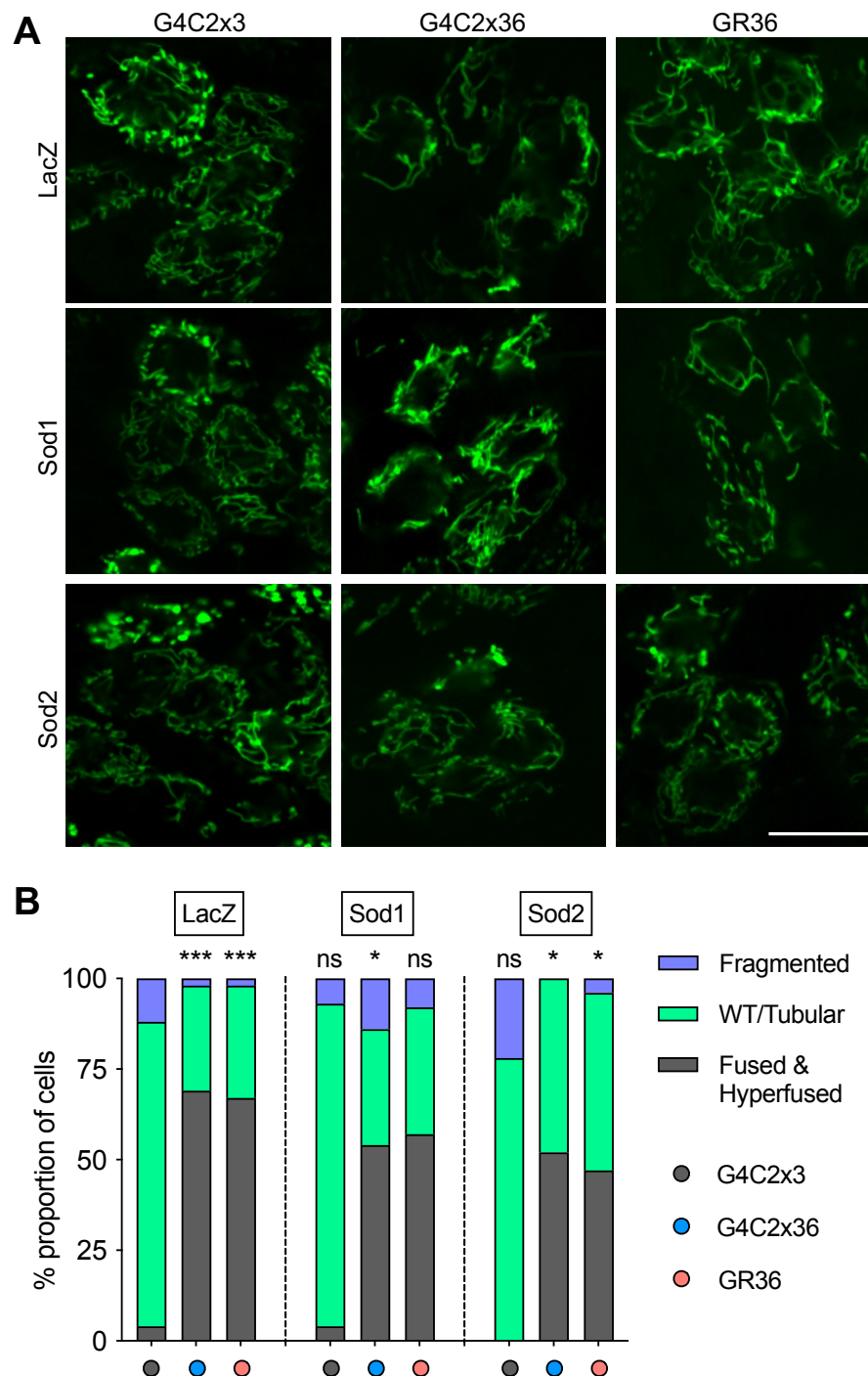


Figure 4.9 Changes in morphology are observed when overexpressing Sod1 and Sod2

(A) Confocal microscopy of the ventral ganglion of larval brains. Mitochondria are labelled with mito.GFP when overexpressed with pan-neuronal driver *nSyb-GAL4*, scale bar = 10 μ m. Genetic manipulations overexpressing Sod1 and Sod2 in *C9orf72* conditions. **(B)** Quantification of mitochondrial morphology using a scoring system established in Figure 3.6. Statistical analysis was performed using Chi squared test. Comparisons for the first LacZ group are against G4C2x3, LacZ. Otherwise, all the comparisons are against their respective control (LacZ) condition. * $p < 0.05$, *** $p < 0.001$, ns = not significant, n=8-10.

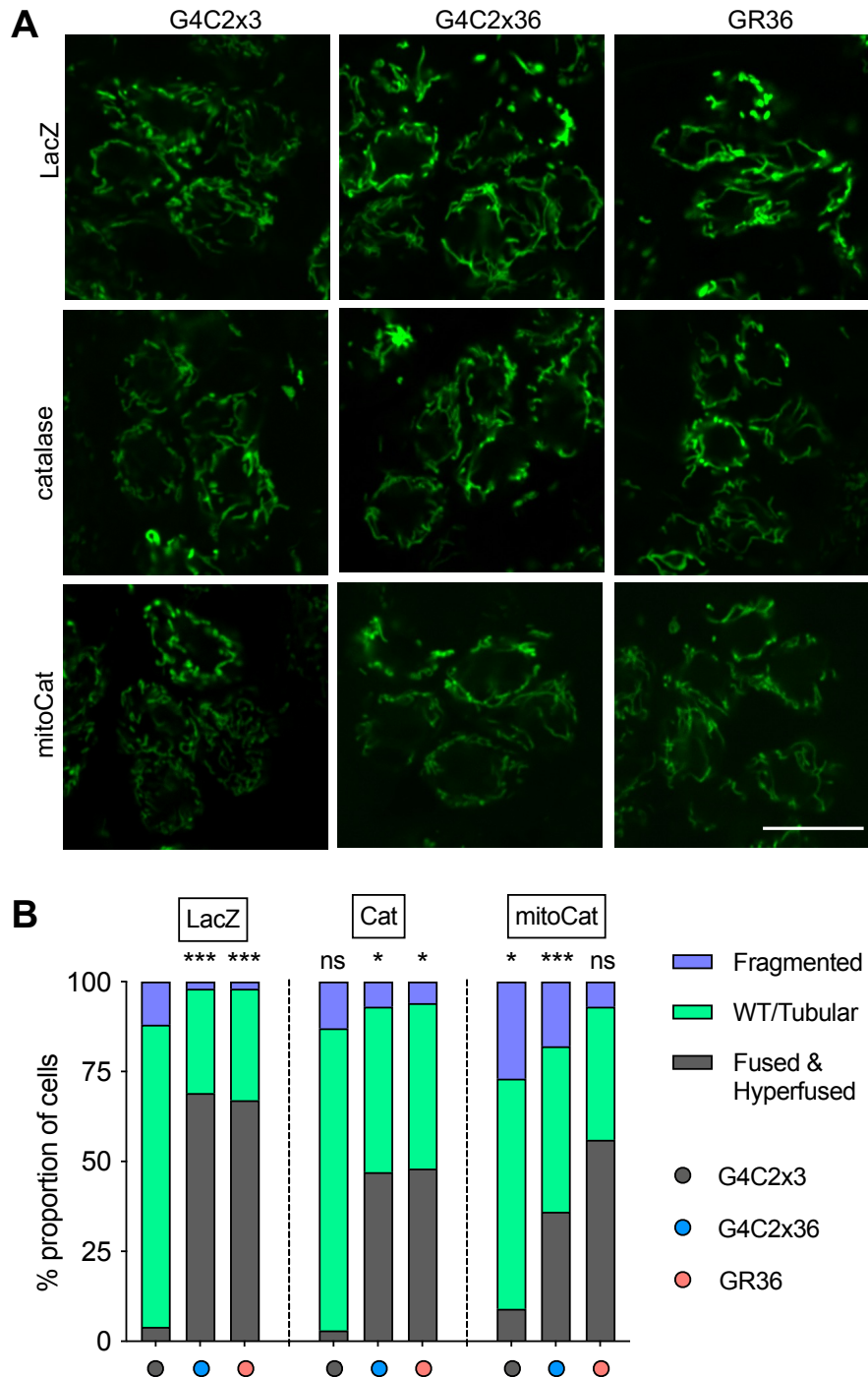


Figure 4.10 Changes in morphology are observed when overexpressing catalases

(A) Confocal microscopy of the ventral ganglion of larval brains. Mitochondria are labelled with mito.GFP when overexpressed with pan-neuronal driver *nSyb-GAL4*, scale bar = 10 μ m. Genetic manipulations overexpressing Cat and mitochondrial catalase (mito.Cat) in *C9orf72* conditions. **(B)** Quantification of mitochondrial morphology using a scoring system established in Figure 3.6. Statistical analysis was performed using Chi squared test. Comparisons for the first LacZ group are against G4C2x3, LacZ. Otherwise, all the comparisons are against their respective control (LacZ) condition. * $p < 0.05$, *** $p < 0.001$, ns = not significant, $n = 8-10$.

4.4.3 No additive effect was observed when overexpressing Sod2 and catalase together

Since we saw beneficial effects from mitochondrial Sod2 and cytosolic catalase, each partially suppressing the locomotor phenotype, we hypothesised that combining the two antioxidant enzymes together may provide a better rescue. Additionally, since Sod1 was detrimental, we decided to test whether combination with Sod2 or catalase would be less deleterious. Therefore, to assess the relative contribution that the different antioxidant enzymes have to the observed phenotypes, we decided to analyse the dual overexpression of the Sods and catalase.

Recombinant fly lines to overexpress all combinations of Sod1, Sod2, catalase and mito.Cat were generated. When overexpressing Sod1 with either Sod2, catalase or mito.Cat, the larval crawling phenotype for G4C2x36 and GR36 was the same as overexpression of Sod1 alone and did not improve the phenotype (Figure 4.11). This suggests that Sod1 is the overriding factor that is responsible for worsening the motor deficit phenotype.

In contrast, overexpressing Sod2 and catalase as well as Sod2 and mito.Cat together rescues the larval locomotion back to control levels for G4C2x36 (Figure 4.11). However, it must be noted that although the number of peristaltic waves significantly improved, the larvae were not moving around the plate as much as G4C2x3 control genotypes suggesting that their motor function is not fully rescued (data not shown). For GR36, there was a significant improvement in crawling too but the phenotype is probably too strong to rescue in its entirety.

Finally, the combination of catalase and mito.Cat together with G4C2x36 and GR36 did not rescue the crawling impairment (Figure 4.11). This potentially suggests that excessive overexpression of catalase may not be beneficial as the cell may be removing too much hydrogen peroxide which has important signalling properties in the cell.

Taken together, the data further support that Sod2 and catalase have beneficial effects in this model, but Sod1 is detrimental. It will be interesting to unravel the mechanism to understand why this is the case.

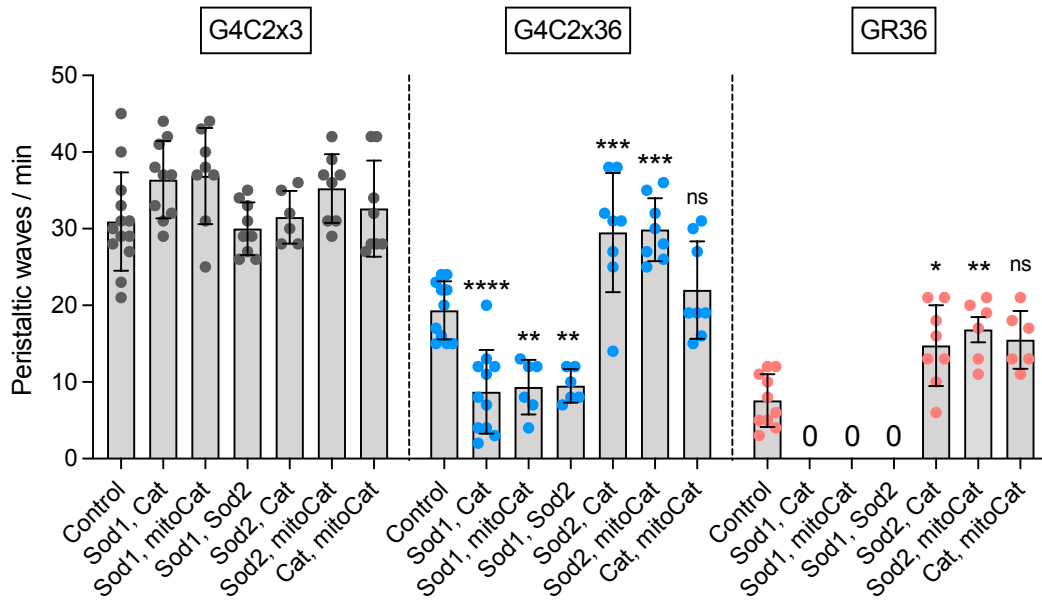


Figure 4.11 Overexpressing both Sod2 and catalase together rescues *C9orf72* crawling phenotype

Larval crawling was assessed by overexpressing the repeats and DPRs with combinations of antioxidant enzymes (Sod1+catalase, Sod1+mito.Cat, Sod1+Sod2; Sod2+catalase; Sod2+mito.Cat, Cat+mito.Cat) using the pan-neuronal driver – *nSyb-GAL4*. A 2xUAS control was used (UAS-mCD8.GFP, UAS-mito.GFP) to compensate for the additional UAS-antioxidant added with dual co-expression with the repeats and DPRs. Statistical analysis was performed using one-way ANOVA with Bonferroni multiple comparison test: * $p < 0.05$, ** $p < 0.01$, *** $p < 0.001$, 0 indicates no moving larvae could be selected for experimenting. Chart shows mean \pm SD, $n = 10-15$.

4.4.4 Overexpression of mitochondrial Sod2 and catalase also partially rescued adult climbing deficits observed with GR1000 model at day 10

Furthermore, I wanted to recapitulate the beneficial effects of antioxidants in the GR1000 model as well. Using the pan-neuronal *nSyb-GAL4* driver, I co-expressed the GR1000 with Sod1, Sod2, catalase and mito.Cat and assessed climbing ability at day 2 and day 10. At day 2, there were no climbing deficits for all the controls and experimental genotypes (Figure 4.12A). By day 10, the GR1000 developed a climbing deficit which was partially rescued with overexpression of Sod2 and catalase (Figure 4.12B). There was a trend for improvement in climbing with mito.Cat, however, this did not reach significance. Overexpression of Sod1 had no effect, however, it also did not significantly exacerbate the phenotypes as observed with larval crawling of G4C2x36, Sod1 and GR36, Sod1.

In summary, the GR1000 model supports the data collected with G4C2x36 and GR36. Overexpression of Sod2 and catalases are beneficial. The next step will be to dissect the molecular mechanisms affecting antioxidant systems as well as test therapeutic potential of antioxidants.

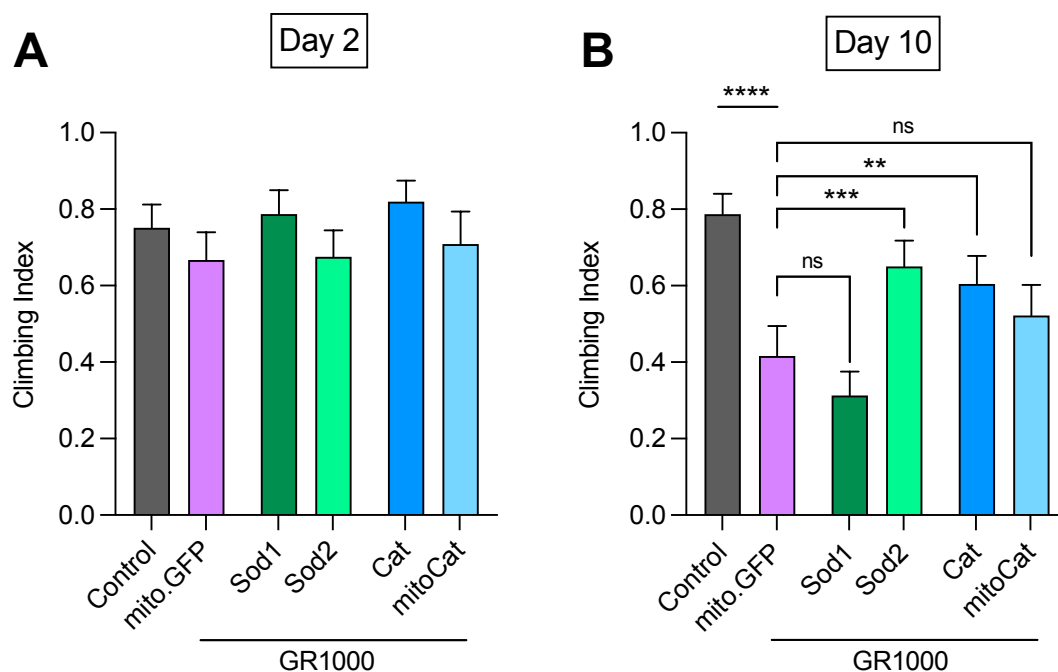


Figure 4.12 Overexpression of Sod2 and catalase partially rescues GR1000 climbing deficit at day 10

Pan-neuronal overexpression of Sod2 and catalase in GR1000 with *nSyb-GAL4* at day 2 (A) and day 10 (B). Control is *nSyb/+*. Statistical analysis was performed using Kruskal-Wallis non parametric test with Dunn's correction: ns = non-significant, ** $p < 0.01$, *** $p < 0.001$ **** $p < 0.0001$. Chart shows mean \pm 95% CI, $n=60-100$ flies.

4.4.5 Partial rescue of mitophagy was observed with overexpression of Sod2

Another downstream consequence that has been established is the reduction in mitophagy in *C9orf72* flies (Figure 3.8, 4.6). To further investigate the beneficial effects of overexpression of antioxidants, mitophagy was assessed using the mito-QC reporter. Overexpression of Sod2 in G4C2x36 and GR36 was able to partially rescue mitophagy phenotypes, however, the number of mitolysosomes per cell did not reach G4C2x3 control numbers (Figure 4.13). Hyperfused mitochondria were still observed which correlate well with the mitochondrial morphology data (Figure 4.9).

In summary, overexpression of antioxidants except for Sod1 are beneficial for *C9orf72* flies but only result in a partial rescue of behavioural locomotion. In addition, overexpression

of antioxidants with GR36 was not sufficient to rescue the L3 developmental lethality. Therefore, this indicates that there are other pathways which contribute to *C9orf72* pathogenesis.

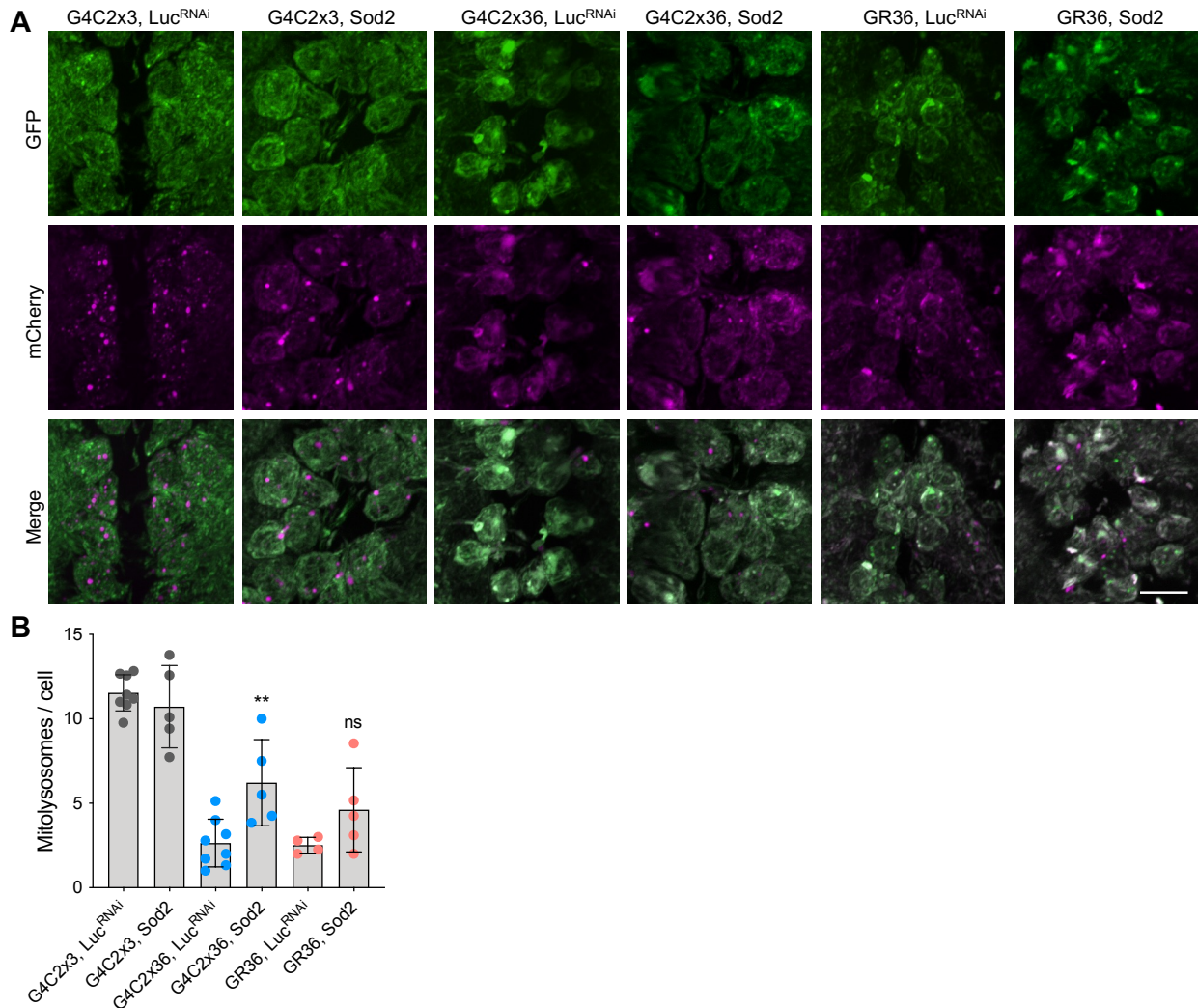


Figure 4.13 Overexpression with *Sod2* partially restores levels of mitophagy

(A) Confocal microscopy images of the mito-QC reporter in *C9orf72* conditions with overexpression of *Sod2* using pan-neuronal driver *nSyb-GAL4* expressed in larval ventral ganglion. Control luciferase RNAi (Luci) was used to balance the UAS/GAL4 ratio. Mitolysosomes are evident as GFP-negative, mCherry-positive red only puncta. Scale bar = 10 μ m. **(B)** Quantification of number of mitolysosomes per cell using IMARIS. Statistical analysis was performed using one-way ANOVA with Bonferroni multiple comparison test: ** $p < 0.01$, ns = not significant, chart shows mean \pm SD, $n = 4-8$.

4.5 Discussion

Modulation of mitochondrial dynamics does not rescue *C9orf72* phenotypes

Neuronal expression of G4C2x36 and GR36 caused hyperfused, elongated mitochondria. To determine whether excess fusion is a primary cause of pathogenesis, I first increased fission by overexpression of the key mitochondrial fission factors, *Mff* (*Tango11* in *Drosophila*) and *Drp1* as well as reducing fusion by using heterozygous mutants of the *Drosophila* homologue of Mitofusin – Marf and Opa1. However, although some differences in morphology were observed when co-expressing mitochondrial dynamics genes with G4C2x36 and GR36, it was not enough to rescue the larval crawling behavioural phenotypes therefore this suggests that fission and fusion do not play an important role in *C9orf72* pathogenesis and the mitochondrial morphology phenotypes observed are likely a downstream consequence.

There are some limitations with using these mitochondrial dynamics transgenic lines as under normal conditions i.e., co-expression with G4C2x3 control, no morphological differences were observed. Firstly, the scoring system used may mask minor changes observed, therefore if we use a more systematic approach i.e., quantify with FIJI, then the results may be clearer. However, it must be stressed that all of these transgenic lines chosen have been shown to modulate mitochondrial fission or fusion and have been tested and used in many studies before. Sandoval *et al* (2014) generated the Marf mutant lines and used ATP5a to label mitochondria in the muscle and observed small rounded mitochondria. When overexpressing mito.GFP in the larval VNC using the motor neuron driver *D42-GAL4*, Sandoval *et al*. (2014) observed that mito.GFP mostly localises to the neuropil in the Marf[B] mutant and showed an obvious reduction in levels of mitochondria in the neuropil therefore since I use the middle section of the VNC, it may not be the ideal localisation to use for investigating mitochondrial morphology. However, in their study, they use Marf[B] homozygous mutants and therefore since I use heterozygotes, the effect might be less strong. DuBoff *et al* (2012) found that a heterozygous loss-of-function mutation in Opa1[s3475] normalised mitochondrial length in neurons of the adult brain and suppresses toxicity in a *Drosophila* tauopathy model. However, in their quantification, the mitochondrial length of the Opa1[s3475] heterozygous mutant without tau had similar morphology compared to control, therefore similar observations were observed compared to my results.

Deng *et al* (2008) overexpressed Drp1 using the same transgenic flies as my study and observed mitochondrial fragmentation in adult indirect flight muscle. Moreover, Tango11 overexpression produce smaller mitochondria in axons (personal communication with Dr Victoria Hewitt). As shown in Figure 4.1, there were often ‘accumulations’ of mitochondria which had a long ‘tail’. These accumulations occur in all the genotypes, even in the control. This often skewed the quantification as there appeared to be more elongated mitochondria in the control, therefore the larval brain may not be the optimal tissue to use in this set-up as well. In summary, further experiments may be needed to investigate in more detail the effects of these genes in a neuronal environment and compare them with other tissues. Another factor that needs to be considered is the UAS/GAL4 ratio. In the co-overexpression experiments, I used one copy of *nSyb-GAL4* driver to express three copies of UAS transgenes including UAS-mito.GFP, UAS-G4C2x36/GR36 and UAS-dynamics. This may mask any effects observed and account for the lack of phenotype observed in the G4C2x3 controls. Finally, Li *et al.* (2020) studied the effect of altering fission-fusion balance by the loss- or gain of function of Drp1, Fis1, or Marf and observed no obvious effect on GR80 toxicity which suggests that modulation of GR80 is unrelated to mitochondrial dynamics which is similar to what I have observed as well.

MICOS

Li *et al.* (2020) emphasised in their study that most studies focus on neuronal settings and therefore they want to investigate cellular mechanisms in muscle cells instead. They showed that as GR is highly positively charged, it is able to enter the mitochondria and interact with components of the MICOS. Genetic manipulation by downregulation of MICOS complex components as well as pharmacological restoration of ion homeostasis with nigericin rescues mitochondrial cristae morphology in GR80 flies.

However, in my studies, I used my neuronal set up instead and observed no changes in behavioural phenotypes with genetic manipulations of the MICOS complex components. This does not invalidate any results but highlights the differences between cell and tissue specific compartments.

Modulation of mitophagy does not rescue *C9orf72* phenotypes

Ubiquitin-specific protease (USP30) is a deubiquitinating enzyme (DUB) found in the OMM and peroxisomes and plays an essential role in PINK1-parkin mediated mitophagy (Wang *et al*, 2022). Previous studies have shown that USP30 opposes PINK1 and parkin-dependent mitophagy (Bingol *et al.*, 2014) where it preferentially cleaves Lys6- and Lys11-linked ubiquitin chains assembled by Parkin on the mitochondria in response to membrane depolarisation (Cunningham *et al.*, 2015). It has been shown that depletion of USP30 in a *Drosophila* model of PD is beneficial by enhancing mitochondrial clearance (Bingol *et al.*, 2014) however, little was known about the role of USP30 *in vivo*. In my setup, I have observed that reducing the levels of USP30 increases the number of mitolysosomes *in vivo*. When combined with G4C2x36 and GR36, despite boosting mitophagy, this was not able to rescue the number of mitolysosomes or the larval crawling deficit in the *C9orf72* models, which suggests that the observed decrease in mitophagy is a downstream consequence and not a primary causation event. Other DUBs such as knockdown of USP15 have also been found to rescue parkin knockdown flies as well as rescue mitophagy defects found in PD patient fibroblasts by counteracting parkin-mediated mitochondrial ubiquitination (Cornelissen *et al*, 2014). Therefore, it would be interesting to investigate *C9orf72* interactions with other DUBs such as USP15 and USP8, as beneficial effects were observed with USP8 knockdown in PD models as well (Alexopoulou *et al*, 2016; von Stockum *et al*, 2019).

PINK1 overexpression has also been used to rescue other models of neurodegenerative diseases. As well as their role in mitophagy, it has been suggested that PINK1 and parkin are essential in regulating fission and fusion by interacting with Drp1 and Opa1 (Berman *et al*, 2008) and that this pathway regulates morphology by tipping the balance towards fission (Poole *et al*, 2008; Yu *et al*, 2011). Overexpression of PINK1 enhances mitochondrial fission independent of parkin and autophagy by phosphorylating Drp1 on serine 616 (Han *et al*, 2020). Du *et al* (2017) showed that increasing PINK1 expression enhances amyloid- β clearance via activation of OPTN and NDP52 signals in an mAPP Alzheimer's mouse model. Khalil *et al.* (2015) found mitochondrial spheroids in non-apoptotic photoreceptor neurons in a *Drosophila* model of Huntington's Disease. These spheroids are characteristic of cells where mitophagy is blocked. They found that *PINK1* overexpression alleviated mitochondrial spheroid formation and counteracted neurotoxicity by restoring ATP levels, and neuronal integrity thereby improving survival. In light of these results, I aimed to overexpress PINK1 in G4C2x36 and GR36 to both boost mitophagy and rescue the mitochondrial elongation morphology phenotype, however, I saw the opposite effect where overexpression of PINK1 or parkin mildly exacerbated the phenotype instead. It has to be

noted that overexpression of PINK1 has not necessarily been shown to boost mitophagy and therefore whilst the theory and thought process may be correct, this point needs to be proven first.

Furthermore, there are alternative pathways that have been reported to trigger mitophagy that are PINK1/Parkin independent. Other mitophagy receptors that are located on the OMM containing LC3 interacting region (LIR) motifs which also interact with LC3 (Khalil & Lievens, 2017) include Bcl-2 and adenovirus E1B 19 kDa-interacting protein 3 (BNIP3) and Nix/BNIP3L (BNIP3-Like) (Novak *et al.*, 2010; Rikka *et al.*, 2011), Autophagy and BECLIN 1 regulator 1 (AMBRA1) (Strappazzon *et al.*, 2015) and FUN14 domain-containing protein 1 (FUNDC1) (Liu *et al.*, 2012). Apart from mitophagy receptors, cardiolipin can be translocated from the IMM to the OMM where it recruits phagophores by association with LC3 (Chu *et al.*, 2013). Finally, *in vivo* work in mice and *Drosophila* revealed that PINK1 and Parkin are dispensable for basal mitophagy, indicating that other pathways may compensate for the PINK1/Parkin mitophagy pathway under physiological mitophagy (Lee *et al.*, 2018; McWilliams *et al.*, 2018). Different stimuli and stress-induced mitophagy may be affected by different regulatory receptors and pathways therefore more work is needed to elucidate the role of mitophagy in *C9orf72* pathogenesis.

Antioxidants

Since an increase in mitochondrial ROS was observed in G4C2x36, GR36 and GR1000 flies, I hypothesised that overexpression of antioxidants would suppress behavioural locomotor phenotypes. However, only overexpression of Sod2 and catalase rescued the *C9orf72* phenotypes whereas Sod1 exacerbated larval crawling impairment in G4C2x36 and GR36 larvae and had little effect on GR1000 climbing. Over 150 mutations in SOD1 have been found to cause familial ALS (Forsberg *et al.*, 2019) and it is widely accepted in the field that the normal dimeric Sod1 forms destabilised monomers and aggregates which are the toxic species. Since Sod1 is an ALS gene, it would be interesting to investigate any potential links between *C9orf72*, Sod1 and neurodegeneration. This may provide more insight as to why Sod1 is not able to rescue the *C9orf72* behavioural locomotor impairments. Lopez-Gonzalez *et al.* (2016) found that ectopic expression of hSOD1 and catalase can suppress GR80 toxicity in the fly wing. It has to be noted that their hSOD1 suppression is relatively small. Moreover, overexpression with human Sod1 is not directly comparable with overexpression of *Drosophila* Sod1. These results highlight the importance of mitochondrial

ROS driving disease phenotypes and compartmentalised investigations will allow better understanding to indicate where ROS is most damaging.

Moreover, Filograna *et al* (2016) investigated the beneficial effects of Sod enzymes and used a SOD-mimetic compound M40403 to protect against paraquat (PQ) induced toxicity showing a rescue in lethality in both Sod1 and Sod2 deficient flies. Interestingly, they found that paraquat was able to promote oxidative stress at the mitochondrial level. Of note, Filograna *et al.* (2016) observed that an acute dose of 24 h PQ treatment resulted in increased mitochondrial ROS production only, whereas a longer chronic 48 h dose increased both mitochondrial and cytosolic ROS in SH-SY5Y cells. Overexpression of human SOD1 and SOD2 was used to attempt to protect against PQ toxicity, however only mitochondrial SOD2 was able to confer protection measured by cell viability. Consistent with *in vitro* results, ubiquitous overexpression of *Drosophila* Sod1 had no effect however, flies overexpressing Sod2 were significantly more resistant to acute PQ (5 mM) toxicity measured by survival. This suggests that organismal viability is more affected at the mitochondrial level from ROS compared to the cytosol as only overexpression of Sod2 was able to rescue in acute stress conditions. Next, they investigated chronic exposure of PQ (1 mM for 7 days). Surprisingly, ubiquitous overexpression of Sod1 was able to rescue motor behavioural phenotypes whereas Sod2 had no effect Filograna *et al.* (2016). These results suggest that cytosolic production of superoxide is more damaging with chronic exposure to PQ. These data complement my work and highlights the importance of studying subcellular compartments.

Catalases, are also important antioxidant enzymes which decompose hydrogen peroxide into water and oxygen. It is mainly cytosolic and highly expressed in peroxisomes but absent in the mitochondria. Other enzymes such as glutathione peroxidase (GPX) performs similar function to catalase, but can be found in the mitochondria. Stapper & Jahn (2018) used a roGFP2 reporter probe developed from Albrecht *et al.* (2011) to measure changes in glutathione redox potential in an A β 42 *Drosophila* model therefore, it would also be interesting to adopt a similar approach to investigate glutathione redox potential similar in a *C9orf72* background. Catalases have been used as a therapeutic treatment in *in vivo* models of ALS however, its use is limited due to its short half-life and poor penetration across the blood-brain barrier (BBB) to enter cells (Nandi *et al*, 2019). However, Singhal *et al* (2013) successfully used nanoparticles to deliver catalase to cultured primary human neurons where they observed a decrease in hydrogen peroxide-induced protein oxidation, DNA damage and reduced mitochondrial membrane transition pore opening. Reinholz *et al* (1999) used a putrescine-modified catalase with increased permeability at the BBB and observed a significant delayed age of onset of clinical disease as well as a trend for prolongation of

survival in a hSOD1^{G93A} mouse model. Furthermore, Pehar *et al* (2014) found that mitochondria-targeted catalase reverts neurotoxicity in astrocytes in a hSOD1^{G93A} mouse model but does not extend survival of the animal which implies that preventing peroxide-mediated mitochondrial damage alone is not sufficient to delay the disease. These results support my observations where overexpression of catalase and mito.Cat are generally beneficial in the *C9orf72* models.

4.6 Summary

In summary, amongst all the different genetic manipulations used to reverse mitochondrial phenotypes observed in the previous chapter, only overexpression of antioxidants such as mitochondrial Sod2 and catalase were beneficial. This suggests that oxidative stress is an important upstream pathway that is important when looking at disease pathogenesis. The next step will be to study *C9orf72* flies' defence mechanisms against oxidative stress and therefore investigating the NRF2/Keap1 antioxidant signalling pathway.

Chapter 5 – NRF2/cncC and Keap1 signalling

Chapter 5. NRF2/cncC and Keap1 signalling

Introduction and Aims

In Chapter 3, I showed that the *C9orf72* models have increased mitochondrial ROS and in Chapter 4, genetic manipulations with overexpression of Sod2 and catalase partially rescued *C9orf72* behavioural phenotypes. Taken together, my results suggest that oxidative stress is a main contributing factor in disease pathogenesis. The NRF2-Keap1 system is an evolutionary conserved intracellular defence mechanism to counteract oxidative stress. Under normal basal conditions, cytoplasmic NRF2 is targeted to the proteasome for degradation. Upon oxidative stress, Keap1 inhibition is relieved and detaches from NRF2 allowing NRF2 to translocate to the nucleus, where it heterodimerises with small Maf proteins. This in turn leads to transcription of downstream target genes including a series of antioxidative and cytoprotective proteins including heme oxygenase-1 (HO-1), glutathione peroxidase 1, glutathione S-transferases (GSTs), glutathione reductase (GR), and superoxide dismutase (SOD) (Tu *et al*, 2019). In this chapter, I investigate whether this pathway is involved in the overall pathogenesis of the *C9orf72* models and if its modulation can ameliorate the phenotypes observed in previous chapters.

5.1 Genetic interactions with Keap1

5.1.1 Genetic interactions with Keap1 mutants in heterozygosity rescued larval crawling phenotypes in G4C2x36 and GR36 larvae

It has been shown previously that reducing *Keap1* levels using two independent alleles, was able to extend lifespan as well as rescue neuronal-specific motor deficits in a *Drosophila* model of Alzheimer's Disease (Kerr *et al*, 2017). Therefore, I wanted to test whether reducing Keap1 levels would also rescue *C9orf72* phenotypes.

Firstly, I assessed larval crawling using a heterozygous mutant of *Keap1* as homozygous *Keap1* mutants are developmental lethal. Reduction of *Keap1* was able to significantly improve the larval crawling of both G4C2x36 and GR36 compared to control (Figure 5.1A). Moreover, qualitatively, the larvae did not appear as thin compared to their respective controls with heterozygous loss of *Keap1* (Figure 5.1B).

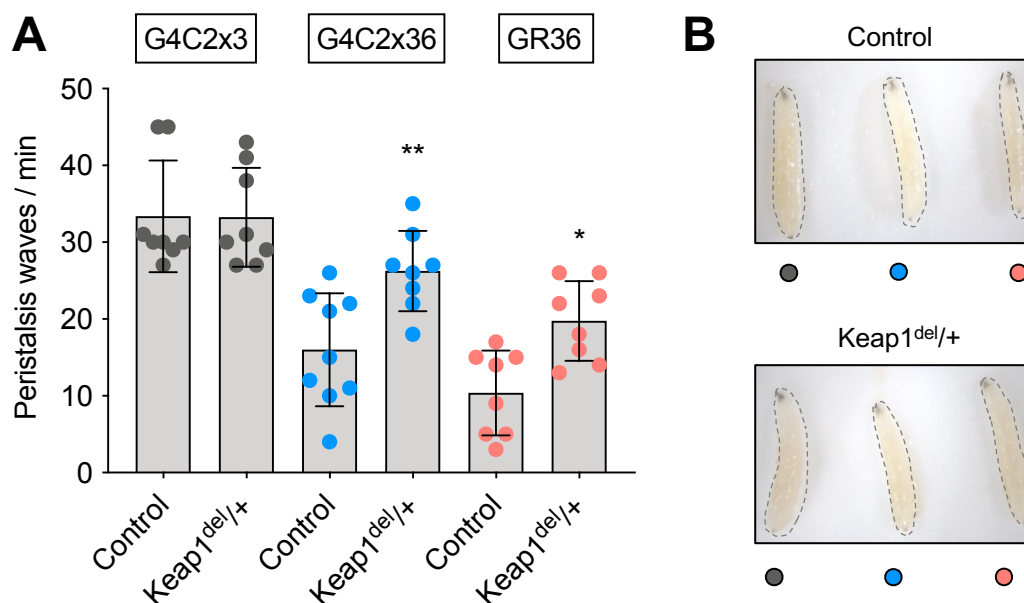


Figure 5.1 Heterozygous loss of Keap1 partially rescues *C9orf72* larval crawling phenotypes

(A) Expression of the repeats and DPRs was achieved using a pan-neuronal driver, *nSyb-GAL4* and the number of peristalsis waves was recorded. Statistical analysis was performed using one-way ANOVA with Bonferroni multiple comparison test: * $p < 0.05$, ** $p < 0.01$, chart shows mean \pm SD, $n = 8-10$, controls are pan-neuronal overexpression of *C9orf72* transgenes only. **(B)** Pan-neuronal expression of the G4C2x36 and GR36 with heterozygous mutants of Keap1. ($n = 6$ images taken, but more than 30 larvae were assessed visually to confirm the phenotypes observed).

5.1.2 Genetic interactions with Keap1 mutants in heterozygosity rescued adult climbing phenotypes in GR1000 flies

Similar experiments were performed using the GR1000 model, where adult climbing was assessed. At day 2, there were no climbing impairments from control or GR1000 that were biologically significant (Figure 5.2A). Flies were aged to d10, where GR1000 in combination with Keap1 in heterozygosity was able to fully rescue the climbing deficit for GR1000 control (Figure 5.2B).

Taken together, the data from all the *C9orf72* models tested suggest that reduction of Keap1 can rescue behavioural motor impairments and therefore may serve as an effective target for the prevention of neurodegeneration in *C9orf72*.

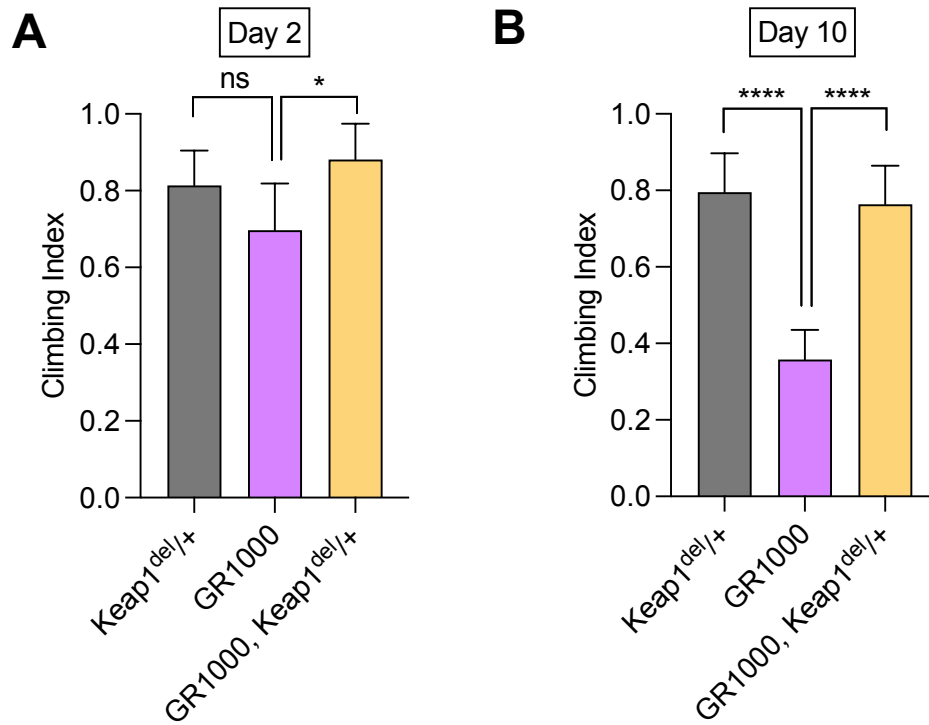


Figure 5.2 Heterozygous loss of Keap1 fully rescues GR1000 climbing deficit

Pan-neuronal expression of GR1000 with *nSyb-GAL4* with heterozygous mutant of *Keap1* at day 2 (**A**) and day 10 (**B**). Statistical analysis was performed using Kruskal-Wallis non parametric test with Dunn's correction: ns = non-significant, **** $p < 0.0001$. Chart shows mean \pm 95% CI, $n=60-100$ flies.

5.2 Characterisation of NRF2/cncC in G4C2x36 flies

5.2.1 Increased nuclear cncC staining is observed in larval brains of G4C2x36 and GR36

Since the behavioural data provided evidence that the NRF2/Keap1 pathway is involved, I hypothesised that there may also be induction of NRF2-ARE-dependent transcription. Increased ROS in *C9orf72* flies would be expected to activate the pathway to provide protection by transcription of antioxidant and cytoprotective genes to counteract oxidative stress.

If my hypothesis were true, NRF2 should translocate to the nucleus to act as a transcription factor. cncC has been shown to be the *Drosophila* homologue for NRF2 (Sykiotis & Bohmann, 2008). To test this hypothesis, I used an anti-cncC antibody from Chew *et al* (2021) and performed immunofluorescence in the larval brain with pan-neuronal expression of G4C2x36 and GR36 using *nSyb-GAL4* (Figure 5.3A). By quantifying the intensity of cncC nuclear staining using Hoechst to label the nucleus, I observed an increase in nuclear cncC in both G4C2x36 and GR36 compared to the G4C2x3 control (Figure 5.3B). This suggests that there is an activation of the NRF2/Keap1 signalling pathway at early stages of the disease pathogenesis.

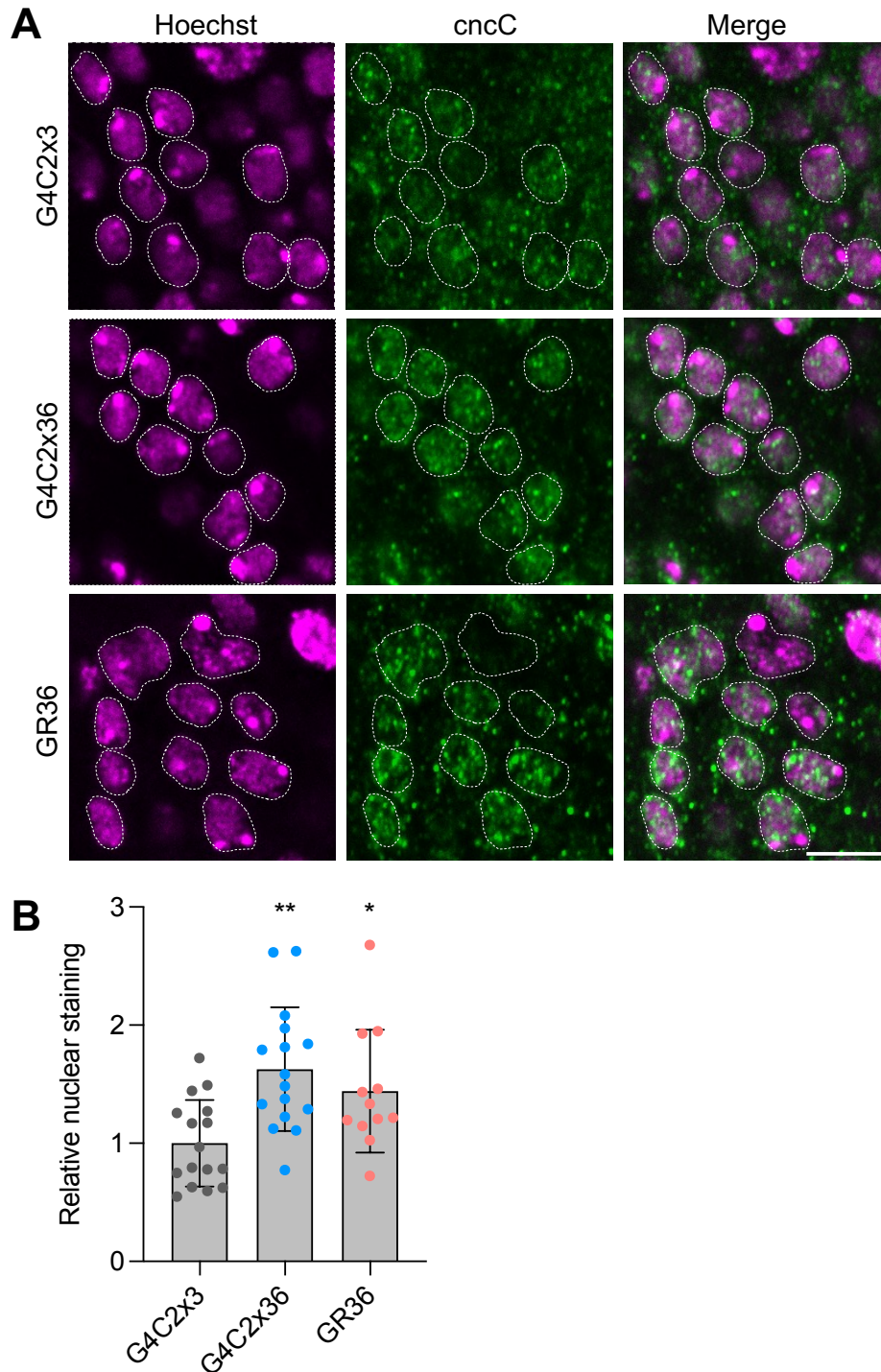


Figure 5.3 Increased *cncC* staining observed in G4C2x36 and GR36 larval brains

(A) Confocal microscopy images of larval brains labelling *cncC* expression, with Hoechst used to identify the nuclei boundaries. Pan-neuronal expression of G4C2x36 and GR36 with *nSyb-GAL4* was used and nuclear intensity was compared to the control, G4C2x3, scale bar = 10 μ m **(B)** Graph showing quantification of relative nuclear staining and statistical analysis was performed using one-way ANOVA with Bonferroni multiple comparison test: * $p < 0.05$, ** $p < 0.01$, chart shows mean \pm SD, $n = 12-16$.

5.2.2 G4C2x36 flies are able to respond to ROS-inducing paraquat treatment

gstD1 is a prototypical oxidative stress response gene and has been confirmed to be a cncC target gene (Sykiotis & Bohmann, 2008). Bohmann's group generated a reporter fly line to monitor the cncC/Keap1 antioxidant and detoxification responses in live conditions. It utilises a transgene that expresses GFP under the control of a 2.7 kb genomic sequence upstream of the *gstD1* gene. This genomic sequence harbours an antioxidant response element (ARE) sequence which is used to control the expression of GFP in the transgenic reporter flies (Figure 5.4A).

Moreover, Sykiotis & Bohmann (2008) validated the reporter function by utilising various oxidants such as paraquat, a free radical generator, diethyl-maleate, a glutathione depleting agent as well as hydrogen peroxide and observed induction of the reporter activity. I treated the control G4C2x3 flies with 5mM paraquat for 24 hours at day 4 and collected the flies at day 5 for immunoblot. With paraquat treatment, there is a significant increase in *gstD1*-GFP levels compared to no treatment (Figure 5.4B,C) therefore validating the reporter and recapitulating the findings from Sykiotis & Bohmann (2008).

At the same time I assessed whether the G4C2x36 flies could also respond to the ROS-inducing paraquat treatment. If they did not respond, this may explain the behavioural deficits of the *C9orf72* flies which have been shown to have increase mitochondrial ROS. Despite only having 2 biological replicates, the results show that there is a response to paraquat from the G4C2x36 flies compared to no treatment as *gstD1*-GFP levels increased (Figure 5.4B,C). This suggests that the *C9orf72* flies are still able to respond to paraquat and therefore their antioxidant response is still functional. But we cannot rule out the possibility that the response may be blunted as G4C2x36 flies induce the reporter to a proportionally lower level compared to control (G4C2x3 vs G4C2x3 PQ FC 3.47; G4C2x36 vs G4C2x36 PQ FC 1.88, Figure 5.4D)

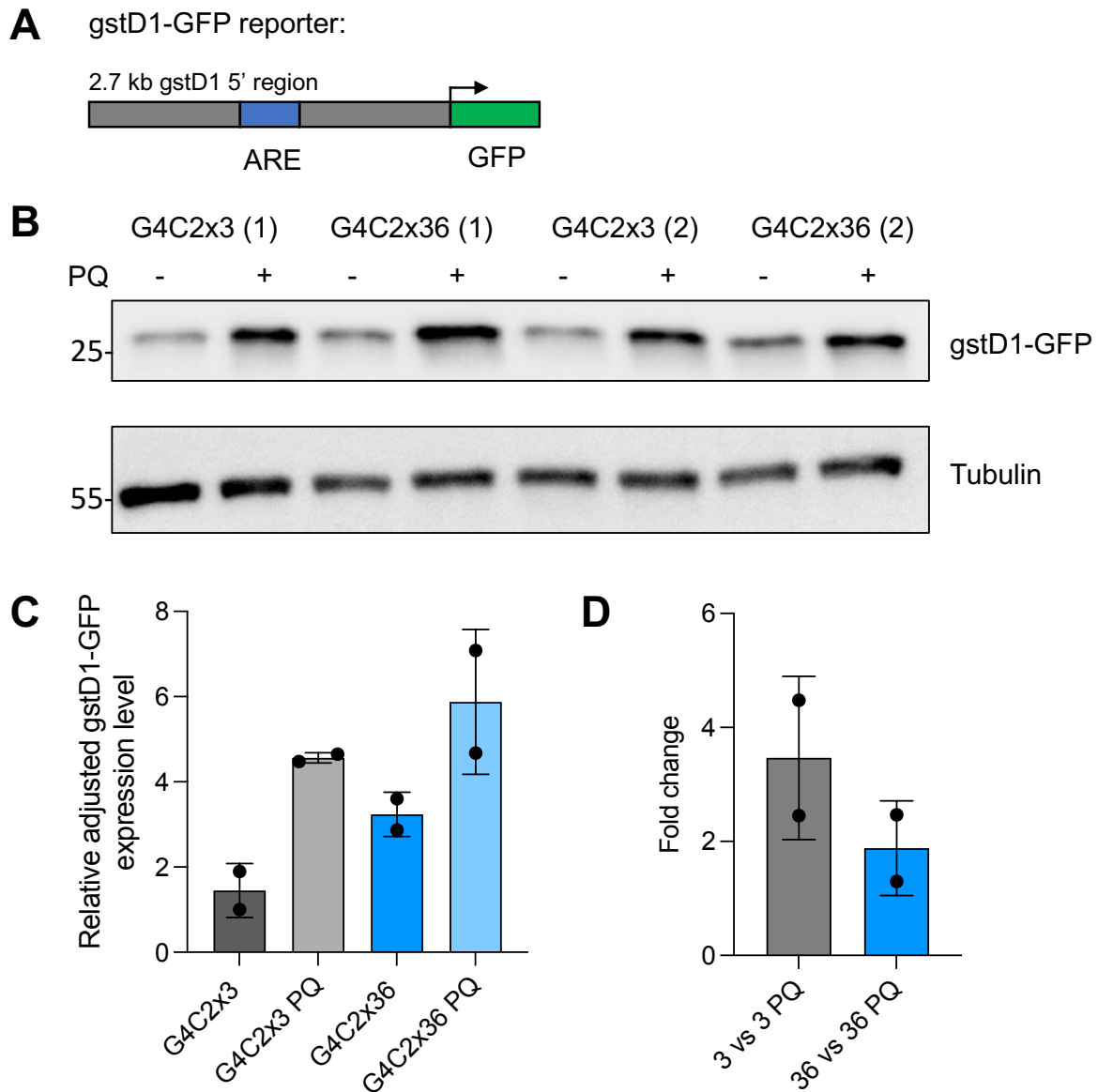


Figure 5.4 Immunoblot using the *gstD1*-GFP reporter in response to paraquat

(A) Schematic depicting *gstD1*-GFP reporter, adapted from Sykiotis and Bohmann (2008). Briefly, the genomic sequence upstream of the *gstD1* gene harbours an antioxidant response element (ARE) sequence which was used to control the expression of GFP in the reporter fly line. **(B)** Pan-neuronal expression of G4C2x36 in combination with the *gstD1*-GFP reporter. Anti-GFP was used to measure the levels of reporter expression at day 5, which is controlled by the ARE sequence in genomic sequence upstream of the *gstD1* gene. Flies were also treated with 5mM paraquat for 24 hours at day 4 and collected at day 5 for immunoblot. Two biological replicates are shown and denoted, anti-tubulin was used as the loading control. **(C)** Quantification of *gstD1*-GFP levels, chart shows mean \pm SD, ns = not significant. **(D)** Bar chart depicting the fold change of *gstD1*-GFP expression levels comparing G4C2x3 vs G4C2x3 PQ and G4C2x36 vs G4C2x36 PQ.

5.2.3 Changes in gstD1-GFP levels were observed across time

The gstD1-GFP reporter has been used in several studies to study NRF2 activity *in vivo*. Kerr *et al.* (2017) utilised this reporter to show a reduction of cncC activity in a *Drosophila* model of Alzheimer's Disease. Moreover, they performed an experiment where they also found a suppression of cncC in flies overexpressing human 0N3R tau as well as GR100, therefore suggesting that it is the accumulation of toxic proteins which leads to the generalised defect in NRF2 signalling across different neurodegenerative diseases (Kerr *et al.*, 2017).

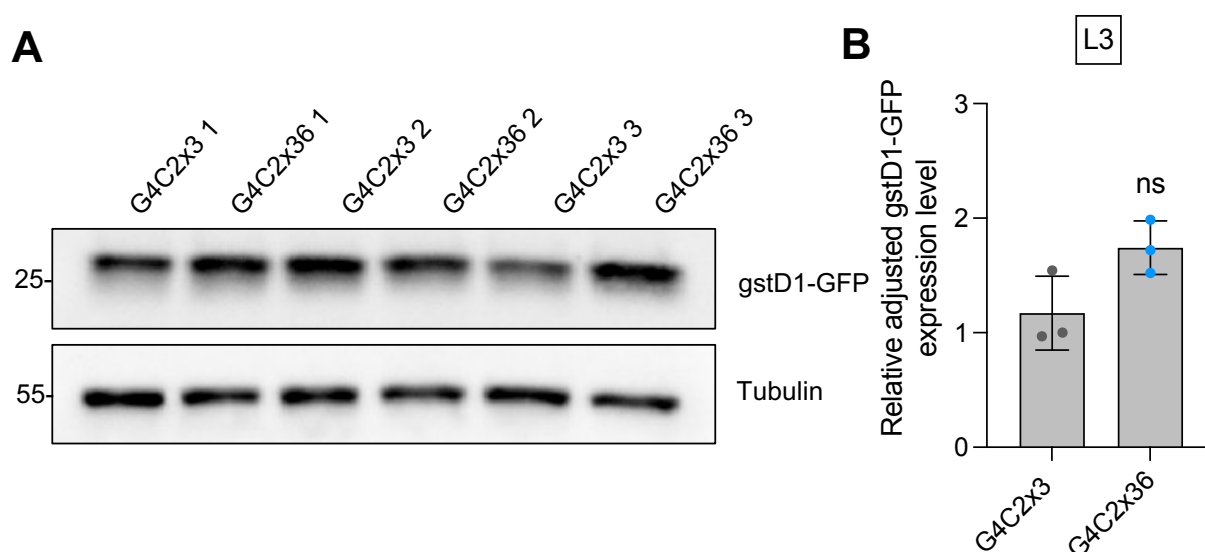


Figure 5.5 Immunoblot using the gstD1-GFP reporter in L3 stage shows no change in NRF2 activity in G4C2x36 flies

(A) Pan-neuronal expression of G4C2x36 in combination with the gstD1-GFP reporter. Anti-GFP was used to measure the levels of reporter expression at the L3 larval stage, which is controlled by the ARE sequence in genomic sequence upstream of the gstD1 gene. Three biological replicates are shown and denoted, anti-tubulin was used as the loading control. **(B)** Quantification of gstD1-GFP levels, chart shows mean \pm SD, ns = not significant.

Since I saw a behavioural rescue with reduction of Keap1 in the *C9ORF72* flies as well as nuclear accumulation of cncC/NRF2, I wanted to use the gstD1-GFP reporter to investigate whether there are changes in NRF2 activity in the *C9ORF72* flies across time. Firstly, I combined the reporter with pan-neuronal expression of G4C2x36 using *nSyb-GAL4*. After dissecting out the larval brains to perform western blot, I observed no changes to gstD1-GFP levels in the larval stage comparing G4C2x36 with the G4C2x3 control (Figure 5.5), despite an increase in nuclear staining of cncC (Figure 5.3).

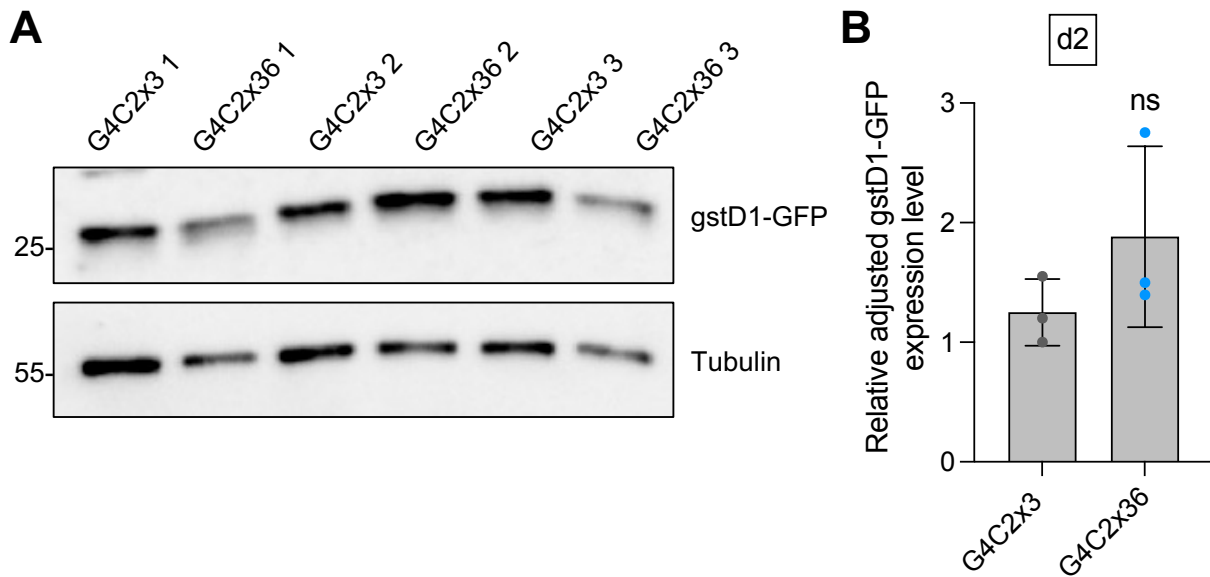


Figure 5.6 Immunoblot using the *gstD1*-GFP reporter at day 2 shows no change in NRF2 activity in G4C2x36 flies

(A) Pan-neuronal expression of G4C2x36 in combination with the *gstD1*-GFP reporter. Anti-GFP was used to measure the levels of reporter expression at day 2, which is controlled by the ARE sequence in genomic sequence upstream of the *gstD1* gene. Three biological replicates are shown and denoted, anti-tubulin was used as the loading control. **(B)** Quantification of *gstD1*-GFP levels, chart shows mean \pm SD, ns = not significant.

Next, I investigated NRF2 activity in the adults, at day 2 and day 5. At day 2, there were still no changes to the *gstD1*-GFP levels (Figure 5.6), however the results were variable and more replicates will give a more definitive answer. At day 5, there was a clear increase in NRF2 activity as reporter levels increased significantly, comparing G4C2x36 to the G4C2x36 control (Figure 5.4 and 5.7). The increase in NRF2 activity contradicts what was observed in Kerr *et al.* (2017) as they reported a decrease in NRF2 activity using the same reporter line in a GR100 model. However, considerations need to be made such as a different *C9orf72* model was used as well as their induction system using gene-switch GAL4 instead.

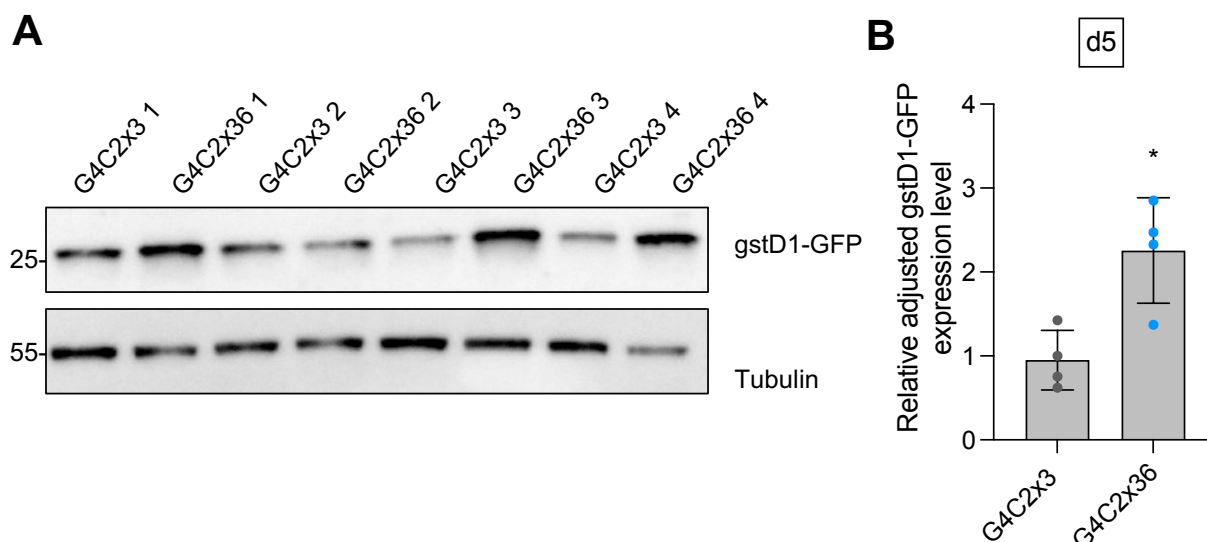


Figure 5.7 Immunoblot using the *gstD1*-GFP reporter at day 5 shows an increase in NRF2 activity in G4C2x36 flies

(A) Pan-neuronal expression of G4C2x36 in combination with the *gstD1*-GFP reporter. Anti-GFP was used to measure the levels of reporter expression at day 5, which is controlled by the ARE sequence in genomic sequence upstream of the *gstD1* gene. Four biological replicates are shown and denoted, anti-tubulin was used as the loading control. **(B)** Quantification of *gstD1*-GFP levels, chart shows mean \pm SD, * $p < 0.05$.

Lastly, I aged the flies to day 12 and collected fly heads to perform an immunoblot. At day 12, there is significantly more *gstD1*-GFP expression in the G4C2x36 flies compared to G4C2x3 control (Figure 5.8). The fold change (FC) is also much higher than at day 5 which suggests that NRF2 activity increases with time.

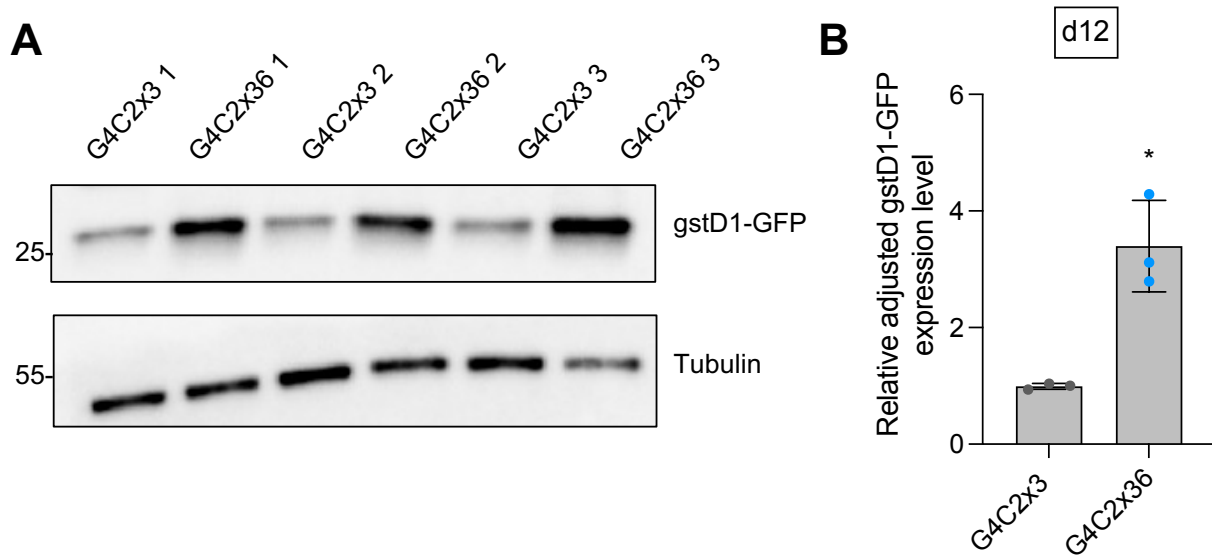


Figure 5.8 Immunoblot using the *gstD1*-GFP reporter at day 12 shows an increase in NRF2 activity in G4C2x36 flies

(A) Pan-neuronal expression of G4C2x36 in combination with the *gstD1*-GFP reporter. Anti-GFP was used to measure the levels of reporter expression at day 12, which is controlled by the ARE sequence in genomic sequence upstream of the *gstD1* gene. Three biological replicates are shown and denoted, anti-tubulin was used as the loading control. **(B)** Quantification of *gstD1*-GFP levels, chart shows mean \pm SD, * $p < 0.05$.

5.2.4 *cncC* target genes show minimal changes at transcript level

Using the *gstD1*-GFP reporter, I showed that there was an increase in NRF2 activity in G4C2x36 with age as well as an increased nuclear localisation of NRF2 in the larval brain. This implies that there could be more transcription of NRF2-ARE genes and therefore the next step was to determine whether there was an increase in transcription of endogenous NRF2 target genes.

Firstly, I wanted to test how the various NRF2 target genes would respond to paraquat treatment. I treated the flies with 5 mM paraquat at day 4 for 24 hours and collected the flies for qRT-PCR at day 5. For the G4C2x3 control, there was an increase in *cncC* and *gstD1* transcripts with paraquat treatment. No differences were observed for Keap1, Sod1 or Sod2 levels (Figure 5.9). In line with observations made earlier, where *gstD1*-GFP levels also increased with paraquat treatment in G4C2x36 flies (Figure 5.4), both *cncC* and *gstD1* mRNA transcripts also increased with paraquat treatment in G4C2x36 flies. Again, no differences

were observed with Keap1 transcript levels. The two datasets validate the experimental set up where paraquat induces an acute oxidative stress and flies can respond by increasing cytoprotective cncC targets transcripts such as *gstD1*, that subsequently will increase its protein levels, as shown by the *gstD1*-GFP reporter line (Figure 5.7, 5.8) and its downstream target transcripts.

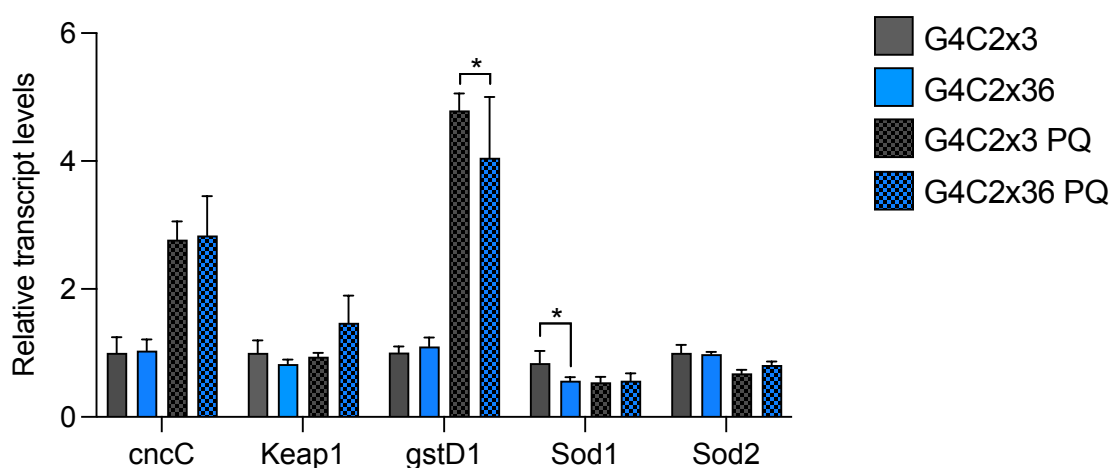


Figure 5.9 Quantitative RT-PCR on G4C2x36 flies at day 5 with paraquat treatment

qRT-PCR was performed using adult heads from day 5 flies with pan-neuronal expression of G4C2x3 as the control and G4C2x36 as the experimental group. For paraquat treatment, flies were fed 5 mM paraquat for 24 hours at day 4 and harvested at day 5. $n=4$ biological replicates, however, a few data points were taken out after quality control checks with the CT means. Statistical analysis was performed using unpaired t-tests with Welch's correction for unequal standard deviation, chart shows mean \pm SD, $*p<0.05$, all other results are non-significant (ns).

However, when investigating at basal levels where no paraquat treatment was added, there were no differences in *cncC*, *Keap1* or *gstD1* transcript levels between G4C2x3 and G4C2x36 flies (Figure 5.10), even though there was an increase in *gstD1*-GFP levels in the reporter line (Figure 5.7). Moreover, *Sod1* and *Sod2* are antioxidant genes that are also NRF2 target genes. Under basal conditions, there was a significant reduction in *Sod1* transcript levels, no changes to *Sod2* transcripts and a significant increase in catalase transcript levels. With paraquat treatment, the expected outcome was an induction of NRF2-target transcripts such as *Sod1* and *Sod2*; however, no differences were observed in their transcript levels in both G4C2x3 control and G4C2x36 flies (Figure 5.9).

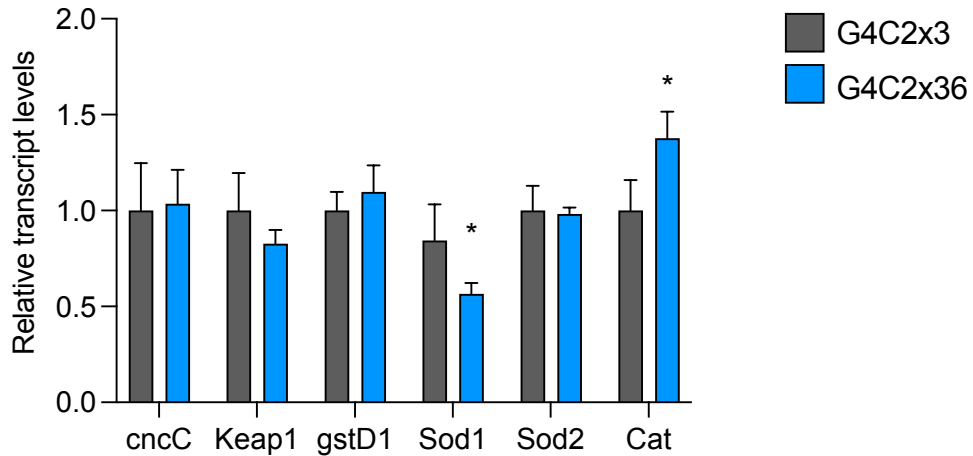


Figure 5.10 Basal transcript levels of cncC target genes in G4C2x36 flies at day 5

qRT-PCR was performed using adult heads from day 5 flies with pan-neuronal expression of G4C2x3 as the control and G4C2x36 as the experimental group. n=4 biological replicates, however, a few data points were taken out after quality control checks with the CT means. Statistical analysis was performed using unpaired t-tests with Welch's correction for unequal standard deviation, chart shows mean \pm SD, *p<0.05, all other results are non-significant (ns).

5.2.5 Transcript levels of cncC related genes comparing larval and adult G4C2x36 flies

Cheng *et al* (2021) used *gstD1*, *gclC* and *gclM* (glutamate-cysteine ligase catalytic/modifier subunits (GclC/GclM) which are the rate-limiting enzymes for glutathione biosynthesis), as their target genes to quantify CncC-regulated mRNAs by RT-PCR. Using a similar approach, I investigated the transcript levels of *cncC*, *Keap1* and *gstD1* at the L3 larval stage and compared this with day 5 adults to determine whether there is a difference in response with age. For both *cncC* and *Keap1*, there were no differences in transcript levels between G4C2x3 and G4C2x36 at L3 compared to day 5. However when comparing *gstD1* mRNA transcripts between late larvae (L3 stage) and mid-aged adult (day 5), there was a significant increase in *gstD1* transcript levels at the larval stage when comparing G4C2x3 control with G4C2x36, yet this increase was lost at day 5 where there were no differences observed (Figure 5.11). This contrasts with an increase in *gstD1*-GFP reporter levels at adult day 5, as assessed by western blot (Figure 5.7). However, it has to be noted that the sample size was relatively small and more experiments would be needed to confirm these results.

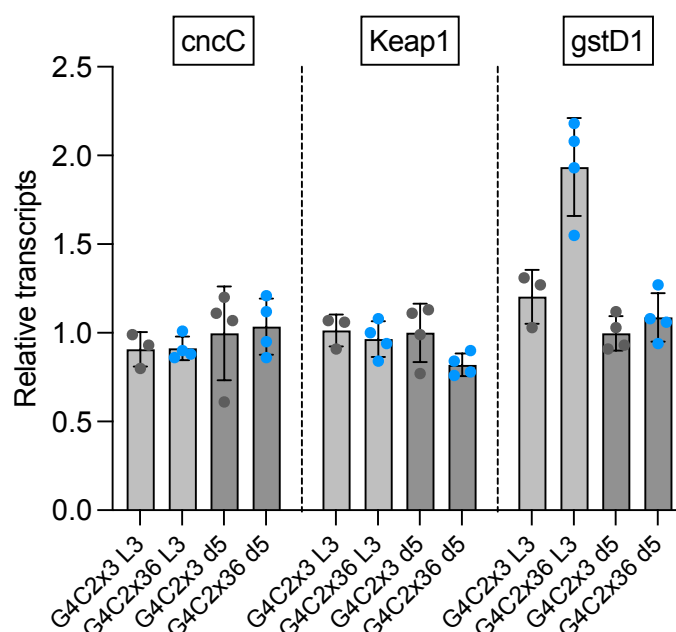


Figure 5.11 Transcript levels of cncC, Keap1 and gstD1 at L3 and day 5 for G4C2x36 flies

qRT-PCR was performed using dissected larval brains for L3 larval stage, and adult heads for day 5 with pan-neuronal expression of G4C2x3 as the control and G4C2x36 as the experimental group. n=4 biological replicates, however, a few data points were taken out after quality control checks with the CT means. Statistical analysis was performed using unpaired t-tests with Welch's correction for unequal standard deviation, chart shows mean \pm SD, *p<0.05, all other results are non-significant (ns).

Next, I chose a few other genes to attempt to understand the cncC target gene transcription landscape better. gclC has been shown to be a cncC target gene (Cheng et al., 2021) and I expected the gclC results would corroborate with the trends observed with gstD1. However, this was not the case as gclC transcript levels did not change in both larval L3 and at day 5 (Figure 5.12). Since I saw a decrease in mitophagy and NRF2 has been shown to regulate PINK1 expression under oxidative stress conditions (Murata *et al*, 2015), I investigated the levels of PINK1 as well but found no differences at larval L3 stage or at day 5-old adult heads too (Figure 5.12). Finally, since I saw an increase in catalase transcript levels at day 5 (Figure 5.11 and 5.12), I quantified catalase transcript levels at larval L3 stage as well. Here, I found no differences at the early stage compared to at day 5 (Figure 5.12). In summary, there are a lot of genes that were expected to change due to the findings from the gstD1 reporter but were not recapitulated with the qRT-PCR results (Figure 5.13), therefore more investigation is needed to investigate NRF2 signalling in this context.

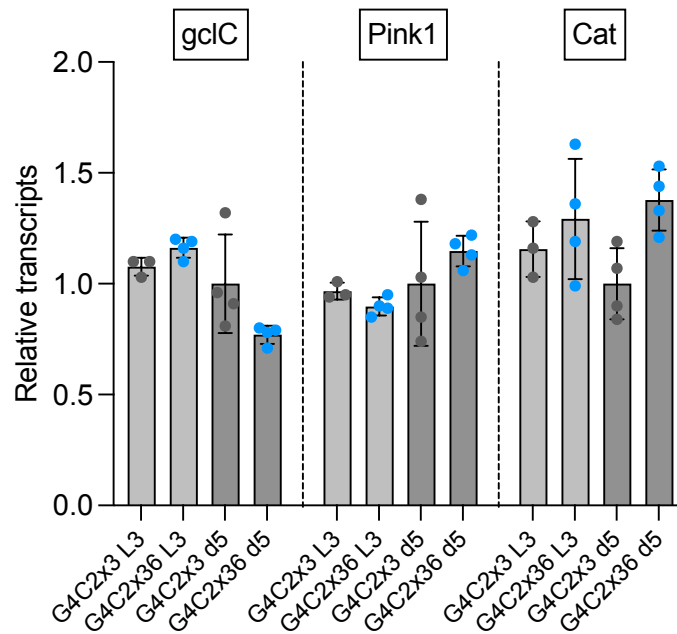


Figure 5.12 Transcript levels of gclC, Pink1 and catalase at L3 and day 5 for G4C2x36 flies

qRT-PCR was performed using dissected larval brains for L3 larval stage, and adult heads for day 5 with pan-neuronal expression of G4C2x3 as the control and G4C2x36 as the experimental group. n=4 biological replicates, however, a few data points were taken out after quality control checks with the CT means. Statistical analysis was performed using unpaired t tests with Welch's correction for unequal standard deviation, chart shows mean \pm SD, *p<0.05, all other results are non-significant (ns).

	cncC	cncC	gstD1	gstD1	
	Localisation	mRNA	mRNA	reporter	
L3	nuclear				Increase
d5	n/a				Trend for increase (ns)
d12	n/a	n/a	n/a		No change

Figure 5.13 Summary of findings

Table depicts a summary of all the NRF2/cncC findings using the immunoblot with anti-cncC, measuring cncC and gstD1 transcript levels and gstD1-GFP reporter, a proxy for NRF2 activity. Key: gray – no change, light green – trend for increase (results not statistically significant), dark green – statistically significant increase and n/a – not tested.

5.3 Treatment with NRF2/cncC activator dimethyl fumarate (DMF)

5.3.1 DMF treatment rescued climbing phenotypes in G4C2x36 and GR36 flies

Dimethyl fumarate (DMF) is an antioxidative and anti-inflammatory drug which is licensed under the name of Tecfidera, to treat relapsing forms of multiple sclerosis. It is thought to work by activating the NRF2 pathway, resulting in immunomodulatory and anti-inflammatory effects. It has also been shown to be beneficial in other inflammatory diseases and cancers, as well as exhibiting neuroprotective effects in other animal models of neurodegenerative diseases such as AD, PD and HD (Majkutewicz, 2022). Granatiero *et al* (2019) used DMF for NRF2 activation in human SOD1^{G93A} iPSC-derived astrocytes (iPSAs) and found that DMF was able to rescue calcium dysregulation as well as motor neuron toxicity. Since I saw beneficial effects with heterozygous knockdown of Keap1 and also differences using the *gstD1*-GFP reporter, I wanted to use DMF to activate the NRF2 pathway in my *C9orf72* models as well.

For this experiment, it was necessary to use a GAL4 driver which would overexpress the G4C2x36 and GR36 repeats but produce viable adults in order to test the longer-term effects of disease progression as well as perform longer drug treatments and use the climbing assay instead to measure behaviour phenotypes. *DIP-γ-GAL4* is a predominantly motor neuron driver (Venkatasubramanian & Mann, 2019) and when used to overexpress G4C2x36 allows the recovery of viable adults that show an age-dependent climbing phenotype whereby at day 3, the climbing behaviour is comparable to the G4C2x3 control (Figure 5.14A). However, by day 10, there is a significant impairment in climbing when compared to age-matched G4C2x3 control (Figure 5.14B). For GR36, there were viable adults compared to lethality at the L3 larval stage when using pan-neuronal expression with *nSyb-GAL4*. Moreover, there was a climbing phenotype for GR36 at day 3 when compared to G4C2x3 control (Figure 5.14A), which deteriorates and has an even stronger climbing phenotype by day 10 (Figure 5.14B).

To test whether activating NRF2 is beneficial in *C9orf72* flies, DMF was added to the food, with ethanol added instead to use for the control. To my knowledge, only one group have successfully used DMF in *Drosophila* for their investigations. Solana-Manrique *et al* (2020) used 7 μM DMF to attenuate the climbing deficit exhibited by DJ-1β mutants as well as

demonstrate a significant reduction of hydrogen peroxide production in these mutants supplemented with DMF. Using the same concentration of DMF, once eclosed, the *C9orf72* flies were raised on food containing 7 μ M DMF and their climbing ability was assessed. At day 3, flies supplemented with DMF showed no significant differences in climbing ability compared with their respective controls i.e. same genotype raised in food supplemented with ethanol (Figure 5.14A). At day 10, control G4C2x3 flies exhibited no differences in climbing between DMF and ethanol-supplemented food which demonstrates that this dose of DMF is tolerable. However, for both G4C2x36 and GR36, flies climbed significantly better raised on DMF food compared to ethanol control which suggests that DMF is beneficial and can attenuate *C9orf72* behavioural phenotypes (Figure 5.14B).

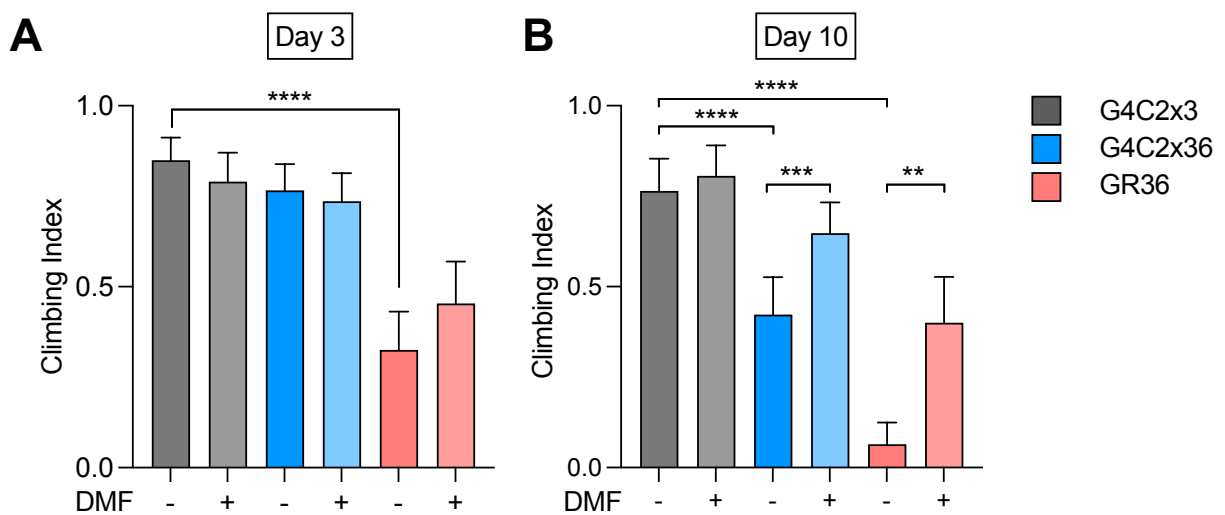


Figure 5.14 DMF treatment is able to rescue *C9orf72* climbing phenotypes

Adult climbing ability was assessed by expression in motor neurons using *DIP- γ -GAL4*. Flies were raised on food supplemented with either 7 μ M DMF or ethanol as control. Climbing was assessed at **(A)** day 3 and **(B)** day 10. Statistical analysis was performed using Kruskal-Wallis non parametric test with Dunn's correction: ** $p < 0.01$, *** $p < 0.001$, **** $p < 0.0001$, chart shows mean \pm 95% CI.

5.3.2 DMF treatment had little effect on climbing phenotypes in GR1000 flies

I repeated the same experiment with GR1000 flies which were raised on food supplemented with 7 μ M DMF and their climbing behaviour was assessed. No behavioural differences were observed at day 3 (Figure 5.15A). At day 10, the GR1000 climbing deficit was not significantly rescued by DMF supplementation however, there was a trend for improvement (Figure 5.15B). In the future, I would like to increase the dose of DMF to repeat

the experiment. Moreover, a later time point can be tested to develop a clearer idea of whether DMF supplementation is beneficial in GR1000 flies. Taken together, the results suggest that activating the NRF2 pathway with DMF can be beneficial and therefore a potential therapeutic target to treat *C9orf72* ALS/FTD.

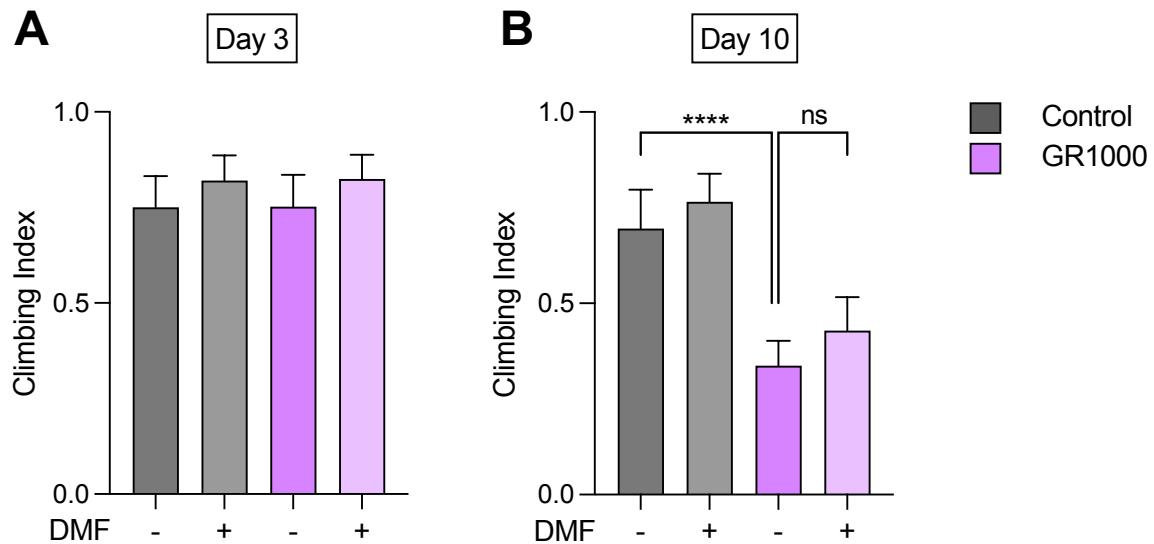


Figure 5.15 DMF treatment is not able to rescue GR1000 climbing phenotype at day 10 but shows trend for improvement

Adult climbing ability was assessed by expression in using pan-neuronal driver *nSyb-GAL4*. Flies were raised on food supplemented with either 7 μ M DMF or ethanol as control. Climbing was assessed at **(A)** day 3 and **(B)** day 10. Statistical analysis was performed using Kruskal-Wallis non parametric test with Dunn's correction: **** $p < 0.0001$, ns = non-significant, chart shows mean \pm 95% CI.

5.4 Discussion

In Chapter 5, I have investigated the role of NRF2 and Keap1 and their cellular response to increased oxidative stress in the *C9orf72* models. Firstly, I have shown that there is increased nuclear translocation of NRF2 in G4C2x36 and GR36 larval brains which suggests that this pathway is activated already at the larval stage. By using the *gstD1*-GFP reporter as a proxy for NRF2 activity with age, I have shown that there is a significant increase in GFP expression levels at day 5 which further increases at day 12. However, when measuring the mRNA transcript levels of NRF2, Keap1 as well as NRF2 targeting genes, there are no substantial changes in transcript levels, except for an increase in *gstD1* transcripts at the larval stage. This may indicate that although the flies are able to detect the oxidative stress environment, a response is mounted but not sufficient and may be blunted. This explains the lack of changes seen in the transcript levels and the behavioural degenerative phenotype observed. However, this pathway indeed plays a role in *C9orf72* pathogenesis, as heterozygous knockdown of Keap1 was able to significantly improve the larval crawling for G4C2x36 and GR36 larvae. Moreover, there was also a rescue in climbing behaviour for GR1000 flies as well. Finally, dimethyl fumarate (DMF) treatment to boost NRF2 activity was able to rescue climbing behaviour of G4C2x36 and GR36 flies using a predominantly motor neuron driver. This is a positive result that promotes NRF2 activation as a potential therapeutic strategy for tackling *C9orf72* ALS/FTD.

Localisation of *cncC*/NRF2

NRF2 has been shown to be translocated into the nucleus to activate ARE antioxidant genes under stress conditions such as oxidative stress. Theodore *et al* (2008) identified nuclear localisation signal (NLS) motifs which are important to drive nuclear translocation of NRF2. Moreover, using immunoprecipitation assays, they demonstrated that importins $\alpha 5$ and $\beta 1$ associate with NRF2 which highlights an important role for the nuclear import system. Other import proteins that have been studied include importin $\alpha 7$, which has been linked to mediating Keap1 nuclear import by interaction with its Kelch domain and thus enhancing the clearance of NRF2 in the nucleus (Sun *et al*, 2011). Interestingly, nucleocytoplasmic transport has been reported to be disrupted in *C9orf72* (Freibaum *et al.*, 2015). I would like to perform further experiments investigating the localisation of NRF2 in adult brains with aging in the neurodegenerative models and therefore ask whether nucleocytoplasmic transport deficits in

C9orf72 disrupt the nuclear translocation of NRF2 which may explain the lack of response to oxidative stress with my results.

cncC/NRF2 activity – using the gstD1-GFP reporter

The gstD1-GFP reporter generated by the Bohmann lab has been an invaluable resource to assess NRF2 activity in various contexts. In a fly model of Batten disease, flies lacking CLN3 (genetic mutations in the CL3 gene lead to early onset Batten disease) function are hypersensitive to oxidative stress and when overexpressed provides increased resistance to it. CLN3 mutant flies are able to perceive conditions of oxidative stress shown by induction of the gstD1 reporter, but are not able to detoxify ROS, suggesting their ability to respond is compromised (Tuxworth *et al*, 2011). There are also numerous studies using the gstD1-GFP reporter in the literature where an increase in ROS usually correlates with an increase in gstD1-GFP reporter expression suggesting an increase in NRF2 activity. In a traumatic brain injury in *Drosophila*, the authors correlated increases in oxidative stress markers from a rat model of TBI with an increase in gstD1-GFP reporter activity in their fly system (Saikumar *et al*, 2020). Another study to use this reporter included Wu *et al* (2017) where they investigated intestinal microbial dysbiosis in an A β 42 *Drosophila* model of AD and explored ROS production by DCF-DA staining to detect an increase in intracellular ROS levels. This was accompanied by an increase in gstD1-GFP reporter activity at day 10 using pan neuronal overexpression of A β 42 with *elav-GAL4*. This contrasts with the results shown in Kerr *et al*. (2017) where they used a slightly different AD model - Arctic mutant A β 42 to show a significant reduction in gstD1-GFP reporter and therefore suggested that inhibition of NRF2 activity is attributed to A β 42 aggregation. Moreover, Kerr *et al*. (2017) also found that the reporter activity was significantly decreased in flies overexpressing human 0N3R tau as well as in a GR100 model for *C9orf72* ALS/FTD indicating that it may be an accumulation of toxic proteins which lead to the generalised defect in NRF2 signalling across various neurodegenerative diseases.

However, my results do not align with the findings from Kerr *et al*. (2017). Under basal conditions, I have observed an increase in mitochondrial ROS with the mito-roGFP2-Orp1 reporter. The accumulation of ROS could be due to a failure to perceive the presence of ROS or it could be the failure to mount a response. To determine whether the accumulated ROS was due to a failure to upregulate antioxidant gene transcription in response to oxidants, I used the gstD1-GFP reporter in the G4C2x36 flies, and also tested its response to paraquat, which generates superoxide anions. In the absence of paraquat, the basal level of GFP

expression is higher in G4C2x36 flies compared to G4C2x3 control (1.23-fold) which suggests that they are trying to respond since they are under an intrinsic oxidative load which corroborates with an increase in mitochondrial ROS observed initially for G4C2x36 flies. Following exposure to 24 h treatment of 5 mM paraquat, the reporter was strongly induced in both control and G4C2x36 flies. However, G4C2x36 flies induce the reporter to a lower level compared to control (G4C2x3 vs G4C2x3 PQ FC 3.47; G4C2x36 vs G4C2x36 PQ FC 1.88) and therefore suggests that although the G4C2x36 flies can perceive the presence of high ROS, their response to oxidative stress may be blunted. This may reflect the absence of a feedback mechanism whereby a sufficient response is needed to combat oxidative damage.

Interestingly, there were changes in the *gstD1*-GFP reporter when I performed a time course tracking G4C2x36 larvae and flies compared to G4C2x3 control. Early developmental stages represented by larval L3 stage showed no changes with the reporter activity even though there is a strong behavioural phenotype accompanied by an increase in mitochondrial ROS. There were also no changes at day 2 which may suggest that there is a delay in responding to the oxidative stress environment for G4C2x36 flies. This also suggests that the system is trying to compensate and respond which is why there is an increase in *gstD1*-GFP reporter expression at day 5 which further increases at day 12, the later time point. If we compare the fold change at day 12 with paraquat treated control flies at day 5 (G4C2x3 vs G4C2x3 PQ FC 3.47 compared to G4C2x3 vs G4C2x36 d12 FC 3.4), it shows that the response at day 12 is similar to the response a control fly would have with paraquat-induced oxidative stress. This highlights the capability for the G4C2x36 flies to respond but the response may be blunted or delayed and therefore the flies are not able to counteract the overload of ROS in the cells. I showed in Chapter 4 that overexpression of antioxidants such as *Sod2* and catalase partially rescue *C9orf72* behavioural phenotypes. This indicates that it is a very tightly regulated system and that the response to oxidative stress is pivotal to investigating disease initiation and pathogenesis in *C9orf72* ALS/FTD.

cncC/NRF2 activity – transcript levels

As I observed an increase in the expression of GFP levels using the *gstD1*-GFP reporter with age in G4C2x36, I hypothesised that since NRF2 activity is enhanced, this suggests that there is more transcription of NRF2 targeting genes and therefore their relative transcript levels are boosted. There were many results that were not expected when I conducted qRT-PCR to measure transcript levels. Firstly, I used paraquat as a positive control to induce an acute stress whereby NRF2-mediated transcription should be boosted. Both *cncC* and *gstD1* transcripts were significantly elevated with paraquat treatment. This suggests that the paraquat treatment worked and a response is elicited. However, surprisingly, *Sod1* and *Sod2* transcripts did not increase with paraquat treatment, even though it has been suggested in the literature that they are antioxidant genes targeted by NRF2-ARE transcription. Of note, Filograna *et al.* (2016) observed that an acute dose of 24 h PQ treatment resulted in increased mitochondrial ROS production only, whereas a longer chronic 48 h dose increased both mitochondrial and cytosolic ROS in SH-SY5Y cells (Rodriguez-Rocha *et al.*, 2013; Filograna *et al.*, 2016). These findings suggest that in my experimental set up, I apply an acute stress only which may not be enough to elicit a full response therefore the antioxidant genes may not be substantially affected.

Kirby *et al.* (2005) performed microarray analysis in a motor neuron-like NSC34 cell line transfected with SOD1^{G93A} and found that NRF2 and its targeted genes were markedly reduced. Post mortem tissue from ALS patients revealed a reduction of NRF2 mRNA and protein expression in neurons in the motor cortex and spinal cord, whereas Keap1 mRNA expression was increased in the motor cortex only, however similar protein expression levels were observed (Sarlette *et al.*, 2008). To summarise, if the NRF2 pathway is activated, there should be increased transcription of NRF2 and its target genes, however, previous literature has shown that the opposite result can be observed. Interestingly, a meta-analysis of microarray sets from Alzheimer's Disease (AD) and Parkinson's Disease (PD) found that NRF2 was upregulated yet identified 31 common downregulated ARE-driven genes such as detoxification genes NQO-1 and SOD1 (Wang *et al.*, 2017). The authors speculated that NRF2 may be part of a complex regulatory network and must be affected by other transcription factors and regulatory mechanisms. They found that sMAF, in particular MAFF, was highly expressed in AD and PD. sMAF proteins can form homodimers among themselves and can act as transcriptional repressors therefore overexpression of MAFF represses NRF2 dependent gene transcription, resulting in NRF2 target gene downregulation (Wang *et al.*,

2017). These findings may explain why minimal changes were observed in the G4C2x36 flies. As described earlier, there is increased ROS with a blunted NRF2 mediated response and potentially, sMAF proteins may be dysregulated. It will be interesting to investigate the mRNA transcripts of sMAF as well as test genetic interactions with C9orf72 conditions.

Therapeutic treatments – DMF

Dimethyl fumarate (DMF) has been successfully used to treat relapsing multiple sclerosis and has also been shown to be beneficial in some animal models of neurodegenerative disease (Yamazaki *et al*, 2015; Majkutewicz, 2022). NRF2 has many functions; the most important being the induction of transcription of cytoprotective enzymes and antioxidant genes such as NAD(P)H-quinone oxidoreductase 1 (NQO1), glutamate-cysteine ligase catalytic subunit (GCLc), glutathione S-transferases (GSTs) and heme oxygenase 1 (HO-1). DMF acts by the inactivation of Keap1 via succination of its cysteine residues, more specifically, mass spectrometry experiments found that monomethyl fumarate led to direct modification at cysteine 151 (Linker *et al*, 2011; Yamamoto *et al*, 2018).

Another mode of action mediated by DMF includes the inhibition of pro-inflammatory nuclear factor kappa-light-chain-enhancer of activated B cells (NF- κ B) pathway (Giridharan & Srinivasan, 2018). Similar to NRF2, NF- κ B is a transcription factor normally localised in the cytoplasm and is inhibited by inhibitor of kappa B protein (I κ B), as Keap1 is to NRF2. Under oxidative stress or exposure to bacterial and viral antigens, I κ B is phosphorylated and subsequently degraded, therefore releasing its inhibition on NF- κ B, which is allowed to translocate to the nucleus which activates expression of genes associated with inflammatory responses and tumorigenesis. It has been shown that DMF inhibits NF- κ B activity by covalently modifying p65, which is an important component of the NF- κ B complex in breast cancer cells. However, Gillard *et al* (2015) demonstrated that inhibition of NF- κ B by DMF was independent of NRF2 as DMF treatment inhibited pro-inflammatory cytokine production in both cultured wild-type and NRF2 knockout splenocytes. Conversely, DMF can indirectly inhibit the NF- κ B pathway indirectly via the NRF2 pathway. NRF2 activation has been shown to induce transcription of genes responsible for mounting an inflammatory response such as interleukin 1 β (IL-1 β), interleukin 6 (IL-6) and tumour necrosis factor α (TNF- α) (Pan *et al*, 2012). As described previously, NRF2 also promotes transcription of HO-1, as carbon oxide, a product derived from HO-1 activity can exert anti-inflammatory effects on macrophages by inhibiting

the NF- κ B pathway (Lee *et al*, 2003). Moreover, both NRF2 and p65 compete to bind with transcriptional co-activator CREB-binding protein-p300 complex (CBP-p300) and therefore overexpression of NRF2 by DMF may tip the balance for NRF2 mediated ARE transcription bound to CBP-p300 instead thereby limiting NF- κ B activity (Liu *et al*, 2008; Majkutewicz, 2022). Finally, Keap1 has another role as an inhibitor of kappa B protein kinase ubiquitination, therefore when DMF acts via succination of Keap1, its depletion would lead to stabilisation of the kinase and hence upregulation of NF- κ B activity (Lee *et al*, 2009).

Since I have observed a partial rescue of the *C9orf72* phenotypes with reduction of Keap1 as well as DMF treatment despite a weak NRF2 response, as observed by minimal changes of mRNA transcripts of NRF2 and its targeting genes, it would be interesting to study how Keap1 is acting, and whether the rescue is NRF2 related. Moreover, the DMF rescue could be via NRF2 independent pathways, therefore more research is needed to determine what the reasons behind the rescue experiments are and whether there is crosstalk between the two pathways.

5.5 Summary

In summary, I have used various techniques to investigate the NRF2/Keap1 pathway. In G4C2x36 larvae, there is increased nuclear cncC localisation which suggests that the pathway is induced early in disease pathogenesis. Moreover, in G4C2x36 day 5 flies, increased NRF2 activity was observed using the *gstD1*-GFP reporter. Lastly, heterozygous loss of Keap1 partially rescues G4C2x36 larval locomotion and therapeutic treatment with DMF suppressed G4C2x36 climbing motor impairment which suggests that targeting the NRF2/Keap1 pathway may be beneficial.

Chapter 6 – General discussion and future work

Chapter 6 – General Discussion and future work

6.1 Summary of Findings

Mitochondrial dysfunction has been widely reported in many neurodegenerative diseases including ALS/FTD. The role of mitochondria specifically in *C9orf72* ALS/FTD has been relatively understudied, especially in an *in vivo* system. Excess production of reactive oxygen species has been reported (Lopez-Gonzalez *et al.*, 2016) but it is not clear whether these phenomena are causative or a consequence of the pathogenic process. The aim of this thesis was to use *C9orf72* transgenic *Drosophila* models to investigate and characterise mitochondrial phenotypes and determine their relevance in driving the pathogenic mechanisms.

In Chapter 3, I was able to recapitulate established phenotypic characterisation that have been previously published. Strong larval crawling and adult climbing behavioural phenotypes were observed with pan-neuronal expression of G4C2x36 in the pure repeats model (Mizielinska *et al.*, 2014) as well as the alternative codon GR-only constructs – GR36 (Mizielinska *et al.*, 2014) and GR1000 (West *et al.*, 2020). Their locomotor impairment allowed me to use it as a readout for testing different genetic manipulations to modulate their behavioural phenotypes. Next, I investigated mitochondrial morphology. Mitochondrial fragmentation and swollen mitochondria were commonly found in *C9orf72* patient fibroblasts and iPSCs (Dafinca *et al.*, 2016; Onesto *et al.*, 2016). Similar findings were observed in flies where mitochondria were swollen when GR80 was expressed in the fly muscle (Li *et al.*, 2020). However, when I pan-neuronally expressed the G4C2x36 and GR36 in the larval brain, elongated and hyperfused mitochondria were observed. Differences in morphology between the studies are likely due to the different model systems used as well as cell types (muscle vs neurons). Impaired mitophagy has also been implicated in many neurodegenerative diseases including ALS however, to my knowledge, mitophagy has been relatively understudied in specifically in *C9orf72*. Therefore, I employed our *Drosophila* mitophagy reporter, mito-QC (Lee *et al.*, 2018) and found a reduction of mitolysosomes in G4C2x36 and GR36. These results complement observations where perturbed autophagy is found in G4C2x36 and GR36. A reduction in the number of autolysosomes was observed using an autophagic flux GFP-mCherry-Atg8a reporter as well as increased expression of Ref(2)P and a reduction in Atg8a-II levels by immunoblot. My results also corroborate with recent findings from (Cunningham *et al.*, 2020) where they reported disrupted autophagy in their G4C2x30 repeats model as well. Finally, I observed a reduction in complex I and complex II linked respiration in G4C2x36 flies as well as increased mitochondrial ROS in both G4C2x36 and GR36 measured with the mito-

roGFP2-Orp1 reporter and in the GR1000 model measured with MitoSOX. My results are in line with findings from Choi *et al.* (2019) where they found an increase in DNA damage, oxidative stress and decreased activities of mitochondrial complexes I and V. The next step was to investigate the underlying pathogenic mechanisms associated with changes in mitochondrial morphology, defective mitophagy and oxidative stress-associated neurodegeneration.

In Chapter 4, genetic manipulation to restore mitochondrial fission/fusion dynamics by promoting fission (overexpression of Tango11 or Drp1) or reducing fusion (heterozygous Opa1 and Marf mutants) did not rescue G4C2x36 and GR36 locomotor deficits contrary to my expectations. Li *et al.* (2020) studied the effect of altering fission-fusion balance by the loss- or gain-of-function of Drp1, Fis1, or Marf and also observed no obvious effect on GR80 toxicity. Moreover, boosting mitophagy by knockdown of USP30 or PINK1/parkin overexpression was not able to rescue the G4C2x36 and GR36 phenotypes. Taken together, these data corroborate the lack of behavioural rescue and suggests that aberrant mitochondrial dynamics and reduced mitophagy are not primary causes but downstream consequences in *C9orf72* pathogenesis. However, genetic upregulation of antioxidants such as mitochondrial superoxide dismutase 2 (Sod2) and catalase were able to rescue behavioural impairment phenotypes in G4C236, GR36 and GR1000. Surprisingly, overexpression of cytosolic superoxide dismutase 1 (Sod1) exacerbated larval crawling phenotypes in G4C2x36 and GR36 and had no effect in GR1000 flies. This is contrary to Lopez-Gonzalez *et al.* (2016) where they found that ectopic expression of hSOD1 and catalase can suppress GR80 toxicity in the fly wing. It has to be noted that their hSOD1 suppression is small and also not directly comparable with overexpression of *Drosophila* Sod1. My results highlight the importance of mitochondrial ROS driving disease phenotypes and compartmentalised studies allow better understanding to indicate where ROS is most damaging. In summary, these data suggest a causative link between mitochondrial dysfunction, ROS and behavioural phenotypes.

Finally in Chapter 5, I aimed to study one of the key defence mechanisms against oxidative stress: the NRF2/Keap1 pathway. NRF2 was found to be translocated to the nucleus in G4C2x36 and GR36 larval brains suggesting an activation of the pathway. Moreover, there was increased NRF2 activity in G4C2x36 flies observed using a *gstD1*-GFP reporter. These flies are also able to respond to paraquat treatment. Taken together, these data suggest that *C9orf72* flies can respond to oxidative stress. However, minimal changes were observed with NRF2 mRNA transcripts as well as NRF2 target transcript genes. This suggests that whilst the pathway is activated, the response may be blunted. Furthermore, genetic reduction in *Keap1* and pharmacological treatment with an NRF2 activator, dimethyl fumarate (DMF),

showed a behavioural rescue in climbing activity of G4C2x36 and GR36 flies, suggesting targeting the NRF2/Keap1 signalling pathway could be a viable therapeutic strategy for ALS/FTD.

6.2 Expanding on our knowledge of compartmentalised ROS damage

Since I have observed a suppression of behavioural phenotypes with mitochondrial Sod2 but not cytosolic Sod1, it highlights the importance of mitochondrial ROS driving toxicity. Filograna *et al.* (2016) investigated the effects of Sod enzymes protection against paraquat induced toxicity. Acute treatment of paraquat resulted in an increase in mitochondrial ROS production only. They only observed a suppression in cell viability with overexpression of Sod2, but not Sod1. Similar to my results, it suggests that organismal viability is more affected at the mitochondrial level from ROS compared to the cytosol as only overexpression of Sod2 was able to rescue under stress conditions. It has been shown in the literature that oxidative stress is increased in *C9orf72* conditions (Lopez-Gonzalez *et al.*, 2016) therefore showing the relevance of ROS in different cellular compartments is interesting and would allow better targeted treatments. I would like to perform a more detailed study analysing the contribution of various ROS species i.e. testing the production of superoxides compared to hydrogen peroxide as well as their cytosolic vs mitochondrial involvement. Cells may be a better system to use considering all the limitations of flies I have described throughout the thesis. I have acquired Neuro2a cells expressing G4C2x45 (kind gift from Dr. Guillaume Hautbergue) and have characterised the cells for future experiments. Preliminary experiments using this model system showed an increased signal was observed with MitoSOX after flow cytometry analysis comparing G4C2x35 to control (data not shown). Flow cytometry is an easy, fast and high throughput approach to measure different ROS species produced. Mitochondrial superoxide can be measured using MitoSOX whereas cytosolic superoxide production can be measured using DHE. Furthermore, mitochondrial hydrogen peroxide production can be detected using Amplex Red from isolated mitochondria while H₂DCFDA can be used to measure cytosolic hydrogen peroxide production (Dikalov & Harrison, 2014; Murphy *et al.*, 2022). Additionally, I can also use the mito-roGFP vs cyto-roGFP in cells as well.

In *Drosophila*, I would also like to use another *in vivo* roGFP2-based probe - cyto-Grx1-roGFP2 and mito-roGFP2-Grx1 (Albrecht *et al.*, 2011). Glutathione (GSH) is the most abundant antioxidant in cells (Dringen, 2000; Stapper & Jahn, 2018) where it cycles between a reduced (GSH) and an oxidised (GSSG) state. Therefore, measurement of its redox

potential (E_{GSH}) is widely used to assess cellular redox homeostasis where an increased GSSG:GSH ratio is an indication of oxidative stress. Similar to the mito-roGFP2-Orp1, glutaredoxin 1 (Grx1), a small redox enzyme maintained by non-enzymatic reduction by GSH, mediates roGFP2 oxidation by GSSG (Albrecht *et al.*, 2011). Stapper & Jahn (2018) used both roGFP2 probes in a *Drosophila* model of Alzheimer's disease where they found that changes in E_{GSH} correlated with disease onset and progression but did not find any changes in hydrogen peroxide levels suggesting that it is not the driving factor for onset of neurotoxicity, but stresses the significance of glutathione redox homeostasis. This highlights the importance of studying different aspects of oxidative stress, as many studies generically show an 'increase in oxidative stress' without any in-depth analysis of the ROS species produced or information regarding distinct subcellular compartments.

Since I have emphasised the importance of studying different ROS species, I have reflected on the use of only paraquat (PQ) in my studies. PQ is used as a redox cyler used to stimulate superoxide production in the mitochondrial matrix through interactions with complex I (Cocheme & Murphy, 2008). Moreover, further studies by Filograna *et al.*, (2013) have shown that an acute dose of 24 h PQ treatment resulted in increased mitochondrial ROS production only, whereas a longer chronic 48 h dose increased both mitochondrial and cytosolic ROS in SH-SY5Y cells (Rodriguez-Rocha *et al.*, 2013; Filograna *et al.*, 2016). Therefore, it may be interesting to conduct an experiment investigating the differences between acute and chronic exposure to PQ, or even use mitoPQ. I would also like to perform a lifespan survival assay to determine whether the *C9orf72* flies are more susceptible to stress in a complementary way. Furthermore, different oxidants can be used to test different species of ROS production, including arsenic, a heavy metal; di-ethyl maleate (DEM), a glutathione depleting agent, mitoParaquat or hydrogen peroxide itself. These potential experiments will expand on my findings where mitochondrial Sod2 suppressed *C9orf72* behavioural phenotypes, but not cytosolic Sod1. It will provide a better understanding to what 'an increase in ROS' really means as well as investigate ROS production and the cell's regulation in different subcellular compartments.

6.3 Alternative oxidative stress responses & contribution from other pathogenic mechanisms

In my study, I have shown that the NRF2/Keap1 pathway is involved in *C9orf72* disease pathogenesis. However, some of my results are inconclusive and may appear contradictory and ultimately, the underlying mechanisms are yet to be resolved. The main discrepancy is that I observe suppression of behavioural phenotypes with genetic manipulations and drug treatments which activate the NRF2 pathway, however, even though a *gstD1*-GFP reporter indicates that NRF2 activity is upregulated, the mRNA transcripts examined are not changed. This suggests that there may be post translational changes and modifications, or that translation itself is perturbed. Moujalled *et al.* (2017) had a similar finding using ALS patient fibroblasts harbouring a TDP-43^{M337V} mutation and NSC-34 motor neuronal cell lines carrying the TDP-43^{Q331K} mutation where they performed RNA binding immunoprecipitation studies. This revealed an enrichment of NRF2 and GPX1 transcripts bound to heterogeneous nuclear ribonucleoprotein K (hnRNP K) protein, which is an RNA binding protein. hnRNP K was found to be mislocalised and its altered metabolism subsequently impairs the oxidative stress response in cells due to aberrant translation of key antioxidant proteins. Similarly, various hnRNPs have been found to interact with both sense and antisense RNA foci including hnRNP H (Conlon *et al.*, 2016), hnRNP A1 (Sareen *et al.*, 2013; Cooper-Knock *et al.*, 2014), hnRNP A3 (Mori *et al.*, 2013) and hnRNP H1/F (Lee *et al.*, 2013; Cooper-Knock *et al.*, 2014). Since there is precedence that hnRNPs are disrupted and sequestered by RNA foci in *C9orf72*, it may suggest that a similar mechanism has occurred whereby alterations in hnRNPs impair translation of key antioxidant proteins and therefore is worth further investigation.

Moreover, NRF2 is regulated by several transcription factors such as aryl hydrocarbon receptor (AhR) (Miao *et al.*, 2005) and NF- κ B (Nair *et al.*, 2008). NRF2 can also regulate its own *NFE2L2* mRNA transcription, as the gene itself has an ARE within its promoter therefore can directly activate its own transcription, creating a positive feedback loop to enhance NRF2 effects (Kwak *et al.*, 2002). But there must be negative regulation of this feedback. Apart from the Keap1-CUL3-RBX1 ubiquitin ligase complex, other ubiquitin ligases have been shown to target NRF2 for ubiquitination and ultimately degradation such as glycogen synthase kinase (GSK)3/ β -TrCP-dependent Cul1-based ubiquitin ligase (Rada *et al.*, 2011; Chowdhry *et al.*, 2013). There also may be alternative oxidative stress responses as well as compensatory pathways activated which include NF- κ B pathway as discussed in Chapter 5 (He *et al.*, 2020). Transcriptional activation of NRF2 target genes also require the recruitment of small Maf

proteins (sMAFs) such as MAFF, MAFG and MAFK to form a heterodimer with NRF2 before transcription can proceed. Interestingly, Wang *et al.* (2017) conducted a meta-analysis of microarray sets from Alzheimer's Disease (AD) and Parkinson's Disease (PD) and found that although NRF2 was upregulated, they identified 31 common downregulated ARE-driven genes such as detoxification genes NQO-1 and SOD1 (Wang *et al.*, 2017). The authors speculated that NRF2 may be part of a complex regulatory network and must be affected by other transcription factors and regulatory mechanisms as I have eluded to in this discussion. They found that MAFF was highly expressed in AD and PD and speculated that sMAF proteins can form homodimers among themselves and subsequently act as transcriptional repressors therefore overexpression of MAFF represses NRF2 dependent gene transcription, result in in NRF2 target gene downregulation (Wang *et al.*, 2017). These findings may explain why minimal changes were observed in the G4C2x36 flies. As described earlier, there is increased ROS with a blunted NRF2-mediated response and potentially, sMAF proteins may be dysregulated. I plan to test genetic manipulations with overexpression and knockdown of sMAF with the *C9orf72* flies. The sole *Drosophila* homolog of sMAF proteins is the product of the CG9954 gene, MafS (Veraksa *et al.*, 2000). Rahman *et al.* (2013) also confirmed that MafS is required for NRF2-like functions of cncC. It will also be interesting to measure MafS mRNA and protein levels and test whether the hypothesis of transcription repression due to excess MafS could explain the lack of NRF2 target transcripts in *C9orf72* ALS/FTD as well.

Lastly, there may be multiple pathogenic mechanisms in play which trigger pathology and toxicity. In this thesis, I have concentrated my efforts to characterise mitochondrial phenotypes and oxidative stress, and despite showing important influences on pathology, a greater emphasis on *C9orf72* as a whole may be important, including exploring other pathogenic mechanisms involved. Arginine-rich DPRs have been associated with defective nucleocytoplasmic transport (NCT) deficits (Freibaum *et al.*, 2015; Jovicic *et al.*, 2015), translation disruption (Moens *et al.*, 2019) and stress granule dysfunction (Lee *et al.*, 2016; Boeynaems *et al.*, 2017). Boeynaems *et al.* (2016) performed a targeted modifier screen based on the findings from Jovicic *et al.* (2015) using eye degeneration as a readout for suppressors and enhancers of PR25 toxicity. They consolidated findings from the yeast screens to show that nucleocytoplasmic transport players such as karyopherins, nuclear pore complex components and enzymes involved in generating the Ran-GTP gradient, play an important role and are major contributing factors to *C9orf72* toxicity. Interestingly, KPNA6 (Importin $\alpha 7$)-mediated nuclear import of Keap1 represses the Nrf2-dependent antioxidant response (Sun *et al.*, 2011), therefore it will be useful to investigate if there is a link between NCT defects and the NRF2 signalling pathway. Other experiments that will strengthen the study include investigating other phenotypes besides behavioural assays. Are the DPRs levels

affected when suppression of behavioural phenotypes is observed with Sod2, catalase, Keap1 and DMF treatment? GR was found to be spread diffusely throughout the cytosol, and PR to be both nuclear and cytoplasmic (Yang *et al.*, 2015; Solomon *et al.*, 2018; West *et al.*, 2020). Is the localisation of GR affected with the suppression of the behavioural phenotypes too? To summarise, more experiments will strengthen the story and may provide more hints to explain the mechanism behind *C9orf72* pathogenesis.

6.4 Mitophagy and autophagy

In my investigation, I found that mitophagy was perturbed in G4C2x36 and GR36. Overexpression of Sod2 was able to suppress the behavioural phenotypes and significantly restore mitophagy, however, not back to control levels. Mitophagy is an interesting topic to further investigate as it has been relatively understudied in *C9orf72* ALS/FTD. Although no causative relation has been established between NRF2 and mitophagy, there is evidence that NRF2 may play a role in mitochondrial quality control under oxidative stress conditions (Dinkova-Kostova & Abramov, 2015). In a sepsis mouse model, oxidative stress and inflammation was observed. NRF2 and its downstream target genes such as Sod2 and HO-1 were increased, suggesting that there was a mitochondrial adaptive response to oxidative stress. Next, they observed a decrease in Ref(2)P/p62 and using a LC3-GFP reporter mice, LC3 signal and citrate synthase staining were increased, which suggests that there is increased mitochondrial biogenesis as well as increased mitophagy as there was a strong colocalisation between the LC3 puncta with mitochondria. Most importantly, these phenotypes were suppressed in NRF2 knockout mice compared to WT control mice which indicates that NRF2 plays a key role in redox-sensitive mitophagy (Chang *et al.*, 2015). Recently, Gumeni *et al.* (2021) showed that NRF2 activation can induce mitophagy and reverse Pink1/parkin knockdown mediated neuronal and muscle degeneration. The paper supports the hypothesis that NRF2 is involved in regulating mitophagy however, there are limitations to this study from my perspective, as their use of the mito-QC reporter from my experience, is not analysed very well.

Other than mitophagy, I have shown that autophagy is perturbed in G4C2x36 and GR36 flies. However, the immunoblots of GABARAP and Ref(2)P lack some biological repeats and control conditions with chloroquine as it is important to measure the amount of Atg8a-II delivered to the lysosomes by comparing in the presence and absence of bafilomycin A1 (a vacuolar H⁺-ATPase inhibitor) or lysosomotropic agents (e.g., chloroquine) to inhibit lysosomal degradation of Atg8a-II hence determine the basal autophagic activity (Jiang & Mizushima,

2015). I have shown an increase in Ref(2)P levels, albeit not significant, therefore more biological replicates will determine whether this result holds. However, Cunningham *et al.* (2020) have also shown perturbed autophagy and accumulation of Ref(2)P and it is also widely documented that ALS/FTD patients also exhibit Ref(2)P/p62 and ubiquitin-positive inclusions in degenerating neurons. The formation of p62 inclusions is likely to interfere with the autophagy process, therefore impacting cellular homeostasis (Chitiprolu *et al.*, 2018). Interestingly, p62 has been shown to interact with the NRF2 binding site on Keap1 and therefore competes with NRF2 (Komatsu *et al.*, 2010). Moreover, p62 is also an NRF2 target gene as it contains an ARE in its promoter region therefore can create a positive regulatory feedback loop (Komatsu *et al.*, 2010, Jain *et al.*, 2010). East *et al.* (2014) generated a p62-mediated mitophagy inducer (PMI, HB229) as a small molecule which upregulates p62 and disrupts the Nrf2-Keap1 interaction therefore stabilising NRF2 to drive mitophagy, acting downstream of the Pink1/parkin pathway. However, Jain *et al.* (2015) discovered that this positive feedback loop between NRF2 and Ref(2)P is not conserved in *Drosophila*. They found that similar to mammals, Ref(2)P interacts directly with Atg8a (LC3 in mammals) through a LIR motif and Ref(2)P also has an ARE region that is recognised by cncC (NRF2), but it does not bind directly to Keap1 as it lacks an ETGE-like motif. Despite the absence of a Ref(2)P mediated positive feedback loop, the authors found that cncC was able to induce Atg8a levels and stimulate autophagy. It will be interesting to investigate a potential link between C9orf72 – NRF2/cncC – Ref(2)P/p62 – mitophagy/autophagy.

6.5 Therapeutic treatments - DMF

One of the more exciting findings from my investigation is that dimethyl fumarate (DMF) could suppress behavioural phenotypes in G4C2x36 and GR36, though some further clarifications are needed. For instance, while an increase in nuclear localisation of cncC was observed in larval brains of G4C2x36 and GR36, there was no significant increase in NRF2 activity measured using the *gstD1*-GFP reporter. However, at day 5, NRF2 activity is significantly increased therefore it would be interesting to investigate the expression levels and localisation of cncC in adult brains as well. Moreover, it will be interesting to determine whether a similar result is achieved using the GR1000 flies. Lastly, since I have observed a suppression of behavioural phenotypes in G4C2x36 and GR36, it would be essential to combine with the *gstD1*-GFP reporter as well as testing mRNA transcripts to understand the physiological landscape in the rescue flies. Complementary experiments can also be performed using the N2a G4C2x45 cell model with DMF treatment and additional antioxidants

such as Trolox or other NRF2 activators such as sulforaphane can also be tested to determine whether they are able to rescue *C9orf72* phenotypes as well.

DMF is a prodrug which is hydrolysed by esterases to monomethyl fumarate (MMF) *in vivo*. Both fumarates have been shown to activate the NRF2 pathway and show immunosuppressive and anti-inflammatory properties through several mechanisms including the inhibition of the NF- κ B pathway (Majkutewicz, 2022). In fact, DMF has been used in many neurodegenerative models including AD, PD and HD, where the general consensus is that DMF is beneficial and attenuates phenotypes such as alleviated oxidative stress, neurodegeneration and gliosis, reviewed in detail by Majkutewicz (2022). DMF has mostly been administered in *in vitro* models and *in vivo* mouse models however, there was a study investigating the effect of DMF in a *Drosophila* model of PD (Solana-Manrique *et al.*, 2020). DJ-1 β mutant flies fed with DMF food exhibited improved climbing ability than standard medium food and showed that the levels of hydrogen peroxide and protein carbonylation were lower whereas phosphofructokinase, a glycolytic enzyme was higher compared to DJ-1 β mutant flies with longer treatment of DMF. This highlights the potential benefits of using DMF as a therapeutic treatment for neurodegenerative diseases however, there are currently no cellular models or animal models testing DMF in ALS. Still, a clinical trial of DMF where a phase 2 multi-centre, randomised, placebo-controlled, double-blind clinical trial aimed at assessing the efficacy and safety of Tecfidera (brand name for DMF) in patients with sporadic ALS has been conducted (Vucic *et al.*, 2020). Unfortunately, although the drug was safe and well tolerated, there was a lack of efficacy and no significant differences were observed in the Amyotrophic Lateral Sclerosis Functional Rating Scale-Revised (ALSFRS-R) at week 36. However, beneficial effects on the neurophysiological index was observed, suggesting preservation of lower motor neuron function, although this needs verification in a larger trial. Moreover, the authors raised the point that participants showed an 'unusually slow disease progression' during the study and suggested that future trials should include rapidly progressing ALS patients (Vucic *et al.*, 2021). Taken together, DMF treatment shows promise but more scientific research understanding the underlying mechanisms behind disease pathogenesis and progression, as well as clinical trials on a more homogenous cohort may provide more conclusive results.

6.6 Relevance of work

In summary, I have used three well established *Drosophila* models of *C9orf72* ALS/FTD to investigate mitochondrial dysfunction. *Drosophila melanogaster* is a useful *in vivo*

model and has been extensively used to study *C9orf72*. However, not many studies to date have comprehensively characterised mitochondrial phenotypes, therefore my work has provided a strong groundwork to first understand what has gone wrong in the mitochondria before setting out to attenuate and rescue toxic phenotypes. Investigations in mitochondrial morphology in a neuronal setting, changes in mitochondrial respiration and perturbed autophagy add to known findings in the literature and can complement *post mortem* tissue data, *in vitro* and other *in vivo* models discoveries. I have also uncovered some novel results, highlighting the importance of studying ROS in different subcellular compartments. Moreover, a reduction in mitophagy was observed which has been a severely understudied topic in *C9orf72*. While the NRF2/Keap1 pathway is by no means a new pathway to investigate, but currently, there are no studies providing direct evidence linking *C9orf72* with NRF2 and therefore my work adds to our understanding of *C9orf72* disease pathogenesis and progression.

Moreover, I was also interested in investigating potential differences between repeat RNA vs DNA DPR-mediated toxicity by using a pure repeat model (G4C2x36) and two GR-only models (GR36 and GR1000) developed by Mizielinska *et al.* (2014) and West *et al.* (2020). However, I have not been able to find any differences or deviations in results with the rescue experiments performed. Both overexpression of mitochondrial Sod2 and catalase, as well as using heterozygous Keap1 mutants were able to suppress G4C2x36, GR36 and GR1000 behavioural phenotypes. This meant I could not able to discern the differences between repeat RNA and DPR toxicity and distinguish the relative contribution of each to toxicity or rescue, however, it is encouraging to know that all these genetic manipulations were able to rescue all the disease models. It was also useful to study a shorter length GR36 model compared to the GR1000 model. Expressing GR1000 in the fly eye did not yield a rough eye phenotype but still exhibited a shorter lifespan and climbing motor impairments with age West *et al.* (2020). The less acute toxicity in the GR1000 model could be considered to be more representative of the disease where it can be aged to examine the effects of DPRs throughout the lifetime of the fly (West *et al.*, 2020). Surprisingly, I observed very similar results between the GR36 and GR1000 models. Taken together, all the disease models I used followed a similar pattern and more work will be needed to disentangle the differences between repeat RNA vs DPR toxicity by using all the different DPR only constructs as well as RNA only constructs too. Moreover, co-expression of DPRs may provide a better understanding the relative contribution of each DPR to effects on disease pathogenesis.

6.7 Conclusions

In conclusion, I have used three different *Drosophila* models of *C9orf72* ALS/FTD to perform a comprehensive characterisation of mitochondrial dysfunction. I found alterations in mitochondrial morphology, specifically elongated and hyperfused mitochondria. Moreover, a reduction in mitophagy and impaired mitochondrial respiration was found as well as increased mitochondrial ROS production in a neuronal context. Unexpectedly, genetic manipulation to restore mitochondrial fission/fusion dynamics or boosting mitophagy were unable to rescue the locomotor deficits in larvae. However, genetic upregulation of antioxidants such as mitochondrial superoxide dismutase 2 (*Sod2*) and catalase was able to rescue impaired larval locomotion. Surprisingly, overexpression of cytosolic superoxide dismutase 1 (*Sod1*) exacerbated larval crawling phenotypes. Together, these data suggest a causative link between mitochondrial dysfunction, ROS and behavioural phenotypes. Lastly, I investigated the NRF2/Keap1 signalling pathway as it has a crucial role in the maintenance of cellular redox homeostasis. I found that NRF2 was translocated to the nucleus suggesting that the pathway is activated. However, minimal changes to NRF2 target transcript genes were observed although increased GFP expression was found using a *gstD1*-GFP reporter, a proxy for NRF2 activity. Despite these variable effects, both genetic reduction in Keap1 and pharmacological treatment with the NRF2 activator, dimethyl fumarate (DMF) could suppress behavioural motor impairments. While more research is needed, these results provide compelling evidence that mitochondrial oxidative stress is a major upstream pathogenic mechanism leading to downstream mitochondrial dysfunction such as alterations in mitochondrial function and turnover. Consequently, targeting one of the main intracellular defence mechanisms to counteract oxidative stress – the NRF2/Keap1 signalling pathway – could be a viable therapeutic strategy for ALS/FTD.

References

- Al-Sarraj S, King A, Troakes C, Smith B, Maekawa S, Bodi I, Rogelj B, Al-Chalabi A, Hortobagyi T, Shaw CE (2011) p62 positive, TDP-43 negative, neuronal cytoplasmic and intranuclear inclusions in the cerebellum and hippocampus define the pathology of C9orf72-linked FTLN and MND/ALS. *Acta Neuropathol* 122: 691-702
- Albrecht SC, Barata AG, Grosshans J, Teleman AA, Dick TP (2011) In vivo mapping of hydrogen peroxide and oxidized glutathione reveals chemical and regional specificity of redox homeostasis. *Cell Metab* 14: 819-829
- Alexopoulou Z, Lang J, Perrett RM, Elschami M, Hurry ME, Kim HT, Mazaraki D, Szabo A, Kessler BM, Goldberg AL *et al* (2016) Deubiquitinase Usp8 regulates alpha-synuclein clearance and modifies its toxicity in Lewy body disease. *Proc Natl Acad Sci U S A* 113: E4688-4697
- Amick J, Roczniak-Ferguson A, Ferguson SM (2016) C9orf72 binds SMCR8, localizes to lysosomes, and regulates mTORC1 signaling. *Mol Biol Cell* 27: 3040-3051
- Amick J, Tharkeshwar AK, Amaya C, Ferguson SM (2018) WDR41 supports lysosomal response to changes in amino acid availability. *Mol Biol Cell* 29: 2213-2227
- Amick J, Tharkeshwar AK, Talaia G, Ferguson SM (2020) PQLC2 recruits the C9orf72 complex to lysosomes in response to cationic amino acid starvation. *J Cell Biol* 219
- Anoar S, Woodling NS, Niccoli T (2021) Mitochondria Dysfunction in Frontotemporal Dementia/Amyotrophic Lateral Sclerosis: Lessons From Drosophila Models. *Front Neurosci* 15: 786076
- Aoki Y, Manzano R, Lee Y, Dafinca R, Aoki M, Douglas AGL, Varela MA, Sathyaprakash C, Scaber J, Barbagallo P *et al* (2017) C9orf72 and RAB7L1 regulate vesicle trafficking in amyotrophic lateral sclerosis and frontotemporal dementia. *Brain* 140: 887-897
- Arai T, Hasegawa M, Akiyama H, Ikeda K, Nonaka T, Mori H, Mann D, Tsuchiya K, Yoshida M, Hashizume Y *et al* (2006) TDP-43 is a component of ubiquitin-positive tau-negative inclusions in frontotemporal lobar degeneration and amyotrophic lateral sclerosis. *Biochem Biophys Res Commun* 351: 602-611
- Area-Gomez E, Guardia-Laguarta C, Schon EA, Przedborski S (2019) Mitochondria, OxPhos, and neurodegeneration: cells are not just running out of gas. *J Clin Invest* 129: 34-45
- Ash PE, Bieniek KF, Gendron TF, Caulfield T, Lin WL, DeJesus-Hernandez M, van Blitterswijk MM, Jansen-West K, Paul JW, 3rd, Rademakers R *et al* (2013) Unconventional translation of C9ORF72 GGGGCC expansion generates insoluble polypeptides specific to c9FTD/ALS. *Neuron* 77: 639-646
- Atanasio A, Decman V, White D, Ramos M, Ikiz B, Lee HC, Siao CJ, Brydges S, LaRosa E, Bai Y *et al* (2016) C9orf72 ablation causes immune dysregulation characterized by leukocyte expansion, autoantibody production, and glomerulonephropathy in mice. *Sci Rep* 6: 23204

References

- Atkinson RA, Fernandez-Martos CM, Atkin JD, Vickers JC, King AE (2015) C9ORF72 expression and cellular localization over mouse development. *Acta Neuropathol Commun* 3: 59
- Baldwin KR, Godena VK, Hewitt VL, Whitworth AJ (2016) Axonal transport defects are a common phenotype in Drosophila models of ALS. *Hum Mol Genet* 25: 2378-2392
- Balendra R, Isaacs AM (2018) C9orf72-mediated ALS and FTD: multiple pathways to disease. *Nat Rev Neurol* 14: 544-558
- Batra R, Lee CW (2017) Mouse Models of C9orf72 Hexanucleotide Repeat Expansion in Amyotrophic Lateral Sclerosis/ Frontotemporal Dementia. *Front Cell Neurosci* 11: 196
- Beck J, Poulter M, Hensman D, Rohrer JD, Mahoney CJ, Adamson G, Campbell T, Uphill J, Borg A, Fratta P *et al* (2013) Large C9orf72 hexanucleotide repeat expansions are seen in multiple neurodegenerative syndromes and are more frequent than expected in the UK population. *Am J Hum Genet* 92: 345-353
- Bedont JL, Toda H, Shi M, Park CH, Quake C, Stein C, Kolesnik A, Sehgal A (2021) Short and long sleeping mutants reveal links between sleep and macroautophagy. *Elife* 10
- Belzil VV, Bauer PO, Prudencio M, Gendron TF, Stetler CT, Yan IK, Pregent L, Daugherty L, Baker MC, Rademakers R *et al* (2013) Reduced C9orf72 gene expression in c9FTD/ALS is caused by histone trimethylation, an epigenetic event detectable in blood. *Acta Neuropathol* 126: 895-905
- Berman SB, Pineda FJ, Hardwick JM (2008) Mitochondrial fission and fusion dynamics: the long and short of it. *Cell Death Differ* 15: 1147-1152
- Bingol B, Tea JS, Phu L, Reichelt M, Bakalarski CE, Song Q, Foreman O, Kirkpatrick DS, Sheng M (2014) The mitochondrial deubiquitinase USP30 opposes parkin-mediated mitophagy. *Nature* 510: 370-375
- Boeynaems S, Bogaert E, Kovacs D, Konijnenberg A, Timmerman E, Volkov A, Guharoy M, De Decker M, Jaspers T, Ryan VH *et al* (2017) Phase Separation of C9orf72 Dipeptide Repeats Perturbs Stress Granule Dynamics. *Mol Cell* 65: 1044-1055 e1045
- Boeynaems S, Bogaert E, Michiels E, Gijssels I, Sieben A, Jovicic A, De Baets G, Scheveneels W, Steyaert J, Cuijt I *et al* (2016) Drosophila screen connects nuclear transport genes to DPR pathology in c9ALS/FTD. *Sci Rep* 6: 20877
- Bono S, Feligioni M, Corbo M (2021) Impaired antioxidant KEAP1-NRF2 system in amyotrophic lateral sclerosis: NRF2 activation as a potential therapeutic strategy. *Mol Neurodegener* 16: 71
- Braems E, Swinnen B, Van Den Bosch L (2020) C9orf72 loss-of-function: a trivial, stand-alone or additive mechanism in C9 ALS/FTD? *Acta Neuropathol* 140: 625-643
- Brand AH, Perrimon N (1993) Targeted gene expression as a means of altering cell fates and generating dominant phenotypes. *Development* 118: 401-415
- Brand MD (2010) The sites and topology of mitochondrial superoxide production. *Exp Gerontol* 45: 466-472
- Brown RH, Al-Chalabi A (2017) Amyotrophic Lateral Sclerosis. *N Engl J Med* 377: 162-172

- Burberry A, Suzuki N, Wang JY, Moccia R, Mordes DA, Stewart MH, Suzuki-Uematsu S, Ghosh S, Singh A, Merkle FT *et al* (2016) Loss-of-function mutations in the C9ORF72 mouse ortholog cause fatal autoimmune disease. *Sci Transl Med* 8: 347ra393
- Burberry A, Wells MF, Limone F, Couto A, Smith KS, Keaney J, Gillet G, van Gastel N, Wang JY, Pietilainen O *et al* (2020) C9orf72 suppresses systemic and neural inflammation induced by gut bacteria. *Nature* 582: 89-94
- Burguete AS, Almeida S, Gao FB, Kalb R, Akins MR, Bonini NM (2015) GGGGCC microsatellite RNA is neuritically localized, induces branching defects, and perturbs transport granule function. *Elife* 4: e08881
- Cali CP, Patino M, Tai YK, Ho WY, McLean CA, Morris CM, Seeley WW, Miller BL, Gaig C, Vonsattel JPG *et al* (2019) C9orf72 intermediate repeats are associated with corticobasal degeneration, increased C9orf72 expression and disruption of autophagy. *Acta Neuropathol* 138: 795-811
- Cao YL, Meng S, Chen Y, Feng JX, Gu DD, Yu B, Li YJ, Yang JY, Liao S, Chan DC *et al* (2017) MFN1 structures reveal nucleotide-triggered dimerization critical for mitochondrial fusion. *Nature* 542: 372-376
- Celona B, Dollen JV, Vatsavayai SC, Kashima R, Johnson JR, Tang AA, Hata A, Miller BL, Huang EJ, Krogan NJ *et al* (2017) Suppression of C9orf72 RNA repeat-induced neurotoxicity by the ALS-associated RNA-binding protein Zfp106. *Elife* 6
- Chan DC (2012) Fusion and fission: interlinked processes critical for mitochondrial health. *Annu Rev Genet* 46: 265-287
- Chang AL, Ulrich A, Suliman HB, Piantadosi CA (2015) Redox regulation of mitophagy in the lung during murine *Staphylococcus aureus* sepsis. *Free Radic Biol Med* 78: 179-189
- Chang YJ, Jeng US, Chiang YL, Hwang IS, Chen YR (2016) The Glycine-Alanine Dipeptide Repeat from C9orf72 Hexanucleotide Expansions Forms Toxic Amyloids Possessing Cell-to-Cell Transmission Properties. *J Biol Chem* 291: 4903-4911
- Chatterjee N, Bohmann D (2012) A versatile PhiC31 based reporter system for measuring AP-1 and Nrf2 signaling in *Drosophila* and in tissue culture. *PLoS One* 7: e34063
- Cheng Y, Pitoniak A, Wang J, Bohmann D (2021) Preserving transcriptional stress responses as an anti-aging strategy. *Aging Cell* 20: e13297
- Chew J, Gendron TF, Prudencio M, Sasaguri H, Zhang YJ, Castanedes-Casey M, Lee CW, Jansen-West K, Kurti A, Murray ME *et al* (2015) Neurodegeneration. C9ORF72 repeat expansions in mice cause TDP-43 pathology, neuronal loss, and behavioral deficits. *Science* 348: 1151-1154
- Chew LY, Zhang H, He J, Yu F (2021) The Nrf2-Keap1 pathway is activated by steroid hormone signaling to govern neuronal remodeling. *Cell Rep* 36: 109466
- Chitiprolu M, Jagow C, Tremblay V, Bondy-Chorney E, Paris G, Savard A, Palidwor G, Barry FA, Zinman L, Keith J *et al* (2018) A complex of C9ORF72 and p62 uses arginine methylation to eliminate stress granules by autophagy. *Nat Commun* 9: 2794

References

- Choi SY, Lopez-Gonzalez R, Krishnan G, Phillips HL, Li AN, Seeley WW, Yao WD, Almeida S, Gao FB (2019) C9ORF72-ALS/FTD-associated poly(GR) binds Atp5a1 and compromises mitochondrial function in vivo. *Nat Neurosci* 22: 851-862
- Chowdhry S, Zhang Y, McMahon M, Sutherland C, Cuadrado A, Hayes JD (2013) Nrf2 is controlled by two distinct beta-TrCP recognition motifs in its Neh6 domain, one of which can be modulated by GSK-3 activity. *Oncogene* 32: 3765-3781
- Chu CT, Ji J, Dagda RK, Jiang JF, Tyurina YY, Kapralov AA, Tyurin VA, Yanamala N, Shrivastava IH, Mohammadyani D *et al* (2013) Cardiolipin externalization to the outer mitochondrial membrane acts as an elimination signal for mitophagy in neuronal cells. *Nat Cell Biol* 15: 1197-1205
- Ciura S, Lattante S, Le Ber I, Latouche M, Tostivint H, Brice A, Kabashi E (2013) Loss of function of C9orf72 causes motor deficits in a zebrafish model of amyotrophic lateral sclerosis. *Ann Neurol* 74: 180-187
- Cocheme HM, Murphy MP (2008) Complex I is the major site of mitochondrial superoxide production by paraquat. *J Biol Chem* 283: 1786-1798
- Cocheme HM, Quin C, McQuaker SJ, Cabreiro F, Logan A, Prime TA, Abakumova I, Patel JV, Fearnley IM, James AM *et al* (2011) Measurement of H₂O₂ within living *Drosophila* during aging using a ratiometric mass spectrometry probe targeted to the mitochondrial matrix. *Cell Metab* 13: 340-350
- Cohen MM, Tareste D (2018) Recent insights into the structure and function of Mitofusins in mitochondrial fusion. *F1000Res* 7
- Cohen TJ, Lee VM, Trojanowski JQ (2011) TDP-43 functions and pathogenic mechanisms implicated in TDP-43 proteinopathies. *Trends Mol Med* 17: 659-667
- Conlon EG, Lu L, Sharma A, Yamazaki T, Tang T, Shneider NA, Manley JL (2016) The C9ORF72 GGGGCC expansion forms RNA G-quadruplex inclusions and sequesters hnRNP H to disrupt splicing in ALS brains. *Elife* 5
- Cooper-Knock J, Higginbottom A, Stopford MJ, Highley JR, Ince PG, Wharton SB, Pickering-Brown S, Kirby J, Hautbergue GM, Shaw PJ (2015) Antisense RNA foci in the motor neurons of C9ORF72-ALS patients are associated with TDP-43 proteinopathy. *Acta Neuropathol* 130: 63-75
- Cooper-Knock J, Walsh MJ, Higginbottom A, Robin Highley J, Dickman MJ, Edbauer D, Ince PG, Wharton SB, Wilson SA, Kirby J *et al* (2014) Sequestration of multiple RNA recognition motif-containing proteins by C9orf72 repeat expansions. *Brain* 137: 2040-2051
- Cornelissen T, Haddad D, Wauters F, Van Humbeeck C, Mandemakers W, Koentjoro B, Sue C, Gevaert K, De Strooper B, Verstreken P *et al* (2014) The deubiquitinase USP15 antagonizes Parkin-mediated mitochondrial ubiquitination and mitophagy. *Hum Mol Genet* 23: 5227-5242
- Coyne AN, Zaepfel BL, Hayes L, Fitchman B, Salzberg Y, Luo EC, Bowen K, Trost H, Aigner S, Rigo F *et al* (2020) G(4)C(2) Repeat RNA Initiates a POM121-Mediated Reduction in Specific Nucleoporins in C9orf72 ALS/FTD. *Neuron* 107: 1124-1140 e11111

- Cunningham CN, Baughman JM, Phu L, Tea JS, Yu C, Coons M, Kirkpatrick DS, Bingol B, Corn JE (2015) USP30 and parkin homeostatically regulate atypical ubiquitin chains on mitochondria. *Nat Cell Biol* 17: 160-169
- Cunningham KM, Maulding K, Ruan K, Senturk M, Grima JC, Sung H, Zuo Z, Song H, Gao J, Dubey S *et al* (2020) TFEB/Mitf links impaired nuclear import to autophagolysosomal dysfunction in C9-ALS. *Elife* 9
- Dafinca R, Scaber J, Ababneh N, Lalic T, Weir G, Christian H, Vowles J, Douglas AG, Fletcher-Jones A, Browne C *et al* (2016) C9orf72 Hexanucleotide Expansions Are Associated with Altered Endoplasmic Reticulum Calcium Homeostasis and Stress Granule Formation in Induced Pluripotent Stem Cell-Derived Neurons from Patients with Amyotrophic Lateral Sclerosis and Frontotemporal Dementia. *Stem Cells* 34: 2063-2078
- DeJesus-Hernandez M, Finch NA, Wang X, Gendron TF, Bieniek KF, Heckman MG, Vasilevich A, Murray ME, Rousseau L, Weesner R *et al* (2017) In-depth clinico-pathological examination of RNA foci in a large cohort of C9ORF72 expansion carriers. *Acta Neuropathol* 134: 255-269
- DeJesus-Hernandez M, Mackenzie IR, Boeve BF, Boxer AL, Baker M, Rutherford NJ, Nicholson AM, Finch NA, Flynn H, Adamson J *et al* (2011) Expanded GGGGCC hexanucleotide repeat in noncoding region of C9ORF72 causes chromosome 9p-linked FTD and ALS. *Neuron* 72: 245-256
- Deng H, Dodson MW, Huang H, Guo M (2008) The Parkinson's disease genes pink1 and parkin promote mitochondrial fission and/or inhibit fusion in *Drosophila*. *Proc Natl Acad Sci U S A* 105: 14503-14508
- Deng HX, Chen W, Hong ST, Boycott KM, Gorrie GH, Siddique N, Yang Y, Fecto F, Shi Y, Zhai H *et al* (2011) Mutations in UBQLN2 cause dominant X-linked juvenile and adult-onset ALS and ALS/dementia. *Nature* 477: 211-215
- Dikalov SI, Harrison DG (2014) Methods for detection of mitochondrial and cellular reactive oxygen species. *Antioxid Redox Signal* 20: 372-382
- Dinkova-Kostova AT, Abramov AY (2015) The emerging role of Nrf2 in mitochondrial function. *Free Radic Biol Med* 88: 179-188
- Donnelly CJ, Zhang PW, Pham JT, Haeusler AR, Mistry NA, Vidensky S, Daley EL, Poth EM, Hoover B, Fines DM *et al* (2013) RNA toxicity from the ALS/FTD C9ORF72 expansion is mitigated by antisense intervention. *Neuron* 80: 415-428
- Dringen R (2000) Metabolism and functions of glutathione in brain. *Prog Neurobiol* 62: 649-671
- Du F, Yu Q, Yan S, Hu G, Lue LF, Walker DG, Wu L, Yan SF, Tieu K, Yan SS (2017) PINK1 signalling rescues amyloid pathology and mitochondrial dysfunction in Alzheimer's disease. *Brain* 140: 3233-3251
- Dubey SK, Maulding K, Sung H, Lloyd TE (2022) Nucleoporins are degraded via upregulation of ESCRT-III/Vps4 complex in *Drosophila* models of C9-ALS/FTD. *Cell Rep* 40: 111379
- DuBoff B, Gotz J, Feany MB (2012) Tau promotes neurodegeneration via DRP1 mislocalization in vivo. *Neuron* 75: 618-632

References

- East DA, Fagiani F, Crosby J, Georgakopoulos ND, Bertrand H, Schaap M, Fowkes A, Wells G, Campanella M (2014) PMI: a DeltaPsim independent pharmacological regulator of mitophagy. *Chem Biol* 21: 1585-1596
- Edbauer D, Haass C (2016) An amyloid-like cascade hypothesis for C9orf72 ALS/FTD. *Curr Opin Neurobiol* 36: 99-106
- Farg MA, Sundaramoorthy V, Sultana JM, Yang S, Atkinson RA, Levina V, Halloran MA, Gleeson PA, Blair IP, Soo KY *et al* (2014) C9ORF72, implicated in amyotrophic lateral sclerosis and frontotemporal dementia, regulates endosomal trafficking. *Hum Mol Genet* 23: 3579-3595
- Fecto F, Yan J, Vemula SP, Liu E, Yang Y, Chen W, Zheng JG, Shi Y, Siddique N, Arrat H *et al* (2011) SQSTM1 mutations in familial and sporadic amyotrophic lateral sclerosis. *Arch Neurol* 68: 1440-1446
- Filograna R, Godena VK, Sanchez-Martinez A, Ferrari E, Casella L, Beltramini M, Bubacco L, Whitworth AJ, Bisaglia M (2016) Superoxide Dismutase (SOD)-mimetic M40403 Is Protective in Cell and Fly Models of Paraquat Toxicity: IMPLICATIONS FOR PARKINSON DISEASE. *J Biol Chem* 291: 9257-9267
- Forsberg K, Graffmo K, Pakkenberg B, Weber M, Nielsen M, Marklund S, Brannstrom T, Andersen PM (2019) Misfolded SOD1 inclusions in patients with mutations in C9orf72 and other ALS/FTD-associated genes. *J Neurol Neurosurg Psychiatry* 90: 861-869
- Fratia P, Polke JM, Newcombe J, Mizielinska S, Lashley T, Poulter M, Beck J, Preza E, Devoy A, Sidle K *et al* (2015) Screening a UK amyotrophic lateral sclerosis cohort provides evidence of multiple origins of the C9orf72 expansion. *Neurobiol Aging* 36: 546 e541-547
- Freeman HC, Hugill A, Dear NT, Ashcroft FM, Cox RD (2006) Deletion of nicotinamide nucleotide transhydrogenase: a new quantitative trait locus accounting for glucose intolerance in C57BL/6J mice. *Diabetes* 55: 2153-2156
- Freibaum BD, Lu Y, Lopez-Gonzalez R, Kim NC, Almeida S, Lee KH, Badders N, Valentine M, Miller BL, Wong PC *et al* (2015) GGGGCC repeat expansion in C9orf72 compromises nucleocytoplasmic transport. *Nature* 525: 129-133
- Freibaum BD, Taylor JP (2017) The Role of Dipeptide Repeats in C9ORF72-Related ALS-FTD. *Front Mol Neurosci* 10: 35
- Frezza C, Cipolat S, Martins de Brito O, Micaroni M, Beznoussenko GV, Rudka T, Bartoli D, Polishuck RS, Danial NN, De Strooper B *et al* (2006) OPA1 controls apoptotic cristae remodeling independently from mitochondrial fusion. *Cell* 126: 177-189
- Frick P, Sellier C, Mackenzie IRA, Cheng CY, Tahraoui-Bories J, Martinat C, Pasterkamp RJ, Prudlo J, Edbauer D, Oulad-Abdelghani M *et al* (2018) Novel antibodies reveal presynaptic localization of C9orf72 protein and reduced protein levels in C9orf72 mutation carriers. *Acta Neuropathol Commun* 6: 72
- Friedman JR, Lackner LL, West M, DiBenedetto JR, Nunnari J, Voeltz GK (2011) ER tubules mark sites of mitochondrial division. *Science* 334: 358-362
- Fuse Y, Kobayashi M (2017) Conservation of the Keap1-Nrf2 System: An Evolutionary Journey through Stressful Space and Time. *Molecules* 22

- Gao FB, Almeida S, Lopez-Gonzalez R (2017) Dysregulated molecular pathways in amyotrophic lateral sclerosis-frontotemporal dementia spectrum disorder. *EMBO J* 36: 2931-2950
- Gijssels I, Van Mossevelde S, van der Zee J, Sieben A, Engelborghs S, De Bleecker J, Ivanoiu A, Deryck O, Edbauer D, Zhang M *et al* (2016) The C9orf72 repeat size correlates with onset age of disease, DNA methylation and transcriptional downregulation of the promoter. *Mol Psychiatry* 21: 1112-1124
- Gillard GO, Collette B, Anderson J, Chao J, Scannevin RH, Huss DJ, Fontenot JD (2015) DMF, but not other fumarates, inhibits NF-kappaB activity in vitro in an Nrf2-independent manner. *J Neuroimmunol* 283: 74-85
- Giridharan S, Srinivasan M (2018) Mechanisms of NF-kappaB p65 and strategies for therapeutic manipulation. *J Inflamm Res* 11: 407-419
- Granatiero V, Konrad C, Bredvik K, Manfredi G, Kawamata H (2019) Nrf2 signaling links ER oxidative protein folding and calcium homeostasis in health and disease. *Life Sci Alliance* 2
- Green KM, Glineburg MR, Kearse MG, Flores BN, Linsalata AE, Fedak SJ, Goldstrohm AC, Barmada SJ, Todd PK (2017) RAN translation at C9orf72-associated repeat expansions is selectively enhanced by the integrated stress response. *Nat Commun* 8: 2005
- Greene AW, Grenier K, Aguilera MA, Muise S, Farazifard R, Haque ME, McBride HM, Park DS, Fon EA (2012) Mitochondrial processing peptidase regulates PINK1 processing, import and Parkin recruitment. *EMBO Rep* 13: 378-385
- Gumeni S, Papanagnou ED, Manola MS, Trougakos IP (2021) Nrf2 activation induces mitophagy and reverses Parkin/Pink1 knock down-mediated neuronal and muscle degeneration phenotypes. *Cell Death Dis* 12: 671
- Guo Q, Lehmer C, Martinez-Sanchez A, Rudack T, Beck F, Hartmann H, Perez-Berlanga M, Frottin F, Hipp MS, Hartl FU *et al* (2018) In Situ Structure of Neuronal C9orf72 Poly-GA Aggregates Reveals Proteasome Recruitment. *Cell* 172: 696-705 e612
- Guo Y, Zhang Y, Wen D, Duan W, An T, Shi P, Wang J, Li Z, Chen X, Li C (2013) The modest impact of transcription factor Nrf2 on the course of disease in an ALS animal model. *Lab Invest* 93: 825-833
- Gutschner M, Sobotta MC, Wabnitz GH, Ballikaya S, Meyer AJ, Samstag Y, Dick TP (2009) Proximity-based protein thiol oxidation by H₂O₂-scavenging peroxidases. *J Biol Chem* 284: 31532-31540
- Hadano S, Mitsui S, Pan L, Otomo A, Kubo M, Sato K, Ono S, Onodera W, Abe K, Chen X *et al* (2016) Functional links between SQSTM1 and ALS2 in the pathogenesis of ALS: cumulative impact on the protection against mutant SOD1-mediated motor dysfunction in mice. *Hum Mol Genet* 25: 3321-3340
- Haeusler AR, Donnelly CJ, Periz G, Simko EA, Shaw PG, Kim MS, Maragakis NJ, Troncoso JC, Pandey A, Sattler R *et al* (2014) C9orf72 nucleotide repeat structures initiate molecular cascades of disease. *Nature* 507: 195-200
- Han D, Williams E, Cadenas E (2001) Mitochondrial respiratory chain-dependent generation of superoxide anion and its release into the intermembrane space. *Biochem J* 353: 411-416

References

- Han H, Tan J, Wang R, Wan H, He Y, Yan X, Guo J, Gao Q, Li J, Shang S *et al* (2020) PINK1 phosphorylates Drp1(S616) to regulate mitophagy-independent mitochondrial dynamics. *EMBO Rep* 21: e48686
- Hardiman O, Al-Chalabi A, Chio A, Corr EM, Logroscino G, Robberecht W, Shaw PJ, Simmons Z, van den Berg LH (2017) Amyotrophic lateral sclerosis. *Nat Rev Dis Primers* 3: 17071
- Hardy J, Rogaeva E (2014) Motor neuron disease and frontotemporal dementia: sometimes related, sometimes not. *Exp Neurol* 262 Pt B: 75-83
- Harms M, Benitez BA, Cairns N, Cooper B, Cooper P, Mayo K, Carrell D, Faber K, Williamson J, Bird T *et al* (2013) C9orf72 hexanucleotide repeat expansions in clinical Alzheimer disease. *JAMA Neurol* 70: 736-741
- Harris DA, Das AM (1991) Control of mitochondrial ATP synthesis in the heart. *Biochem J* 280 (Pt 3): 561-573
- Hautbergue GM, Castelli LM, Ferraiuolo L, Sanchez-Martinez A, Cooper-Knock J, Higginbottom A, Lin YH, Bauer CS, Dodd JE, Myszczyńska MA *et al* (2017) SRSF1-dependent nuclear export inhibition of C9ORF72 repeat transcripts prevents neurodegeneration and associated motor deficits. *Nat Commun* 8: 16063
- Hayes JD, Dinkova-Kostova AT (2014) The Nrf2 regulatory network provides an interface between redox and intermediary metabolism. *Trends Biochem Sci* 39: 199-218
- He F, Ru X, Wen T (2020) NRF2, a Transcription Factor for Stress Response and Beyond. *Int J Mol Sci* 21
- Hirotsu Y, Katsuoka F, Funayama R, Nagashima T, Nishida Y, Nakayama K, Engel JD, Yamamoto M (2012) Nrf2-MafG heterodimers contribute globally to antioxidant and metabolic networks. *Nucleic Acids Res* 40: 10228-10239
- Hirth F (2010) Drosophila melanogaster in the study of human neurodegeneration. *CNS Neurol Disord Drug Targets* 9: 504-523
- Holmstrom KM, Finkel T (2014) Cellular mechanisms and physiological consequences of redox-dependent signalling. *Nat Rev Mol Cell Biol* 15: 411-421
- Holmstrom KM, Kostov RV, Dinkova-Kostova AT (2016) The multifaceted role of Nrf2 in mitochondrial function. *Curr Opin Toxicol* 1: 80-91
- Itoh K, Nakamura K, Iijima M, Sesaki H (2013) Mitochondrial dynamics in neurodegeneration. *Trends Cell Biol* 23: 64-71
- Jackson JL, Finch NA, Baker MC, Kachergus JM, DeJesus-Hernandez M, Pereira K, Christopher E, Prudencio M, Heckman MG, Thompson EA *et al* (2020) Elevated methylation levels, reduced expression levels, and frequent contractions in a clinical cohort of C9orf72 expansion carriers. *Mol Neurodegener* 15: 7
- Jain A, Rusten TE, Katheder N, Elvenes J, Bruun JA, Sjøttem E, Lamark T, Johansen T (2015) p62/Sequestosome-1, Autophagy-related Gene 8, and Autophagy in Drosophila Are Regulated by Nuclear Factor Erythroid 2-related Factor 2 (NRF2), Independent of Transcription Factor TFEB. *J Biol Chem* 290: 14945-14962

- Jiang J, Zhu Q, Gendron TF, Saberi S, McAlonis-Downes M, Seelman A, Stauffer JE, Jafar-Nejad P, Drenner K, Schulte D *et al* (2016) Gain of Toxicity from ALS/FTD-Linked Repeat Expansions in C9ORF72 Is Alleviated by Antisense Oligonucleotides Targeting GGGGCC-Containing RNAs. *Neuron* 90: 535-550
- Jiang P, Mizushima N (2015) LC3- and p62-based biochemical methods for the analysis of autophagy progression in mammalian cells. *Methods* 75: 13-18
- Jimenez-Villegas J, Ferraiuolo L, Mead RJ, Shaw PJ, Cuadrado A, Rojo AI (2021) NRF2 as a therapeutic opportunity to impact in the molecular roadmap of ALS. *Free Radic Biol Med* 173: 125-141
- Johnson JO, Mandrioli J, Benatar M, Abramzon Y, Van Deerlin VM, Trojanowski JQ, Gibbs JR, Brunetti M, Gronka S, Wu J *et al* (2010) Exome sequencing reveals VCP mutations as a cause of familial ALS. *Neuron* 68: 857-864
- Jovicic A, Mertens J, Boeynaems S, Bogaert E, Chai N, Yamada SB, Paul JW, 3rd, Sun S, Herdy JR, Bieri G *et al* (2015) Modifiers of C9orf72 dipeptide repeat toxicity connect nucleocytoplasmic transport defects to FTD/ALS. *Nat Neurosci* 18: 1226-1229
- Kedersha N, Panas MD, Achorn CA, Lyons S, Tisdale S, Hickman T, Thomas M, Lieberman J, McInerney GM, Ivanov P *et al* (2016) G3BP-Caprin1-USP10 complexes mediate stress granule condensation and associate with 40S subunits. *J Cell Biol* 212: 845-860
- Kerr F, Sofola-Adesakin O, Ivanov DK, Gatliff J, Gomez Perez-Nievas B, Bertrand HC, Martinez P, Callard R, Snoeren I, Cocheme HM *et al* (2017) Direct Keap1-Nrf2 disruption as a potential therapeutic target for Alzheimer's disease. *PLoS Genet* 13: e1006593
- Khalil B, El Fissi N, Aouane A, Cabirol-Pol MJ, Rival T, Lievens JC (2015) PINK1-induced mitophagy promotes neuroprotection in Huntington's disease. *Cell Death Dis* 6: e1617
- Khalil B, Lievens JC (2017) Mitochondrial quality control in amyotrophic lateral sclerosis: towards a common pathway? *Neural Regen Res* 12: 1052-1061
- Khosravi B, LaClair KD, Riemenschneider H, Zhou Q, Frottin F, Mareljic N, Czuppa M, Farny D, Hartmann H, Michaelson M *et al* (2020) Cell-to-cell transmission of C9orf72 poly-(Gly-Ala) triggers key features of ALS/FTD. *EMBO J* 39: e102811
- Kim I, Rodriguez-Enriquez S, Lemasters JJ (2007) Selective degradation of mitochondria by mitophagy. *Arch Biochem Biophys* 462: 245-253
- Kirby J, Halligan E, Baptista MJ, Allen S, Heath PR, Holden H, Barber SC, Loynes CA, Wood-Allum CA, Lunec J *et al* (2005) Mutant SOD1 alters the motor neuronal transcriptome: implications for familial ALS. *Brain* 128: 1686-1706
- Klionsky DJ, Abdel-Aziz AK, Abdelfatah S, Abdellatif M, Abdoli A, Abel S, Abeliovich H, Abildgaard MH, Abudu YP, Acevedo-Arozena A *et al* (2021) Guidelines for the use and interpretation of assays for monitoring autophagy (4th edition)(1). *Autophagy* 17: 1-382
- Kobayashi M, Itoh K, Suzuki T, Osanai H, Nishikawa K, Katoh Y, Takagi Y, Yamamoto M (2002) Identification of the interactive interface and phylogenetic conservation of the Nrf2-Keap1 system. *Genes Cells* 7: 807-820

References

- Komatsu M, Kurokawa H, Waguri S, Taguchi K, Kobayashi A, Ichimura Y, Sou YS, Ueno I, Sakamoto A, Tong KI *et al* (2010) The selective autophagy substrate p62 activates the stress responsive transcription factor Nrf2 through inactivation of Keap1. *Nat Cell Biol* 12: 213-223
- Konrad C, Kawamata H, Bredvik KG, Arreguin AJ, Cajamarca SA, Hupf JC, Ravits JM, Miller TM, Maragakis NJ, Hales CM *et al* (2017) Fibroblast bioenergetics to classify amyotrophic lateral sclerosis patients. *Mol Neurodegener* 12: 76
- Koppers M, Blokhuis AM, Westeneng HJ, Terpstra ML, Zundel CA, Vieira de Sa R, Schellevis RD, Waite AJ, Blake DJ, Veldink JH *et al* (2015) C9orf72 ablation in mice does not cause motor neuron degeneration or motor deficits. *Ann Neurol* 78: 426-438
- Kraft AD, Resch JM, Johnson DA, Johnson JA (2007) Activation of the Nrf2-ARE pathway in muscle and spinal cord during ALS-like pathology in mice expressing mutant SOD1. *Exp Neurol* 207: 107-117
- Kwak MK, Itoh K, Yamamoto M, Kensler TW (2002) Enhanced expression of the transcription factor Nrf2 by cancer chemopreventive agents: role of antioxidant response element-like sequences in the nrf2 promoter. *Mol Cell Biol* 22: 2883-2892
- Kwon I, Xiang S, Kato M, Wu L, Theodoropoulos P, Wang T, Kim J, Yun J, Xie Y, McKnight SL (2014) Poly-dipeptides encoded by the C9orf72 repeats bind nucleoli, impede RNA biogenesis, and kill cells. *Science* 345: 1139-1145
- Laflamme C, McKeever PM, Kumar R, Schwartz J, Kolahdouzan M, Chen CX, You Z, Benaliouad F, Gileadi O, McBride HM *et al* (2019) Implementation of an antibody characterization procedure and application to the major ALS/FTD disease gene C9ORF72. *Elife* 8
- Lagier-Tourenne C, Baughn M, Rigo F, Sun S, Liu P, Li HR, Jiang J, Watt AT, Chun S, Katz M *et al* (2013) Targeted degradation of sense and antisense C9orf72 RNA foci as therapy for ALS and frontotemporal degeneration. *Proc Natl Acad Sci U S A* 110: E4530-4539
- Lazarou M, Sliter DA, Kane LA, Sarraf SA, Wang C, Burman JL, Sideris DP, Fogel AI, Youle RJ (2015) The ubiquitin kinase PINK1 recruits autophagy receptors to induce mitophagy. *Nature* 524: 309-314
- Lee DF, Kuo HP, Liu M, Chou CK, Xia W, Du Y, Shen J, Chen CT, Huo L, Hsu MC *et al* (2009) KEAP1 E3 ligase-mediated downregulation of NF-kappaB signaling by targeting IKKbeta. *Mol Cell* 36: 131-140
- Lee JJ, Sanchez-Martinez A, Martinez Zarate A, Beninca C, Mayor U, Clague MJ, Whitworth AJ (2018) Basal mitophagy is widespread in Drosophila but minimally affected by loss of Pink1 or parkin. *J Cell Biol* 217: 1613-1622
- Lee KH, Zhang P, Kim HJ, Mitrea DM, Sarkar M, Freibaum BD, Cika J, Coughlin M, Messing J, Molliex A *et al* (2016) C9orf72 Dipeptide Repeats Impair the Assembly, Dynamics, and Function of Membrane-Less Organelles. *Cell* 167: 774-788 e717
- Lee TS, Tsai HL, Chau LY (2003) Induction of heme oxygenase-1 expression in murine macrophages is essential for the anti-inflammatory effect of low dose 15-deoxy-Delta 12,14-prostaglandin J2. *J Biol Chem* 278: 19325-19330

- Lee YB, Chen HJ, Peres JN, Gomez-Deza J, Attig J, Stalekar M, Troakes C, Nishimura AL, Scotter EL, Vance C *et al* (2013) Hexanucleotide repeats in ALS/FTD form length-dependent RNA foci, sequester RNA binding proteins, and are neurotoxic. *Cell Rep* 5: 1178-1186
- Levine TP, Daniels RD, Gatta AT, Wong LH, Hayes MJ (2013) The product of C9orf72, a gene strongly implicated in neurodegeneration, is structurally related to DENN Rab-GEFs. *Bioinformatics* 29: 499-503
- Lewis SC, Uchiyama LF, Nunnari J (2016) ER-mitochondria contacts couple mtDNA synthesis with mitochondrial division in human cells. *Science* 353: aaf5549
- Li JL, Lin TY, Chen PL, Guo TN, Huang SY, Chen CH, Lin CH, Chan CC (2021) Mitochondrial Function and Parkinson's Disease: From the Perspective of the Electron Transport Chain. *Front Mol Neurosci* 14: 797833
- Li S, Wu Z, Li Y, Tantray I, De Stefani D, Mattarei A, Krishnan G, Gao FB, Vogel H, Lu B (2020) Altered MICOS Morphology and Mitochondrial Ion Homeostasis Contribute to Poly(GR) Toxicity Associated with C9-ALS/FTD. *Cell Rep* 32: 107989
- Liesa M, Palacin M, Zorzano A (2009) Mitochondrial dynamics in mammalian health and disease. *Physiol Rev* 89: 799-845
- Liesa M, Van der Bliek A, Shirihai OS (2019) To Fis or not to Fuse? This is the question! *EMBO J* 38
- Lin J, Chen K, Chen W, Yao Y, Ni S, Ye M, Zhuang G, Hu M, Gao J, Gao C *et al* (2020) Paradoxical Mitophagy Regulation by PINK1 and TUFm. *Mol Cell* 80: 607-620 e612
- Lin Y, Mori E, Kato M, Xiang S, Wu L, Kwon I, McKnight SL (2016) Toxic PR Poly-Dipeptides Encoded by the C9orf72 Repeat Expansion Target LC Domain Polymers. *Cell* 167: 789-802 e712
- Ling SC, Polymenidou M, Cleveland DW (2013) Converging mechanisms in ALS and FTD: disrupted RNA and protein homeostasis. *Neuron* 79: 416-438
- Linker RA, Lee DH, Ryan S, van Dam AM, Conrad R, Bista P, Zeng W, Hronowsky X, Buko A, Chollate S *et al* (2011) Fumaric acid esters exert neuroprotective effects in neuroinflammation via activation of the Nrf2 antioxidant pathway. *Brain* 134: 678-692
- Liu GH, Qu J, Shen X (2008) NF-kappaB/p65 antagonizes Nrf2-ARE pathway by depriving CBP from Nrf2 and facilitating recruitment of HDAC3 to MafK. *Biochim Biophys Acta* 1783: 713-727
- Liu L, Feng D, Chen G, Chen M, Zheng Q, Song P, Ma Q, Zhu C, Wang R, Qi W *et al* (2012) Mitochondrial outer-membrane protein FUNDC1 mediates hypoxia-induced mitophagy in mammalian cells. *Nat Cell Biol* 14: 177-185
- Liu Y, Pattamatta A, Zu T, Reid T, Bardhi O, Borchelt DR, Yachnis AT, Ranum LP (2016) C9orf72 BAC Mouse Model with Motor Deficits and Neurodegenerative Features of ALS/FTD. *Neuron* 90: 521-534
- Liu YJ, McIntyre RL, Janssens GE, Houtkooper RH (2020) Mitochondrial fission and fusion: A dynamic role in aging and potential target for age-related disease. *Mech Ageing Dev* 186: 111212

References

- Lo JY, Spatola BN, Curran SP (2017) WDR23 regulates NRF2 independently of KEAP1. *PLoS Genet* 13: e1006762
- Lomen-Hoerth C, Anderson T, Miller B (2002) The overlap of amyotrophic lateral sclerosis and frontotemporal dementia. *Neurology* 59: 1077-1079
- Lopez-Gonzalez R, Lu Y, Gendron TF, Karydas A, Tran H, Yang D, Petrucelli L, Miller BL, Almeida S, Gao FB (2016) Poly(GR) in C9ORF72-Related ALS/FTD Compromises Mitochondrial Function and Increases Oxidative Stress and DNA Damage in iPSC-Derived Motor Neurons. *Neuron* 92: 383-391
- Loson OC, Song Z, Chen H, Chan DC (2013) Fis1, Mff, MiD49, and MiD51 mediate Drp1 recruitment in mitochondrial fission. *Mol Biol Cell* 24: 659-667
- Lubos E, Loscalzo J, Handy DE (2011) Glutathione peroxidase-1 in health and disease: from molecular mechanisms to therapeutic opportunities. *Antioxid Redox Signal* 15: 1957-1997
- Mackenzie IR, Frick P, Grasser FA, Gendron TF, Petrucelli L, Cashman NR, Edbauer D, Kremmer E, Prudlo J, Troost D *et al* (2015) Quantitative analysis and clinico-pathological correlations of different dipeptide repeat protein pathologies in C9ORF72 mutation carriers. *Acta Neuropathol* 130: 845-861
- Maharjan N, Kunzli C, Buthey K, Saxena S (2017) C9ORF72 Regulates Stress Granule Formation and Its Deficiency Impairs Stress Granule Assembly, Hypersensitizing Cells to Stress. *Mol Neurobiol* 54: 3062-3077
- Majkutewicz I (2022) Dimethyl fumarate: A review of preclinical efficacy in models of neurodegenerative diseases. *Eur J Pharmacol* 926: 175025
- Masrori P, Van Damme P (2020) Amyotrophic lateral sclerosis: a clinical review. *Eur J Neurol* 27: 1918-1929
- Mattie S, Riemer J, Wideman JG, McBride HM (2018) A new mitofusin topology places the redox-regulated C terminus in the mitochondrial intermembrane space. *J Cell Biol* 217: 507-515
- Mauvezin C, Ayala C, Braden CR, Kim J, Neufeld TP (2014) Assays to monitor autophagy in *Drosophila*. *Methods* 68: 134-139
- May S, Hornburg D, Schludi MH, Arzberger T, Rentzsch K, Schwenk BM, Grasser FA, Mori K, Kremmer E, Banzhaf-Strathmann J *et al* (2014) C9orf72 FTL/ALS-associated Gly-Ala dipeptide repeat proteins cause neuronal toxicity and Unc119 sequestration. *Acta Neuropathol* 128: 485-503
- Mazat JP, Ransac S, Heiske M, Devin A, Rigoulet M (2013) Mitochondrial energetic metabolism-some general principles. *IUBMB Life* 65: 171-179
- McWilliams TG, Prescott AR, Montava-Garriga L, Ball G, Singh F, Barini E, Muqit MMK, Brooks SP, Ganley IG (2018) Basal Mitophagy Occurs Independently of PINK1 in Mouse Tissues of High Metabolic Demand. *Cell Metab* 27: 439-449 e435
- Mears JA, Lackner LL, Fang S, Ingeman E, Nunnari J, Hinshaw JE (2011) Conformational changes in Dnm1 support a contractile mechanism for mitochondrial fission. *Nat Struct Mol Biol* 18: 20-26

- Mehta AR, Gregory JM, Dando O, Carter RN, Burr K, Nanda J, Story D, McDade K, Smith C, Morton NM *et al* (2021) Mitochondrial bioenergetic deficits in C9orf72 amyotrophic lateral sclerosis motor neurons cause dysfunctional axonal homeostasis. *Acta Neuropathol* 141: 257-279
- Miao W, Hu L, Scrivens PJ, Batist G (2005) Transcriptional regulation of NF-E2 p45-related factor (NRF2) expression by the aryl hydrocarbon receptor-xenobiotic response element signaling pathway: direct cross-talk between phase I and II drug-metabolizing enzymes. *J Biol Chem* 280: 20340-20348
- Mimoto T, Miyazaki K, Morimoto N, Kurata T, Satoh K, Ikeda Y, Abe K (2012) Impaired antioxidant Keap1/Nrf2 system and the downstream stress protein responses in the motor neuron of ALS model mice. *Brain Res* 1446: 109-118
- Mishra P, Chan DC (2016) Metabolic regulation of mitochondrial dynamics. *J Cell Biol* 212: 379-387
- Mizielinska S, Gronke S, Niccoli T, Ridler CE, Clayton EL, Devoy A, Moens T, Norona FE, Woollacott IOC, Pietrzyk J *et al* (2014) C9orf72 repeat expansions cause neurodegeneration in Drosophila through arginine-rich proteins. *Science* 345: 1192-1194
- Moens TG, Mizielinska S, Niccoli T, Mitchell JS, Thoeng A, Ridler CE, Gronke S, Esser J, Heslegrave A, Zetterberg H *et al* (2018) Sense and antisense RNA are not toxic in Drosophila models of C9orf72-associated ALS/FTD. *Acta Neuropathol* 135: 445-457
- Moens TG, Niccoli T, Wilson KM, Atilano ML, Birsa N, Gittings LM, Holbling BV, Dyson MC, Thoeng A, Neeves J *et al* (2019) C9orf72 arginine-rich dipeptide proteins interact with ribosomal proteins in vivo to induce a toxic translational arrest that is rescued by eIF1A. *Acta Neuropathol* 137: 487-500
- Mohler J, Vani K, Leung S, Epstein A (1991) Segmentally restricted, cephalic expression of a leucine zipper gene during Drosophila embryogenesis. *Mech Dev* 34: 3-9
- Moore AS, Holzbaur EL (2016) Dynamic recruitment and activation of ALS-associated TBK1 with its target optineurin are required for efficient mitophagy. *Proc Natl Acad Sci U S A* 113: E3349-3358
- Mordes DA, Morrison BM, Ament XH, Cantrell C, Mok J, Eggan P, Xue C, Wang JY, Eggan K, Rothstein JD (2020) Absence of Survival and Motor Deficits in 500 Repeat C9ORF72 BAC Mice. *Neuron* 108: 775-783 e774
- Mori K, Weng SM, Arzberger T, May S, Rentzsch K, Kremmer E, Schmid B, Kretzschmar HA, Cruts M, Van Broeckhoven C *et al* (2013) The C9orf72 GGGGCC repeat is translated into aggregating dipeptide-repeat proteins in FTL/ALS. *Science* 339: 1335-1338
- Moujalled D, Grubman A, Acevedo K, Yang S, Ke YD, Moujalled DM, Duncan C, Caragounis A, Perera ND, Turner BJ *et al* (2017) TDP-43 mutations causing amyotrophic lateral sclerosis are associated with altered expression of RNA-binding protein hnRNP K and affect the Nrf2 antioxidant pathway. *Hum Mol Genet* 26: 1732-1746
- Murata H, Takamatsu H, Liu S, Kataoka K, Huh NH, Sakaguchi M (2015) NRF2 Regulates PINK1 Expression under Oxidative Stress Conditions. *PLoS One* 10: e0142438

References

- Murphy MP, Bayir H, Belousov V, Chang CJ, Davies KJA, Davies MJ, Dick TP, Finkel T, Forman HJ, Janssen-Heininger Y *et al* (2022) Guidelines for measuring reactive oxygen species and oxidative damage in cells and in vivo. *Nat Metab* 4: 651-662
- Nagy P, Varga A, Kovacs AL, Takats S, Juhasz G (2015) How and why to study autophagy in *Drosophila*: it's more than just a garbage chute. *Methods* 75: 151-161
- Nair S, Doh ST, Chan JY, Kong AN, Cai L (2008) Regulatory potential for concerted modulation of Nrf2- and Nfkb1-mediated gene expression in inflammation and carcinogenesis. *Br J Cancer* 99: 2070-2082
- Nandi A, Yan LJ, Jana CK, Das N (2019) Role of Catalase in Oxidative Stress- and Age-Associated Degenerative Diseases. *Oxid Med Cell Longev* 2019: 9613090
- Nanou A, Higginbottom A, Valori CF, Wyles M, Ning K, Shaw P, Azzouz M (2013) Viral delivery of antioxidant genes as a therapeutic strategy in experimental models of amyotrophic lateral sclerosis. *Mol Ther* 21: 1486-1496
- Nardo G, Iennaco R, Fusi N, Heath PR, Marino M, Trolese MC, Ferraiuolo L, Lawrence N, Shaw PJ, Bendotti C (2013) Transcriptomic indices of fast and slow disease progression in two mouse models of amyotrophic lateral sclerosis. *Brain* 136: 3305-3332
- Neumann M, Sampathu DM, Kwong LK, Truax AC, Micsenyi MC, Chou TT, Bruce J, Schuck T, Grossman M, Clark CM *et al* (2006) Ubiquitinated TDP-43 in frontotemporal lobar degeneration and amyotrophic lateral sclerosis. *Science* 314: 130-133
- Nezis IP, Shrivage BV, Sagona AP, Lamark T, Bjorkoy G, Johansen T, Rusten TE, Brech A, Baehrecke EH, Stenmark H (2010) Autophagic degradation of dBruce controls DNA fragmentation in nurse cells during late *Drosophila melanogaster* oogenesis. *J Cell Biol* 190: 523-531
- Nguyen L, Laboissonniere LA, Guo S, Pilotto F, Scheidegger O, Oestmann A, Hammond JW, Li H, Hyysalo A, Peltola R *et al* (2020a) Survival and Motor Phenotypes in FVB C9-500 ALS/FTD BAC Transgenic Mice Reproduced by Multiple Labs. *Neuron* 108: 784-796 e783
- Nguyen L, Montrasio F, Pattamatta A, Tusi SK, Bardhi O, Meyer KD, Hayes L, Nakamura K, Banez-Coronel M, Coyne A *et al* (2020b) Antibody Therapy Targeting RAN Proteins Rescues C9 ALS/FTD Phenotypes in C9orf72 Mouse Model. *Neuron* 105: 645-662 e611
- Nguyen TN, Padman BS, Lazarou M (2016) Deciphering the Molecular Signals of PINK1/Parkin Mitophagy. *Trends Cell Biol* 26: 733-744
- Nicholls DG, Budd SL (2000) Mitochondria and neuronal survival. *Physiol Rev* 80: 315-360
- Nickel AG, von Hardenberg A, Hohl M, Loffler JR, Kohlhaas M, Becker J, Reil JC, Kazakov A, Bonnekoh J, Stadelmaier M *et al* (2015) Reversal of Mitochondrial Transhydrogenase Causes Oxidative Stress in Heart Failure. *Cell Metab* 22: 472-484
- Novak I, Kirkin V, McEwan DG, Zhang J, Wild P, Rozenknop A, Rogov V, Lohr F, Popovic D, Occhipinti A *et al* (2010) Nix is a selective autophagy receptor for mitochondrial clearance. *EMBO Rep* 11: 45-51
- O'Rourke JG, Bogdanik L, Yanez A, Lall D, Wolf AJ, Muhammad AK, Ho R, Carmona S, Vit JP, Zarrow J *et al* (2016) C9orf72 is required for proper macrophage and microglial function in mice. *Science* 351: 1324-1329

- Oakes JA, Davies MC, Collins MO (2017) TBK1: a new player in ALS linking autophagy and neuroinflammation. *Mol Brain* 10: 5
- Onesto E, Colombrita C, Gumina V, Borghi MO, Dusi S, Doretti A, Fagiolari G, Invernizzi F, Moggio M, Tiranti V *et al* (2016) Gene-specific mitochondria dysfunctions in human TARDBP and C9ORF72 fibroblasts. *Acta Neuropathol Commun* 4: 47
- Otera H, Ishihara N, Mihara K (2013) New insights into the function and regulation of mitochondrial fission. *Biochim Biophys Acta* 1833: 1256-1268
- Otera H, Miyata N, Kuge O, Mihara K (2016) Drp1-dependent mitochondrial fission via MiD49/51 is essential for apoptotic cristae remodeling. *J Cell Biol* 212: 531-544
- Pan H, Wang H, Wang X, Zhu L, Mao L (2012) The absence of Nrf2 enhances NF-kappaB-dependent inflammation following scratch injury in mouse primary cultured astrocytes. *Mediators Inflamm* 2012: 217580
- Pang W, Hu F (2021) Cellular and physiological functions of C9ORF72 and implications for ALS/FTD. *J Neurochem* 157: 334-350
- Parkinson N, Ince PG, Smith MO, Highley R, Skibinski G, Andersen PM, Morrison KE, Pall HS, Hardiman O, Collinge J *et al* (2006) ALS phenotypes with mutations in CHMP2B (charged multivesicular body protein 2B). *Neurology* 67: 1074-1077
- Pehar M, Beeson G, Beeson CC, Johnson JA, Vargas MR (2014) Mitochondria-targeted catalase reverts the neurotoxicity of hSOD1G(9)(3)A astrocytes without extending the survival of ALS-linked mutant hSOD1 mice. *PLoS One* 9: e103438
- Pehar M, Vargas MR, Robinson KM, Cassina P, Diaz-Amarilla PJ, Hagen TM, Radi R, Barbeito L, Beckman JS (2007) Mitochondrial superoxide production and nuclear factor erythroid 2-related factor 2 activation in p75 neurotrophin receptor-induced motor neuron apoptosis. *J Neurosci* 27: 7777-7785
- Peters OM, Cabrera GT, Tran H, Gendron TF, McKeon JE, Metterville J, Weiss A, Wightman N, Salameh J, Kim J *et al* (2015) Human C9ORF72 Hexanucleotide Expansion Reproduces RNA Foci and Dipeptide Repeat Proteins but Not Neurodegeneration in BAC Transgenic Mice. *Neuron* 88: 902-909
- Pitoniak A, Bohmann D (2015) Mechanisms and functions of Nrf2 signaling in Drosophila. *Free Radic Biol Med* 88: 302-313
- Poole AC, Thomas RE, Andrews LA, McBride HM, Whitworth AJ, Pallanck LJ (2008) The PINK1/Parkin pathway regulates mitochondrial morphology. *Proc Natl Acad Sci U S A* 105: 1638-1643
- Qi Y, Yan L, Yu C, Guo X, Zhou X, Hu X, Huang X, Rao Z, Lou Z, Hu J (2016) Structures of human mitofusin 1 provide insight into mitochondrial tethering. *J Cell Biol* 215: 621-629
- Rada P, Rojo AI, Chowdhry S, McMahon M, Hayes JD, Cuadrado A (2011) SCF/ β -TrCP promotes glycogen synthase kinase 3-dependent degradation of the Nrf2 transcription factor in a Keap1-independent manner. *Mol Cell Biol* 31: 1121-1133
- Rademakers R, Neumann M, Mackenzie IR (2012) Advances in understanding the molecular basis of frontotemporal dementia. *Nat Rev Neurol* 8: 423-434

References

- Rahman MM, Sykietis GP, Nishimura M, Bodmer R, Bohmann D (2013) Declining signal dependence of Nrf2-MafS-regulated gene expression correlates with aging phenotypes. *Aging Cell* 12: 554-562
- Rana A, Oliveira MP, Khamoui AV, Aparicio R, Rera M, Rossiter HB, Walker DW (2017) Promoting Drp1-mediated mitochondrial fission in midlife prolongs healthy lifespan of *Drosophila melanogaster*. *Nat Commun* 8: 448
- Reinholz MM, Merkle CM, Poduslo JF (1999) Therapeutic benefits of putrescine-modified catalase in a transgenic mouse model of familial amyotrophic lateral sclerosis. *Exp Neurol* 159: 204-216
- Renton AE, Majounie E, Waite A, Simon-Sanchez J, Rollinson S, Gibbs JR, Schymick JC, Laaksovirta H, van Swieten JC, Myllykangas L *et al* (2011) A hexanucleotide repeat expansion in C9ORF72 is the cause of chromosome 9p21-linked ALS-FTD. *Neuron* 72: 257-268
- Rikka S, Quinsay MN, Thomas RL, Kubli DA, Zhang X, Murphy AN, Gustafsson AB (2011) Bnip3 impairs mitochondrial bioenergetics and stimulates mitochondrial turnover. *Cell Death Differ* 18: 721-731
- Rizzu P, Blauwendraat C, Heetveld S, Lynes EM, Castillo-Lizardo M, Dhingra A, Pyz E, Hobert M, Synofzik M, Simon-Sanchez J *et al* (2016) C9orf72 is differentially expressed in the central nervous system and myeloid cells and consistently reduced in C9orf72, MAPT and GRN mutation carriers. *Acta Neuropathol Commun* 4: 37
- Robberecht W, Philips T (2013) The changing scene of amyotrophic lateral sclerosis. *Nat Rev Neurosci* 14: 248-264
- Rodriguez-Rocha H, Garcia-Garcia A, Pickett C, Li S, Jones J, Chen H, Webb B, Choi J, Zhou Y, Zimmerman MC *et al* (2013) Compartmentalized oxidative stress in dopaminergic cell death induced by pesticides and complex I inhibitors: distinct roles of superoxide anion and superoxide dismutases. *Free Radic Biol Med* 61: 370-383
- Rohrer JD, Isaacs AM, Mizielińska S, Mead S, Lashley T, Wray S, Sidle K, Fratta P, Orrell RW, Hardy J *et al* (2015) C9orf72 expansions in frontotemporal dementia and amyotrophic lateral sclerosis. *Lancet Neurol* 14: 291-301
- Rossmann MP, Dubois SM, Agarwal S, Zon LI (2021) Mitochondrial function in development and disease. *Dis Model Mech* 14
- Rubino E, Rainero I, Chio A, Rogaeva E, Galimberti D, Fenoglio P, Grinberg Y, Isaia G, Calvo A, Gentile S *et al* (2012) SQSTM1 mutations in frontotemporal lobar degeneration and amyotrophic lateral sclerosis. *Neurology* 79: 1556-1562
- Rutherford NJ, Heckman MG, Dejesus-Hernandez M, Baker MC, Soto-Ortolaza AI, Rayaprolu S, Stewart H, Finger E, Volkening K, Seeley WW *et al* (2012) Length of normal alleles of C9ORF72 GGGGCC repeat do not influence disease phenotype. *Neurobiol Aging* 33: 2950 e2955-2957
- Saberi S, Stauffer JE, Jiang J, Garcia SD, Taylor AE, Schulte D, Ohkubo T, Schloffman CL, Maldonado M, Baughn M *et al* (2018) Sense-encoded poly-GR dipeptide repeat proteins correlate to neurodegeneration and uniquely co-localize with TDP-43 in dendrites of repeat-expanded C9orf72 amyotrophic lateral sclerosis. *Acta Neuropathol* 135: 459-474

- Saikumar J, Byrns CN, Hemphill M, Meaney DF, Bonini NM (2020) Dynamic neural and glial responses of a head-specific model for traumatic brain injury in *Drosophila*. *Proc Natl Acad Sci U S A* 117: 17269-17277
- Sandoval H, Yao CK, Chen K, Jaiswal M, Donti T, Lin YQ, Bayat V, Xiong B, Zhang K, David G *et al* (2014) Mitochondrial fusion but not fission regulates larval growth and synaptic development through steroid hormone production. *Elife* 3
- Sareen D, O'Rourke JG, Meera P, Muhammad AK, Grant S, Simpkinson M, Bell S, Carmona S, Ornelas L, Sahabian A *et al* (2013) Targeting RNA foci in iPSC-derived motor neurons from ALS patients with a C9ORF72 repeat expansion. *Sci Transl Med* 5: 208ra149
- Sarlette A, Krampfl K, Grothe C, Neuhoff N, Dengler R, Petri S (2008) Nuclear erythroid 2-related factor 2-antioxidative response element signaling pathway in motor cortex and spinal cord in amyotrophic lateral sclerosis. *J Neuropathol Exp Neurol* 67: 1055-1062
- Sazanov LA (2015) A giant molecular proton pump: structure and mechanism of respiratory complex I. *Nat Rev Mol Cell Biol* 16: 375-388
- Schludi MH, May S, Grasser FA, Rentzsch K, Kremmer E, Kupper C, Klopstock T, German Consortium for Frontotemporal Lobar D, Bavarian Brain Banking A, Arzberger T *et al* (2015) Distribution of dipeptide repeat proteins in cellular models and C9orf72 mutation cases suggests link to transcriptional silencing. *Acta Neuropathol* 130: 537-555
- Schmitz A, Pinheiro Marques J, Oertig I, Maharjan N, Saxena S (2021) Emerging Perspectives on Dipeptide Repeat Proteins in C9ORF72 ALS/FTD. *Front Cell Neurosci* 15: 637548
- Schwarzlander M, Fricker MD, Muller C, Marty L, Brach T, Novak J, Sweetlove LJ, Hell R, Meyer AJ (2008) Confocal imaging of glutathione redox potential in living plant cells. *J Microsc* 231: 299-316
- Scott RC, Juhasz G, Neufeld TP (2007) Direct induction of autophagy by Atg1 inhibits cell growth and induces apoptotic cell death. *Curr Biol* 17: 1-11
- Scotter EL, Chen HJ, Shaw CE (2015) TDP-43 Proteinopathy and ALS: Insights into Disease Mechanisms and Therapeutic Targets. *Neurotherapeutics* 12: 352-363
- Sellier C, Campanari ML, Julie Corbier C, Gaucherot A, Kolb-Cheynel I, Oulad-Abdelghani M, Ruffenach F, Page A, Ciura S, Kabashi E *et al* (2016) Loss of C9ORF72 impairs autophagy and synergizes with polyQ Ataxin-2 to induce motor neuron dysfunction and cell death. *EMBO J* 35: 1276-1297
- Sen A, Cox RT (2017) Fly Models of Human Diseases: *Drosophila* as a Model for Understanding Human Mitochondrial Mutations and Disease. *Curr Top Dev Biol* 121: 1-27
- Shahheydari H, Ragagnin A, Walker AK, Toth RP, Vidal M, Jagaraj CJ, Perri ER, Konopka A, Sultana JM, Atkin JD (2017) Protein Quality Control and the Amyotrophic Lateral Sclerosis/Frontotemporal Dementia Continuum. *Front Mol Neurosci* 10: 119
- Sharpe JL, Harper NS, Garner DR, West RJH (2021) Modeling C9orf72-Related Frontotemporal Dementia and Amyotrophic Lateral Sclerosis in *Drosophila*. *Front Cell Neurosci* 15: 770937

References

- Shchepinova MM, Cairns AG, Prime TA, Logan A, James AM, Hall AR, Vidoni S, Arndt S, Caldwell ST, Prag HA *et al* (2017) MitoNeoD: A Mitochondria-Targeted Superoxide Probe. *Cell Chem Biol* 24: 1285-1298 e1212
- Shi Y, Lin S, Staats KA, Li Y, Chang WH, Hung ST, Hendricks E, Linares GR, Wang Y, Son EY *et al* (2018) Haploinsufficiency leads to neurodegeneration in C9ORF72 ALS/FTD human induced motor neurons. *Nat Med* 24: 313-325
- Singhal A, Morris VB, Labhasetwar V, Ghorpade A (2013) Nanoparticle-mediated catalase delivery protects human neurons from oxidative stress. *Cell Death Dis* 4: e903
- Sivadasan R, Hornburg D, Drepper C, Frank N, Jablonka S, Hansel A, Lojewski X, Sternecker J, Hermann A, Shaw PJ *et al* (2016) C9ORF72 interaction with cofilin modulates actin dynamics in motor neurons. *Nat Neurosci* 19: 1610-1618
- Skibinski G, Parkinson NJ, Brown JM, Chakrabarti L, Lloyd SL, Hummerich H, Nielsen JE, Hodges JR, Spillantini MG, Thusgaard T *et al* (2005) Mutations in the endosomal ESCRTIII-complex subunit CHMP2B in frontotemporal dementia. *Nat Genet* 37: 806-808
- Smeyers J, Banchi EG, Latouche M (2021) C9ORF72: What It Is, What It Does, and Why It Matters. *Front Cell Neurosci* 15: 661447
- Smith EF, Shaw PJ, De Vos KJ (2019) The role of mitochondria in amyotrophic lateral sclerosis. *Neurosci Lett* 710: 132933
- Solana-Manrique C, Sanz FJ, Ripolles E, Bano MC, Torres J, Munoz-Soriano V, Paricio N (2020) Enhanced activity of glycolytic enzymes in *Drosophila* and human cell models of Parkinson's disease based on DJ-1 deficiency. *Free Radic Biol Med* 158: 137-148
- Solomon DA, Stepto A, Au WH, Adachi Y, Diaper DC, Hall R, Rekhi A, Boudi A, Tziortzouda P, Lee YB *et al* (2018) A feedback loop between dipeptide-repeat protein, TDP-43 and karyopherin- α mediates C9orf72-related neurodegeneration. *Brain* 141: 2908-2924
- St Johnston D (2002) The art and design of genetic screens: *Drosophila melanogaster*. *Nat Rev Genet* 3: 176-188
- Stapper ZA, Jahn TR (2018) Changes in Glutathione Redox Potential Are Linked to Abeta42-Induced Neurotoxicity. *Cell Rep* 24: 1696-1703
- Strappazzon F, Nazio F, Corrado M, Cianfanelli V, Romagnoli A, Fimia GM, Campello S, Nardacci R, Piacentini M, Campanella M *et al* (2015) AMBRA1 is able to induce mitophagy via LC3 binding, regardless of PARKIN and p62/SQSTM1. *Cell Death Differ* 22: 419-432
- Su MY, Fromm SA, Zoncu R, Hurley JH (2020) Structure of the C9orf72 ARF GAP complex that is haploinsufficient in ALS and FTD. *Nature* 585: 251-255
- Sullivan PM, Zhou X, Robins AM, Paushter DH, Kim D, Smolka MB, Hu F (2016) The ALS/FTLD associated protein C9orf72 associates with SMCR8 and WDR41 to regulate the autophagy-lysosome pathway. *Acta Neuropathol Commun* 4: 51
- Sun Z, Wu T, Zhao F, Lau A, Birch CM, Zhang DD (2011) KPNA6 (Importin α 7)-mediated nuclear import of Keap1 represses the Nrf2-dependent antioxidant response. *Mol Cell Biol* 31: 1800-1811

- Swaminathan A, Bouffard M, Liao M, Ryan S, Callister JB, Pickering-Brown SM, Armstrong GAB, Drapeau P (2018) Expression of C9orf72-related dipeptides impairs motor function in a vertebrate model. *Hum Mol Genet* 27: 1754-1762
- Swinnen B, Bento-Abreu A, Gendron TF, Boeynaems S, Bogaert E, Nuyts R, Timmers M, Scheveneels W, Hersmus N, Wang J *et al* (2018) A zebrafish model for C9orf72 ALS reveals RNA toxicity as a pathogenic mechanism. *Acta Neuropathol* 135: 427-443
- Sykitotis GP, Bohmann D (2008) Keap1/Nrf2 signaling regulates oxidative stress tolerance and lifespan in *Drosophila*. *Dev Cell* 14: 76-85
- Tang D, Sheng J, Xu L, Zhan X, Liu J, Jiang H, Shu X, Liu X, Zhang T, Jiang L *et al* (2020) Cryo-EM structure of C9ORF72-SMCR8-WDR41 reveals the role as a GAP for Rab8a and Rab11a. *Proc Natl Acad Sci U S A* 117: 9876-9883
- Teulier L, Weber JM, Crevier J, Darveau CA (2016) Proline as a fuel for insect flight: enhancing carbohydrate oxidation in hymenoptera. *Proc Biol Sci* 283
- Theodore M, Kawai Y, Yang J, Kleshchenko Y, Reddy SP, Villalta F, Arinze IJ (2008) Multiple nuclear localization signals function in the nuclear import of the transcription factor Nrf2. *J Biol Chem* 283: 8984-8994
- Therrien M, Rouleau GA, Dion PA, Parker JA (2013) Deletion of C9ORF72 results in motor neuron degeneration and stress sensitivity in *C. elegans*. *PLoS One* 8: e83450
- Tilokani L, Nagashima S, Paupe V, Prudent J (2018) Mitochondrial dynamics: overview of molecular mechanisms. *Essays Biochem* 62: 341-360
- Tran H, Almeida S, Moore J, Gendron TF, Chalasani U, Lu Y, Du X, Nickerson JA, Petrucelli L, Weng Z *et al* (2015) Differential Toxicity of Nuclear RNA Foci versus Dipeptide Repeat Proteins in a *Drosophila* Model of C9ORF72 FTD/ALS. *Neuron* 87: 1207-1214
- Tu W, Wang H, Li S, Liu Q, Sha H (2019) The Anti-Inflammatory and Anti-Oxidant Mechanisms of the Keap1/Nrf2/ARE Signaling Pathway in Chronic Diseases. *Aging Dis* 10: 637-651
- Tuxworth RI, Chen H, Vivancos V, Carvajal N, Huang X, Tear G (2011) The Batten disease gene CLN3 is required for the response to oxidative stress. *Hum Mol Genet* 20: 2037-2047
- Ugolino J, Ji YJ, Conchina K, Chu J, Nirujogi RS, Pandey A, Brady NR, Hamacher-Brady A, Wang J (2016) Loss of C9orf72 Enhances Autophagic Activity via Deregulated mTOR and TFEB Signaling. *PLoS Genet* 12: e1006443
- van Blitterswijk M, Gendron TF, Baker MC, DeJesus-Hernandez M, Finch NA, Brown PH, Daugherty LM, Murray ME, Heckman MG, Jiang J *et al* (2015) Novel clinical associations with specific C9ORF72 transcripts in patients with repeat expansions in C9ORF72. *Acta Neuropathol* 130: 863-876
- van Es MA, Hardiman O, Chio A, Al-Chalabi A, Pasterkamp RJ, Veldink JH, van den Berg LH (2017) Amyotrophic lateral sclerosis. *Lancet* 390: 2084-2098
- Vargas MR, Burton NC, Kutzke J, Gan L, Johnson DA, Schafer M, Werner S, Johnson JA (2013) Absence of Nrf2 or its selective overexpression in neurons and muscle does not affect survival in ALS-linked mutant hSOD1 mouse models. *PLoS One* 8: e56625

References

- Venkatasubramanian L, Mann RS (2019) The development and assembly of the Drosophila adult ventral nerve cord. *Curr Opin Neurobiol* 56: 135-143
- Veraksa A, McGinnis N, Li X, Mohler J, McGinnis W (2000) Cap 'n' collar B cooperates with a small Maf subunit to specify pharyngeal development and suppress deformed homeotic function in the Drosophila head. *Development* 127: 4023-4037
- von Stockum S, Sanchez-Martinez A, Corra S, Chakraborty J, Marchesan E, Locatello L, Da Re C, Cusumano P, Caicci F, Ferrari V *et al* (2019) Inhibition of the deubiquitinase USP8 corrects a Drosophila PINK1 model of mitochondria dysfunction. *Life Sci Alliance* 2
- Vucic S, Henderson RD, Mathers S, Needham M, Schultz D, Kiernan MC, group Ts (2021) Safety and efficacy of dimethyl fumarate in ALS: randomised controlled study. *Ann Clin Transl Neurol* 8: 1991-1999
- Vucic S, Ryder J, Mekhael L, Rd H, Mathers S, Needham M, Dw S, Mc K, group Ts (2020) Phase 2 randomized placebo controlled double blind study to assess the efficacy and safety of tecfidera in patients with amyotrophic lateral sclerosis (TEALS Study): Study protocol clinical trial (SPIRIT Compliant). *Medicine (Baltimore)* 99: e18904
- Waite AJ, Baumer D, East S, Neal J, Morris HR, Ansorge O, Blake DJ (2014) Reduced C9orf72 protein levels in frontal cortex of amyotrophic lateral sclerosis and frontotemporal degeneration brain with the C9ORF72 hexanucleotide repeat expansion. *Neurobiol Aging* 35: 1779 e1775-1779 e1713
- Wang F, Gao Y, Zhou L, Chen J, Xie Z, Ye Z, Wang Y (2022) USP30: Structure, Emerging Physiological Role, and Target Inhibition. *Front Pharmacol* 13: 851654
- Wang H, Liu K, Geng M, Gao P, Wu X, Hai Y, Li Y, Li Y, Luo L, Hayes JD *et al* (2013) RXRalpha inhibits the NRF2-ARE signaling pathway through a direct interaction with the Neh7 domain of NRF2. *Cancer Res* 73: 3097-3108
- Wang P, Deng J, Dong J, Liu J, Bigio EH, Mesulam M, Wang T, Sun L, Wang L, Lee AY *et al* (2019) TDP-43 induces mitochondrial damage and activates the mitochondrial unfolded protein response. *PLoS Genet* 15: e1007947
- Wang Q, Li WX, Dai SX, Guo YC, Han FF, Zheng JJ, Li GH, Huang JF (2017) Meta-Analysis of Parkinson's Disease and Alzheimer's Disease Revealed Commonly Impaired Pathways and Dysregulation of NRF2-Dependent Genes. *J Alzheimers Dis* 56: 1525-1539
- Wang T, Liu H, Itoh K, Oh S, Zhao L, Murata D, Sesaki H, Hartung T, Na CH, Wang J (2021) C9orf72 regulates energy homeostasis by stabilizing mitochondrial complex I assembly. *Cell Metab* 33: 531-546 e539
- Wang W, Wang L, Lu J, Siedlak SL, Fujioka H, Liang J, Jiang S, Ma X, Jiang Z, da Rocha EL *et al* (2016a) The inhibition of TDP-43 mitochondrial localization blocks its neuronal toxicity. *Nat Med* 22: 869-878
- Wang Y, Branicky R, Noe A, Hekimi S (2018) Superoxide dismutases: Dual roles in controlling ROS damage and regulating ROS signaling. *J Cell Biol* 217: 1915-1928
- Wang ZH, Clark C, Geisbrecht ER (2016b) Analysis of mitochondrial structure and function in the Drosophila larval musculature. *Mitochondrion* 26: 33-42

- Watts GD, Wymer J, Kovach MJ, Mehta SG, Mumm S, Darvish D, Pestronk A, Whyte MP, Kimonis VE (2004) Inclusion body myopathy associated with Paget disease of bone and frontotemporal dementia is caused by mutant valosin-containing protein. *Nat Genet* 36: 377-381
- Webster CP, Smith EF, Bauer CS, Moller A, Hautbergue GM, Ferraiuolo L, Myszczyńska MA, Higginbottom A, Walsh MJ, Whitworth AJ *et al* (2016) The C9orf72 protein interacts with Rab1a and the ULK1 complex to regulate initiation of autophagy. *EMBO J* 35: 1656-1676
- Wen X, Tan W, Westergard T, Krishnamurthy K, Markandaiah SS, Shi Y, Lin S, Shneider NA, Monaghan J, Pandey UB *et al* (2014) Antisense proline-arginine RAN dipeptides linked to C9ORF72-ALS/FTD form toxic nuclear aggregates that initiate in vitro and in vivo neuronal death. *Neuron* 84: 1213-1225
- West RJH, Sharpe JL, Voelzmann A, Munro AL, Hahn I, Baines RA, Pickering-Brown S (2020) Co-expression of C9orf72 related dipeptide-repeats over 1000 repeat units reveals age- and combination-specific phenotypic profiles in Drosophila. *Acta Neuropathol Commun* 8: 158
- Westrate LM, Drocco JA, Martin KR, Hlavacek WS, MacKeigan JP (2014) Mitochondrial morphological features are associated with fission and fusion events. *PLoS One* 9: e95265
- Wong YC, Holzbaur EL (2014) Optineurin is an autophagy receptor for damaged mitochondria in parkin-mediated mitophagy that is disrupted by an ALS-linked mutation. *Proc Natl Acad Sci U S A* 111: E4439-4448
- Wu SC, Cao ZS, Chang KM, Juang JL (2017) Intestinal microbial dysbiosis aggravates the progression of Alzheimer's disease in Drosophila. *Nat Commun* 8: 24
- Xiao S, MacNair L, McGoldrick P, McKeever PM, McLean JR, Zhang M, Keith J, Zinman L, Rogueva E, Robertson J (2015) Isoform-specific antibodies reveal distinct subcellular localizations of C9orf72 in amyotrophic lateral sclerosis. *Ann Neurol* 78: 568-583
- Xu Z, Poidevin M, Li X, Li Y, Shu L, Nelson DL, Li H, Hales CM, Gearing M, Wingo TS *et al* (2013) Expanded GGGGCC repeat RNA associated with amyotrophic lateral sclerosis and frontotemporal dementia causes neurodegeneration. *Proc Natl Acad Sci U S A* 110: 7778-7783
- Yamamoto M, Kensler TW, Motohashi H (2018) The KEAP1-NRF2 System: a Thiol-Based Sensor-Effector Apparatus for Maintaining Redox Homeostasis. *Physiol Rev* 98: 1169-1203
- Yamazaki H, Tanji K, Wakabayashi K, Matsuura S, Itoh K (2015) Role of the Keap1/Nrf2 pathway in neurodegenerative diseases. *Pathol Int* 65: 210-219
- Yang D, Abdallah A, Li Z, Lu Y, Almeida S, Gao FB (2015) FTD/ALS-associated poly(GR) protein impairs the Notch pathway and is recruited by poly(GA) into cytoplasmic inclusions. *Acta Neuropathol* 130: 525-535
- Yang M, Liang C, Swaminathan K, Herrlinger S, Lai F, Shiekhhattar R, Chen JF (2016) A C9ORF72/SMCR8-containing complex regulates ULK1 and plays a dual role in autophagy. *Sci Adv* 2: e1601167
- Yim WW, Mizushima N (2020) Lysosome biology in autophagy. *Cell Discov* 6: 6
- Youle RJ, Narendra DP (2011) Mechanisms of mitophagy. *Nat Rev Mol Cell Biol* 12: 9-14

References

- Youle RJ, van der Bliek AM (2012) Mitochondrial fission, fusion, and stress. *Science* 337: 1062-1065
- Yu R, Jin SB, Lendahl U, Nister M, Zhao J (2019) Human Fis1 regulates mitochondrial dynamics through inhibition of the fusion machinery. *EMBO J* 38
- Yu W, Sun Y, Guo S, Lu B (2011) The PINK1/Parkin pathway regulates mitochondrial dynamics and function in mammalian hippocampal and dopaminergic neurons. *Hum Mol Genet* 20: 3227-3240
- Zemirli N, Morel E, Molino D (2018) Mitochondrial Dynamics in Basal and Stressful Conditions. *Int J Mol Sci* 19
- Zhang D, Iyer LM, He F, Aravind L (2012) Discovery of Novel DENN Proteins: Implications for the Evolution of Eukaryotic Intracellular Membrane Structures and Human Disease. *Front Genet* 3: 283
- Zhang K, Donnelly CJ, Haeusler AR, Grima JC, Machamer JB, Steinwald P, Daley EL, Miller SJ, Cunningham KM, Vidensky S *et al* (2015) The C9orf72 repeat expansion disrupts nucleocytoplasmic transport. *Nature* 525: 56-61
- Zhang YJ, Gendron TF, Ebbert MTW, O'Raw AD, Yue M, Jansen-West K, Zhang X, Prudencio M, Chew J, Cook CN *et al* (2018) Poly(GR) impairs protein translation and stress granule dynamics in C9orf72-associated frontotemporal dementia and amyotrophic lateral sclerosis. *Nat Med* 24: 1136-1142
- Zhang YJ, Gendron TF, Grima JC, Sasaguri H, Jansen-West K, Xu YF, Katzman RB, Gass J, Murray ME, Shinohara M *et al* (2016) C9ORF72 poly(GA) aggregates sequester and impair HR23 and nucleocytoplasmic transport proteins. *Nat Neurosci* 19: 668-677
- Zhang YJ, Jansen-West K, Xu YF, Gendron TF, Bieniek KF, Lin WL, Sasaguri H, Caulfield T, Hubbard J, Daugherty L *et al* (2014) Aggregation-prone c9FTD/ALS poly(GA) RAN-translated proteins cause neurotoxicity by inducing ER stress. *Acta Neuropathol* 128: 505-524
- Zhao RZ, Jiang S, Zhang L, Yu ZB (2019) Mitochondrial electron transport chain, ROS generation and uncoupling (Review). *Int J Mol Med* 44: 3-15
- Zhu CL, Yao RQ, Li LX, Li P, Xie J, Wang JF, Deng XM (2021) Mechanism of Mitophagy and Its Role in Sepsis Induced Organ Dysfunction: A Review. *Front Cell Dev Biol* 9: 664896
- Zhu Q, Jiang J, Gendron TF, McAlonis-Downes M, Jiang L, Taylor A, Diaz Garcia S, Ghosh Dastidar S, Rodriguez MJ, King P *et al* (2020) Reduced C9ORF72 function exacerbates gain of toxicity from ALS/FTD-causing repeat expansion in C9orf72. *Nat Neurosci* 23: 615-624
- Zielonka J, Sikora A, Hardy M, Joseph J, Dranka BP, Kalyanaraman B (2012) Boronate probes as diagnostic tools for real time monitoring of peroxynitrite and hydroperoxides. *Chem Res Toxicol* 25: 1793-1799
- Zielonka J, Vasquez-Vivar J, Kalyanaraman B (2008) Detection of 2-hydroxyethidium in cellular systems: a unique marker product of superoxide and hydroethidine. *Nat Protoc* 3: 8-21